



UNIVERSITÉ CATHOLIQUE DE LOUVAIN

INSTITUT DE RECHERCHE EN  
MATHÉMATIQUE ET PHYSIQUE

---

## Applications of the line bundle Laplacian to spanning forests and related lattice models

---

Adrien PONCELET

Thesis submitted in partial fulfillment of the requirements for  
the degree of Docteur en Sciences

### Dissertation committee

Prof. Philippe RUELLE (Supervisor)	UCL, Belgium
Prof. Marino GRAN (President)	UCL, Belgium
Prof. Tom CLAEYS (Secretary)	UCL, Belgium
Prof. Christian HAGENDORF	UCL, Belgium
Prof. Vyatcheslav B. PRIEZZHEV	JINR, Russia

JANUARY 2018



# Remerciements

La personne que je souhaite remercier en premier est mon promoteur, Philippe Ruelle, pour son soutien tant sur le plan technique qu'humain au long de ces six années de doctorat, mais également pour m'avoir lancé sur un thème de recherche si porteur et passionnant. Sa patience, sa grande disponibilité et ses remarques toujours pertinentes ont été extrêmement précieuses lors de mon apprentissage du métier de chercheur.

Je suis redevable à Christian Hagendorf d'avoir attiré mon attention sur la formule de Schramm pour la marche aléatoire à boucles effacées, et d'avoir entrepris les premiers calculs avec moi. Ce qui devait n'être au départ qu'une simple collection de quelques résultats explicites s'est finalement transformé en un solide sujet de recherche, constituant près de la moitié de ma thèse. Merci aussi à lui de m'avoir motivé à améliorer mon encadrement en tant qu'assistant.

Je remercie également les membres de mon jury, les professeurs Tom Claeys, Marino Gran, Christian Hagendorf et Vyatcheslav B. Priezzhev pour le temps qu'ils ont consacré à la lecture de mon texte, ainsi que pour leurs remarques et suggestions en vue de son amélioration. J'ai une pensée particulière pour le professeur Priezzhev, récemment décédé, dont j'ai apprécié l'attitude positive et constructive lors des discussions autour de ma défense privée en décembre.

Le cadre de travail agréable dans lequel j'ai baigné a été essentiel à l'aboutissement de ce travail de longue haleine. Pour la bonne humeur, les moments de décompression, les partages d'expériences, les astuces mathématiques, les conseils techniques et pratiques, je tiens à remercier

tous mes collègues (anciens et actuels) du groupe de physique statistique et mathématique : Alexi, Bernard, Bryan, Gilles, Jean et Lise ; et aussi David de CP3, avec qui j'ai partagé un bureau pendant près d'un an. Un grand merci plus largement à l'ensemble des membres MATH/GPP de l'IRMP pour l'ambiance chaleureuse régnant au cyclotron.

À côté des aspects liés à la recherche, une part conséquente de mon temps pendant ces six années a été consacrée à l'enseignement. En tant qu'assistant, il n'a pas toujours été facile de bien équilibrer encadrement, recherche et vie privée, dans un cadre professionnel exigeant. Ce volet de mon expérience doctorale s'est cependant avéré fort enrichissant, grâce à la compétence et à la bonne volonté des nombreux collègues assistants, techniciens et professeurs avec qui j'ai eu la chance d'échanger et de collaborer au fil des ans—en particulier Matthieu, Benoit, Francisco, Manu et Thierry, dans le cadre du cours de physique générale en médecine vétérinaire. D'autre part, je tiens aussi à remercier les étudiants que j'ai encadrés lors de séances d'exercices et de laboratoires. J'ai beaucoup appris à leur contact, tant d'un point de vue scientifique et pédagogique que personnel. C'a été un réel plaisir de contribuer modestement à leur formation.

Enfin, merci aux amis pour leur présence, pour arriver sans peine à me changer les idées, et pour les innombrables séances sportives partagées ensemble. Merci à ma famille pour son intérêt dans mes travaux, et pour son soutien constant et inconditionnel.

# Contents

<b>Introduction</b>	<b>1</b>
<b>1 Spanning trees and the line bundle Laplacian</b>	<b>11</b>
1.1 The matrix-tree theorem . . . . .	11
1.2 The line bundle Laplacian . . . . .	14
1.3 Cycle-rooted groves . . . . .	16
1.3.1 Oriented cycle-rooted groves . . . . .	17
1.4 Annular-one graphs . . . . .	20
1.5 Graphs with free boundary conditions . . . . .	25
<b>2 The Abelian sandpile model</b>	<b>29</b>
2.1 Review of the Abelian sandpile model . . . . .	30
2.1.1 The burning algorithm . . . . .	33
2.1.2 Height probabilities . . . . .	36
2.1.3 Multisite height probabilities . . . . .	38
2.2 Single-site probabilities on the plane . . . . .	45
2.3 Multisite probabilities on the plane . . . . .	51
2.3.1 Two-site probabilities . . . . .	52

---

2.3.2	Three-site probabilities . . . . .	56
2.4	Probabilities on the upper half-plane . . . . .	58
2.4.1	One-site probabilities on the upper half-plane . . .	58
2.4.2	One-site probabilities on the diagonal upper half- plane . . . . .	61
2.4.3	Mixed bulk-boundary two-site correlations . . . . .	64
2.4.4	Bulk two-site correlations . . . . .	65
2.5	Height probabilities on the triangular lattice . . . . .	66
2.5.1	On the plane . . . . .	67
2.5.2	On the upper half-plane . . . . .	72
2.6	Height probabilities on the hexagonal lattice . . . . .	74
2.6.1	On the plane . . . . .	76
2.6.2	On upper half-planes . . . . .	78
2.6.3	On boundaries . . . . .	82
2.7	Conformal field theory . . . . .	84
2.7.1	Correlations on the plane . . . . .	90
2.7.2	Bulk-boundary correlations . . . . .	95
2.7.3	Two-point bulk correlations on the upper half-plane	98
2.7.4	Other lattices . . . . .	102
<b>3</b>	<b>Loop-erased random walks</b>	<b>105</b>
3.1	Paths in spanning forests and Schramm's formula . . . . .	107
3.1.1	Measures on paths in forests and groves . . . . .	107
3.1.2	Schramm's formula . . . . .	110
3.2	Explicit results for passage probabilities . . . . .	114

---

3.2.1	The upper half-plane . . . . .	114
3.2.2	The cylinder . . . . .	118
3.2.3	The Möbius strip . . . . .	126
3.3	Passage probabilities for multiple paths . . . . .	139
3.3.1	Two paths . . . . .	141
3.3.2	More than two paths . . . . .	145
3.4	Correspondence with loop-erased random walks . . . . .	156
3.4.1	Single walks . . . . .	157
3.4.2	Multiple walks . . . . .	163
3.5	Comparison with SLE/CFT results . . . . .	166
	<b>Conclusion</b>	<b>171</b>
	<b>A Green functions</b>	<b>175</b>
A.1	Zipper on the plane . . . . .	175
A.2	Zipper on the upper half-plane . . . . .	180
A.3	Modified graphs . . . . .	184
A.4	Triangular lattice . . . . .	192
A.4.1	Values of Green functions . . . . .	192
A.4.2	Green function derivative for small distances . . . . .	193
A.4.3	Green function derivative for large distances . . . . .	194
	<b>B Symmetries and maps between predecessor diagrams on half-planes</b>	<b>201</b>
	<b>C Jacobi's theta and elliptic functions</b>	<b>211</b>

C.1	Jacobi's theta functions . . . . .	211
C.2	Jacobi's elliptic functions . . . . .	213
<b>D</b>	<b>Technical proofs</b>	<b>215</b>
	<b>Bibliography</b>	<b>225</b>

# Introduction

Phase transitions in physics refer to the appearance of significant macroscopic changes of a system, induced by a small variation of a global parameter such as the temperature or an external magnetic field. Two of the most common examples consist in the transition between liquid and gaseous phases of a body, and spontaneous magnetization in ferromagnets. The latter in particular was studied in the 1920s by Ising through a simple model for ferromagnetism on square lattices  $\mathbb{Z}^d$  introduced by Lenz. Although Ising determined the absence of phase transition in one dimension, it was shown in 1936 by Peierls that the model—now renowned as the *Ising model*—undergoes a phase transition in any dimension strictly larger than one. In 1941, Kramers and Wannier identified the temperature  $T_c$  corresponding to the *critical point* in  $d = 2$  dimensions, namely the particular value of  $T$  marking the separation between the ordered and disordered phases. After Onsager computed in 1944 the free energy of the 2D model (in the absence of an external magnetic field), thus giving access to some of its thermodynamical properties, the two-dimensional Ising model became one of the most thoroughly investigated statistical models exhibiting an order-disorder transition.

In particular, it was observed that a number of macroscopic quantities of the Ising model, such as the specific heat, the magnetization or the correlation length, are described near the critical temperature by power laws, whose exponents are called *critical exponents*. Due to their power-law behavior, these functions do not possess a characteristic scale, hence they are said to be *scale invariant*. This observation resulted in the introduction of the renormalization group in the 1960s, which led

to a better understanding of the critical regime of various statistical models—in particular the Ising model—from a physical point of view. Roughly speaking, the idea of renormalization consists in looking at a given physical system at a larger scale, at which the microscopic degrees of freedom have been replaced by fewer effective ones (see for instance the block-spin technique for the Ising model). Iterating the process many times leads to the notion of *scaling limit*, which can alternatively be viewed as considering the statistical model on a large graph with a very small mesh size. The loss of information caused by the renormalization procedure suggests that the scaling limit of a model should be independent of a number of microscopic details, in particular the specific lattice on which the model is defined. According to this idea, a large number of models should therefore be described by the same set of critical exponents, in which case they are said to belong to the same *universality class*.

Two key features of phase transitions in statistical models such as the Ising model are that (i) the system is at equilibrium and (ii) the critical point corresponds to specific, fine-tuned values of global parameters (the temperature  $T$  and the magnetic field  $H$  for the Ising model). Approximate scale invariance is however observed in many natural phenomena. For instance, spatial power-law correlations describe the height profile of mountain ranges, the shape of coastlines or the catchment area of river flows; and temporal power-law correlations describe the luminosity of stars, the frequency of rain of a given intensity or the frequency of earthquakes. As these systems are out of equilibrium and evolve over decades, external variables such as the temperature are expected to vary significantly over time, so their fine-tuning is rather unlikely. To justify the existence of power laws in the various phenomena listed above, Bak, Tang and Wiesenfeld proposed in 1987 a generic underlying mechanism called *self-organized criticality* (SOC) [6]. Dynamical systems exhibiting this property are kept out of equilibrium by a slow driving process (e.g. the accumulation of water in clouds through evaporation), such that their overall properties are unchanged over the time scale of an observation (these systems are said to be in a nonequilibrium steady state). Moreover, they possess a burst-like relaxation procedure that provides a form of dissipation (e.g. precipitations), whose time scale is much smaller than that of the driving process. Bak et al. argued that the dy-

---

namics of such systems then naturally evolve toward their critical state, without any fine-tuning required. Their paper was followed by a few others on models in which SOC is conjectured to occur: earthquakes [121], pulsars [118], forest fires [44] or fluctuations in economics [5].

To give a concrete illustration of SOC, Bak et al. [6] defined a toy model on a square grid, in which grains of sand are piled up at the vertices. The driving process consists in increasing the heights of the sandpiles until they reach a critical value, causing the piles to collapse and to distribute grains to their neighbors on the grid, which may in turn topple, thus yielding an avalanche. The first analytic treatment of this model is due to Dhar [39], who showed in particular its Abelian property, in the sense that the order in which simultaneously unstable sandpiles collapse does not influence the resulting stable state. The model has subsequently been called the *Abelian sandpile model* (ASM)—it is also known as the *chip-firing game* in the mathematics community, see e.g. [16]—and has been the subject of numerous papers since then, for three main reasons. First, as the ASM is one of the simplest, prototypical SOC model, studying it is a way to probe and discover generic aspects of self-organized criticality. Second, the ASM turns out to be interesting in itself, as it has been shown to be connected with several well-known statistical models, namely the uniform spanning tree (UST) [112], dimers [155], the  $q \rightarrow 0$  Potts model [54, 158] and the loop-erased random walk [126, 157] (via their connection with the UST for the latter three models). Systems having a similar dynamics, such as the Manna model [114] and Eulerian walkers [138] (also known as the rotor-router model [67]), also share features with the original model of Bak et al. Third, the Abelian property of the ASM—which is believed to be conformally invariant in the scaling limit—makes it particularly amenable to analytical and numerical computations, most of which being related to the microscopic degrees of freedom of the model, namely the height variables.

Among the exact results obtained on square grids are single-site probabilities on the full lattice or half-lattice [81, 137], various joint probabilities of heights at isolated sites or between a certain type of clusters [79, 110, 111, 130, 131], the effects of boundary conditions and boundary probabilities [18, 73, 78, 80, 128, 141, 142], finite-size corrections [81, 112, 141] and the insertion of dissipation [78, 80, 110, 127]. Some attention has been

paid to other regular lattices, in particular the triangular and hexagonal (or honeycomb) ones, for which height probabilities have been estimated using renormalization group transformations and numerical simulations [70, 109, 124]. More recently, multisite height-one probabilities have been evaluated exactly on the hexagonal lattice [4], and the sandpile density (i.e. the average height per site) has been computed for a variety of regular lattices [84]. It should be noted that the model has also been studied away from its critical point (by introducing dissipation at each site of the lattice). Analytical results include joint probabilities of unit heights or between a certain type of clusters [110] and joint boundary probabilities [128].

Other variables have been studied in the ASM, namely those associated with an avalanche, such as the total number of topplings  $s$ , the number of distinct sites toppled  $s_d$ , the radius  $R$  of the avalanche cluster, the duration  $T$ , and the number of waves  $n_w$ . It is conjectured that all these variables can be written as powers of one another, and that

$$\mathbb{P}(X \geq x) \propto x^{1-\tau_X} f(x/x_c),$$

where  $X$  is any of the random variables  $s, s_d, R, T, n_w$ , the parameter  $x_c$  is a cutoff that scales with the size of the system, and  $\tau_X$  denotes the critical exponent associated with  $X$ . Although the four avalanche exponents have been determined by scaling arguments and numerical simulations [41, 74, 75, 94, 139] (see also [40] for a review), exact lattice computations remains to be done. Another mathematical aspect of the model that has been investigated concerns the operators  $a_i$  that drop a grain of sand at site  $i$  on the lattice and relax the system through the toppling of unstable sites. These operators—which depend on the graph  $\mathcal{G}$  on which the ASM is defined—map the set of stable configurations onto itself, and generate a finite Abelian group  $G(\mathcal{G})$ , called the sandpile (or critical) group of  $\mathcal{G}$ . Many papers have been written on this topic, dealing mostly with the identification of the group structure of  $G(\mathcal{G})$  for generic or specific classes of graphs [15, 35, 38, 42, 69, 77, 156], or with the description of the identity element of  $G(\mathcal{G})$  [24, 36, 42, 106].

In the scaling limit—that is, as the lattice mesh goes to zero—statistical models are expected to be described by quantum field theories. More precisely, a specific field is associated with each (local) lattice observable

---

in such a way that lattice correlators converge to field-theoretical ones. Due to the power-law behavior observed for many critical models, it was argued that the corresponding quantum field theories must be scale invariant, in addition to being translation and rotation invariant. With a few supplementary assumptions, they were said to exhibit *global* conformal invariance [135]. The existence of a much stronger symmetry for two-dimensional systems was inferred in 1984 by Belavin, Polyakov and Zamolodchikov [12], namely *local* conformal invariance. In two dimensions, local conformal maps are given by holomorphic functions, which yield an infinite-dimensional Lie algebra symmetry. This assumption of conformal invariance led to the development of *conformal field theories* (CFTs), which are (partially) classified by a real number  $c$  called the *central charge*. As a consequence of their heavily constrained nature, the study of CFTs has led to a myriad of explicit results over the years regarding the classification of 2D critical models and the inventory of the possible scaling fields in each theory, the finite-size behavior and analytical computation of critical correlators, and the exact determination of critical exponents (see [72] for a collection of the original papers on these topics). Outside of statistical physics, CFTs have also found many applications in condensed matter physics, from the Kondo effect [1], the Fermi edge singularity [2] or the fractional quantum Hall effect [117] to entanglement entropy [20] or quantum quenches [21, 22]. Conformal invariance has also been used in string theory [55], in particular via the AdS/CFT correspondence [113]. Due to its prevalence in modern theoretical physics, conformal field theory has therefore been the subject of many reviews and books, among which are the following well-known references [26, 43, 61].

Although early developments of CFTs led to tremendous progress in the comprehension of many critical systems in two dimensions, it was noticed in the 1990s that richer and more complicated theories were required to describe the behavior of certain observables in diverse models, in particular those exhibiting nonlocal properties. Among the characteristic features of those CFTs are their nonunitarity and the inclusion of reducible but indecomposable representations [140]. In more physical terms, the latter property means that the Hamiltonian is nondiagonalizable, which leads to the appearance of logarithms in correlation functions (in such a way that conformal invariance is preserved) [63]. Those

theories have therefore been called *logarithmic conformal field theories* (LCFTs). While much progress has been made since then (see the recent special issue on the subject [59]), LCFTs are still far from being fully understood—at least, to the extent nonlogarithmic, usual CFTs are understood today. In this regard, studying lattice realizations of LCFTs should prove very useful to probe and try to better understand certain aspects of these theories.

The first objective of this dissertation is therefore to carry out explicit calculations of correlations in the lattice sandpile model, without referring to LCFTs. A number of computations have already been done using standard graph-theoretical methods to write height correlations as fractions of spanning trees with certain nonlocal topological properties (see for instance [81, 130, 131, 137]). However, in view of their technical complexity and clumsiness, these methods have somehow delivered all what they could. Recent ideas put forward by Kenyon and Wilson [88, 91] to compute partition functions for spanning forests have much improved the situation, since they dramatically reduce the complexity of calculations. These techniques are directly relevant to the evaluation of sandpile correlations and therefore allow one to obtain new explicit results, which can in turn be compared to LCFT predictions.

The large success met by the use of conformal field theories to study critical lattice systems has also inspired significant developments related to conformal invariance in the mathematics community. In particular, papers pertaining to crossing probabilities in the percolation model published in the early 1990s [28, 97] attracted a number of mathematicians to the domain. The description of random interfaces and paths appearing in critical lattice models was at that time very limited, and the few important results derived using CFTs had nothing to do with systematic techniques. The major breakthrough came in 2000, when Schramm proposed a natural candidate for families of nonintersecting curves to describe the continuum limit of the loop-erased random walk (LERW) and the uniform spanning tree (UST) [144]. He introduced what is now called the *Schramm-Loewner evolution with parameter  $\kappa > 0$*  ( $\text{SLE}_\kappa$ ), defined as the random Loewner evolution with driving process  $\sqrt{\kappa} B_t$ , where  $(B_t)_{t \geq 0}$  is a standard Brownian motion (the value of  $\kappa$  depending on the specific lattice model considered). Its two key properties

are (i) conformal invariance and (ii) a domain Markov property. Together with Lawler and Werner, Schramm proved in 2004 the convergence of the LERW and the UST to  $\text{SLE}_2$  and  $\text{SLE}_8$ , respectively, in the celebrated paper [105]. Since then, SLEs have been proved to be the scaling limit of interfaces and paths appearing in a variety of models: percolation [23, 151], the discrete Gaussian free field [146, 147] and the critical Ising and FK-Ising models [29, 31]. SLEs have also been extended in several directions, for instance on multiply connected domains [11, 102, 160] and for the description of multiple nonintersecting curves [10, 45, 76, 93, 95, 101, 125, 159]. The connection with the CFT framework has been made in [8, 56], and relates the central charge  $c$  to the parameter  $\kappa$  as follows:

$$c = \frac{(6 - \kappa)(3\kappa - 8)}{2\kappa},$$

which is invariant under  $\kappa \rightarrow 16/\kappa$  and implies that  $c \leq 1$ .

More recently, another approach to conformal invariance of 2D critical lattice models has come from *discrete complex analysis*, pioneered by Smirnov in the late 2000s (see [152] for an overview) based on early developments appearing in the work of Kenyon [85, 87]. Several rigorous results have been obtained by identifying lattice observables of the Ising model and the dimer model—and more generally of  $O(n)$  models—that satisfy discrete Cauchy-Riemann equations and possess a conformally invariant limit, on a large class of planar graphs [30, 31, 47, 68] (see also [46] for a summary thereof).

As far as explicit computations are concerned, one of the simplest results obtained in the SLE framework for a single curve is *Schramm's formula*, which gives the probability that a marked point lies to the left (or right) of an  $\text{SLE}_\kappa$  curve between fixed boundary points [145]. This formula has been adapted in several ways, namely to curves in doubly connected domains for  $\kappa = 2$  [64] and  $\kappa = 4$  [66], and for the left-passage probability with respect to two marked points  $z_1, z_2$  for  $\kappa = 8/3$  [13, 150]. The generalization to multiple curves passing left or right of one marked point has also been investigated in [60], in which the passage probabilities were explicitly computed for two curves only, for  $\kappa = 0, 2, 4, 8/3, 8$  (with more rigorous proofs given later in [107]). Most of the results regarding Schramm's formula, including the original paper [145], have

been directly obtained in the continuum. A notable exception is [71], in which an explicit expression for the left-passage probability with respect to a specific type of marked points is given on the lattice, for the percolation model. The second objective of this dissertation is to derive the equivalent of Schramm's formula at the lattice level for a specific model, namely the loop-erased random walk. Due to the well-known correspondence between the LERW and branches of the UST [126, 157], the probability of interest may be expressed as a ratio of partition functions for spanning forests with a certain topological property. Techniques recently developed by Kenyon and Wilson [88, 91] may be used to obtain a discrete combinatorial form for Schramm's formula. Its explicit evaluation on rectangular grids approximating well-known domains such as the upper half-plane and the cylinder allow for a comparison with SLE computations in the scaling limit. Moreover, the same formalism allows one to find a generalization of Schramm's formula for multiple LERWs.

The layout of this dissertation is the following. In the first chapter, we first recall well-known definitions and results in graph theory regarding spanning trees and the combinatorial Laplacian, most notably the matrix-tree theorem and its generalization for minors of the Laplacian. We then introduce the concept of a connection on a graph and the line bundle Laplacian (which specializes to the usual graph Laplacian for a trivial connection). We present the results of [53, 88, 91], in particular the grove theorem, which constitutes the mathematical foundation of our work. The second and third chapters concern the Abelian sandpile model and the loop-erased random walk, respectively (a detailed description of their contents is included at the beginning of both chapters). For both models, exact lattice results are obtained through the correspondence with the spanning tree model, using theorems recalled in the first chapter. Their comparison in the scaling limit to predictions arising from LCFTs and SLEs is then discussed. Finally, four appendices collect technical material related to the explicit computations presented in the second and third chapters of this dissertation.

The results presented in this thesis have been published in the following articles:

- PONCELET, A, AND RUELLE, P. Multipoint correlators in the Abelian sandpile model. *J. Stat. Mech.* (2017), 123102.
- PONCELET, A, AND RUELLE, P. Sandpile probabilities on triangular and hexagonal lattices. *J. Phys. A* 51, 1 (2018), 015002.
- PONCELET, A. Schramm's formula for multiple loop-erased random walks. [arXiv:1801.03126](https://arxiv.org/abs/1801.03126) [cond-mat.stat-mech].



# Chapter 1

## Spanning trees and the line bundle Laplacian

In this chapter, we recall definitions and classical results in graph theory. We give an overview of some new techniques pertaining to graphs equipped with a connection, introduced in [53, 88, 91], which are relevant for the computations of later chapters. For the most part, we follow the formalism of [91].

### 1.1 The matrix-tree theorem

Let  $\mathcal{G}$  be an unoriented connected graph, with a set of vertices  $\mathcal{V}$  and edges  $\mathcal{E}$ . We assume that there are no self-loops or multiple edges in  $\mathcal{E}$ . We shall denote by  $(u, v)$  and  $\{u, v\}$  the oriented edge and the unoriented edge from  $u$  to  $v$ , respectively (with  $\{v, u\} = \{u, v\}$ ). Let  $s$  be an additional vertex, called the *root*, connected to a subset  $\mathcal{D} \subset \mathcal{V}$  by a set of edges  $\mathcal{E}_s$ , which may contain multiple edges. We denote by  $\mathcal{G}_s$  the extended graph with vertices  $\mathcal{V} \cup \{s\}$  and edges  $\mathcal{E} \cup \mathcal{E}_s$ .

A *spanning tree* on  $\mathcal{G}_s$  is a connected subgraph without loops that contains all the vertices of  $\mathcal{V} \cup \{s\}$  (see Fig. 1.1). In what follows, we shall make the distinction between a spanning tree and a *rooted* spanning tree,

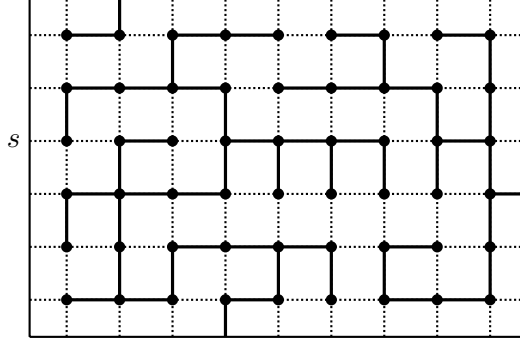


Figure 1.1: Spanning tree on a rectangular  $9 \times 6$  grid (whose edges are drawn as dotted lines), extended by a unique root  $s$ , represented as the box surrounding the grid.

in which all edges are oriented toward a single vertex, usually taken to be the root  $s$ .

We define a conductance function  $c : \mathcal{E} \cup \mathcal{E}_s \rightarrow \mathbb{R}_+^*$ , associating a weight  $c_{u,v} = c_{v,u}$  with each unoriented edge  $\{u,v\} \in \mathcal{E}$ . We further choose a unit conductance for the edges  $\{u,s\}$  in  $\mathcal{E}_s$ :  $c_{u,s} = c_{s,u} = 1$ . The weight of a spanning tree  $\mathcal{T}$  on  $\mathcal{G}_s$  is given by

$$w(\mathcal{T}) = \prod_{\{u,v\} \in \mathcal{T}} c_{u,v}. \quad (1.1)$$

The standard Laplacian of the graph  $\mathcal{G}_s$  is denoted by  $\Delta_{\mathcal{G}_s}$ , and is defined for any  $u, v \in \mathcal{V} \cup \{s\}$  by

$$(\Delta_{\mathcal{G}_s})_{u,v} = \begin{cases} \deg_s(u) & \text{if } v = u, \\ -c_{u,v} & \text{if } \{u,v\} \in \mathcal{E} \cup \mathcal{E}_s, \\ 0 & \text{otherwise,} \end{cases} \quad (1.2)$$

where  $\deg_s(u)$  is the (weighted) degree of  $u$  on the graph  $\mathcal{G}_s$ , given by

$$\deg_s(u) = \sum_{w: \{u,w\} \in \mathcal{E} \cup \mathcal{E}_s} c_{u,w}. \quad (1.3)$$

One sees that  $\Delta_{\mathcal{G}_s}$  is singular since it has a zero eigenvalue, whose corresponding eigenspace is generated by  $(1, 1, \dots, 1)^t$  (this Laplacian is sometimes denoted by  $\Delta_0$ , the index referring to its zero eigenvalue).

Therefore, it is customary to define  $\Delta_{\mathcal{G}_s}^{(s)}$ , the Laplacian of  $\mathcal{G}_s$  with Dirichlet boundary conditions at  $s$ , as the submatrix of  $\Delta_{\mathcal{G}_s}$  from which the row and column indexed by  $s$  have been removed. In what follows, we shall drop the subscript  $\mathcal{G}_s$  and the superscript  $(s)$ , and simply refer to this Dirichlet Laplacian as  $\Delta$ . Moreover, we shall call *wired* the vertices of  $\mathcal{D}$  (i.e. those that are connected to the root  $s$  by an edge in  $\mathcal{E}_s$ ), and *free* or *unwired* the vertices in  $\mathcal{V} \setminus \mathcal{D}$ .

In this thesis, we shall consider planar graphs embedded on surfaces bounded by Jordan curves. We shall call *boundary vertices* the vertices in  $\mathcal{V}$  belonging to these curves, and take  $\mathcal{D}$  to be a subset thereof. A graph in which all boundary vertices belong to  $\mathcal{D}$  (resp.  $\mathcal{V} \setminus \mathcal{D}$ ) will be said to have a *wired boundary* (resp. *free boundary*).

A well-known result in graph theory, the *matrix-tree theorem*—which is also known as Kirchhoff’s theorem—states that the determinant of the Dirichlet Laplacian  $\Delta$  is equal to the weighted sum of spanning trees on  $\mathcal{G}_s$ .

**Theorem 1.1** ([92]). *Let  $\mathcal{T}$  denote the set of spanning trees on the graph  $\mathcal{G}_s$ , and let  $\Delta$  be the Dirichlet Laplacian of  $\mathcal{G}_s$ . Then*

$$\det \Delta = \sum_{\mathcal{T} \in \mathcal{T}} w(\mathcal{T}), \quad (1.4)$$

where the weight of a spanning tree is defined by Eq. (1.1).

More generally, we shall consider spanning forests on  $\mathcal{G}_s$ , that is, multiply connected spanning subgraphs in which each component is a tree. The natural weight of a spanning forest is given by the product of the weights of its tree components. The generalization of Kirchhoff’s theorem for spanning forests, called the *all-minors matrix-tree theorem*, is as follows.

**Theorem 1.2** ([32]). *In addition to the root  $s$ , let  $R = \{r_1, \dots, r_k\}$ ,  $S = \{s_1, \dots, s_k\}$  and  $T = \{t_1, \dots, t_\ell\}$  be three disjoint subsets of  $\mathcal{V}$ , and*

$$\sigma = r_1 s_1 | \dots | r_k s_k | t_1 | \dots | t_\ell | s \quad (1.5)$$

be a partial pairing of these vertices (the vertical bars separating the pairs and singletons). One denotes by  $Z[\sigma]$  the weighted sum of spanning

forests on  $\mathcal{G}_s$  in which each of the  $k+\ell+1$  trees contains either  $s$ , a single  $t_i$ , or a single pair  $\{r_i, s_i\}$ . Then the following sum rule holds:

$$\det \Delta \det G_{R \cup T}^{S \cup T} = \sum_{\rho \in S_k} \epsilon(\rho) Z[r_1 s_{\rho(1)} | \dots | r_k s_{\rho(k)} | t_1 | \dots | t_\ell | s], \quad (1.6)$$

where the sum is over all permutations of the symmetric group on  $k$  objects and  $\epsilon(\rho)$  is the signature of  $\rho$ . The notation  $G_{R \cup T}^{S \cup T}$  refers to the restriction of the Green matrix  $G = \Delta^{-1}$  to the rows (resp. columns) indexed by the vertices of  $R \cup T$  (resp.  $S \cup T$ ), where  $\Delta$  is the Laplacian of  $\mathcal{G}_s$  with Dirichlet boundary conditions at  $s$ .

To simplify notations, the matrix  $G_{R \cup T}^{S \cup T} = G_{\{r_1, \dots, r_k\} \cup \{t_1, \dots, t_\ell\}}^{\{s_1, \dots, s_k\} \cup \{t_1, \dots, t_\ell\}}$  will from now on be written as  $G_{R, T}^{S, T}$  or  $G_{r_1, \dots, r_k, t_1, \dots, t_\ell}^{s_1, \dots, s_k, t_1, \dots, t_\ell}$ . A useful variant of Theorem 1.2 consists in taking the root  $s$  in  $S$ , i.e. setting  $s_k \equiv s$ . In such a case, the all-minors matrix-tree theorem is as follows.

**Theorem 1.3** ([32]).

$$\det \Delta \det \widehat{G}_{R, T}^{S, T} = \sum_{\rho \in S_k} \epsilon(\rho) Z[r_1 s_{\rho(1)} | \dots | r_k s_{\rho(k)} | t_1 | \dots | t_\ell], \quad (1.7)$$

where  $\widehat{G}_{u, v} = G_{u, v}$  for  $v \neq s$  and  $\widehat{G}_{u, s} = 1$ , for any  $u \in \mathcal{V}$ .

Note that the sum on the right-hand side of Theorem 1.3 is over  $(k+\ell)$ -component spanning forests, instead of  $k+\ell+1$  as in Theorem 1.2.

## 1.2 The line bundle Laplacian

The Dirichlet graph Laplacian  $\Delta$ , acting on complex-valued functions on the graph, can be generalized in the following way. For a fixed vector space  $V$ , a *vector bundle*  $B$  over the graph  $\mathcal{G}_s$  is the assignment to each vertex  $v \in \mathcal{V} \cup \{s\}$  of a vector space  $V_v$  isomorphic to  $V$ . A *section*  $f \in B$  is an element of  $V_{\mathcal{G}_s} = \bigoplus_v V_v$ . We focus here on the one-dimensional case  $V_v \simeq V = \mathbb{C}$  for each  $v \in \mathcal{V} \cup \{s\}$ , which was first envisaged in [53] (the higher-dimensional analogue has been considered in [88]). Since  $\dim V = 1$ , the vector bundle  $B$  is called a *line bundle*.

A *connection*  $\Phi$  is the choice, for each oriented edge  $(v, w) \in \mathcal{E} \cup \mathcal{E}_s$ , of an isomorphism  $\phi_{v,w} : V_v \rightarrow V_w$  called a *parallel transport*, such that  $\phi_{w,v} = \phi_{v,w}^{-1}$ . For  $V = \mathbb{C}$ , the parallel transport is just the multiplication by a nonzero complex number,  $\phi_{v,w} \in \mathbb{C}^*$ . The generalized Laplacian that includes complex parallel transports, called the *line bundle Laplacian* [88], will be written as  $\Delta$  (in bold). For Dirichlet boundary conditions at  $s$ , the Laplacian  $\Delta$  is restricted to sections that vanish at  $s$ . Its action on such sections  $f$  is given for  $v \neq s$  by

$$\begin{aligned} \Delta f(v) &= \sum_{w \sim v} c_{v,w} [f(v) - \phi_{w,v} f(w)] \\ &= \deg_s(v) f(v) - \sum_{w \sim v} c_{v,w} \phi_{w,v} f(w), \end{aligned} \tag{1.8}$$

where the sum is over the vertices  $w$  such that  $\{v, w\} \in \mathcal{E} \cup \mathcal{E}_s$ . As a matrix, the line bundle Laplacian yields, for  $u, v \in \mathcal{V}$ ,

$$\Delta_{u,v} = \begin{cases} \deg_s(u) & \text{if } v = u, \\ -c_{u,v} \phi_{v,u} & \text{if } \{u, v\} \in \mathcal{E}, \\ 0 & \text{otherwise.} \end{cases} \tag{1.9}$$

An example of a line bundle Laplacian on a graph with five vertices is given in Fig. 1.2. Clearly, the usual Dirichlet Laplacian  $\Delta$  is recovered when  $\phi_{v,w} = 1$  for each edge  $(v, w) \in \mathcal{E}$ , that is,

$$\Delta = \lim_{\Phi \rightarrow \mathbb{I}} \Delta. \tag{1.10}$$

The analogue of the matrix-tree theorem for graphs with a connection counts combinatorial objects called *oriented cycle-rooted spanning forests*. An OCRSF consists in the union of a single tree containing the root  $s$  and *cycle-rooted trees* (CRTs, also known as *unicycles*), which are connected subgraphs containing a single cycle. The tree attached to the root  $s$ —which can possibly be degenerate or spanning—is naturally oriented toward  $s$ . In a cycle-rooted tree, all edges in branches point toward the cycle, which can be oriented in either direction (so that there is a unique outgoing arrow at each vertex of the CRT). The theorem is the following.

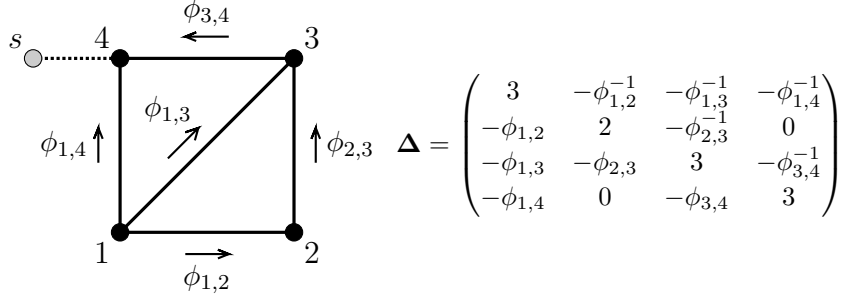


Figure 1.2: On the left: five-vertex graph equipped with the most general complex-valued connection with unit conductances ( $c_{u,v} = 1$  for any  $u, v \in \mathcal{V}$ ), such that the vertex 4 is connected to the root  $s$ . On the right: the corresponding line bundle Laplacian with Dirichlet boundary conditions at  $s$ .

**Theorem 1.4** ([53, 88]).

$$\det \Delta = \sum_{\text{OCRSFs } \mathcal{C}} w(\mathcal{C}), \quad \text{with } w(\mathcal{C}) = \prod_{\{u,v\} \in \mathcal{C}} c_{u,v} \prod_{\text{cycles } \alpha \in \mathcal{C}} (1 - \varpi_\alpha), \quad (1.11)$$

where  $\varpi_\alpha$  is the monodromy of the cycle  $\alpha = (v_0, v_1, \dots, v_k, v_{k+1} \equiv v_0)$  ( $k \geq 1$ ), defined as the product of all parallel transports along  $\alpha$ :

$$\varpi_\alpha = \prod_{i=0}^k \phi_{v_i, v_{i+1}}. \quad (1.12)$$

As the  $\phi$ 's are complex numbers, the starting point of a cycle is arbitrary. One also notes that cycles of length 2 have vanishing weight, due to the inverse property of parallel transports, i.e.  $\phi_{v_0, v_1} = \phi_{v_1, v_0}^{-1}$ .

### 1.3 Cycle-rooted groves

Let us select a subset  $\mathcal{N} \ni s$  of distinguished vertices of  $\mathcal{G}_s$  and call them *nodes*, which we number from 1 to  $n = |\mathcal{N}|$ . As a convention, we assume that node  $n$  is the root  $s$  of the graph. The vertices of  $\mathcal{V} \setminus \mathcal{N}$  are called *interior vertices*. A *cycle-rooted grove* (CRG), in the sense of [91], is an unoriented subgraph of  $\mathcal{G}_s$  containing all vertices such that

each component is either a cycle-rooted tree without any node or a tree containing at least one node<sup>1</sup>. The weight of a CRG on a graph is the same as that of an OCRSF, namely, it is given by the product of the conductances of its edges, with an extra factor  $(1 - \varpi_\alpha) + (1 - \varpi_\alpha^{-1}) = 2 - \varpi_\alpha - \varpi_\alpha^{-1}$  for each unoriented cycle  $\alpha$ .

CRGs on a graph can be classified according to the way nodes are distributed in the trees. A specific way to distribute the nodes will be called a partition; the nodes belonging to distinct components will be separated by bars. For instance, if  $\mathcal{N} = \{1, 2, 3, 4, 5=s\}$ ,  $\sigma = 134|25$  specifies CRGs with two tree components, containing respectively nodes  $\{1, 3, 4\}$  and  $\{2, 5\}$  (see the example in Fig. 1.3). Let us note that, depending on the positions of the nodes, certain partitions cannot be realized by CRGs, for topological reasons. For a partition  $\sigma$  of the nodes, the partition function  $\mathbf{Z}[\sigma]$  is defined as the weighted sum over all CRGs whose nodes are distributed in trees according to  $\sigma$ ,

$$\mathbf{Z}[\sigma] = \sum_{\sigma\text{-CRGs}} \prod_{\text{edges } \{u,v\} \in \text{CRG}} c_{u,v} \prod_{\text{cycles } \alpha \in \text{CRG}} (2 - \varpi_\alpha - \varpi_\alpha^{-1}). \quad (1.13)$$

In particular, for a trivial connection,  $\mathbf{Z}[12\dots n] = Z[12\dots n]$  is simply the weighted sum of spanning trees on  $\mathcal{G}_s$  (since all cycle contributions vanish).

### 1.3.1 Oriented cycle-rooted groves

A particular type of partitions of the nodes consists in partial pairings, connecting  $2k$  nodes in pairs and leaving  $\ell$  nodes on their own tree, i.e.  $\sigma = r_1 s_1 | \dots | r_k s_k | t_1 | \dots | t_\ell$ . For such partitions, we define an *oriented cycle-rooted grove* (OCRG) as a spanning subgraph of  $\mathcal{G}_s$  whose components are either:

- a rooted tree containing exactly two nodes  $r_i, s_i$ , in which all edges point toward node  $s_i$ ;

<sup>1</sup>Similar geometrical objects, comprising trees and cycle-rooted trees, were considered in the context of the monomer-dimer model [17, 133], where they arose from the Temperley correspondence, and were called spanning webs. In particular, for the dimer model on a cylinder, the distribution of the number of loops was obtained by using a technique closely related to a connection [19].

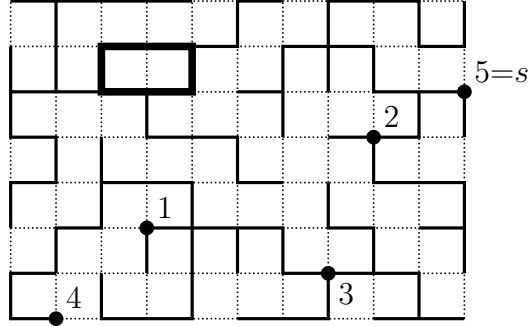


Figure 1.3: Cycle-rooted grove of type  $\sigma = 134|25$  on a graph with five nodes (the fifth one being the root  $s$ ). The component with no nodes is a cycle-rooted tree, whose unique cycle is highlighted with a heavy line.

- a rooted tree containing a single node  $t_i$ , in which all edges point toward  $t_i$ ;
- a cycle-rooted tree not containing any node, in which all branch edges point toward the unique cycle, which can be oriented in either direction.

An illustration of an OCRG on a graph with four nodes is provided in Fig. 1.4. We shall speak of *oriented partial pairings* when referring to OCRGs with a fixed distribution of the nodes in oriented tree components, and shall denote them using a vector notation:

$$\vec{\sigma} = \begin{matrix} s_1 \\ r_1 \end{matrix} | \cdots | \begin{matrix} s_k \\ r_k \end{matrix} | t_1 | \cdots | t_\ell. \quad (1.14)$$

Let then  $\Gamma_{\vec{\sigma}}$  be an OCRG with  $2k + \ell$  nodes distributed in trees according to the oriented partition  $\vec{\sigma}$  written above, that is, in which each rooted tree containing a pair  $r_i, s_i$  is oriented toward  $s_i$ . The weight of  $\Gamma_{\vec{\sigma}}$  is given by the same formula as for an OCRSF (1.11), with an extra factor accounting for (the inverse of) the product of parallel transports  $\phi_{r_i \rightarrow s_i}$  along the unique path from node  $r_i$  to node  $s_i$  in each rooted tree ( $1 \leq i \leq k$ ):

$$w(\Gamma_{\vec{\sigma}}) = \prod_{\{u,v\} \in \Gamma_{\vec{\sigma}}} c_{u,v} \prod_{\text{cycles } \alpha \in \Gamma_{\vec{\sigma}}} (1 - \varpi_\alpha) \times \prod_{i=1}^k \phi_{r_i \rightarrow s_i}^{-1}. \quad (1.15)$$

We shall use the notation  $\mathbf{Z}[\vec{\sigma}]$  for the partition function for all OCRGs whose nodes are distributed in rooted trees according to the oriented pairing  $\vec{\sigma}$ .

For an oriented partial pairing  $\vec{\sigma}$  of the form (1.14) and its unoriented version  $\sigma$ , the distinction between the corresponding partition functions,  $\mathbf{Z}[\vec{\sigma}]$  and  $\mathbf{Z}[\sigma]$ , lies in the incorporation of the product of (the inverse of) parallel transports along the paths from  $r_i$  to  $s_i$  in each of the  $k$  trees. Consequently, these two functions coincide in the limit of a trivial connection,

$$\lim_{\Phi \rightarrow \mathbb{1}} \mathbf{Z}[\vec{\sigma}] = \lim_{\Phi \rightarrow \mathbb{1}} \mathbf{Z}[\sigma] = Z[\sigma], \quad (1.16)$$

where  $Z[\sigma]$  is the weighted sum of spanning forests of the type  $\sigma$ , introduced in Theorem 1.2.

The partition functions  $\mathbf{Z}[\vec{\sigma}]$  satisfy the *grove theorem*, which generalizes Theorems 1.2 and 1.3.

**Theorem 1.5** ([91]). *Let  $\mathcal{N} = R \cup S \cup T$  be the set of nodes on a graph  $\mathcal{G}_s$ , split as a disjoint union  $R \cup S \cup T$ , where  $R = \{r_1, \dots, r_k\}$ ,  $S = \{s_1, \dots, s_k\}$ ,  $T = \{t_1, \dots, t_\ell\}$ . Let  $\Delta$  be the line bundle Laplacian of  $\mathcal{G}_s$  with Dirichlet boundary conditions at  $s$ , and  $\mathbf{G}$  its inverse, called the line bundle Green function. Moreover, let  $\mathbf{Z} = \det \Delta$ .*

*If the root  $s$  belongs to  $T$ , one may assume that  $s = t_\ell$  without loss of generality. If  $\tilde{T}$  is defined as  $T \setminus \{s\}$ , the following sum rule holds,*

$$\mathbf{Z} \det \mathbf{G}_{R, \tilde{T}}^{S, \tilde{T}} = \sum_{\rho \in \mathcal{S}_k} \epsilon(\rho) \mathbf{Z} \left[ \begin{smallmatrix} s_{\rho(1)} \\ r_1 \end{smallmatrix} \mid \cdots \mid \begin{smallmatrix} s_{\rho(k)} \\ r_k \end{smallmatrix} \mid t_1 \mid \cdots \mid t_{\ell-1} \mid s \right]. \quad (1.17)$$

*If rather  $s \in R \cup S$ , one may assume that  $s = s_k$  (up to relabeling the nodes and exchanging the roles of  $R$  and  $S$ ). Let  $\Delta_0$  be the line bundle Laplacian of  $\mathcal{G}_s$  without Dirichlet boundary conditions, and let  $\hat{\Delta}$  be the matrix defined by*

$$\hat{\Delta}_{u,v} = (\Delta_0)_{u,v}, \quad \hat{\Delta}_{u,s} = (\Delta_0)_{u,s}, \quad \hat{\Delta}_{s,v} = 0, \quad \hat{\Delta}_{s,s} = 1, \quad (1.18)$$

*for  $u, v \in \mathcal{V}$ , and let  $\hat{\mathbf{G}} = \hat{\Delta}^{-1}$ . Then  $\det \hat{\Delta} = \det \Delta$ ,  $\hat{\mathbf{G}}_{u,v} = \mathbf{G}_{u,v}$  for any  $u, v \in \mathcal{V}$  and*

$$\mathbf{Z} \det \hat{\mathbf{G}}_{R,T}^{S,T} = \sum_{\rho \in \mathcal{S}_k} \epsilon(\rho) \mathbf{Z} \left[ \begin{smallmatrix} s_{\rho(1)} \\ r_1 \end{smallmatrix} \mid \cdots \mid \begin{smallmatrix} s_{\rho(k)} \\ r_k \end{smallmatrix} \mid t_1 \mid \cdots \mid t_\ell \right]. \quad (1.19)$$

The grove theorem, due to Kenyon and Wilson [91], lies at the core of this thesis. Indeed, OCRG partition functions  $\mathbf{Z}[\vec{\sigma}]$  will be the main quantities of interest in sandpile computations in Chapter 2. More precisely, we shall be interested in evaluating the partition functions  $Z[\sigma]$ , using the property

$$Z[\sigma] = \lim_{\Phi \rightarrow \mathbb{I}} \mathbf{Z}[\vec{\sigma}]. \quad (1.20)$$

A natural question is the following: Why bother to introduce a connection on the graph and then take its trivial limit? First, we shall see that Theorem 1.2 and Theorem 1.3 do not suffice to compute the partition functions  $Z[\sigma]$ . Indeed, the system of linear relations one can obtain for all possible choices of disjoint subsets  $R, S, T$  (such that  $\mathcal{N} = R \cup S \cup T$ ) is not invertible for generic positions of the nodes.

On certain types of graphs, namely so-called *annular-one graphs* [91], using Theorem 1.5 with a nontrivial connection produces an invertible system of equations. It follows that the partition functions  $\mathbf{Z}[\vec{\sigma}]$  can be written as linear combinations of minors of the modified line bundle Green function  $\widehat{\mathbf{G}}$ . Taking the limit  $\Phi \rightarrow \mathbb{I}$  yields formulas for the  $Z[\sigma]$ 's, in which a dependence on the connection remains manifest, as we shall see below. Introducing a connection  $\Phi$  to compute the  $Z[\sigma]$ 's and then taking its limit  $\Phi \rightarrow \mathbb{I}$  (in an appropriate manner) is therefore not a trivial operation.

## 1.4 Annular-one graphs

Let us now consider a planar graph  $\mathcal{G}_s$  embedded on the plane, such that the root  $s$  is connected to a subset  $\mathcal{D}$  of boundary vertices (i.e. those located along the outer face of the graph). Let  $\mathcal{N} = \{1, \dots, n\}$  be a set of nodes, such that nodes 1 to  $n-1$  lie in counterclockwise order on the boundary of a single marked face  $f$  of the graph, and such that the root  $s$  is the  $n$ th node. Such a graph is called an *annular-one graph* [91].

We equip the graph with a connection  $\Phi$ , chosen to be trivial everywhere except on the edges crossed by a *zipper*, i.e. a path on the dual graph from  $f$  to the outer face. On such edges  $\{k, \ell\}$ —called *zipper edges*—we put a parallel transport  $\phi_{k,\ell} = z \in \mathbb{C}^*$  in the direction of the oriented

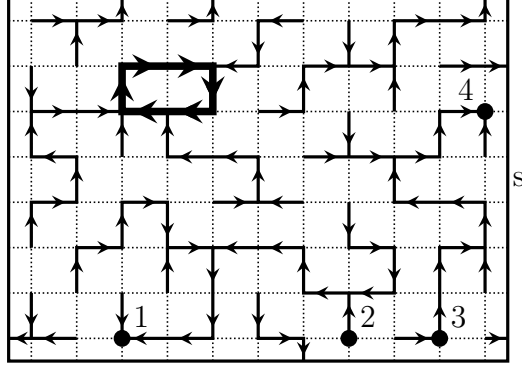


Figure 1.4: Oriented cycle-rooted grove on a rectangular grid with wired boundary, where the root  $s$  is drawn as a box surrounding the grid. The graph contains five nodes paired according to  $\vec{\sigma} = \frac{1}{2} \frac{4}{3} | s$ . The grove has four connected components: three trees  $\mathcal{T}_s$ ,  $\mathcal{T}_{2 \rightarrow 1}$ ,  $\mathcal{T}_{3 \rightarrow 4}$  and a cycle-rooted tree without nodes, whose cycle is highlighted with a heavy line. All the edges in  $\mathcal{T}_{2 \rightarrow 1}$  (resp.  $\mathcal{T}_{3 \rightarrow 4}$ ) are oriented toward node 1 (resp. node 4).

edge  $(k, \ell)$ . The opposite edges,  $(\ell, k)$ , must then have a parallel transport  $\phi_{\ell, k} = \phi_{k, \ell}^{-1} = z^{-1}$ . Up to relabeling, we may assume that the zipper edge belonging to the boundary of  $f$  lies between nodes 1 and  $n-1$ .

As an example, let us consider an annular-one graph with four nodes, i.e.  $\mathcal{N} = \{1, 2, 3, 4\}$  as in Fig. 1.5, and compute the number of spanning forests of type  $12|34$  (that is, forests that contain two trees: one with nodes 1 and 2, and the other with nodes 3 and 4). With  $T = \emptyset$ , and for three different choices of subsets  $R, S$ , Theorem 1.5 yields

$$\begin{aligned} \mathbf{Z} \det \widehat{\mathbf{G}}_{1,2}^{3,4} &= \mathbf{Z} \left[ \begin{array}{c|c} 3 & 4 \\ \hline 1 & 2 \end{array} \right] - \mathbf{Z} \left[ \begin{array}{c|c} 4 & 3 \\ \hline 1 & 2 \end{array} \right], \\ \mathbf{Z} \det \widehat{\mathbf{G}}_{1,3}^{2,4} &= \mathbf{Z} \left[ \begin{array}{c|c} 2 & 4 \\ \hline 1 & 3 \end{array} \right] - \mathbf{Z} \left[ \begin{array}{c|c} 4 & 2 \\ \hline 1 & 3 \end{array} \right], \\ \mathbf{Z} \det \widehat{\mathbf{G}}_{2,3}^{1,4} &= \mathbf{Z} \left[ \begin{array}{c|c} 1 & 4 \\ \hline 2 & 3 \end{array} \right] - \mathbf{Z} \left[ \begin{array}{c|c} 4 & 1 \\ \hline 2 & 3 \end{array} \right]. \end{aligned} \quad (1.21)$$

The path joining a node  $r_1 \in \{1, 2, 3\}$  and node 4 in  $\mathbf{Z} \left[ \begin{array}{c|c} s_2 & 4 \\ \hline r_2 & r_1 \end{array} \right]$  can cross the zipper any number of times in both directions, so  $\phi_{4 \rightarrow r_1}$  varies from grove to grove. We note that these groves do not contain cycle-rooted trees, since any cycle would have a trivial monodromy. Moreover, the path between the two remaining nodes  $r_2, s_2$  in  $\mathcal{N} \setminus \{r_1, 4\}$  is such that  $\phi_{s_2 \rightarrow r_2}$  is constant over all groves in  $\mathbf{Z} \left[ \begin{array}{c|c} s_2 & 4 \\ \hline r_2 & r_1 \end{array} \right]$ , because  $\mathcal{G}_s$  is planar. For

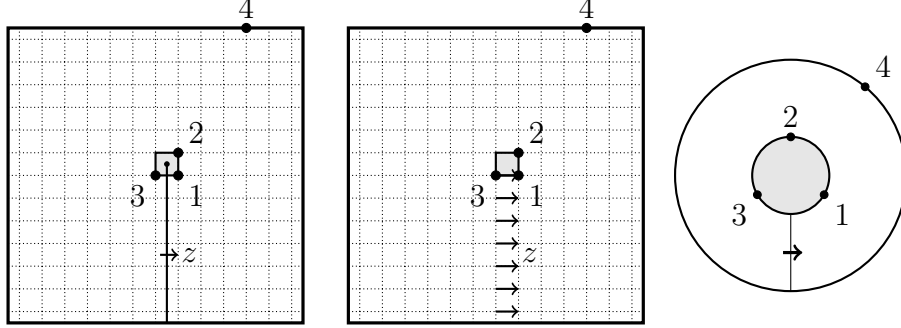


Figure 1.5: Finite square grid with four nodes and wired boundary, with Dirichlet boundary conditions at node 4. On the left: zipper on the dual graph going from the face adjacent to nodes 1, 2, 3 to the outer face. In the middle: the edges crossed by the zipper are equipped with a parallel transport  $z \in \mathbb{C}^*$  in the direction of the arrows, from left to right (and  $z^{-1}$  from right to left). On the right: schematic representation of the nodes and the zipper on an annulus.

instance,  $\phi_{3 \rightarrow 1} = z$  in  $\mathbf{Z}^{\left[ \begin{smallmatrix} 3 & 4 \\ 1 & 2 \end{smallmatrix} \right]}$  and  $\phi_{1 \rightarrow 3} = z^{-1}$  in  $\mathbf{Z}^{\left[ \begin{smallmatrix} 1 & 4 \\ 3 & 2 \end{smallmatrix} \right]}$ , so

$$\mathbf{Z}^{\left[ \begin{smallmatrix} 3 & 4 \\ 1 & 2 \end{smallmatrix} \right]} = z^2 \mathbf{Z}^{\left[ \begin{smallmatrix} 1 & 4 \\ 3 & 2 \end{smallmatrix} \right]}. \quad (1.22)$$

Likewise, we see that  $\phi_{3 \rightarrow 2} = 1$  in  $\mathbf{Z}^{\left[ \begin{smallmatrix} 3 & 4 \\ 2 & 1 \end{smallmatrix} \right]}$  and  $\phi_{2 \rightarrow 1} = 1$  in  $\mathbf{Z}^{\left[ \begin{smallmatrix} 2 & 4 \\ 1 & 3 \end{smallmatrix} \right]}$ , resulting in two further identities:

$$\mathbf{Z}^{\left[ \begin{smallmatrix} 3 & 4 \\ 2 & 1 \end{smallmatrix} \right]} = \mathbf{Z}^{\left[ \begin{smallmatrix} 2 & 4 \\ 3 & 1 \end{smallmatrix} \right]}, \quad \mathbf{Z}^{\left[ \begin{smallmatrix} 1 & 4 \\ 2 & 3 \end{smallmatrix} \right]} = \mathbf{Z}^{\left[ \begin{smallmatrix} 2 & 4 \\ 1 & 3 \end{smallmatrix} \right]}. \quad (1.23)$$

This reduces the number of independent quantities to 3 and allows one, for  $z \neq \pm 1$ , to invert the linear system (1.21). One obtains in particular

$$\begin{aligned} \frac{\mathbf{Z}^{\left[ \begin{smallmatrix} 2 & 4 \\ 1 & 3 \end{smallmatrix} \right]}}{\mathbf{Z}} &= \frac{\det \widehat{\mathbf{G}}_{1,3}^{2,4} + z^2 \det \widehat{\mathbf{G}}_{3,2}^{1,4} + \det \widehat{\mathbf{G}}_{2,1}^{3,4}}{1 - z^2} \\ &= \frac{\widehat{\mathbf{G}}_{1,2} \widehat{\mathbf{G}}_{3,4} - z^2 \widehat{\mathbf{G}}_{2,1} \widehat{\mathbf{G}}_{3,4} - \widehat{\mathbf{G}}_{1,3} \widehat{\mathbf{G}}_{2,4}}{1 - z^2} \\ &\quad + \frac{z^2 \widehat{\mathbf{G}}_{3,1} \widehat{\mathbf{G}}_{2,4} + \widehat{\mathbf{G}}_{2,3} \widehat{\mathbf{G}}_{1,4} - \widehat{\mathbf{G}}_{3,2} \widehat{\mathbf{G}}_{1,4}}{1 - z^2}. \end{aligned} \quad (1.24)$$

Remember that the hat over the quantities  $\widehat{\mathbf{G}}$  serves as a reminder that it is defined with respect to a perturbed line bundle Laplacian  $\widehat{\Delta}$  (see Theorem 1.5). A natural question is the following: Is it possible to write

a formula for  $\mathbf{Z}[\frac{2}{1}|\frac{4}{3}]$  in terms of the Dirichlet line bundle Laplacian  $\Delta$  instead? Indeed, the latter matrix and its inverse  $\mathbf{G}$  should be easier to manipulate in concrete applications, at least in the limit  $z \rightarrow 1$ , in which they converge respectively to the well-known matrices  $\Delta$  and  $G$ . By definition,  $\widehat{\mathbf{G}}_{i,j} = \mathbf{G}_{i,j}$ ,  $\widehat{\mathbf{G}}_{n,j} = 0$  and  $\widehat{\mathbf{G}}_{n,n} = 1$  for  $1 \leq i, j \leq n-1$ , but what about  $\widehat{\mathbf{G}}_{i,n}$ ? The answer to that question was provided in [91], in which the authors proved the following result.

**Theorem 1.6** ([91]). *Let  $\vec{\sigma}$  be an oriented partial pairing of  $n$  nodes on an annular-one graph  $\mathcal{G}_s$ , such that node  $n$  is the root  $s$ . Then the partition function  $\mathbf{Z}[\vec{\sigma}]$  can be written as  $\mathbf{Z}$  times a polynomial in the variables  $\widehat{\mathbf{G}}_{i,j}$ , for  $1 \leq i \leq n-1$  and  $1 \leq j \leq n$ . Moreover, in the limit  $z \rightarrow 1$ ,  $\mathbf{Z}[\vec{\sigma}]$  can be computed in terms of the variables  $\mathbf{G}_{i,j}$ , according to the following substitution rule:*

$$\widehat{\mathbf{G}}_{i,n} \rightarrow 1 \quad \text{for } 1 \leq i \leq n. \quad (1.25)$$

In the example presented above, Theorem 1.6 yields the following expression:

$$\lim_{z \rightarrow 1} \frac{\mathbf{Z}[\frac{2}{1}|\frac{4}{3}]}{\mathbf{Z}} = \lim_{z \rightarrow 1} \frac{\mathbf{G}_{1,2} - z^2 \mathbf{G}_{2,1} - \mathbf{G}_{1,3} + z^2 \mathbf{G}_{3,1} + \mathbf{G}_{2,3} - \mathbf{G}_{3,2}}{1 - z^2}. \quad (1.26)$$

In that limit, both the numerator and denominator of Eq. (1.26) vanish since  $\lim_{z \rightarrow 1} \mathbf{G}_{u,v} = G_{u,v} = G_{v,u}$  is symmetric in  $u, v$ . The ratio however converges to

$$\begin{aligned} \frac{Z[12|34]}{Z} &= \lim_{z \rightarrow 1} \frac{\mathbf{Z}[\frac{2}{1}|\frac{4}{3}]}{\mathbf{Z}} \\ &= \lim_{z \rightarrow 1} \frac{\mathbf{G}'_{1,2} - 2z \mathbf{G}'_{2,1} - z^2 \mathbf{G}'_{2,1} - \mathbf{G}'_{1,3} + 2z \mathbf{G}'_{3,1} + z^2 \mathbf{G}'_{3,1} + \mathbf{G}'_{2,3} - \mathbf{G}'_{3,2}}{-2z} \\ &= G_{2,1} - G_{3,1} - \frac{1}{2} \left\{ [G'_{1,2} - G'_{2,1}] - [G'_{1,3} - G'_{3,1}] + [G'_{2,3} - G'_{3,2}] \right\} \\ &= G_{1,2} - G_{1,3} - G'_{1,2} + G'_{1,3} - G'_{2,3}, \end{aligned} \quad (1.27)$$

where  $\mathbf{G}'_{u,v} \equiv \partial_z \mathbf{G}_{u,v}$  and  $G'_{u,v} = -G'_{v,u} = \lim_{z \rightarrow 1} \partial_z \mathbf{G}_{u,v}$ , the latter of which is called the *derivative of the Green function*. Since the connection

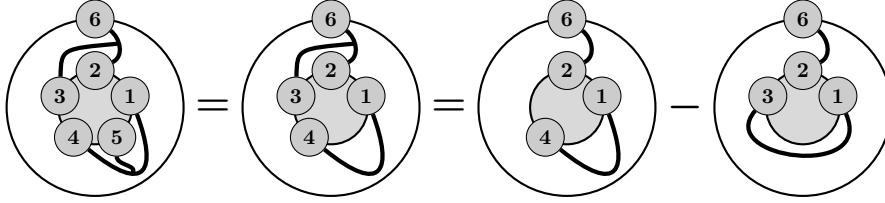


Figure 1.6: Reduction of a generic partition to partial pairings for a trivial connection on an annular-one graph with six nodes.

depends on a single parameter  $z$  (and its inverse  $z^{-1}$ ), it is straightforward to obtain a formula for  $G'_{u,v}$  in terms of the Green function  $G$  [91]:

$$G'_{u,v} = \sum_{(k,\ell): \phi_{k,\ell}=z} c_{u,v}(G_{u,\ell} G_{k,v} - G_{u,k} G_{\ell,v}), \quad (1.28)$$

where the sum is over all oriented edges equipped with a parallel transport  $z$ . To compute  $Z[12|34]$ , we see that the full dependence of the Green function  $\mathbf{G}$  in the variable  $z$  is not required, but only its zeroth and first order in  $z-1$  (this remains true for a generic partition  $\sigma$  in which node  $n$  is paired [91]). Technicalities about the way they can actually be computed are collected in Appendix A.

In sandpile computations in Chapter 2, we shall need to compute partition functions  $Z[\tau]$  for which  $\tau$  is not a partial pairing (i.e. corresponding to spanning forests in which at least one tree contains three or more nodes). Although the grove theorem is not directly applicable in this case, it is possible to write  $Z[\tau]$  as a linear combination of  $Z[\sigma]$ 's, where the  $\sigma$ 's are partial pairings, assuming node  $n$  (the root  $s$ ) is not in a singleton. We illustrate the method on the partition  $145|236$ , shown in Fig. 1.6.

For a trivial connection,  $Z[145|236]$  is the number of two-component spanning forests in which  $1, 4, 5$  lie on one tree and  $2, 3, 6$  on the other tree. Let us first observe that in spanning forests of type  $14|236$ , node  $5$  necessarily belongs to the tree containing the nodes  $1$  and  $4$ . Therefore,  $Z[145|236] = Z[14|236]$ , and node  $5$  can be considered as an interior vertex (which may, in principle, belong to any tree in the forest).

Let us consider next the partition  $14|26$ . Node  $3$  can either lie on a tree with  $2$  and  $6$ , or with  $1$  and  $4$ , so  $Z[14|26] = Z[134|26] + Z[14|236]$ . By

the same argument used above,  $Z[134|26] = Z[13|26]$ , and we find

$$\begin{aligned} Z[145|236] &= Z[14|236] = Z[14|26] - Z[134|26] \\ &= Z[14|26] - Z[13|26], \end{aligned} \quad (1.29)$$

where  $14|26$  and  $13|26$  are partial pairings. Their respective partition functions can therefore be computed via Theorem 1.5.

## 1.5 Graphs with free boundary conditions

Up to this point, we have considered a graph  $\mathcal{G}$  with a root  $s$ , for which the Dirichlet Laplacian  $\Delta$  is invertible. For such a graph, a subset  $\mathcal{D}$  of the vertices  $\mathcal{V}$  are wired to  $s$ , while the vertices of  $\mathcal{V} \setminus \mathcal{D}$  are free. A particular case occurs when  $\mathcal{D} = \emptyset$ , namely, if all vertices are free. As the root  $s$  is isolated from all the vertices of  $\mathcal{G}$ , it may be eliminated altogether. Although this situation may seem the most natural from the graph-theoretical point of view, the singularity of the standard Laplacian  $\Delta_0$  raises technical difficulties, as we shall see below (the subscript 0 serves as a reminder that  $\Delta_0$  has a zero eigenvalue).

Let us denote by  $V_0 = \langle |f_0 \rangle \rangle \subset V = \mathbb{C}^N$  the one-dimensional eigenspace associated with the eigenvalue  $\lambda_0 = 0$ , where  $N = |\mathcal{V}|$  (recall that the multiplicity of  $\lambda_0$  is the number of connected components of  $\mathcal{G}$ ). Let  $\Delta'$  stand for the restriction of  $\Delta_0$  to  $V \setminus V_0$ , and  $G$  stand for the inverse of  $\Delta'$ . We shall call  $G$  the *regularized Green function* of the graph  $\mathcal{G}^2$ . We further denote by  $\mathcal{P}_0 = |f_0 \rangle \langle f_0|$  the projector onto  $V_0$  and by  $G_0$  the matrix defined by

$$\Delta_0 G_0 = \mathbb{I} - \mathcal{P}_0 = G_0 \Delta_0. \quad (1.30)$$

In the canonical basis of  $V$ ,  $(\mathcal{P}_0)_{u,v} = 1/N$  for any  $u, v \in \mathcal{V}$ . Explicitly, if we write  $V = V_0 \oplus V_0^\perp$ , then  $\Delta_0$  and  $G_0$  read, in the canonical basis for the direct sum:

$$\Delta_0 = \begin{pmatrix} 0 & 0 \\ 0 & \Delta' \end{pmatrix}, \quad G_0 = \begin{pmatrix} \alpha & 0 \\ 0 & (\Delta')^{-1} \end{pmatrix}. \quad (1.31)$$

---

<sup>2</sup>We use the same symbol,  $G$ , to refer to both the Dirichlet Green function on graphs with a root  $s$  and the regularized Green function on graphs without roots. No confusion should occur, as it is clear from the beginning whether the graph has a root or not.

The parameter  $\alpha$  is free, since  $G_0$  is only defined up to a term proportional to  $\mathcal{P}_0$ . For simplicity, we choose the value  $\alpha = 0$ . Using Eq. (1.31), it is then straightforward to see that the following relations hold:

$$\det(\Delta_0 + q\mathcal{P}_0) = q \det \Delta', \quad (\Delta_0 + q\mathcal{P}_0)^{-1} = G + q^{-1}\mathcal{P}_0, \quad (1.32)$$

for any nonzero parameter  $q$ . In terms of the eigenvalues  $\lambda$  and the orthonormal eigenfunctions  $|f_\lambda\rangle$  of  $\Delta_0$ , the regularized Green function takes the more explicit and familiar form

$$G = \sum_{\lambda \neq 0} \frac{1}{\lambda} |f_\lambda\rangle \langle f_\lambda|. \quad (1.33)$$

We now show how to adapt Theorems 1.2 and 1.5 to graphs with free boundary conditions, in terms of the regularized Green function  $G$ . Note that for a generic connection  $\Phi$ , the line bundle Laplacian  $\Delta_0$  is nonsingular, so its inverse  $\mathbf{G}_0$  is well defined. It is therefore possible to write a version of Theorem 1.5 in terms of these two matrices. However, it may often be difficult to control the singular behavior of  $\mathbf{G}_0$  in the limit  $\Phi \rightarrow \mathbb{I}$ . In such a case, we can consider a small perturbation of the line bundle Laplacian,  $\Delta_0 + q\mathcal{P}_0$ , and denote by  $\mathbf{G}_q$  its inverse. The analogue of Theorems 1.2 and 1.5 is given by

**Proposition 1.7.** *Let  $R = \{r_1, \dots, r_k\}$ ,  $S = \{s_1, \dots, s_k\}$  and  $T = \{t_1, \dots, t_\ell\}$  be disjoint subsets of vertices of  $\mathcal{G}$ , with  $k \geq 2$ . We denote by  $(\mathbf{G}_q)_{R,T}^{S,T}$  the submatrix of  $\mathbf{G}_q$  whose rows and columns are indexed by  $R \cup T$  and  $S \cup T$ , respectively. Then*

$$\lim_{q \rightarrow 0} \det(\Delta_0 + q\mathcal{P}_0) \det(\mathbf{G}_q)_{R,T}^{S,T} = \sum_{\rho \in \mathbb{S}_k} \epsilon(\rho) \mathbf{Z} \left[ \begin{matrix} s_{\rho(1)} \\ r_1 \end{matrix} \mid \dots \mid \begin{matrix} s_{\rho(k)} \\ r_k \end{matrix} \mid t_1 \mid \dots \mid t_\ell \right]. \quad (1.34)$$

In the limit  $\Phi \rightarrow \mathbb{I}$ , the preceding equation reads

$$\begin{aligned} & \frac{1}{N} \det \Delta' \times \det \begin{pmatrix} 1 & G_{r_1, s_2} - G_{r_1, s_1} & \cdots & G_{r_1, t_\ell} - G_{r_1, s_1} \\ \vdots & \vdots & & \vdots \\ 1 & G_{t_\ell, s_2} - G_{t_\ell, s_1} & \cdots & G_{t_\ell, t_\ell} - G_{t_\ell, s_1} \end{pmatrix} \\ &= \sum_{\rho \in \mathbb{S}_k} \epsilon(\rho) Z[r_1 s_{\rho(1)} \mid \dots \mid r_k s_{\rho(k)} \mid t_1 \mid \dots \mid t_\ell], \end{aligned} \quad (1.35)$$

where  $\det \Delta' / N$  is equal to the weighted sum of spanning trees on  $\mathcal{G}$  by Kirchhoff's theorem.

*Proof.* Using Cramer's formula for minors, we find that

$$\begin{aligned} \lim_{q \rightarrow 0} \det(\mathbf{\Delta}_0 + q\mathcal{P}_0) \det(\mathbf{G}_q)_{R,T}^{S,T} &= \lim_{q \rightarrow 0} (-1)^{\Sigma R + \Sigma S} \det(\mathbf{\Delta}_0 + q\mathcal{P}_0)_{\mathcal{V} \setminus R \cup T}^{\mathcal{V} \setminus R \cup T} \\ &= (-1)^{\Sigma R + \Sigma S} \det(\mathbf{\Delta}_0)_{\mathcal{V} \setminus S \cup T}^{\mathcal{V} \setminus R \cup T}, \end{aligned} \quad (1.36)$$

where  $\Sigma R$  (resp.  $\Sigma S$ ) denotes the sum of the indices of the columns of  $\mathbf{\Delta}_0 + q\mathcal{P}_0$  indexed by elements of  $R$  (resp.  $S$ ). The latter (signed) determinant corresponds precisely to the right-hand side of Eq. (1.34) (see Theorem 4.4 in [91]). In the limit  $\Phi \rightarrow \mathbb{I}$ , the left-hand side of Eq. (1.34) yields

$$\lim_{q \rightarrow 0} \det \Delta' \times q \det(G + q^{-1}\mathcal{P}_0)_{R,T}^{S,T},$$

which can be evaluated by subtracting the first column of  $(G + q^{-1}\mathcal{P}_0)_{R,T}^{S,T}$  from its other columns to isolate the  $q^{-1}$  dependence in the first column only (recall that  $(\mathcal{P}_0)_{u,v} = 1/N$  for any  $u, v \in \mathcal{V}$ ).  $\square$

For concrete applications, we shall use Proposition 1.7 for a connection  $\Phi$  with parallel transports 1,  $z$  or  $z^{-1}$ . In particular, we shall need to compute the first-order expansion of the line bundle Green function  $\mathbf{G}_q$  around  $z = 1$ , which reads

$$\begin{aligned} (\mathbf{G}_q)_{u,v} &= (G_{u,v} + q^{-1}N^{-1}) \\ &+ (z-1) \sum_{(k,\ell): \phi_{k,\ell}=z} c_{k,\ell} (G_{u,\ell} G_{k,v} - G_{u,k} G_{\ell,v}) \\ &+ (z-1)q^{-1}N^{-1} \sum_{(k,\ell): \phi_{k,\ell}=z} c_{k,\ell} (G_{u,\ell} + G_{k,v} - G_{u,k} - G_{\ell,v}) + \dots \end{aligned} \quad (1.37)$$

We write the first-order derivative of  $\mathbf{G}_q$  as follows:  $\partial_z \mathbf{G}_q|_{z=1} = G' + q^{-1}N^{-1}\tilde{G}'$ , with

$$\begin{aligned} G'_{u,v} &= \sum_{(k,\ell): \phi_{k,\ell}=z} c_{k,\ell} (G'_{u,\ell} G_{k,v} - G_{u,k} G'_{\ell,v}), \\ \tilde{G}'_{u,v} &= \sum_{(k,\ell): \phi_{k,\ell}=z} c_{k,\ell} (G'_{u,\ell} + G_{k,v} - G_{u,k} - G'_{\ell,v}). \end{aligned} \quad (1.38)$$



## Chapter 2

# The Abelian sandpile model

The purpose of this chapter is twofold. First, we show how the ideas and concepts developed in [88, 91] and presented in Chapter 1 may be used to compute sandpile probabilities, in a much more efficient way than via earlier routes used in [81, 131, 137]. In Section 2.1, we recall the definition of the Abelian sandpile model on a generic graph, together with the bijection between recurrent sandpile configurations with prescribed heights (with at most one different from 1) and certain classes of spanning trees. We take the opportunity to generalize the bijection when several prescribed heights are strictly larger than 1, and give an explicit formula for two-point joint probabilities in terms of fractions of spanning trees. In Sections 2.2, 2.3 and 2.4, we rederive known one-site and two-site results on the square lattice and half-lattice, before computing new joint probabilities on both graphs. We then apply the techniques of Chapter 1 to the calculation of height probabilities on triangular and hexagonal lattices in Sections 2.5 and 2.6.

Second, we compare our new lattice results (in the scaling limit) to CFT correlators, based on the field identifications of [81, 129]. This is done in Section 2.7, in which we find a full agreement with the correlators evaluated on the square lattice. Moreover, we show that the computations on triangular and hexagonal graphs are consistent with the CFT conjectures established from square lattice results.

## 2.1 Review of the Abelian sandpile model

Let us consider a two-dimensional unoriented connected graph  $\mathcal{G} = (\mathcal{V}, \mathcal{E})$  with a discrete random variable  $h_i \in \mathbb{N}^*$  associated with each site  $i \in \mathcal{G}$ . A *sandpile configuration* is a set  $\mathcal{C} = \{h_i\}_{i \in \mathcal{G}}$ , where the *height*  $h_i \geq 1$  counts the number of grains of sand at site  $i$ .

The definition of the model on  $\mathcal{G}$  requires to extend it to  $\mathcal{G}_s = \mathcal{G} \cup \{s\}$  with an additional site  $s$  called the *sink* (or *root*), and edges linking a nonempty subset  $\mathcal{D} \subset \mathcal{V}$  to  $s$  (multiple edges between a site and the sink are allowed, whereas all edges are simple in  $\mathcal{G}$ ). Sites of  $\mathcal{D}$  are called *dissipative* or *open*, while those of  $\mathcal{V} \setminus \mathcal{D}$  are *closed*. We denote by  $z_i$  (resp.  $z_i^*$ ) the degree of  $i$  in  $\mathcal{G}$  (resp.  $\mathcal{G}_s$ ), so that  $z_i^* = z_i$  if  $i$  is closed and  $z_i^* > z_i$  if  $i$  is open. We also define the symmetric *toppling matrix*  $\Delta$  on  $\mathcal{G}$  as follows:

$$\Delta_{i,j} = \begin{cases} z_i^* & \text{if } i = j, \\ -1 & \text{if there exists an edge } \{i, j\} \text{ between } i \text{ and } j, \\ 0 & \text{otherwise.} \end{cases} \quad (2.1)$$

Hence,  $\Delta$  corresponds to the discrete Laplacian on  $\mathcal{G}_s$  with Dirichlet boundary conditions at  $s$ , with unit conductances:  $c_{i,j} = 1$  if  $\{i, j\}$  is an edge of  $\mathcal{G}$ . Open and closed sites simply correspond to wired and free vertices, respectively. A configuration  $\mathcal{C} = \{h_i\}$  is called *stable* if  $1 \leq h_i \leq z_i^* = \Delta_{i,i}$  for each  $i \in \mathcal{G}$ .

The discrete, stochastic dynamics of the sandpile model is defined as follows. Let  $\mathcal{C}_t$  be a stable configuration at time  $t$ . The configuration  $\mathcal{C}_{t+1}$  is obtained in two steps:

- (i) *Seeding*: A grain of sand is dropped on a random site  $i$  of  $\mathcal{G}$ , producing new height values,  $h_j^{\text{new}} = h_j^{\text{old}} + \delta_{j,i}$ . If  $h_i^{\text{new}} \leq \Delta_{i,i}$ , the new configuration is stable, and defines  $\mathcal{C}_{t+1}$ .
- (ii) *Relaxation*: If  $h_i^{\text{new}} > \Delta_{i,i}$ , then the whole system is updated according to  $h_j^{\text{new}} \rightarrow h_j^{\text{new}} - \Delta_{i,j}$  for each  $j \in \mathcal{G}$ , as well as  $s \rightarrow s + z_i^* - z_i$ . In other words, site  $i$  *topples*: it loses  $z_i^*$  grains of sand and gives one grain to each of its neighbors on the graph  $\mathcal{G}_s$ . If one of the updated heights  $h_j$  on  $\mathcal{G}$  in turn exceeds  $\Delta_{j,j}$ , the toppling

process is repeated until all sites are stable, thus defining  $\mathcal{C}_{t+1}$  (see Fig. 2.1). We note that each time a dissipative site is toppled, a certain number of grains leave  $\mathcal{G}$  and are transferred to the sink.

Since the sink  $s$  is never toppled, its height is unboundedly increasing over time. This property implies that the dynamics is well defined, in the sense that the relaxation of an unstable configuration on  $\mathcal{G}$  terminates after a finite number of topplings [39]. The Abelian property stems from the fact that the stable configuration obtained after all unstable sites have toppled does not depend on the order in which the topplings are carried out.

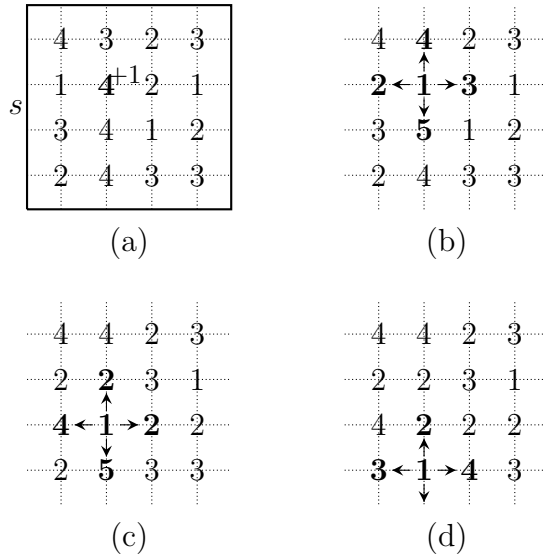


Figure 2.1: Relaxation of a configuration on a  $4 \times 4$  square grid with dissipative sites on its (geometrical) boundary after a grain is dropped on a site  $i$  with height  $h_i = 4$ . Its toppling creates another height  $h_j = 5$ , which in turn topples. On the last step, the grain of sand “falling off the grid” arrives into the sink  $s$ , marked as the contour line surrounding the grid in panel (a). The dotted lines indicate the edges in  $\mathcal{G}_s$ .

The dynamics described above defines a discrete Markov chain on a finite state space, namely the space of stable configurations. It can be shown [39] that it has a unique invariant measure  $\mathbb{P}_{\mathcal{G}}^*$ , which is moreover

uniform on the subset  $\mathcal{R}$  of recurrent configurations:

$$\mathbb{P}_{\mathcal{G}}^*(\mathcal{C}) = \begin{cases} \frac{1}{|\mathcal{R}|} & \text{if } \mathcal{C} \in \mathcal{R}, \\ 0 & \text{if } \mathcal{C} \notin \mathcal{R}. \end{cases} \quad (2.2)$$

Hence, recurrent configurations are the only ones to keep reoccurring in the repeated image of the dynamics; they all do so infinitely often, with equal frequency. In the continuum limit, the measures  $\mathbb{P}_{\mathcal{G}}^*$  are expected to converge to the field-theoretical measure  $\mathbb{P}$  of a conformal field theory of central charge  $c = -2$  [112], which is believed to be logarithmic, see the recent review [143].

In practice, recurrent versus nonrecurrent (transient) configurations can be characterized in terms of certain subconfigurations. For example, the subconfiguration consisting in two neighboring 1s cannot be part of a recurrent configuration on a square grid, since it cannot be produced by topplings (because a height  $h_i = z_i^* + 1$  that topples to become a 1 gives one grain of sand to each of its neighbors, making their height at least equal to 2). Similarly, the block 121 is also forbidden because its production by topplings means that it contained a block 11 before. More generally, a *forbidden subconfiguration* (FSC)  $F$  is such that its heights satisfy

$$h_i \leq z_i^{(F)} = \#\{\text{neighbors of } i \text{ in } F\}, \quad \text{for all } i \in F. \quad (2.3)$$

Then a stable configuration is recurrent if and only if it contains no FSCs [39, 112]. The condition for a configuration to be recurrent is nonlocal, because one has to scan the whole graph to make sure that no such subconfigurations appear. For example, the stable configuration  $h_i = z_i$  for each  $i \in \mathcal{G}$  is not recurrent and contains  $F = \mathcal{G}$  as the smallest FSC.

The recurrence criterion in terms of FSCs shows that the configuration obtained by increasing the height of any site in a recurrent configuration (without making it unstable) is recurrent. Decreasing the heights in a recurrent configuration may however result in nonrecurrent configurations.

Up to this point, it should be noted that the definition of the Abelian sandpile model holds on any unoriented connected graph  $\mathcal{G}_s$ . In what

follows, we shall particularize the discussion to the square lattice, on which most of our results have been obtained.

### 2.1.1 The burning algorithm

Height variables are the most natural degrees of freedom in the Abelian sandpile model, and evolve according to local toppling rules. However, as observed above, the characterization of recurrent configurations in terms of FSCs is highly nonlocal.

The *burning algorithm* [112] gives a bijection between recurrent sandpile configurations on  $\mathcal{G}$  and rooted spanning trees on  $\mathcal{G}_s$ , which turn out to be more convenient for concrete calculations. We shall view the sink  $s$  as the root of the tree, since the burning algorithm will produce trees as growing from  $s$ .

Given a stable configuration on  $\mathcal{G}$ , the burning algorithm describes the propagation of a fire front throughout the grid  $\mathcal{G}_s$ , starting from the root  $s$ ; when the algorithm stops, the various fire lines form a rooted spanning tree on  $\mathcal{G}_s$  if the configuration we started from is recurrent. The fire propagation depends on the height values of the configuration one considers, and so does the resulting spanning tree. It is defined as follows.

At any time<sup>1</sup>  $t$ , the sites of  $\mathcal{G}_s$  belong to one of the following three disjoint sets,  $\mathcal{U}_t$ ,  $\mathcal{B}_t$  and  $\mathcal{E}_t$  (for more clarity, we omit the explicit dependence of these sets on the configuration one is looking at).  $\mathcal{U}_t$  contains the sites that have not burnt yet at time  $t$ ,  $\mathcal{B}_t$  contains those that are burning at time  $t$  and the rest goes in  $\mathcal{E}_t$ , which contains the extinct sites. At the initial time  $t = 0$ , only the sink/root is burning while all other sites are unburnt, so  $\mathcal{U}_0 = \mathcal{G}$ ,  $\mathcal{B}_0 = \{s\}$  and  $\mathcal{E}_0 = \emptyset$ . From then on, the three sets evolve by the following rules.

The sites in  $\mathcal{B}_t$  keep burning for just one time unit, so that  $\mathcal{E}_{t+1} = \mathcal{E}_t \cup \mathcal{B}_t$ . The unburnt sites in  $\mathcal{U}_t$  whose height is strictly larger than their number

---

<sup>1</sup>This time variable is used to describe the propagation of the fire front, and should not be confused with the time used in the previous subsection to describe the dynamics of the model.

of neighbors in  $\mathcal{U}_t$  move to  $\mathcal{B}_{t+1}$ , whereas the others form  $\mathcal{U}_{t+1}$ :

$$\mathcal{B}_{t+1} = \{i \in \mathcal{U}_t : h_i > z_i^{(\mathcal{U}_t)}\}, \quad \mathcal{U}_{t+1} = \mathcal{U}_t \setminus \mathcal{B}_{t+1}. \quad (2.4)$$

Therefore, the size of the set  $\mathcal{U}_t$  decreases in time, while that of  $\mathcal{E}_t$  increases. The algorithm stops when the three sets no longer change, that is, at the first time  $\tau$  for which  $\mathcal{B}_\tau = \emptyset$  (and  $\mathcal{E}_{\tau+1} = \mathcal{E}_\tau$ ,  $\mathcal{U}_\tau = \mathcal{U}_{\tau-1}$ ). From the definitions, we see that the set  $\mathcal{U}_\tau$ , if nonempty, is an FSC. A configuration is therefore recurrent if and only if the algorithm stops after all sites have burnt, namely  $\mathcal{E}_\tau = \mathcal{G}_s$  or  $\mathcal{U}_\tau = \emptyset$ .

Let us observe that for all times  $0 < t < \tau$ , every site of  $\mathcal{B}_t$  has at least one nearest neighbor that was in  $\mathcal{B}_{t-1}$ , since otherwise that site would have been burning at an earlier time. For instance, at time  $t = 1$ , the sites of  $\mathcal{B}_1$  must be dissipative sites, i.e. neighbors of the sink. In this way, we can imagine the fire as propagating along edges connecting nearest neighbors; these edges eventually form the spanning tree.

The spanning tree starts from the root, and connects it to the dissipative sites in  $\mathcal{B}_1$ . Edges are subsequently added as the algorithm is running. If a site  $j$  in  $\mathcal{B}_t$  has only one nearest neighbor  $i$  in  $\mathcal{B}_{t-1}$ , we say that  $j$  catches fire from  $i$ , and we add the edge connecting  $i$  to  $j$  to the tree under construction. More generally, if  $j$  has  $k \geq 1$  nearest neighbors in  $\mathcal{B}_{t-1}$ , the height at  $j$  satisfies

$$z_j^{(\mathcal{N}_{t-1})} + 1 \leq h_j \leq z_j^{(\mathcal{N}_{t-2})} = z_j^{(\mathcal{N}_{t-1})} + k, \quad (2.5)$$

where the lower bound is because  $j$  is in  $\mathcal{B}_t$  and the upper bound is because  $j$  was not in  $\mathcal{B}_{t-1}$ . Therefore, the height  $h_j$  can possibly take  $k$  different values. If the actual value is  $h_j = z_j^{(\mathcal{N}_{t-1})} + m$ , we use the additional prescription that  $j$  catches fire from its  $m$ th neighbor in  $\mathcal{B}_{t-1}$ , once these neighbors are ordered clockwise starting from the northern one. We also add the corresponding edge to the tree.

The algorithm is illustrated in Fig. 2.2. The site in bold is in  $\mathcal{U}_2$  where it has two neighbors, then belongs to  $\mathcal{B}_3$  with two of its neighbors, E and S, in  $\mathcal{B}_2$ . Its height is  $h_j = 3 = z_j^{(\mathcal{N}_2)} + 1$  and so  $m = 1$ . Therefore, it catches fire from its E neighbor, the first of his neighbors in  $\mathcal{B}_2$  with respect to the ordering N-E-S-W. The same prescription has been used at  $t = 1$  to decide which edges propagate the fire to the three burning corner sites.

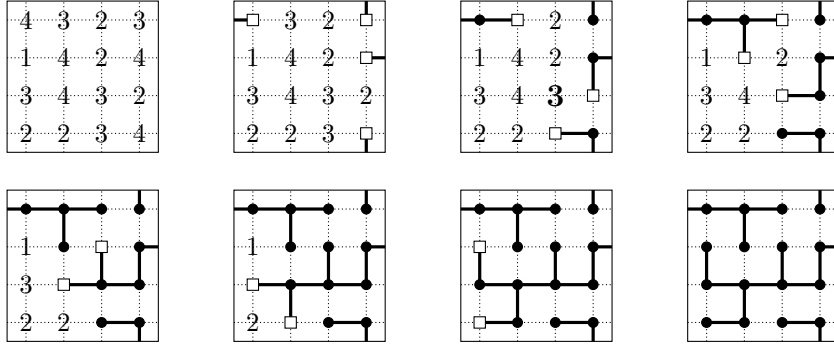


Figure 2.2: Construction of the spanning tree associated with a recurrent configuration on a  $4 \times 4$  grid (the box represents the sink). The burning algorithm stops at time  $\tau = 7$ . Each panel shows a snapshot for times  $t$  between 0 and 7: sites in sets  $\mathcal{U}_t$  are shown by their height, those in  $\mathcal{B}_t$  and  $\mathcal{E}_t$  are marked by white squares and black dots, respectively.

The burning algorithm clearly defines an injective map from the set  $\mathcal{R}$  of recurrent configurations to the set  $\mathcal{T}$  of spanning trees on  $\mathcal{G}_s$  rooted at the sink. Since the two sets have equal size [112], the map is bijective. It follows that the probability measure on spanning trees induced by that on recurrent configurations is uniform. Moreover the size of each set defines the partition function,

$$Z = |\mathcal{R}| = |\mathcal{T}| = \det \Delta. \quad (2.6)$$

It is important to bear in mind that the above algorithm, which we shall refer to as the standard algorithm, is only one among the many possible burning algorithms. One may decide to choose an ordering different from N-E-S-W, or even use a distinct but fixed ordering at each site. One can also delay the burning of a portion of the grid, something we shall do in the next section. All these different algorithms are perfectly admissible but would typically assign trees with many different shapes to a given height configuration. Each one however provides a bijective map if consistently applied to all height configurations.

### 2.1.2 Height probabilities

The burning algorithm associates a rooted spanning tree with each recurrent configuration. Since there is a unique path connecting every site to the root, the edges of the spanning tree can be oriented toward the root, as pictured in Fig. 2.3 (this orientation is opposite to the fire propagation). We define the notion of *predecessor* by saying that  $j$  is a predecessor of  $i$  on a rooted spanning tree if the path from  $j$  to the root goes through  $i$ .

Since the stationary sandpile measure  $\mathbb{P} = \mathbb{P}_{\mathcal{G}}^*$  is uniform over the set  $\mathcal{R}$  of recurrent configurations, the probability  $\mathbb{P}_a(i) \equiv \mathbb{P}(h_i = a)$  that a given site  $i$  has height  $h_i = a$  is given by the ratio of the number of recurrent configurations with  $h_i = a$  to the total number of recurrent configurations. To compute these probabilities relative to the site  $i$ , we partition  $\mathcal{R}$  into four disjoint subsets  $\mathcal{R}_k(i)$ ,  $1 \leq k \leq 4$ , defined as

$$\mathcal{R}_k(i) = \{\text{configurations that are recurrent for } k \leq h_i \leq 4, \\ \text{transient for } 1 \leq h_i \leq k-1\}. \quad (2.7)$$

Since each  $\mathcal{R}_k(i)$  contains an equal number of configurations where  $h_i = k, k+1, \dots, 4$ , one readily finds that the probabilities are given by

$$\mathbb{P}_1(i) = \frac{|\mathcal{R}_1(i)|}{4|\mathcal{R}|}, \quad \mathbb{P}_2(i) = \mathbb{P}_1(i) + \frac{|\mathcal{R}_2(i)|}{3|\mathcal{R}|}, \\ \mathbb{P}_3(i) = \mathbb{P}_2(i) + \frac{|\mathcal{R}_3(i)|}{2|\mathcal{R}|}, \quad \mathbb{P}_4(i) = \mathbb{P}_3(i) + \frac{|\mathcal{R}_4(i)|}{|\mathcal{R}|}. \quad (2.8)$$

The sets  $\mathcal{R}_k(i)$  can be characterized in terms of spanning trees [137]. To see this, we use a slight modification of the standard algorithm. Namely, we keep the reference site  $i$  in the set of unburnt sites as long as possible, that is, until no other site is ready to burn. At that point,  $i$  and possibly other sites form a cluster  $F_i$  of unburnt sites. The whole of  $F_i$  will then subsequently burn following the standard procedure. With respect to this modified algorithm, and since  $i$  is necessarily the first site in  $F_i$  to burn, all the other sites of  $F_i$  are predecessors of  $i$ . Now let  $\mathcal{C}$  be a configuration in  $\mathcal{R}_k(i)$ , to which we apply the modified burning algorithm just described. Since the cluster  $F_i$  will eventually burn for whatever value of  $h_i \geq k$ ,  $F_i$  must contain exactly  $k-1$  nearest neighbors of  $i$ .



### 2.1.3 Multisite height probabilities

We provide a detailed discussion for two-site probabilities  $\mathbb{P}_{a,b}(i, j) \equiv \mathbb{P}(h_i=a, h_j=b)$ , assuming the reference sites  $i$  and  $j$  are not neighbors and do not share common neighbors. By analogy with one-site probabilities, it seems natural to define the following subsets [73],

$$\begin{aligned} \mathcal{R}_{k,\ell}(i, j) = \{ \text{configurations that are recurrent if } k \leq h_i \leq 4 \\ \text{and } \ell \leq h_j \leq 4, \text{ and transient otherwise} \}, \end{aligned} \quad (2.10)$$

and try to characterize the trees contributing to  $\mathbb{P}_{a,b}(i, j)$  in terms of these sets.

However, it was observed in [80] that some recurrent configurations do not belong to any  $\mathcal{R}_{k,\ell}$ . Consider for example a rectangular grid  $\mathcal{G}$  of arbitrary size, with reference sites  $i$  and  $j$  respectively located at the top left and bottom right corners of the grid, and the configuration  $\mathcal{C}_0$  such that  $h_k = z_k$  for any site  $k \neq i, j$ , and  $h_i = z_i + 1 = 3$ ,  $h_j = z_j + 1 = 3$  (see Fig. 2.4). The configuration  $\mathcal{C}_0$  is recurrent, and remains recurrent if *either*  $h_i$  or  $h_j$  is decreased by one or two. However  $\mathcal{C}_0$  becomes transient if *both*  $h_i, h_j$  are set to 2. In particular  $\mathcal{C}_0$  does not belong to  $\mathcal{R}_{1,3}(i, j)$ , since  $\{h_i \geq 1, h_j \geq 3\}$  is a sufficient but not *necessary* condition for  $\mathcal{C}_0$  to be recurrent; similarly it does not belong to  $\mathcal{R}_{3,1}(i, j)$  either. More generally, we see that  $\mathcal{C}_0$  does not belong to any of the subsets  $\mathcal{R}_{k,\ell}(i, j)$ , which therefore do not form a partition of the set of recurrent configurations.

To solve this issue, Jeng proposed an alternative division of  $\mathcal{R}$  [80], which we do not state here explicitly. Instead we propose the following definition, equivalent to that of Jeng:

$$\begin{aligned} \tilde{\mathcal{R}}_{k,\ell}(i, j) = \{ \text{configurations that are recurrent for } (h_i, h_j) = (k, \ell), \\ \text{transient for } (h_i, h_j) = (k-1, \ell) \text{ or } (k, \ell-1) \}. \end{aligned} \quad (2.11)$$

It follows that  $\mathcal{R}_{k,\ell}(i, j) \subset \tilde{\mathcal{R}}_{k,\ell}(i, j)$ . However, the two subsets are not equal, as  $\tilde{\mathcal{R}}_{k,\ell}(i, j) \setminus \mathcal{R}_{k,\ell}(i, j)$  contains configurations that remain recurrent for certain heights  $h_i, h_j$  such that  $h_i > k$  and  $h_j < \ell$ , or  $h_i < k$  and  $h_j > \ell$ .

<b>3</b>	3	- - -	3	2
3	4	- - -	4	3
⋮	⋮	⋮	⋮	⋮
⋮	⋮	⋮	⋮	⋮
⋮	⋮	⋮	⋮	⋮
3	4	- - -	4	3
2	3	- - -	3	<b>3</b>

Figure 2.4: Recurrent sandpile configuration  $\mathcal{C}_0$  on a rectangular grid, with reference sites  $i, j$  located at the top left and bottom right corners, that does not belong to any  $\mathcal{R}_{k,\ell}(i, j)$ , but to  $\tilde{\mathcal{R}}_{1,3}(i, j)$  and  $\tilde{\mathcal{R}}_{3,1}(i, j)$ .

While any recurrent configuration belongs to a subset  $\tilde{\mathcal{R}}_{k,\ell}(i, j)$ , it might not be unique. For instance, the configuration  $\mathcal{C}_0$  described above belongs to both subsets  $\tilde{\mathcal{R}}_{1,3}(i, j)$  and  $\tilde{\mathcal{R}}_{3,1}(i, j)$ . The subsets  $\tilde{\mathcal{R}}_{k,\ell}$  can therefore be used for sandpile computations, but prove to be impractical (see for example the discussion of  $\mathbb{P}_{2,2}(i, j)$  along a closed boundary on the upper half-plane in [80]).

Instead we set up a specific one-to-one correspondence between recurrent configurations and spanning trees based on a slight modification of the burning algorithm. We begin by making the following observation: the classification of rooted spanning trees according to the number of predecessors of  $i$  and  $j$  is not sufficient to compute two-site probabilities if the heights at the two reference sites are both strictly larger than 1. Indeed, let us define  $X_{k,\ell}(i, j)$  as the fraction of spanning trees in which  $i$  and  $j$  have respectively  $k$  and  $\ell$  predecessors among their own nearest neighbors. Then trees in a given class  $X_{k,\ell}(i, j)$  can contribute differently to two-site probabilities.

Consider for example the trees making the fraction  $X_{1,1}(i, j)$ . A tree in that set such that  $i$  and its neighbors are not predecessors of  $j$  or any of its neighbors, and vice versa, will contribute equally to  $\mathbb{P}_{a,b}(i, j)$  for all values  $a, b \geq 2$ . The situation is different for those trees such that  $i$  and  $j$  are not predecessors of each other, but where two neighbors of  $i$  (resp.  $j$ ) are predecessors of  $j$  (resp.  $i$ ), as illustrated in Fig. 2.5. Using the standard burning algorithm (or a modified version of it), we see that  $i$

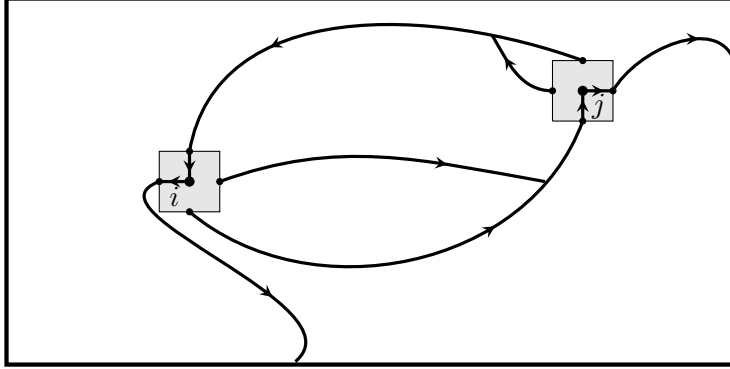


Figure 2.5: Schematic representation of a rooted spanning tree contributing to  $X_{1,1}(i, j)$  with 2 neighbors of  $i$  (resp.  $j$ ) that are predecessors of  $j$  (resp.  $i$ ). Here, only the paths connecting  $i, j$ , their neighbors and the root are shown.

or  $j$  (or both) must be burnable at a time when only one of its neighbors is burnt. It follows that  $h_i$  and/or  $h_j$  must necessarily be equal to 4, and therefore these spanning trees in  $X_{1,1}(i, j)$  do not contribute to  $\mathbb{P}_{2,2}$ ,  $\mathbb{P}_{2,3}$ ,  $\mathbb{P}_{3,2}$  or  $\mathbb{P}_{3,3}$ .

We see that a naive generalization of the characterization of recurrent configurations in terms of spanning trees (established for one-site probabilities) fails. A more detailed characterization including the predecessorship between  $i, j$  and their neighbors is therefore required. To do so, we partition the set of spanning trees on  $\mathcal{G}_s$  according to whether one of the reference sites is a predecessor of the other. More precisely, we define the following three quantities, seen as refined versions of the  $X_{k,\ell}(i, j)$ 's. In all three cases,  $k$  and  $\ell$  denote the number of nearest neighbors that are predecessors of  $i$  and  $j$  respectively.

- $X_{k,\ell}^{m,0}(i \rightarrow j)$  is the fraction of spanning trees on  $\mathcal{G}_s$  in which  $i$  is a predecessor of  $j$ , and  $m$  nearest neighbors of  $i$  are predecessors of  $j$  but not of  $i$  itself; so  $1 \leq \ell \leq 3$ ,  $1 \leq m \leq 4$  and  $1 \leq k + m \leq 4$ .
- $X_{k,\ell}^{0,n}(i \leftarrow j)$  is similarly the fraction of spanning trees on  $\mathcal{G}_s$  in which  $j$  is a predecessor of  $i$ , and  $n$  nearest neighbors of  $j$  are predecessors of  $i$  but not of  $j$ ; so  $1 \leq k \leq 3$ ,  $1 \leq n \leq 4$  and  $1 \leq \ell + n \leq 4$ .

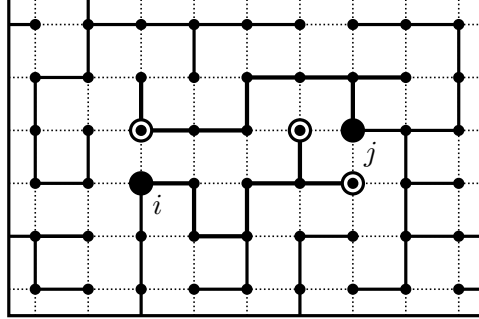


Figure 2.6: Spanning tree accounted for in  $X_{1,1}^{1,2}(i|j)$ . The northern neighbor of  $i$  is a predecessor of  $j$ , while the southern and western neighbors of  $j$  are predecessors of  $i$ .

- $X_{k,\ell}^{m,n}(i|j)$  is the fraction of spanning trees in which neither  $i$  nor  $j$  is a predecessor of the other, and in which  $m$  neighbors of  $i$  are predecessors of  $j$ , and  $n$  neighbors of  $j$  are predecessors of  $i$ ; here  $0 \leq k + m \leq 3$  and  $0 \leq \ell + n \leq 3$ , with the additional conditions that  $m = 0$  if  $\ell = 0$  and  $n = 0$  if  $k = 0$ . A tree of this type, contributing to  $X_{1,1}^{1,2}(i|j)$ , is pictured in Fig. 2.6.

In order to relate these fractions to two-site probabilities, we modify the standard burning algorithm in a way similar to what we did in the previous subsection, so that any recurrent configuration on  $\mathcal{G}$  is now associated with a three-component spanning forest on  $\mathcal{G}_s$ . We proceed in three steps.

1. First we let the fire propagate on the grid except for  $i$  and  $j$ , which we prevent from burning. We denote by  $\tau$  the time at which  $i$  and/or  $j$  are the only burnable sites left.
2. If both  $i$  and  $j$  are burnable at that time, they burn simultaneously and propagate the fire to the remaining unburnt sites.
3. If  $i$  is burnable at time  $\tau$  but  $j$  is not, we burn every burnable site except for  $j$ . Then we allow  $j$  to burn until all sites of the grid are burnt. Otherwise  $j$  is burnable at time  $\tau$  and  $i$  is not, then we burn  $j$  first and  $i$  second.

Let us consider the three-component spanning forest  $\mathcal{F}$  on  $\mathcal{G}_s$  whose components are the trees rooted at  $s, i, j$  respectively:  $\mathcal{F} = \mathcal{T}_s \cup \mathcal{T}_i \cup \mathcal{T}_j$ . We assume that  $\mathcal{T}_i$  (resp.  $\mathcal{T}_j$ ) contains  $k$  (resp.  $m$ ) nearest neighbors of  $i$  and  $n$  (resp.  $\ell$ ) nearest neighbors of  $j$ ; then  $\mathcal{T}_s$  contains  $4-k-m$  neighbors of  $i$  and  $4-\ell-n$  neighbors of  $j$ .

The spanning forest  $\mathcal{F}$  can be extended into a spanning tree on  $\mathcal{G}_s$  by adding two extra edges: one between  $i$  and one of its neighbors, and one between  $j$  and one of its neighbors (so that no loop is formed). If  $i$  is linked to one of its  $4-k-m$  neighbors in  $\mathcal{T}_s$ , and  $j$  is linked to one of its  $4-\ell-n$  neighbors in  $\mathcal{T}_s$ , the resulting spanning tree on  $\mathcal{G}_s$  contributes to the fraction  $X_{k,\ell}^{m,n}(i|j)$ . If rather  $i$  is linked to  $\mathcal{T}_s$  and  $j$  to  $\mathcal{T}_i$  the spanning tree is included in  $X_{k+m,\ell}^{0,n}(i \leftarrow j)$ . Likewise if  $i$  is grafted to  $\mathcal{T}_j$  and  $j$  to  $\mathcal{T}_s$ , the tree belongs to  $X_{k,\ell+n}^{m,0}(i \rightarrow j)$ . It follows that

$$\begin{aligned} \frac{1}{(4-k-m)(4-\ell-n)} X_{k,\ell}^{m,n}(i|j) &= \frac{1}{(4-k-m)n} X_{k+m,\ell}^{0,n}(i \leftarrow j) \\ &= \frac{1}{m(4-\ell-n)} X_{k,\ell+n}^{m,0}(i \rightarrow j), \end{aligned} \quad (2.12)$$

since these three quantities (if the denominators do not vanish) equal the number of spanning forests of the type specified above.

On the other hand, a three-component spanning forest  $\mathcal{F}$ , together with the information that  $i|j$ ,  $i \rightarrow j$  or  $i \leftarrow j$ , is in one-to-one correspondence with a sandpile configuration  $\mathcal{C}_{i,j}$  on  $\mathcal{G} \setminus \{i, j\}$  through the standard burning algorithm (starting from the roots  $s, i$  and  $j$ ). Let us now discuss the possible values of the pair  $(h_i, h_j)$  such that the configuration  $\mathcal{C} \equiv \mathcal{C}_{i,j} \cup \{h_i, h_j\}$  on the whole grid  $\mathcal{G}$  is recurrent:

- If  $\mathcal{F}$  is extended to a tree contributing to  $X_{k,\ell}^{m,n}(i|j)$ , both  $i$  and  $j$  must be burnable after the first step of the modified burning algorithm described above. Since at that time,  $i$  (resp.  $j$ ) has  $k+m$  (resp.  $\ell+n$ ) unburnt neighbors, we obtain the inequality  $k+m+1 \leq h_i \leq 4$  (resp.  $\ell+n+1 \leq h_j \leq 4$ ).
- If  $\mathcal{F}$  is extended to a tree contributing to  $X_{k+m,\ell}^{0,n}(i \leftarrow j)$ ,  $i$  must be burnable after the first step of the burning algorithm while  $j$  is not burnable at that time. However  $j$  must be burnable after the

second step of the algorithm. Therefore,  $k + m + 1 \leq h_i \leq 4$  and  $\ell + 1 \leq h_j \leq \ell + n$ .

- Similarly if  $\mathcal{F}$  is extended to a tree contributing to  $X_{k,\ell+n}^{m,0}(i \rightarrow j)$ , then  $k + 1 \leq h_i \leq k + m$  and  $\ell + n + 1 \leq h_j \leq 4$ .

In all three cases, the number of admissible heights for  $i$  and  $j$  is equal to the number of ways the trees  $\mathcal{T}_i$  and  $\mathcal{T}_j$  can be grafted to one another and/or to  $\mathcal{T}_s$  to form a spanning tree on  $\mathcal{G}_s$  of a given subclass  $i|j$ ,  $i \leftarrow j$  or  $i \rightarrow j$ . Therefore, a given fraction  $X$  contributes equally to all pairs of admissible heights.

It is then straightforward to express two-site probabilities  $\mathbb{P}_{a,b}(i, j)$  in terms of these fractions:

$$\begin{aligned} \mathbb{P}_{a,b}(i, j) = & \sum_{\substack{* \\ 0 \leq k+m \leq a-1 \\ 0 \leq \ell+n \leq b-1}} \frac{X_{k,\ell}^{m,n}(i|j)}{(4-k-m)(4-\ell-n)} + \sum_{\substack{(k,m) \in U(a) \\ (\ell,n) \in V(b)}} \frac{X_{k+m,\ell}^{0,n}(i \leftarrow j)}{(4-k-m)n} \\ & + \sum_{\substack{(k,m) \in V(a) \\ (\ell,n) \in U(b)}} \frac{X_{k,\ell+n}^{m,0}(i \rightarrow j)}{m(4-\ell-n)}, \end{aligned} \quad (2.13)$$

where the symbol  $*$  over the sum is a reminder for the conditions that  $k = 0$  implies  $n = 0$ , and  $\ell = 0$  implies  $m = 0$ .  $U(h)$  and  $V(h)$  are subsets of  $\{0, 1, 2, 3, 4\}^2$  defined by

$$\begin{aligned} U(h) &= \{(x, y) : 1 \leq x + y \leq h - 1\}, \\ V(h) &= \{(x, y) : x + 1 \leq h \leq x + y \leq 4\}. \end{aligned} \quad (2.14)$$

If  $b = 1$ , then Eq. (2.13) simplifies to

$$\mathbb{P}_{a,1}(i, j) = \frac{X_{0,0}^{0,0}(i|j)}{16} \quad \text{for } a = 1, \quad (2.15)$$

$$\mathbb{P}_{a,1}(i, j) = \sum_{k=0}^{a-1} \frac{X_{k,0}^{0,0}(i|j)}{4(4-k)} + \sum_{k=1}^{a-1} \sum_{n=1}^4 \frac{X_{k,0}^{0,n}(i \leftarrow j)}{(4-k)n} \quad \text{for } a > 1. \quad (2.16)$$

Alternatively, these probabilities can be written in terms of the fractions

$$\begin{aligned} X_{0,0}(i, j) &= X_{0,0}^{0,0}(i|j), \\ X_{k,0}(i, j) &= \sum_{n=0}^3 X_{k,0}^{0,n}(i|j) + \sum_{n=1}^4 X_{k,0}^{0,n}(i \leftarrow j) \quad \text{for } k > 0. \end{aligned} \quad (2.17)$$

They are easier to compute, since they only take into account the number of predecessors of  $i$  among its neighbors (with  $j$  having none among its own neighbors). Using Eq. (2.12) with  $\ell = m = 0$ , we find that

$$\begin{aligned}
\mathbb{P}_{a,1}(i, j) &= \sum_{k=0}^{a-1} \frac{X_{k,0}^{0,0}(i|j)}{4(4-k)} + \sum_{k=1}^{a-1} \sum_{n=1}^4 \frac{X_{k,0}^{0,n}(i \leftarrow j)}{4(4-k)} \\
&\quad + \sum_{k=1}^{a-1} \sum_{n=1}^3 \frac{(4-n)X_{k,0}^{0,n}(i \leftarrow j)}{4(4-k)n} \\
&= \sum_{k=0}^{a-1} \frac{X_{k,0}^{0,0}(i|j)}{4(4-k)} + \sum_{k=1}^{a-1} \sum_{n=1}^4 \frac{X_{k,0}^{0,n}(i \leftarrow j)}{4(4-k)} + \sum_{k=1}^{a-1} \sum_{n=1}^3 \frac{X_{k,0}^{0,n}(i|j)}{4(4-k)} \\
&= \sum_{k=0}^{a-1} \frac{X_{k,0}(i, j)}{4(4-k)}.
\end{aligned} \tag{2.18}$$

In principle, it is possible to write similar relations between  $n$ -site probabilities  $\mathbb{P}_{a_1, \dots, a_n}$  and fractions of spanning trees with various types of connectivities. Clearly, the discussion is already quite involved for  $n = 2$ , and will certainly get more complicated for a general value of  $n > 2$  (indeed the number of classes of trees grows exponentially with  $n$ ). It is however possible to deal rather simply with the particular case  $a_j = 1$  for  $2 \leq j \leq n$  (all the probabilities computed in this chapter are of this form).

Following [111], we define a modified graph  $\tilde{\mathcal{G}}$  by removing three edges around each site  $i_2, \dots, i_n$ , so that these sites have only one neighbor left on  $\tilde{\mathcal{G}}$ . In doing so, the degree of each site belonging to a removed edge is decreased by 1; in particular the degree of the sites  $i_2, \dots, i_n$  is 1 on  $\tilde{\mathcal{G}}$ . It is not difficult to see that there is a one-to-one correspondence between recurrent configurations on  $\mathcal{G}$  with  $h_{i_2} = \dots = h_{i_n} = 1$ , and recurrent configurations on  $\tilde{\mathcal{G}}$ . Therefore, the probability that a recurrent configuration on  $\mathcal{G}$  has heights 1 at  $i_2, \dots, i_n$  is given by the ratio  $\det \Delta_{\tilde{\mathcal{G}}} / \det \Delta_{\mathcal{G}}$ . Furthermore, it does not depend on which specific edges have been removed around the reference sites. The  $n$ -point probability

on the original graph can therefore be written as

$$\begin{aligned} \mathbb{P}_{a,1,\dots,1}^{\mathcal{G}}(i_1, i_2, \dots, i_n) &= \mathbb{P}_a^{\mathcal{G}}(i_1 | h_{i_j}=1, 2 \leq j \leq n) \times \mathbb{P}_{1,\dots,1}^{\mathcal{G}}(i_2, \dots, i_n) \\ &= \mathbb{P}_a^{\tilde{\mathcal{G}}}(i_1) \times \frac{\det \Delta_{\tilde{\mathcal{G}}}}{\det \Delta_{\mathcal{G}}}. \end{aligned} \quad (2.19)$$

We see that evaluating an  $n$ -site probability with  $n-1$  heights 1 amounts to computing a one-site probability on a modified graph, which is how we proceed for the calculations of Sections 2.3 and 2.4.

Equivalently, we can write the probability (2.19) in terms of spanning tree fractions, as computed in (2.18) for  $n = 2$ . Consider a spanning tree contributing to  $X_k^{\tilde{\mathcal{G}}}(i_1)$ : sites  $i_2, \dots, i_n$  have only one neighbor on  $\tilde{\mathcal{G}}$ , so they are necessarily leaves in that tree (that is, they have no predecessors). On the other hand, spanning trees in  $X_{k,0,\dots,0}^{\mathcal{G}}(i_1, i_2, \dots, i_n)$  are such that  $i_{j \geq 2}$  are leaves, which can be connected to any of their four neighbors. It follows that

$$\det \Delta_{\mathcal{G}} \times X_{k,0,\dots,0}^{\mathcal{G}}(i_1, i_2, \dots, i_n) = 4^{n-1} \times \det \Delta_{\tilde{\mathcal{G}}} \times X_k^{\tilde{\mathcal{G}}}(i_1). \quad (2.20)$$

Using (2.9) applied to  $\tilde{\mathcal{G}}$ , one obtains the relation

$$\begin{aligned} \mathbb{P}_{a,1,\dots,1}^{\mathcal{G}}(i_1, i_2, \dots, i_n) &= \frac{\det \Delta_{\tilde{\mathcal{G}}}}{\det \Delta_{\mathcal{G}}} \times \sum_{k=0}^{a-1} \frac{X_k^{\tilde{\mathcal{G}}}(i_1)}{4-k} \\ &= \sum_{k=0}^{a-1} \frac{X_{k,0,\dots,0}^{\mathcal{G}}(i_1, i_2, \dots, i_n)}{4^{n-1}(4-k)}, \end{aligned} \quad (2.21)$$

which indeed coincides with (2.18) for  $n = 2$ .

## 2.2 Single-site probabilities on the plane

In order to illustrate the application of the grove theorem (Theorem 1.5) to sandpile calculations, and because it forms the core of the calculations that will follow, we revisit the computation, on the infinite square lattice, of the well-known one-site probabilities  $\mathbb{P}_a(i)$ , as given by (2.9). Their full computation by standard graph-theoretical methods spanned a period of twenty years [25, 81, 91, 111, 132, 134, 137], while the use of the

grove theorem reduces the calculation to a few elementary steps. Because of translational invariance, the numbers  $\mathbb{P}_a(i) = \mathbb{P}_a$  do not depend explicitly on  $i$ .

The height-one probability  $\mathbb{P}_1 = \frac{1}{4}X_0$  is the simplest one, since the definition of  $X_0$  in terms of spanning trees is entirely *local*: it requires that site  $i$  be a leaf of the spanning tree (no predecessor among its neighbors).  $\mathbb{P}_1$  can be computed by resorting to a new graph  $\tilde{\mathcal{G}}$  obtained from  $\mathcal{G} = \mathbb{Z}^2$  by removing three of the adjacent edges of  $i$ .  $\mathbb{P}_1$  is then simply the ratio of the total number of spanning trees on  $\tilde{\mathcal{G}}$  to that on  $\mathcal{G}_s$ , namely the ratio of the partition functions  $\tilde{Z}$  and  $Z$  pertaining respectively to  $\tilde{\mathcal{G}}$  and  $\mathcal{G}$ . The computation does not require a nontrivial line bundle, and reduces to a finite determinant involving the standard Green function on the plane [111]:

$$\mathbb{P}_1 = \frac{\tilde{Z}}{Z} = \frac{2(\pi - 2)}{\pi^3} \simeq 0.0736. \quad (2.22)$$

The probabilities for heights greater than one are more complicated, because they involve classes of spanning trees with nonlocal restrictions, namely that  $i$  must have a fixed number of predecessors among its nearest neighbors. These restrictions can however be seen as corresponding to groves with specific node connectivities. To see this, let us denote the reference site  $i$  by 5, and its eastern, northern, western and southern neighbors by 1, 2, 3, 4 respectively. We can assume without loss of generality that  $i$  is the origin of the lattice. Node 6 is taken as the root  $s$ , and is sent to infinity. From Eq. (2.9),  $\mathbb{P}_2$  is given by

$$\mathbb{P}_2 = \mathbb{P}_1 + \frac{1}{3}X_1, \quad (2.23)$$

where  $X_1$  is the fraction of spanning trees rooted at infinity such that node 5 has exactly one predecessor among its nearest neighbors 1, 2, 3, 4. By rotation invariance, we may assume without loss of generality that node 4 is the only predecessor of node 5 and later multiply the result by 4. The arrow going out from node 5 can be oriented toward node 1, 2 or 3, but again these three cases are equivalent. By including an extra factor 3, we may choose to orient it toward node 1, so that a typical configuration looks like the one depicted in Fig. 2.7.

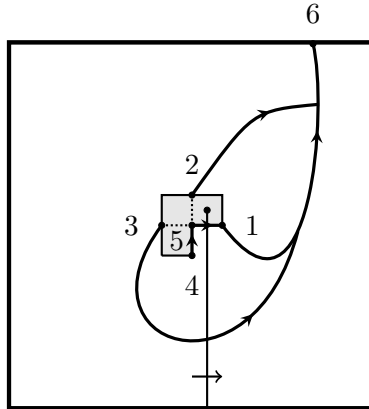


Figure 2.7: Choice of nodes and edge cuts for  $\mathbb{P}_2$ . Edges belonging to the grove are schematically indicated by heavy lines. Node 5 is conventionally chosen to be the origin of the lattice.

Let us consider the modified graph  $\bar{\mathcal{G}}$  (not to be confused with the one defined above for  $\mathbb{P}_1$ ) obtained by removing the unoriented edges  $\{5, 2\}$  and  $\{5, 3\}$ . Then spanning forests on  $\bar{\mathcal{G}}$  of the type  $4|12356$  are in one-to-one correspondence with those rooted spanning trees contributing to  $X_1$  and containing the prescribed arrows  $4 \rightarrow 5$  and  $5 \rightarrow 1$ , the bijection consisting in adding or removing the edge  $\{5, 4\}$ . The fact that nodes 2 and 3 are not in the same component as 4 ensures that they are not predecessors<sup>2</sup> of 5. The fraction  $X_1$  is therefore given by

$$X_1 = 12 \frac{\bar{Z}[4|12356]}{Z} = 12 \frac{\bar{Z}}{Z} \times \frac{\bar{Z}[4|12356]}{\bar{Z}}, \quad (2.24)$$

where  $\bar{Z}$  denotes the total number of spanning trees on the modified graph  $\bar{\mathcal{G}}$ .

Since  $\bar{\mathcal{G}}$  is an annular-one graph, we can reduce the planar partition  $\sigma = 4|12356$  to a linear combination of partial pairings, as illustrated in Fig. 2.8. Notice first that nodes 1 and 2 can be considered as interior vertices since they must necessarily belong to the same tree component as 3,5,6 (recall that an interior vertex can in principle belong to any tree component, so its index is simply erased from the partition). Therefore

<sup>2</sup>This nonlocal constraint, automatically accounted for by specifying the partition type  $4|12356$ , was handled in the old treatment by introducing  $\Theta$ -graphs, making the ensuing calculations much more complicated [81, 137].

we can write

$$\bar{Z}[4|12356] = \bar{Z}[4|356] = \bar{Z}[4|56] - \bar{Z}[34|56], \quad (2.25)$$

since  $\bar{Z}[4|56] = \bar{Z}[34|56] + \bar{Z}[4|356]$ .

To use Theorem 1.5, we introduce a nontrivial connection that is supported on a zipper starting at the face whose lower left corner is the origin (i.e. node 5), and going down vertically to infinity (see Fig. 2.7). All oriented edges of the form  $(k, \ell)$  with  $k = (0, m)$  and  $\ell = (1, m)$ , for  $m \leq 0$ , are equipped with a parallel transport  $\phi_{k, \ell} = z \in \mathbb{C}^*$ . According to the grove theorem, we obtain the equations

$$\frac{\bar{Z}[4|56]}{\bar{Z}} = \lim_{z \rightarrow 1} \frac{\bar{Z}[4|56]}{\bar{Z}} = \bar{G}_{4,4} - \bar{G}_{4,5}, \quad (2.26)$$

$$\frac{\bar{Z}[34|56]}{\bar{Z}} = \lim_{z \rightarrow 1} \frac{\bar{Z}[34|56]}{\bar{Z}} = \bar{G}_{3,4} - \bar{G}_{3,5} - \bar{G}'_{3,4} + \bar{G}'_{3,5} - \bar{G}'_{4,5}, \quad (2.27)$$

where we used  $\bar{G}_{u,v} = \bar{G}_{v,u}$  and  $\bar{G}'_{u,v} = -\bar{G}'_{v,u}$  to simplify both expressions. As illustrated in Appendix A.3, the Woodbury formula (or the Sherman-Morrison formula applied twice, namely once for each removed edge) may be used to compute the Green function and its derivative on the modified graph  $\bar{\mathcal{G}}$  in terms of the same quantities on the original graph  $\mathcal{G}$ , as well as the ratio  $\bar{Z}/Z$  of partition functions. The result reads

$$\mathbb{P}_2 = \mathbb{P}_1 + \frac{12}{3} \frac{\bar{Z}}{Z} \left[ (\bar{G}_{4,4} - \bar{G}_{4,5}) - (\bar{G}_{3,4} - \bar{G}_{3,5} - \bar{G}'_{3,4} + \bar{G}'_{3,5} - \bar{G}'_{4,5}) \right] \quad (2.28)$$

$$\begin{aligned} &= \frac{2(\pi - 2)}{\pi^3} + \frac{4(\pi - 1)}{\pi^2} \left[ \frac{\pi^2 - 5\pi + 8}{2\pi(\pi - 1)} - \frac{\pi^2 - 10\pi + 20}{16(1 - \pi)} \right] \\ &= \frac{1}{4} - \frac{1}{2\pi} - \frac{3}{\pi^2} + \frac{12}{\pi^3} \simeq 0.1739. \end{aligned} \quad (2.29)$$

The computation of the height-three probability  $\mathbb{P}_3$  is similar and makes use of the same modified graph  $\bar{\mathcal{G}}$  as for  $\mathbb{P}_2$ . The spanning trees contributing to  $X_2$ , for which the reference site (node 5) has two predecessors among its nearest neighbors, are of two types: the two predecessors form with node 5 an angle equal to  $\frac{\pi}{2}$  or to  $\pi$ . We denote the corresponding two fractions<sup>3</sup> by  $X_2^{(a)}$  and  $X_2^{(b)}$ .

<sup>3</sup>With respect to the splitting of  $X_2$  in three fractions used in [81], we have  $X_2^{(a)} = X_2^{(1)} + X_2^{(2)}$  and  $X_2^{(b)} = X_2^{(3)}$ .

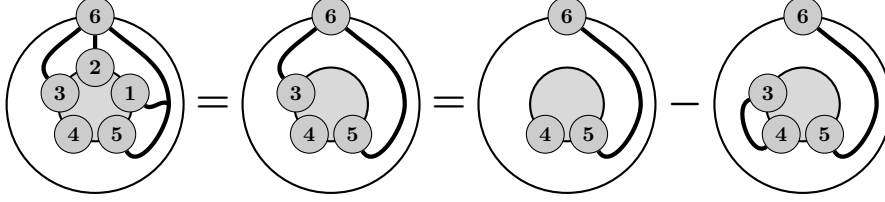


Figure 2.8: Reduction of the partition  $4|12356$  to partial pairings for a trivial connection on an annular-one graph with six nodes.

For type (a), we may assume that the two predecessors of node 5 are the nodes 1 and 4, and that the arrow going out of node 5 points to node 2.  $X_2^{(a)}$  is simply eight times this fraction of specific trees. In such a tree, the nodes 1, 4 and 5 belong to a subtree that becomes disconnected upon the removal of the edge  $\{5, 2\}$ . After the removal, the original spanning tree breaks into two components, one containing the nodes 1, 4 and 5, the other containing 2, 3 and 6. Hence, we obtain  $X_2^{(a)} = 8\bar{Z}[145|236]/Z$  where  $\bar{Z}[145|236]$  is computed on the modified graph  $\bar{\mathcal{G}}$ . Using the reduction to partial pairings shown in (1.29), the same technique used above yields

$$X_2^{(a)} = 8 \frac{\bar{Z}[145|236]}{Z} = 8 \left\{ \frac{\bar{Z}[14|26]}{Z} - \frac{\bar{Z}[13|26]}{Z} \right\} = \frac{3}{2} - \frac{2}{\pi} + \frac{4}{\pi^2} - \frac{32}{\pi^3}. \quad (2.30)$$

For type (b), we may assume, up to a factor 4, that nodes 2 and 4 are predecessors of node 5, and that node 5 is connected to node 1. Such spanning trees are in one-to-one correspondence with the spanning forests associated with the partition  $\sigma = 1356|2|4$ , by removing the edges  $\{2, 5\}$  and  $\{4, 5\}$ , so that  $X_2^{(b)} = 4\bar{Z}[1356|2|4]/Z$ . This can be further simplified by observing that  $\bar{Z}[136|2|4] = \bar{Z}[1356|2|4] + \bar{Z}[136|2|45] = 2\bar{Z}[1356|2|4]$ , because the forests of type  $136|2|45$  are uniquely related to those of type  $1356|2|4$  by connecting node 5 with node 1, rather than with node 4. Therefore we have

$$X_2^{(b)} = 4 \frac{\bar{Z}[1356|2|4]}{Z} = 2 \frac{\bar{Z}[136|2|4]}{Z} = -\frac{5}{4} + \frac{5}{\pi} + \frac{2}{\pi^2} - \frac{16}{\pi^3}. \quad (2.31)$$

Putting these results together, one finds the following expression for the height-three probability:

$$\mathbb{P}_3 = \mathbb{P}_2 + \frac{X_2}{2} = \mathbb{P}_2 + \frac{1}{2}(X_2^{(a)} + X_2^{(b)}) = \frac{3}{8} + \frac{1}{\pi} - \frac{12}{\pi^3} \simeq 0.3063. \quad (2.32)$$

The last probability is simply obtained by subtraction:

$$\mathbb{P}_4 = 1 - \mathbb{P}_1 - \mathbb{P}_2 - \mathbb{P}_3 = \frac{3}{8} - \frac{1}{2\pi} + \frac{1}{\pi^2} + \frac{4}{\pi^3} \simeq 0.4462. \quad (2.33)$$

Although all single-site probabilities are polynomials in  $1/\pi$ , it looks surprising that the *mean height* (also called the *sandpile density*),

$$\langle h \rangle = \sum_{a=1}^4 a \mathbb{P}_a = \frac{25}{8}, \quad (2.34)$$

is a rational number; a conjecture first made by Grassberger in the 1990s from numerical evaluations of height probabilities (in unpublished work). The proof of this result was given in two independent articles [91, 134], via the relation between the mean height and the *return probability* for the loop-erased random walk (LERW, defined in Chapter 3),

$$\mathbb{P}_{\text{ret}} = \frac{\langle h \rangle}{2} - \frac{5}{4} = \frac{5}{16}, \quad (2.35)$$

established in [108, 132]. Here  $\mathbb{P}_{\text{ret}}$  is the probability that a LERW started at the origin  $(0,0)$  of the square lattice and growing toward infinity visits one of its nearest neighbors (e.g.  $(1,0)$ ). The explicit value of  $\mathbb{P}_{\text{ret}}$  was computed in [134] in terms of dimer arrangements, and in [91] in terms of partition functions for spanning forests; thus proving Grassberger's conjecture, and yielding an independent check for the height probabilities  $\mathbb{P}_a$  computed in [25, 81, 111, 137]. However, both techniques still involved powers of  $1/\pi$  in intermediary steps, whose final cancellation remained unexplained.

More recently, Kassel and Wilson [84] gave a simple formula to compute  $\mathbb{P}_{\text{ret}}$  on any planar graph, which made it finally clear why this probability is rational for many (but not all) regular lattices. The mean height can then be obtained from  $\mathbb{P}_{\text{ret}}$  through the generalization of Eq. (2.35), namely [108]

$$\langle h \rangle = \frac{\delta \mathbb{P}_{\text{ret}} + \delta + 1}{2}, \quad (2.36)$$

where  $\delta$  denotes the mean degree of the graph.

## 2.3 Multisite probabilities on the plane

The bijection between recurrent sandpile configurations and spanning trees can in principle be used to compute multisite probabilities of an arbitrary number of heights located at sites  $i_1, \dots, i_n$ . As we eventually want to compare the joint probabilities with conformal correlators, we are especially interested in the regime where all sites are mutually separated by large distances.

As explained in Section 2.2, handling heights 1 poses no serious problem. Counting the configurations where certain sites have a height 1 can be done by computing the total number of recurrent configurations on a locally modified graph, such that each site with height 1 has only one nearest neighbor left (thereby forcing each such site to be a leaf). Multisite height-one probabilities were computed long ago thanks to this technique ([111] for 2-site, [110] for up to 4-site, and [49, 79] for general  $n$ -site).

The computation of a joint probability with two or more heights strictly larger than 1 can in principle be done by using Theorem 1.5. However, in order to invert the linear relations and calculate the grove fractions of interest, the grove theorem requires to work with an annular-one graph, in which the nodes—the sites where the prescribed heights are located, along with their close neighbors—are on the boundary of a single inner face, from which the zipper goes off to infinity. In case the nodes are separated by large distances, this means cutting from the original graph  $\mathbb{Z}^2$  an unboundedly large number of edges to put all the nodes around the same face. This brings two major technical complications: (i) the removal of a large number of edges defines a nonlocal (i.e. macroscopic) modification of the original graph, which makes the calculation of the modified Green function and its derivative much more complicated (for instance the Woodbury formula would require inverting a matrix of unbounded rank), and (ii) the number of groves of interest on the modified graph increases exponentially with the number of removed edges. Approaches involving graphs with more than one inner face and as many zippers, or using a matrix connection, might be more suitable for these computations. However, such generalizations are currently not well enough understood. As a result, the lattice large-distance joint prob-

abilities  $\mathbb{P}_{a,b}(\vec{r})$  of two heights  $a, b > 1$  remain unknown to date (note however that conformal theory predicts their correlations  $\mathbb{P}_{a,b}(\vec{r}) - \mathbb{P}_a \mathbb{P}_b$  to decay like  $\log^2 r / r^4$  for large distance  $r$ ).

The third possible class of joint probabilities, namely those containing a single height larger than or equal to 2, is somewhat simpler. In this class, the only known results concern the three probabilities  $\mathbb{P}_{a,1}(\vec{r})$  that site  $i$  has height  $a = 2, 3$  or 4 and site  $j$  has height 1, when the distance  $r = |i - j|$  is large. Using graph-theoretical techniques developed earlier in [137], it was shown that  $\mathbb{P}_{a,1}(\vec{r}) = \mathbb{P}_a \mathbb{P}_1 + (c_a + d_a \log r) / r^4 + \mathcal{O}(r^{-6} \log^k r)$  for large distance  $r$ , with numerical constants  $c_a, d_a$  explicitly known [130, 131].

In this section, we show how to compute  $\mathbb{P}_{a,1}(\vec{r})$ ,  $a = 2, 3, 4$ , in a more efficient way using the grove theorem and the local graph modifications explained above to handle the height 1. In addition, we extend the known results by explicitly computing the subleading contributions in  $r^{-6}$ . As expected, these subleading terms are not rotationally invariant. We then apply the same method to compute three-site probabilities  $\mathbb{P}_{a,1,1}$  for  $a = 2, 3, 4$ . For the purpose of comparing with field-theoretical correlation functions, it is not the joint probabilities we want to compute, but the correlators

$$\sigma_{a,b}(i_1, i_2) = \mathbb{E} \left[ (\delta_{h_{i_1}, a} - \mathbb{P}_a) (\delta_{h_{i_2}, b} - \mathbb{P}_b) \right] = \mathbb{P}_{a,b}(\vec{r}) - \mathbb{P}_a \mathbb{P}_b, \quad (2.37)$$

and

$$\sigma_{a,b,c}(i_1, i_2, i_3) = \mathbb{E} \left[ (\delta_{h_{i_1}, a} - \mathbb{P}_a) (\delta_{h_{i_2}, b} - \mathbb{P}_b) (\delta_{h_{i_3}, c} - \mathbb{P}_c) \right], \quad (2.38)$$

here restricted to  $b = c = 1$ . As we shall see, because of the subtractions, the calculation of three-site correlators requires the knowledge of two-site probabilities to order  $r^{-6}$ . Higher-order multisite probabilities  $\mathbb{P}_{a,1,\dots,1}$  with more heights 1 could be obtained in the same fashion.

### 2.3.1 Two-site probabilities

As mentioned above, the two-site height-one correlation is well known. We simply recall the result, referring to [111] for further details. If the two heights 1 are located at sites  $i$  and  $j$ , and for  $\vec{r} \equiv j - i = r e^{i\varphi}$ , then

to order 6 in the inverse distance, it is given by

$$\sigma_{1,1}(\vec{r}) = -\frac{\mathbb{P}_1^2}{2r^4} - \frac{4(\pi-2)}{\pi^6 r^6} \{1 + (\pi-2) \cos 4\varphi\} + \mathcal{O}(r^{-7}), \quad (2.39)$$

where the asymptotic series for the Green function given in (A.3) has been used.

For the next case, we assume that site  $i$  (chosen to be the origin) has height 2 while site  $j$  has height 1, and we compute  $\mathbb{P}_{2,1}(\vec{r})$ . From the discussion in Section 2.1.3, it is given, in terms of spanning tree fractions, by

$$\mathbb{P}_{2,1}(\vec{r}) = \mathbb{P}_{1,1}(\vec{r}) + \frac{1}{12} X_{1,0}(\vec{r}), \quad (2.40)$$

where  $X_{1,0}(\vec{r})$  is the fraction of spanning trees rooted at infinity such that  $i$  has exactly one predecessor among its nearest neighbors, while  $j$  has none. As we have seen before, the fact that  $j$  is a leaf may be enforced by removing the connections with three of its nearest neighbors. There are four different ways to do so, but they are all equivalent. Choosing any specific one and multiplying by 4, we can write

$$\mathbb{P}_{2,1}(\vec{r}) = \mathbb{P}_{1,1}(\vec{r}) + \frac{1}{3} \tilde{X}_1(\vec{r}), \quad (2.41)$$

where  $\tilde{X}_1(\vec{r})$  denotes the fraction of spanning trees in which  $i$  has exactly one predecessor among its neighbors, but on the lattice  $\tilde{\mathcal{G}}$  obtained from  $\mathcal{G} = \mathbb{Z}^2$  by removing three edges around  $j$  (in a fixed way, like those shown in Fig. 2.9). As argued in Section 2.1.3, the calculation of  $\mathbb{P}_{2,1}(\vec{r})$  on  $\mathbb{Z}^2$  amounts to computing the height-two probability at a single site but on a lattice that has been modified at a distance  $r$ . The modification around site  $j$  however brings two complications.

The first one is that the removal of three edges at  $j$  breaks the rotational invariance around  $i$ . As a consequence, the question of which one of its nearest neighbors, S, W, N or E, is the predecessor of  $i$  matters because the four cases are no longer equivalent. They are however related by rotations if we simultaneously rotate the height 1. If we denote by  $\tilde{X}_1^S(\vec{r})$  the fraction of spanning trees (on  $\tilde{\mathcal{G}}$ ) in which the southern nearest neighbor of  $i$  is its predecessor, we obtain

$$\tilde{X}_1(\vec{r}) = \tilde{X}_1^S(\vec{r}) + \tilde{X}_1^S(e^{i\pi/2}\vec{r}) + \tilde{X}_1^S(e^{i\pi}\vec{r}) + \tilde{X}_1^S(e^{3i\pi/2}\vec{r}). \quad (2.42)$$

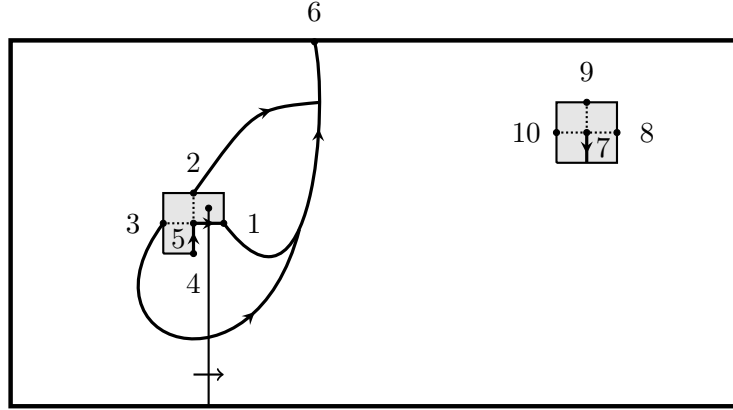


Figure 2.9: Geometrical setting used for the computation of  $\mathbb{P}_{2,1}(\vec{r})$ . The dotted lines represent the removed edges. Node 5 is still at the origin, while site number 7 is located at a large distance  $\vec{r}$ .

In each case, there are still three different possibilities for the arrow going out from  $i$ , but they are equivalent. Up to a factor 3, we can therefore choose to orient it toward its eastern neighbor (node 1) like we did in Section 2.2, see Fig. 2.7.

The calculation of  $\tilde{X}_1^S(\vec{r})$  closely follows that of  $X_1$  carried out in Section 2.2. There the fraction  $X_1^S = \frac{1}{4}X_1$  was expressed as a single grove partition on a lattice modified by the removal of the two edges  $\{5, 2\}$  and  $\{5, 3\}$ . That expression is still valid in the present context, as is the ensuing formula (2.28), which here reads

$$\tilde{X}_1^S(\vec{r}) = 3 \frac{\bar{Z}}{Z} \times \left[ (\bar{G}_{4,4} - \bar{G}_{4,5}) - (\bar{G}_{3,4} - \bar{G}_{3,5} - \bar{G}'_{3,4} + \bar{G}'_{3,5} - \bar{G}'_{4,5}) \right], \quad (2.43)$$

provided we keep in mind that the modifications referred to by the bar are made to the lattice  $\tilde{\mathcal{G}}$ , itself a modification of  $\mathbb{Z}^2$ . Therefore, the full changes on the lattice involve the removal of five edges, two around  $i$  and three around  $j$ , for which a total of seven sites are concerned. In addition to the three nodes 5 ( $= i$ ), 2 and 3, we denote the other four (interior) sites by 7 ( $= j$ ), 8, 9 and 10, as shown in Fig. 2.9.

This double modification of the lattice brings a second technical complication. According to the discussion in Appendix A.3, it requires computing the derivative of the Green function  $G'$  for most pairs of sites among

the seven sites  $\{2, 3, 5, 7, 8, 9, 10\}$  that are concerned, in particular for sites that are far away from the zipper. When the two sites are close to the head of the zipper, the technique already used in the previous section is sufficient. If however one of the two sites is far from the zipper, one sees from the general expression (1.28) giving the derivative of the Green function, that an extra asymptotic analysis is needed. If both sites are far from the zipper, yet another, distinct analysis is required. It is simpler since the use of the asymptotic form of the Green function itself is permitted. Details for these two cases are given in Appendix A.3.

At any rate, after some algebra, we find the following expression for the function  $\tilde{X}_1^S(\vec{r})$  in polar coordinates  $\vec{r} = re^{i\varphi}$ , exact to order  $r^{-6}$  ( $\gamma = 0.577216\dots$  is the Euler constant),

$$\begin{aligned}
\tilde{X}_1^S(\vec{r}) = & \frac{3(\pi-2)(64-20\pi-2\pi^2+\pi^3)}{8\pi^6} - \frac{3(\pi-2)^2 \sin \varphi}{4\pi^6 r^3} \\
& - \frac{3(\pi-2)}{2\pi^6 r^4} \left\{ (\pi-2) \left[ \log r + \gamma + \frac{3}{2} \log 2 \right] + \cos 2\varphi + 10 - \frac{7\pi}{2} \right\} \\
& + \frac{3(\pi-2) \sin \varphi}{4\pi^6 r^5} \left\{ 4 \left[ \log r + \gamma + \frac{3}{2} \log 2 \right] - (4\pi-7) \cos 4\varphi \right. \\
& \quad \left. - (2\pi-3) \cos 2\varphi - \frac{1}{4}(\pi^2+16\pi+16) \right\} \\
& - \frac{1}{8\pi^6 r^6} \left\{ 12(\pi-2) \left[ 1 + 2(\pi-2) \cos 4\varphi \right] \left[ \log r + \gamma + \frac{3}{2} \log 2 \right] \right. \\
& \quad + \frac{3}{2}(9\pi^3-30\pi^2+58\pi-62) \cos 6\varphi - (\pi-2)(97\pi-266) \cos 4\varphi \\
& \quad \left. + \frac{3}{2}(9\pi^3-36\pi^2+38\pi+2) \cos 2\varphi + \frac{3}{2}(\pi^3-3\pi^2-60\pi+148) \right\} + \dots
\end{aligned} \tag{2.44}$$

The summation in (2.42) over the four rotations eliminates all terms whose angular dependence is not a periodic function of  $4\varphi$ , in particular the odd powers of  $r^{-1}$ . The formula (2.41) yields our final result for the correlation  $\sigma_{2,1}(\vec{r})$ , exact to order  $r^{-6}$ ,

$$\begin{aligned}
\sigma_{2,1}(\vec{r}) = & -\frac{\mathbb{P}_1^2}{2r^4} \left\{ \left( \log r + \gamma + \frac{3}{2} \log 2 \right) + \frac{16-5\pi}{2(\pi-2)} \right\} \\
& - \frac{\pi-2}{\pi^6 r^6} \left\{ 2 \left( 1 + 2(\pi-2) \cos 4\varphi \right) \left( \log r + \gamma + \frac{3}{2} \log 2 \right) \right. \\
& \quad \left. - \frac{1}{6}(73\pi-218) \cos 4\varphi + \frac{\pi^3-3\pi^2-44\pi+116}{4(\pi-2)} \right\} + \mathcal{O}(r^{-7}).
\end{aligned} \tag{2.45}$$

The calculation of  $\mathbb{P}_{3,1}(\vec{r})$  proceeds in exactly the same way. Referring to the decomposition of  $\mathbb{P}_3$  in Section 2.2, we write

$$\begin{aligned}\mathbb{P}_{3,1}(\vec{r}) &= \mathbb{P}_{2,1}(\vec{r}) + \frac{1}{8}X_{2,0}(\vec{r}) = \mathbb{P}_{2,1}(\vec{r}) + \frac{1}{2}\tilde{X}_2(\vec{r}) \\ &= \mathbb{P}_{2,1}(\vec{r}) + \frac{1}{2}\left(\tilde{X}_2^{(a)}(\vec{r}) + \tilde{X}_2^{(b)}(\vec{r})\right),\end{aligned}\tag{2.46}$$

where the tilde refers to fractions of spanning trees on the lattice  $\tilde{\mathcal{G}}$ . The fractions  $\tilde{X}_2^{(a)}$  (resp.  $\tilde{X}_2^{(b)}$ ) can be further decomposed into four (resp. two) contributions related by rotations, depending on whether the two predecessors of  $i$  form the pair SE, EN, NW or WS (resp. SN or WE). The calculation then reduces to the computation of the two functions  $\tilde{X}_2^{(a),\text{SE}}(\vec{r})$  and  $\tilde{X}_2^{(b),\text{SN}}(\vec{r})$ , given in terms of the same groves as in Section 2.2, but on the modified lattice  $\tilde{\mathcal{G}}$ . The required Green functions and derivatives thereof are the same as those we needed for  $\mathbb{P}_{2,1}$ .

The final result, to order  $r^{-6}$ , reads

$$\begin{aligned}\sigma_{3,1}(\vec{r}) &= -\frac{(\pi-2)(8-\pi)}{\pi^6 r^4} \left\{ \left( \log r + \gamma + \frac{3}{2} \log 2 \right) - \frac{40-2\pi-\pi^2}{2(8-\pi)} \right\} \\ &\quad - \frac{1}{\pi^6 r^6} \left\{ (8-\pi) \left( 1 + 2(\pi-2) \cos 4\varphi \right) \left( \log r + \gamma + \frac{3}{2} \log 2 \right) \right. \\ &\quad \left. + \frac{1}{12}(\pi-2)(12\pi^2+37\pi-584) \cos 4\varphi + \frac{1}{8}(5\pi^2+50\pi-272) \right\} + \mathcal{O}(r^{-7}).\end{aligned}\tag{2.47}$$

We do not write explicitly the last correlator  $\sigma_{4,1}(\vec{r})$ , easily obtained by subtraction,

$$\sigma_{4,1}(\vec{r}) = -\sigma_{1,1}(\vec{r}) - \sigma_{2,1}(\vec{r}) - \sigma_{3,1}(\vec{r}).\tag{2.48}$$

The dominant terms, proportional to  $r^{-4}$ , in the above expressions of  $\sigma_{a,1}(\vec{r})$  for  $a > 1$ , reproduce the results of [131].

### 2.3.2 Three-site probabilities

We now turn to three-site joint probabilities  $\mathbb{P}_{a,1,1}$  with two heights equal to 1. While  $\mathbb{P}_{1,1,1}$  is known [110], the functions  $\mathbb{P}_{a,1,1}$  for  $a \geq 2$  are new. The way they can be computed follows exactly the way  $\mathbb{P}_{a,1}$  was

computed. The core of the calculation relies on that of  $\mathbb{P}_a$ , which used the grove theorem on the modified lattice  $\bar{\mathcal{G}}$  (see Section 2.2). A second modification around the height 1 allowed the computation of  $\mathbb{P}_{a,1}$ ; now a third (similar) modification around the second height 1 is what is needed to carry out the calculation of  $\mathbb{P}_{a,1,1}$ .

Let us denote by  $i_1, i_2, i_3$  the three sites with height  $a, 1, 1$  respectively. By translation invariance, the joint probability only depends on the two vectors  $\vec{r}_{12} = i_2 - i_1$  and  $\vec{r}_{13} = i_3 - i_1$ . As the dominant term of the connected correlator  $\sigma_{a,1,1}$ ,

$$\begin{aligned} \sigma_{a,1,1}(\vec{r}_{12}, \vec{r}_{13}) &= \mathbb{P}_{a,1,1}(\vec{r}_{12}, \vec{r}_{13}) - \mathbb{P}_a \mathbb{P}_{1,1}(\vec{r}_{23}) - \mathbb{P}_1 \mathbb{P}_{a,1}(\vec{r}_{13}) \\ &\quad - \mathbb{P}_1 \mathbb{P}_{a,1}(\vec{r}_{12}) + 2 \mathbb{P}_a \mathbb{P}_1^2, \end{aligned} \quad (2.49)$$

is expected to be of overall order six in the distances, the knowledge of  $\mathbb{P}_{a,1}(\vec{r})$  up to that order is required, as anticipated above.

For the sake of simplicity, we assume the three sites  $i_1, i_2, i_3$  to be aligned horizontally, so that the vectors  $\vec{r}_{12}$  and  $\vec{r}_{13}$  can be chosen to be along the real axis,  $\vec{r}_{12} = (x_{21}, 0)$  and  $\vec{r}_{13} = (x_{31}, 0)$ . Up to homogeneous terms of order seven or higher in the distances, the three-point correlators read

$$\sigma_{1,1,1}(\vec{r}_{12}, \vec{r}_{13}) = 0 + \dots, \quad (2.50)$$

$$\sigma_{2,1,1}(\vec{r}_{12}, \vec{r}_{13}) = \frac{(\pi - 2)^3}{\pi^9} \frac{1}{x_{21}^3 x_{31}^3} + \dots, \quad (2.51)$$

$$\sigma_{3,1,1}(\vec{r}_{12}, \vec{r}_{13}) = \frac{(\pi - 2)^2 (8 - \pi)}{2\pi^9} \frac{1}{x_{21}^3 x_{31}^3} + \dots, \quad (2.52)$$

$$\sigma_{4,1,1}(\vec{r}_{12}, \vec{r}_{13}) = -\frac{(\pi - 2)^2 (\pi + 4)}{2\pi^9} \frac{1}{x_{21}^3 x_{31}^3} + \dots \quad (2.53)$$

The last correlator  $\sigma_{4,1,1}$  was obtained from the sum rule  $\sum_a \sigma_{a,1,1} = 0$ .

Two observations can be made about these results: (a)  $\sigma_{1,1,1}$  vanishes identically at dominant order, and therefore also in the scaling limit, and (b) the other  $\sigma_{a,1,1}$ 's for  $a \geq 2$  are not logarithmic, unlike the 2-correlators  $\sigma_{a,1}$ . As we shall argue later on, when we discuss the conformal point of view on these correlators, the property (b) is a consequence of (a) and the interpretation of the height-two, height-three and height-four variables as logarithmic partners of the height-one variable, in the

scaling limit. The physical reason as to why the correlation of three heights 1 vanishes remains however unclear.

## 2.4 Probabilities on the upper half-plane

Another case of interest is the lattice computation of height correlations on the upper half-plane (UHP)  $\{(x, y) \in \mathbb{Z}^2 | y > 0\}$ . Again we are interested in the comparison with conformal correlators, so we consider sites separated by large distances. We start by recalling the well-known one-site probabilities  $\mathbb{P}_a(i)$  on the UHP computed in [18] for  $a = 1$  and in [81] for  $a = 2, 3, 4$ . We compare them with the corresponding (new) probabilities on the diagonal upper half-plane (DUHP)  $\{(x, y) \in \mathbb{Z}^2 | y > x\}$ .

We then compute the joint probabilities  $\mathbb{P}_{a,1}(i, j)$  for two heights, a height  $a$  at site  $i$  and a height 1 at site  $j$ . The site  $i$  is chosen to be in the bulk of the UHP (i.e. far from the boundary), while we consider two cases for  $j$ : in the first simpler case,  $j$  is on the boundary of the UHP, and in the second case,  $j$  is also in the bulk and far from  $i$ . The case when the two heights are located on the boundary has been completely solved, for all height values, in [128].

### 2.4.1 One-site probabilities on the upper half-plane

On the upper half-plane with a horizontal boundary, the computations are very similar to those of Sections 2.2 and 2.3, except that the lattice Green functions are those of the UHP. The boundary is the line of sites at  $y = 1$  with boundary condition either fully open or fully closed. The relevant, well-known Green functions are easily found using the image method:

$$G_{(u_1, u_2), (v_1, v_2)}^{\text{op}} = G_{(u_1, u_2), (v_1, v_2)} - G_{(u_1, u_2), (v_1, -v_2)}, \quad (2.54)$$

$$G_{(u_1, u_2), (v_1, v_2)}^{\text{cl}} = G_{(u_1, u_2), (v_1, v_2)} + G_{(u_1, u_2), (v_1, 1-v_2)}, \quad (2.55)$$

where  $G_{u,v}$  is the Green function on the full plane  $\mathbb{Z}^2$  (see Appendix A.1). The UHP with either boundary condition is invariant under horizontal translations, so we can choose without loss of generality the site  $i$  to be

located at  $(0, y)$ . Again we define an annular-one graph  $\bar{\mathcal{G}}$  obtained from  $\mathcal{G} = \mathbb{Z} \times \mathbb{N}^*$  by removing edges between  $i$  and two of its neighbors, so that  $i$  and its four neighbors lie around a single face on  $\bar{\mathcal{G}}$ .

The technique presented in Section 1.4 for the computation of grove probabilities works on the UHP as on the full plane, with however the new feature that the zipper can be taken to be finite or infinite, depending on whether it goes from the marked face to the boundary or off to infinity. As shown in Appendix A.2, the two choices are equivalent but the infinite version is more convenient for practical calculations, since the derivative of the Green function on the UHP can then be written as a linear combination of that on the full plane. Therefore, we choose a zipper going upward to infinity with a nontrivial parallel transport  $z$  on the horizontal edges oriented to the left, namely  $\phi_{(1, y+m), (0, y+m)} = z$  for  $m \geq 1$ , see Fig. 2.10. Then, as shown in Appendix A.2, the derivative of the Green function on the upper half-plane reads:

$$\begin{aligned} G'_{(u_1, u_2), (v_1, v_2)}{}^{\text{op}} &= -G'_{(u_1, -u_2+y+1), (v_1, -v_2+y+1)} - G'_{(u_1, u_2+y+1), (v_1, v_2+y+1)} \\ &\quad + G'_{(u_1, -u_2+y+1), (v_1, v_2+y+1)} + G'_{(u_1, u_2+y+1), (v_1, -v_2+y+1)}, \end{aligned} \quad (2.56)$$

$$\begin{aligned} G'_{(u_1, u_2), (v_1, v_2)}{}^{\text{cl}} &= -G'_{(u_1, -u_2+y+1), (v_1, -v_2+y+1)} - G'_{(u_1, u_2+y), (v_1, v_2+y)} \\ &\quad - G'_{(u_1, -u_2+y+1), (v_1, v_2+y)} - G'_{(u_1, u_2+y), (v_1, -v_2+y+1)}. \end{aligned} \quad (2.57)$$

where  $G'$  on the full plane is computed with respect to the zipper described in Section 2.2 (that is, going down).

The presence of the boundary means that predecessor diagrams are no longer invariant under rotations. In the case of  $\mathbb{P}_2(i)$  for example, one has to compute the fraction  $X_1(i)$  of spanning trees such that  $i$  has exactly one predecessor among its neighbors, either North, East, South or West, see Fig. 2.11. The equality  $X_1^{\text{E}}(i) = X_1^{\text{W}}(i)$  stills holds on the UHP because of the left-right symmetry, so that there are actually three distinct diagrams to consider. In addition, the other two diagrams are related by the following identities,

$$\begin{aligned} X_1^{\text{N}}(i) \Big|_{y \rightarrow -y} &= X_1^{\text{S}}(i) \quad \text{for open b.c.}, \\ X_1^{\text{N}}(i) \Big|_{y \rightarrow 1-y} &= X_1^{\text{S}}(i) \quad \text{for closed b.c.}, \end{aligned} \quad (2.58)$$

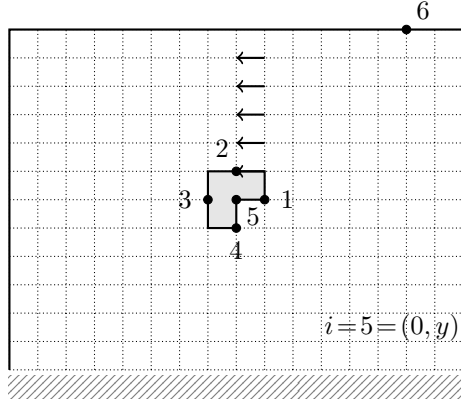


Figure 2.10: Choice of nodes and zipper for the computation of joint height probabilities on the upper half-plane. The zipper extends up to infinity.

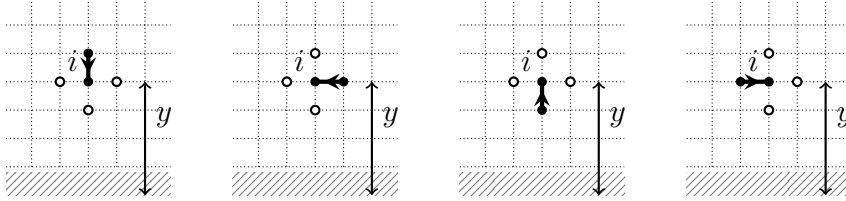


Figure 2.11: The four distinct diagrams contributing to  $X_1(i)$  on the upper half-plane. Neighbors of  $i$  drawn as open circles are *not* predecessors of  $i$ . The boundary of the graph, i.e. the lowest row of sites still included in the graph, is located at  $y = 1$ .

which we prove in Appendix B. The combinatorial significance of these relations is not clear to us.

Although there are roughly twice as many diagrams as for the full plane, their computation procedure using the grove theorem is similar, so we simply mention the final results for one-site height probabilities. We give their expansions in terms of the distance  $r$  between the reference site  $i$  located at  $(0, y)$  and the symmetry axes used in the method of images, namely  $y = 0$  (open boundary) and  $y = 1/2$  (closed boundary):

$$r = y \quad (\text{open b.c.}), \quad r = y - \frac{1}{2} \quad (\text{closed b.c.}) \quad (2.59)$$

For the two boundary conditions, the results read:

$$\sigma_a^{\text{op}}(r) = \frac{1}{r^2} \left( c_a + \frac{d_a}{2} + d_a \log r \right) + \frac{1}{r^4} \left( \frac{c_a}{4} + e_a + \frac{d_a}{4} \log r \right) + \mathcal{O}(r^{-5}), \quad (2.60a)$$

$$\sigma_a^{\text{cl}}(r) = -\frac{1}{r^2} (c_a + d_a \log r) - \frac{1}{r^4} \left( \frac{c_a}{4} + f_a + \frac{d_a}{4} \log r \right) + \mathcal{O}(r^{-5}), \quad (2.60b)$$

with the various coefficients  $c_a, d_a, e_a, f_a$  given in Table 2.1. The dominant terms in  $r^{-2}$ , depending on  $c_a, d_a$  only, were first obtained in [81], whereas the lower-order terms in  $r^{-4}$  are new.

### 2.4.2 One-site probabilities on the diagonal upper half-plane

In addition to the usual upper half-plane with a horizontal boundary, we examine a new form of semi-infinite lattice, namely the diagonal upper half-plane (DUHP), defined as  $\{(x, y) \in \mathbb{Z}^2 | y > x\}$ . Indeed, we note that the Green functions for open and closed boundary conditions can be obtained quite simply by the method of images, and read:

$$G_{(u_1, u_2), (v_1, v_2)}^{\text{op}} = G_{(u_1, u_2), (v_1, v_2)} - G_{(u_1, u_2), (v_2, v_1)}, \quad (2.61)$$

$$G_{(u_1, u_2), (v_1, v_2)}^{\text{cl}} = G_{(u_1, u_2), (v_1, v_2)} + G_{(u_1, u_2), (v_2-1, v_1+1)}. \quad (2.62)$$

Without loss of generality, we can choose the same nodes and zipper as the ones on the UHP (see Fig. 2.12). The derivatives of the Green functions on the DUHP are then given by:

$$\begin{aligned} G'_{(u_1, u_2), (v_1, v_2)}^{\text{op}} &= -G'_{(u_1, y+1-u_2), (v_1, y+1-v_2)} + G'_{(u_1, y+1-u_2), (v_2, y+1-v_1)} \\ &\quad + G'_{(u_2, y+1-u_1), (v_1, y+1-v_2)} - G'_{(u_2, y+1-u_1), (v_2, y+1-v_1)}, \end{aligned} \quad (2.63)$$

$$\begin{aligned} G'_{(u_1, u_2), (v_1, v_2)}^{\text{cl}} &= -G'_{(u_1, y+1-u_2), (v_1, y+1-v_2)} - G'_{(u_1, y+1-u_2), (v_2-1, y-v_1)} \\ &\quad - G'_{(u_2-1, y-u_1), (v_1, y+1-v_2)} - G'_{(u_2-1, y-u_1), (v_2-1, y-v_1)}, \end{aligned} \quad (2.64)$$

where  $G'$  on the full plane is computed with respect to the zipper described in Section 2.2.

	$c_a$	$d_a$	$e_a$	$f_a$
$a = 1$	$\frac{\pi-2}{2\pi^3}$	0	$\frac{\pi+4}{32\pi^3}$	$\frac{8-\pi}{32\pi^3}$
$a = 2$	$\frac{\pi-2}{2\pi^3} (\gamma + \frac{5}{2}\log 2) + \frac{34-11\pi}{8\pi^3}$	$\frac{\pi-2}{2\pi^3}$	$\frac{-76-52\pi+9\pi^2}{384\pi^3}$	$\frac{-196-28\pi+9\pi^2}{384\pi^3}$
$a = 3$	$\frac{8-\pi}{4\pi^3} (\gamma + \frac{5}{2}\log 2) + \frac{-88+5\pi+2\pi^2}{16\pi^3}$	$\frac{8-\pi}{4\pi^3}$	$\frac{8+23\pi}{384\pi^3}$	$\frac{104+17\pi}{384\pi^3}$
$a = 4$	$-\frac{\pi+4}{4\pi^3} (\gamma + \frac{5}{2}\log 2) + \frac{36+9\pi-2\pi^2}{16\pi^3}$	$-\frac{\pi+4}{4\pi^3}$	$\frac{20+17\pi-9\pi^2}{384\pi^3}$	$\frac{-4+23\pi-9\pi^2}{384\pi^3}$

Table 2.1: Numerical coefficients for one-site probabilities on the upper half-plane.

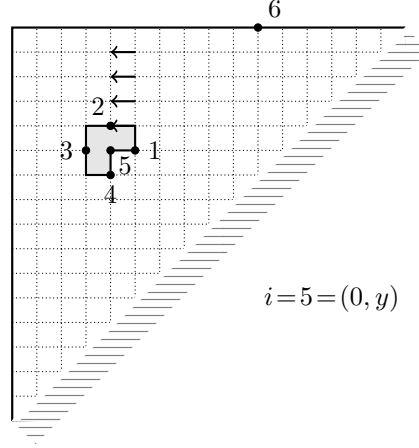


Figure 2.12: Choice of nodes and zipper for the computation of height probabilities on the diagonal upper half-plane. The zipper extends up to infinity.

For the two boundary conditions, we write the results in terms of the Euclidean distance  $r$  between the reference site  $i = (0, y)$  and the reflection axes used in the method of images, namely  $y = x$  (open boundary) and  $y = x + 1$  (closed boundary), so that

$$r = \frac{y}{\sqrt{2}} \quad (\text{open b.c.}), \quad r = \frac{y-1}{\sqrt{2}} \quad (\text{closed b.c.}). \quad (2.65)$$

We find that one-site probabilities on the DUHP read:

$$\sigma_a^{\text{op}}(r) = \frac{1}{r^2} \left( c_a + \frac{d_a}{2} + d_a \log r \right) - \frac{1}{r^4} \left( \frac{c_a}{4} - \tilde{e}_a + \frac{d_a}{4} \log r \right) + \mathcal{O}(r^{-5}), \quad (2.66a)$$

$$\sigma_a^{\text{cl}}(r) = -\frac{1}{r^2} (c_a + d_a \log r) + \frac{1}{r^4} \left( \frac{c_a}{4} - \tilde{f}_a + \frac{d_a}{4} \log r \right) + \mathcal{O}(r^{-5}). \quad (2.66b)$$

The dominant terms in  $r^{-2}$  of  $\sigma_a^{\text{op,cl}}$  are identical on the UHP and the DUHP, as expected. However, the subleading terms in  $r^{-4}$  differ for  $a > 1$ , in the numerical values of the coefficients  $\tilde{e}_a, \tilde{f}_a$ , listed in Table 2.2, and in the overall sign, which, strangely enough, gets swapped.

	$a = 1$	$a = 2$	$a = 3$	$a = 4$
$\tilde{e}_a$	$\frac{\pi+4}{32\pi^3}$	$\frac{-224+22\pi+9\pi^2}{384\pi^3}$	$\frac{152-7\pi}{192\pi^3}$	$\frac{-128-20\pi-9\pi^2}{384\pi^3}$
$\tilde{f}_a$	$\frac{8-\pi}{32\pi^3}$	$\frac{-368+58\pi+9\pi^2}{384\pi^3}$	$\frac{224-13\pi}{192\pi^3}$	$\frac{-176-20\pi-9\pi^2}{384\pi^3}$

Table 2.2: Numerical coefficients for one-site probabilities on the diagonal upper half-plane.

### 2.4.3 Mixed bulk-boundary two-site correlations

In this first case, we compute the two-point probabilities  $\mathbb{P}_{a,1}$ , when the height  $a$  is in the bulk of the UHP, far from the boundary, and the height 1 is on the boundary. For simplicity, we have considered the situation where the two heights are vertically aligned, namely  $h_i = a$  at  $i = (0, y)$  and  $h_j = 1$  at  $j = (0, 1)$ . As before, we actually compute the correlations,

$$\sigma_{a,1}^{\text{bound}}(y) = \mathbb{E}\left[(\delta_{h_i,a} - \mathbb{P}_a)(\delta_{h_j,1} - \mathbb{P}_1^{\text{bound}})\right] = \mathbb{P}_{a,1}(y) - \mathbb{P}_a(y)\mathbb{P}_1^{\text{bound}}, \quad (2.67)$$

where the probabilities  $\mathbb{P}_1^{\text{bound}}$  that a site on the boundary of the UHP has height 1 are given by [18]:

$$\mathbb{P}_1^{\text{op}} = \frac{9}{2} - \frac{42}{\pi} + \frac{320}{3\pi^2} - \frac{512}{9\pi^3} \simeq 0.1038, \quad \mathbb{P}_1^{\text{cl}} = \frac{3}{4} - \frac{2}{\pi} \simeq 0.1134. \quad (2.68)$$

We skip the details of the calculations and merely give the final results:

$$\sigma_{1,1}^{\text{op}}(y) = -\frac{2(\pi-2)(16-3\pi)(32-9\pi)}{9\pi^6 y^4} + \dots, \quad (2.69)$$

$$\sigma_{2,1}^{\text{op}}(y) = -\frac{(16-3\pi)(32-9\pi)}{9\pi^6 y^4} \left\{ 18 - 6\pi + 2(\pi-2) \right. \quad (2.70)$$

$$\left. \times \left( \log y + \gamma + \frac{5}{2} \log 2 \right) \right\} + \dots, \quad (2.71)$$

$$\sigma_{3,1}^{\text{op}}(y) = -\frac{(16-3\pi)(32-9\pi)}{18\pi^6 y^4} \left\{ -48 + 3\pi + \pi^2 + \right. \quad (2.72)$$

$$\left. 2(8-\pi) \left( \log y + \gamma + \frac{5}{2} \log 2 \right) \right\} + \dots, \quad (2.73)$$

$$\sigma_{1,1}^{\text{cl}}(y) = -\frac{2(\pi-2)(3\pi-8)}{\pi^5 y^4} + \dots, \quad (2.74)$$

$$\sigma_{2,1}^{\text{cl}}(y) = -\frac{3\pi-8}{\pi^5 y^4} \left\{ 20 - 7\pi + 2(\pi-2) \left( \log y + \gamma + \frac{5}{2} \log 2 \right) \right\} + \dots, \quad (2.75)$$

$$\sigma_{3,1}^{\text{cl}}(y) = -\frac{3\pi-8}{2\pi^5 y^4} \left\{ -56 + 4\pi + \pi^2 + 2(8-\pi) \left( \log y + \gamma + \frac{5}{2} \log 2 \right) \right\} + \dots \quad (2.76)$$

#### 2.4.4 Bulk two-site correlations

Here we consider the two-site probabilities  $\mathbb{P}_{a,1}(i, j)$  when both heights  $h_i = a$  and  $h_j = 1$  are in the bulk of the UHP, far from the boundary and far from each other. Again, for simplicity, we choose the two sites to be aligned vertically,  $i = (0, y_1)$  and  $j = (0, y_2)$ , with  $y_2 > y_1$ . We have computed, to total order 4 in the inverse distances, the correlations defined as

$$\begin{aligned} \sigma_{a,1}(y_1, y_2) &= \mathbb{E} \left[ (\delta_{h_i, a} - \mathbb{P}_a) (\delta_{h_j, 1} - \mathbb{P}_1) \right] \\ &= \mathbb{P}_{a,b}(y_1, y_2) - \mathbb{P}_a(y_1) \mathbb{P}_b - \mathbb{P}_a \mathbb{P}_b(y_2) + \mathbb{P}_a \mathbb{P}_b, \end{aligned} \quad (2.77)$$

and for the two boundary conditions, open and closed. In terms of the two functions

$$\begin{aligned} P(y_1, y_2) &= \frac{1}{8y_1^2 y_2^2} - \frac{1}{(y_1 - y_2)^4} - \frac{1}{(y_1 + y_2)^4}, \\ Q(y_1, y_2) &= \frac{1}{(y_1 - y_2)^4} - \frac{1}{(y_1 + y_2)^4}, \end{aligned} \quad (2.78)$$

we have found the following results,

$$\sigma_{1,1}^{\text{op}}(y_1, y_2) = \frac{2(\pi-2)^2}{\pi^6} P(y_1, y_2) + \dots, \quad (2.79)$$

$$\begin{aligned} \sigma_{2,1}^{\text{op}}(y_1, y_2) &= \frac{2(\pi-2)^2}{\pi^6} \left[ P(y_1, y_2) \left( \log y_1 + \gamma + \frac{5}{2} \log 2 \right) + Q(y_1, y_2) \log \left| \frac{y_2 + y_1}{y_2 - y_1} \right| \right] \\ &\quad - \frac{\pi-2}{16\pi^6 y_1^2 y_2^2 (y_1^2 - y_2^2)^4} \left[ 3(3\pi-10)(y_1^8 + y_2^8) + 12(58-19\pi)y_1^6 y_2^2 \right. \\ &\quad \left. + 6(482-151\pi)y_1^4 y_2^4 + 4(142-41\pi)y_1^2 y_2^6 \right] + \dots, \end{aligned} \quad (2.80)$$

$$\begin{aligned} \sigma_{3,1}^{\text{op}}(y_1, y_2) &= \frac{(\pi-2)(8-\pi)}{\pi^6} \left[ P(y_1, y_2) \left( \log y_1 + \gamma + \frac{5}{2} \log 2 \right) + Q(y_1, y_2) \log \left| \frac{y_2 + y_1}{y_2 - y_1} \right| \right] \\ &\quad - \frac{\pi-2}{32\pi^6 y_1^2 y_2^2 (y_1^2 - y_2^2)^4} \left[ (2\pi^2 + 3\pi - 72)(y_1^8 + y_2^8) - 4(10\pi^2 + 27\pi - 456)y_1^6 y_2^2 \right. \\ &\quad \left. - 6(30\pi^2 + 61\pi - 1208)y_1^4 y_2^4 - 4(10\pi^2 + 11\pi - 328)y_1^2 y_2^6 \right] + \dots \end{aligned} \quad (2.81)$$

for the open boundary condition, and

$$\sigma_{1,1}^{\text{cl}}(y_1, y_2) = \frac{2(\pi-2)^2}{\pi^6} P(y_1, y_2) + \dots, \quad (2.82)$$

$$\begin{aligned} \sigma_{2,1}^{\text{cl}}(y_1, y_2) &= \frac{2(\pi-2)^2}{\pi^6} \left[ P(y_1, y_2) \left( \log y_1 + \gamma + \frac{5}{2} \log 2 \right) + Q(y_1, y_2) \log \left| \frac{y_2 + y_1}{y_2 - y_1} \right| \right] \\ &\quad - \frac{\pi-2}{16\pi^6 y_1^2 y_2^2 (y_1^2 - y_2^2)^4} \left[ (11\pi-34)(y_1^8 + y_2^8) + 4(194-67\pi)y_1^6 y_2^2 \right. \\ &\quad \left. + 2(1498-479\pi)y_1^4 y_2^4 + 4(98-19\pi)y_1^2 y_2^6 \right] + \dots, \end{aligned} \quad (2.83)$$

$$\begin{aligned} \sigma_{3,1}^{\text{cl}}(y_1, y_2) &= \frac{(\pi-2)(8-\pi)}{\pi^6} \left[ P(y_1, y_2) \left( \log y_1 + \gamma + \frac{5}{2} \log 2 \right) + Q(y_1, y_2) \log \left| \frac{y_2 + y_1}{y_2 - y_1} \right| \right] \\ &\quad - \frac{\pi-2}{32\pi^6 y_1^2 y_2^2 (y_1^2 - y_2^2)^4} \left\{ (\pi+8)(2\pi-11)(y_1^8 + y_2^8) - 4(-536+37\pi+10\pi^2)y_1^6 y_2^2 \right. \\ &\quad \left. - 2(90\pi^2+209\pi-3832)y_1^4 y_2^4 - 4(10\pi^2-11\pi-152)y_1^2 y_2^6 \right\} + \dots \end{aligned} \quad (2.84)$$

for the closed boundary condition. As usual,  $\sigma_{4,1} = -\sigma_{1,1} - \sigma_{2,1} - \sigma_{3,1}$  for both boundary conditions.

## 2.5 Height probabilities on the triangular lattice

Let us now turn to the triangular lattice  $\mathcal{G} = \mathcal{L}_T$ , on which we compute one-site probabilities. We associate with each site  $i \in \mathcal{G}$  a height  $h_i \in \{1, 2, 3, 4, 5, 6\}$  and coordinates  $\vec{r} = (x, y) = x \vec{e}_1 + y \vec{e}_2$ , where the unit

vectors  $\vec{e}_1, \vec{e}_2$  form an angle of  $120^\circ$  (see Fig. 2.13). The six neighbors of the origin  $(0, 0)$  are therefore located at  $(1, 0)$ ,  $(1, 1)$ ,  $(0, 1)$ ,  $(-1, 0)$ ,  $(-1, -1)$  and  $(0, -1)$ . The Euclidean distance  $r$  separating  $\vec{r} = (x, y)$  from the origin  $(0, 0)$  is given by  $r^2 = x^2 + y^2 - xy$ .

### 2.5.1 On the plane

The standard graph Laplacian  $\Delta$  on  $\mathcal{G}$  with a sink  $s$  is defined by Eq. (2.1), with each vertex having degree six on the lattice. As the lattice is invariant under translations, the standard Green function  $G_{u,v} = (\Delta^{-1})_{u,v}$  only depends on the difference  $v - u \equiv (x, y)$ . Its Fourier representation reads

$$\begin{aligned} G_{u,v} &= G(v - u) \equiv G(x, y) \\ &= \int_{-\pi}^{\pi} \frac{d\theta_1}{2\pi} \int_{-\pi}^{\pi} \frac{d\theta_2}{2\pi} \frac{e^{ix\theta_1 + iy\theta_2}}{6 - 2\cos\theta_1 - 2\cos\theta_2 - 2\cos(\theta_1 + \theta_2)}. \end{aligned} \quad (2.85)$$

Due to the symmetries of the triangular lattice, the Green function satisfies twelve identities, which can be obtained by repeated applications of the two following relations,

$$G(x, y) = G(x - y, x) = G(x - y, -y), \quad (2.86)$$

corresponding respectively to a counterclockwise rotation of  $60^\circ$  and a reflection with respect to the horizontal axis. Although the integral (2.85) diverges, the difference  $G(x, y) - G(0, 0)$  is finite, as on the square

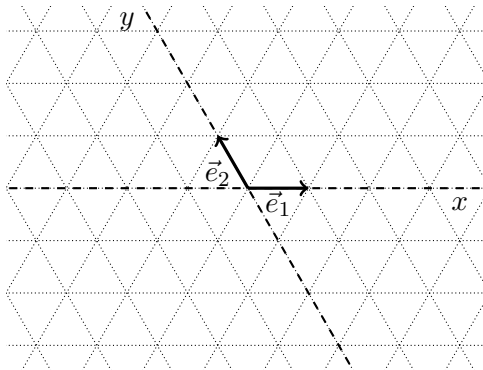


Figure 2.13: Coordinate system on the triangular lattice.

lattice. Its values for short distances, as well as its asymptotic behavior, are collected in Appendix A.

We use the same modified burning algorithm as in Section 2.1.1 to establish a relation between height probabilities and fractions of spanning trees  $X_q(i)$  on  $\mathcal{G}_s$  in which the reference site  $i$  has a fixed number  $q$  of predecessors among its neighbors. The analogue of Eq. (2.9) for the triangular lattice reads

$$\mathbb{P}_a(i) = \sum_{q=0}^{a-1} \frac{X_q(i)}{\deg_s(i) - q} = \mathbb{P}_{a-1}(i) + \frac{X_{a-1}(i)}{\deg_s(i) + 1 - a}, \quad (\mathbb{P}_0(i) \equiv 0), \quad (2.87)$$

for  $1 \leq a \leq \deg_s(i)$ , where the degree of  $i$  on  $\mathcal{G}_s$  is 6.

To compute probabilities for predecessor diagrams, we use a line bundle Laplacian  $\Delta$  with a zipper attached to the face whose lower left corner is the origin (see the left panel of Fig. 2.14). We choose here a non-trivial parallel transport  $z$  on the edges of the form  $((0, k), (1, k))$  and  $((0, k-1), (1, k))$  for  $k \leq 0$ .

The reference site  $i$  is taken to be the origin without loss of generality. The site  $i$ , its six neighbors and the sink  $s$  form the subset of selected vertices called nodes (see Section 1.3). To meet the requirement that all nodes but the sink (i.e. node 8) lie along the boundary of a single face  $f$ , we define a modified graph  $\bar{\mathcal{G}}$  by cutting the edges between  $i$  and four of its neighbors, as depicted on the right panel of Fig. 2.14. We label  $i$  and its neighbors from 1 to 7 in counterclockwise order along the boundary of  $f$ , starting at the right of the zipper.

As on the square lattice, using a line bundle Laplacian is not necessary to compute the fraction  $X_0(i)$ , which can be written in terms of the standard Green function (2.85) evaluated at  $i$  and its neighbors. Its explicit value immediately yields the height-one probability on the triangular lattice:

$$\mathbb{P}_1(i) = \frac{X_0(i)}{6} = -\frac{25}{648} - \frac{55}{72\sqrt{3}\pi} + \frac{7}{3\pi^2} + \frac{11\sqrt{3}}{\pi^3} - \frac{90}{\pi^4} + \frac{54\sqrt{3}}{\pi^5} \simeq 0.054. \quad (2.88)$$

Next we compute the fraction of spanning trees on  $\mathcal{G}_s$  such that  $i$  has exactly one predecessor among its nearest neighbors (see Fig. 2.15), which

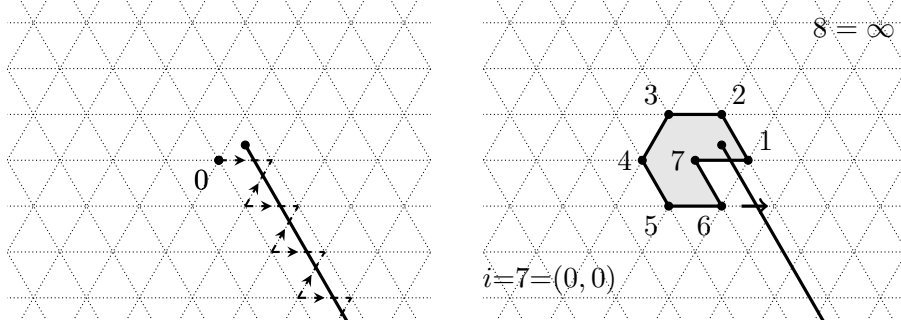


Figure 2.14: Left: zipper line on the triangular lattice, and zipper edges  $(k, \ell)$  with nontrivial parallel transport  $\phi_{k, \ell} = z$ . Right: the modified graph  $\bar{\mathcal{G}}$  obtained by cutting edges between node 7 and its neighbors 2, 3, 4, 5. Node 8 corresponds to the sink/root, and will eventually be sent to infinity in sandpile computations. The zipper extends down to infinity.

we assume to be node 6 at  $(0, -1)$ . By removing the edge between nodes 6 and 7, we can establish a bijection between the spanning trees with a unique predecessor of  $i$  to two-component spanning forests, due to the relative positions of the nodes 1, 6, 7 on  $\bar{\mathcal{G}}$ :

$$X_1(i) = 6 \times 5 \times \frac{\bar{Z}[6|1234578]}{Z} = 30 \times \frac{\bar{Z}[6|578]}{Z}, \quad (2.89)$$

where the combinatorial factor takes into account the number of choices for the unique predecessor of  $i$  among its neighbors (6) and the number of ways to connect  $i$  to the tree with the sink (5). The second equality follows because,  $\bar{\mathcal{G}}$  being planar, the nodes 1 to 4 necessarily belong to the same component as 5, 7, 8. Considering the spanning forests in  $\bar{Z}[6|578]$ , we can write

$$\bar{Z}[6|578] = \bar{Z}[6|78] - \bar{Z}[56|78], \quad (2.90)$$

since node 5 can either be with node 6 or with nodes 7 and 8, implying  $\bar{Z}[6|78] = \bar{Z}[6|578] + \bar{Z}[56|78]$ .

The number of spanning forests of the types  $6|78$  and  $56|78$  on  $\bar{\mathcal{G}}_s$  can be expressed in terms of the usual Green function  $\bar{G}$  and the Green function derivative  $\bar{G}'$ , where the bar is a reminder that these quantities are defined on the modified graph  $\bar{\mathcal{G}}$ . We can compute the number of

forests of the first type directly, as the sum on the right-hand side of Theorem 1.3 contains only one term:

$$\bar{Z}[6|78] = \bar{Z} \det \bar{G}_{\{6,7\}}^{\{6,8\}} = \bar{Z} (\bar{G}_{6,6} \bar{G}_{7,8} - \bar{G}_{6,8} \bar{G}_{7,6}) = \bar{Z} (\bar{G}_{6,6} - \bar{G}_{6,7}), \quad (2.91)$$

where we used  $\bar{G}_{i,8} = 1$  since node 8 is the sink, and  $\bar{G}_{j,i} = \bar{G}_{i,j}$  for an unoriented graph.

The number of spanning forests of the type 56|78, on the other hand, is harder to compute. It requires the use of the Green function derivative  $\bar{G}'$  associated with the zipper. Using the grove theorem, one finds the following result (see Section 5.4 in [91]):

$$\begin{aligned} \bar{Z}[56|78] &= \lim_{z \rightarrow 1} \bar{Z}[56|78] = \lim_{z \rightarrow 1} \bar{Z} \times \frac{\det \bar{G}_{5,7}^{6,8} - \det \bar{G}_{5,6}^{7,8} - z^2 \det \bar{G}_{6,7}^{5,8}}{1 - z^2} \\ &= \bar{Z} \times \frac{\bar{G}'_{5,6} - \bar{G}'_{7,6} - \bar{G}'_{5,7} + \bar{G}'_{6,7} - 2\bar{G}_{6,5} + 2\bar{G}_{7,5} - \bar{G}'_{6,5} + \bar{G}'_{7,5}}{-2} \\ &= \bar{Z} (\bar{G}_{5,6} - \bar{G}_{5,7} - \bar{G}'_{5,6} + \bar{G}'_{5,7} - \bar{G}'_{6,7}), \end{aligned} \quad (2.92)$$

where the substitution rule  $\bar{G}_{i,8} = 1$  and the antisymmetry  $\bar{G}'_{i,j} = -\bar{G}'_{j,i}$  have been used, see Theorem 1.6 and Eq. (1.28).

Both  $\bar{G}, \bar{G}'$  on the modified graph  $\bar{\mathcal{G}}$ , as well as the ratio  $\bar{Z}/Z$ , are given in terms of  $G, G'$  on the original graph  $\mathcal{G}$  using the Woodbury formula, which we recall in Appendix A along with selected values of  $G, G'$ . The resulting analytical value of  $X_1(i)$  on the triangular lattice  $\mathcal{G} = \mathcal{L}_T$  reads:

$$X_1(i) = \frac{485}{1296} + \frac{2395}{36\sqrt{3}\pi} - \frac{345}{2\pi^2} - \frac{200\sqrt{3}}{\pi^3} + \frac{2475}{\pi^4} - \frac{1620\sqrt{3}}{\pi^5} \simeq 0.190, \quad (2.93)$$

which, upon using Eq. (2.87), directly yields the height-two probability  $\mathbb{P}_2(i)$ , shown below.

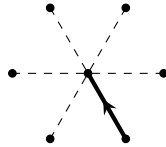


Figure 2.15: Schematic representation of the unique diagram (up to rotations of  $60^\circ$ ) contributing to  $X_1(i)$  on the triangular lattice. The isolated dots represent neighbors of  $i$  that are not its predecessors.

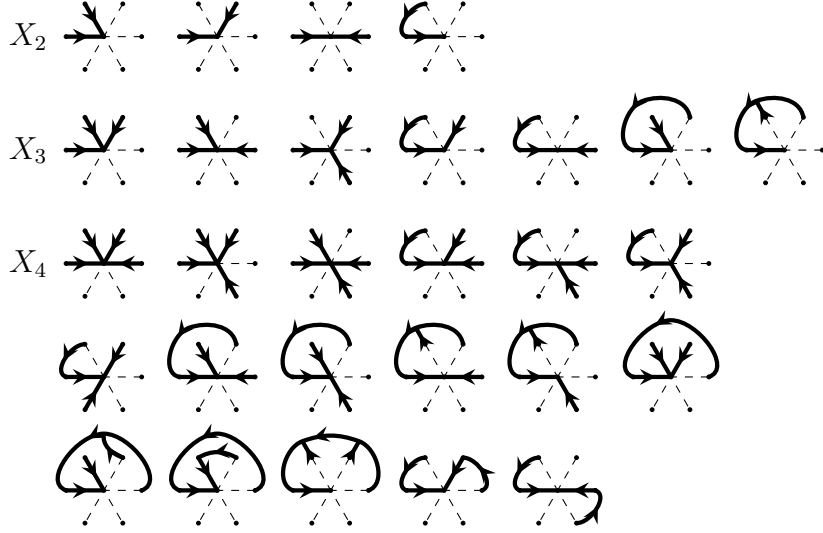


Figure 2.16: Classes of predecessor diagrams contributing to  $X_q(i)$  for  $2 \leq q \leq 4$  on the triangular lattice. A multiplicity (analogous to the factor 30 in Eq. (2.89)) is associated with each class, accounting for the symmetries of the lattice. The ones for the diagrams of  $X_2(i)$ , for instance, are given by 24, 24, 12 and 48, respectively.

Higher-height probabilities on the lattice are computed in the same way, although there are multiple inequivalent predecessor diagrams contributing to the fractions  $X_q(i)$  when  $q \geq 2$  (see Fig. 2.16). The probability of each of these diagrams can be determined similarly to that of the unique one contributing to  $X_1(i)$ . We find the following explicit expressions for  $\mathbb{P}_a(i)$  on  $\mathcal{G} = \mathcal{L}_T$ :

$$\mathbb{P}_1(i) = -\frac{25}{648} - \frac{55}{72\sqrt{3}\pi} + \frac{7}{3\pi^2} + \frac{11\sqrt{3}}{\pi^3} - \frac{90}{\pi^4} + \frac{54\sqrt{3}}{\pi^5} \simeq 0.054, \quad (2.94a)$$

$$\mathbb{P}_2(i) = \frac{47}{1296} + \frac{301}{24\sqrt{3}\pi} - \frac{193}{6\pi^2} - \frac{29\sqrt{3}}{\pi^3} + \frac{405}{\pi^4} - \frac{270\sqrt{3}}{\pi^5} \simeq 0.092, \quad (2.94b)$$

$$\mathbb{P}_3(i) = \frac{3}{8} - \frac{5929}{144\sqrt{3}\pi} + \frac{1441}{12\pi^2} - \frac{9\sqrt{3}}{\pi^3} - \frac{720}{\pi^4} + \frac{540\sqrt{3}}{\pi^5} \simeq 0.137, \quad (2.94c)$$

$$\mathbb{P}_4(i) = \frac{3427}{2592} + \frac{6515}{144\sqrt{3}\pi} - \frac{2125}{12\pi^2} + \frac{91\sqrt{3}}{\pi^3} + \frac{630}{\pi^4} - \frac{540\sqrt{3}}{\pi^5} \simeq 0.189, \quad (2.94d)$$

$$\mathbb{P}_5(i) = -\frac{2663}{1296} - \frac{71\sqrt{3}}{16\pi} + \frac{1331}{12\pi^2} - \frac{94\sqrt{3}}{\pi^3} - \frac{270}{\pi^4} + \frac{270\sqrt{3}}{\pi^5} \simeq 0.242, \quad (2.94e)$$

$$\mathbb{P}_6(i) = \frac{1175}{864} - \frac{365}{144\sqrt{3}\pi} - \frac{289}{12\pi^2} + \frac{30\sqrt{3}}{\pi^3} + \frac{45}{\pi^4} - \frac{54\sqrt{3}}{\pi^5} \simeq 0.286, \quad (2.94f)$$

where we used  $\mathbb{P}_6(i) = 1 - \sum_{a=1}^5 \mathbb{P}_a(i)$  to avoid a direct computation of  $X_5(i)$ , which requires the evaluation of 22 separate predecessor diagrams. As for the square lattice, a nice check of our computations comes from the formula (2.36) relating the mean height to the return probability, whose value on the triangular lattice is  $\mathbb{P}_{\text{ret}} = 5/18$  [84,91]; thus yielding  $\langle h \rangle = 13/3$ , in agreement with (2.94).

### 2.5.2 On the upper half-plane

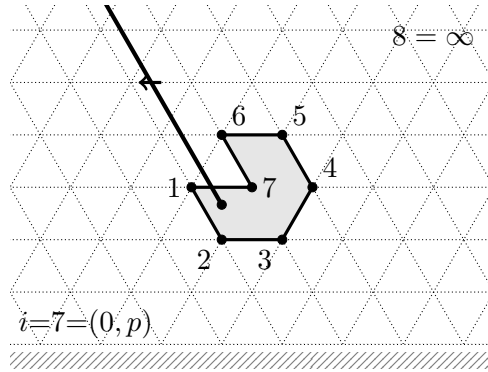


Figure 2.17: The modified graph  $\bar{\mathcal{G}}$  obtained by cutting edges between node 7 and its neighbors 2,3,4,5 on the triangular half-lattice. The sink corresponds to node 8 and is sent to infinity. The zipper extends up to infinity.

In addition to the infinite triangular lattice, we compute one-site probabilities on the semi-infinite lattice with a horizontal boundary, i.e.  $\mathcal{G} = \{(x,y) \in \mathcal{L}_T | y > 0\}$ . Usual boundary conditions on the upper half-plane are either uniformly open or uniformly closed ( $\Delta_{i,i} = 6$  or  $\Delta_{i,i} = 4$  resp. for boundary sites). For the latter, we have not been able to define a suitable reflection in order to use the image method. Therefore, we only discuss the case of an open boundary, for which a simple reflection through the line  $y = 0$  works and yields the following Green function,

$$G_{(x_1,y_1),(x_2,y_2)}^{\text{op}} = G_{(x_1,y_1),(x_2,y_2)} - G_{(x_1,y_1),(x_2-y_2,-y_2)}, \quad (2.95)$$

where  $G$  is the standard Green function on the full triangular lattice (2.85). We choose the reference site  $i$  to be located at  $(0,p)$  with  $p \gg 1$ ,

and take the zipper to be the path on the dual graph crossing the edges of the form  $((0, k), (-1, k))$  and  $((0, k+1), (-1, k))$  for  $k \geq p$  (see Fig. 2.17).

For such a zipper, the Green function derivative  $G'^{\text{op}}$  on the upper half-plane reads:

$$\begin{aligned} G'_{(x_1, y_1), (x_2, y_2)}{}^{\text{op}} = \sum_{k=0}^{\infty} \left[ G_{(x_1, y_1), (-1, p+k)}{}^{\text{op}} G_{(0, p+k), (x_2, y_2)}{}^{\text{op}} \right. \\ \left. - G_{(x_1, y_1), (0, p+k)}{}^{\text{op}} G_{(-1, p+k), (x_2, y_2)}{}^{\text{op}} \right. \\ \left. + G_{(x_1, y_1), (-1, p+k)}{}^{\text{op}} G_{(0, p+k+1), (x_2, y_2)}{}^{\text{op}} \right. \\ \left. - G_{(x_1, y_1), (0, p+k+1)}{}^{\text{op}} G_{(-1, p+k), (x_2, y_2)}{}^{\text{op}} \right]. \end{aligned} \quad (2.96)$$

Using Eq. (2.95), we can write  $G'^{\text{op}}$  in terms of  $G'$  on the full lattice (with respect to the zipper depicted in Fig. 2.14) as follows:

$$\begin{aligned} G'_{(x_1, y_1), (x_2, y_2)}{}^{\text{op}} = G'_{(-x_1, p-y_1), (-x_2, p-y_2)} - G'_{(-x_1, p-y_1), (y_2-x_2, p+y_2)} \\ - G'_{(y_1-x_1, p+y_1), (-x_2, p-y_2)} + G'_{(y_1-x_1, p+y_1), (y_2-x_2, p+y_2)}. \end{aligned} \quad (2.97)$$

For pairs of vertices  $(x_i, y_i)$  close to the head of the zipper (i.e. of the form  $(a_i, p+b_i)$  with  $a_i, b_i = o(1)$ ), the first term of Eq. (2.97) can be computed exactly since it is independent of  $p$ ; the three remaining terms are evaluated as power series in  $1/p$  (see Appendix A for more details).

Similarly to full-plane computations, the reference site  $i$  located at  $(0, p)$  and its six neighbors are chosen as nodes (note that we have relabeled the nodes with respect to Fig. 2.14, so that the new zipper is once again located between nodes 1 and 7). We define a modified graph  $\bar{\mathcal{G}}$  by cutting the edges  $\{7, 2\}$ ,  $\{7, 3\}$ ,  $\{7, 4\}$  and  $\{7, 5\}$ , so that nodes 1 to 7 lie along the boundary of a single face on  $\bar{\mathcal{G}}$ . Since the upper half-plane is not invariant under rotations of  $60^\circ$ , there are in total roughly four times as many distinct diagrams as on the full plane (the left-right symmetry is still preserved). The correspondence between predecessor diagrams and spanning forests with a fixed node partition  $\sigma$  holds on the upper half-plane as well, with  $\bar{Z}[\sigma]/Z$  given as a function of  $G^{\text{op}}, G'^{\text{op}}$  instead of  $G, G'$ . The final results for one-site probabilities at  $i = (0, p)$  on the upper half-plane take the form

$$\sigma_a^{\text{op}}(r) \equiv \mathbb{P}_a^{\text{op}}(r) - \mathbb{P}_a = \frac{1}{r^2} (c_a + d_a \log r) + \dots, \quad (2.98)$$

where  $\mathbb{P}_a$  are the one-site probabilities on the full plane (2.94) and  $r = \sqrt{3}p/2$  is the Euclidean distance between  $i = (0, p)$  and the symmetry axis for the image method,  $y = 0$ . The coefficients  $c_a, d_a$  are given in Table 2.3, from which we see that, as on the square half-lattice, all one-point height probabilities have a logarithmic term except for the height one.

## 2.6 Height probabilities on the hexagonal lattice

The third regular graph we consider is the hexagonal (or honeycomb) lattice  $\mathcal{L}_H$ . In contrast to the square and triangular cases, there are two types of vertices on this lattice, which we call A and B (see Fig. 2.18). Each vertex of type A has three neighbors of type B, and vice versa. We choose the origin of the lattice to be of type A, and pick a coordinate system  $\vec{r} = x \vec{e}_1 + y \vec{e}_2$  where the position of each unit cell is specified by the coordinates  $(x, y) \in \mathbb{Z}^2$  of its A vertex. Each individual vertex of  $\mathcal{L}_H$  is therefore referred to by the complete set of coordinates  $(x, y; \alpha)$ , with  $\alpha = A, B$ . Alternatively, we can use polar coordinates  $(r, \varphi; \alpha)$  with the angle  $\varphi$  measured counterclockwise from the  $x$  axis, which are related to  $(x, y; \alpha)$  through  $x = r \cos \varphi + \frac{r}{\sqrt{3}} \sin \varphi$ ,  $y = \frac{2r}{\sqrt{3}} \sin \varphi$ .

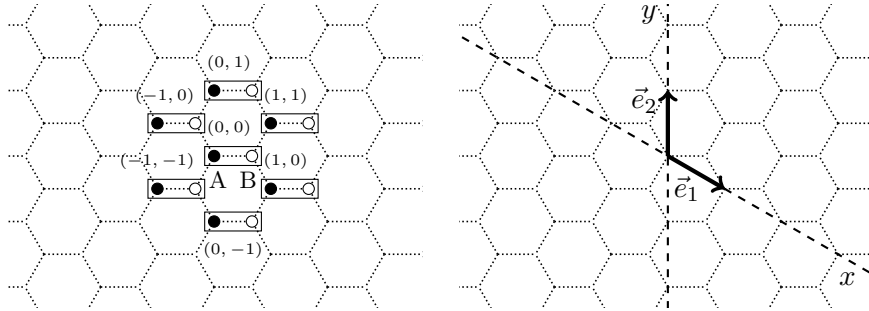


Figure 2.18: Left: unit cells marked by rectangles on the hexagonal lattice. Each of them contains two types of vertices, A and B (resp. in black and in white). Right: coordinate system on the hexagonal lattice, where the positions of A vertices are expressed in terms of the unit vectors  $\vec{e}_1, \vec{e}_2$ .

	$c_a$	$d_a$
$a = 1$	$-\frac{25}{144\sqrt{3}\pi} - \frac{5}{48\pi^2} + \frac{33\sqrt{3}}{8\pi^3} - \frac{99}{4\pi^4} + \frac{27\sqrt{3}}{2\pi^5}$	0
$a = 2$	$\left(-\frac{25}{48\pi^2} + \frac{45\sqrt{3}}{16\pi^3} - \frac{27}{2\pi^4} + \frac{27\sqrt{3}}{4\pi^5}\right) \left(\gamma + \frac{1}{2}\log 48\right)$ $+ \frac{149}{96\sqrt{3}\pi} - \frac{41}{192\pi^2} - \frac{1323\sqrt{3}}{64\pi^3} + \frac{513}{4\pi^4} - \frac{1161\sqrt{3}}{16\pi^5}$	$-\frac{25}{48\pi^2} + \frac{45\sqrt{3}}{16\pi^3} - \frac{27}{2\pi^4} + \frac{27\sqrt{3}}{4\pi^5}$
$a = 3$	$\left(\frac{19}{6\pi^2} - \frac{209\sqrt{3}}{16\pi^3} + \frac{225}{4\pi^4} - \frac{27\sqrt{3}}{\pi^5}\right) \left(\gamma + \frac{1}{2}\log 48\right)$ $- \frac{353}{72\sqrt{3}\pi} + \frac{275}{48\pi^2} + \frac{2491\sqrt{3}}{64\pi^3} - \frac{4275}{16\pi^4} + \frac{621\sqrt{3}}{4\pi^5}$	$\frac{19}{6\pi^2} - \frac{209\sqrt{3}}{16\pi^3} + \frac{225}{4\pi^4} - \frac{27\sqrt{3}}{\pi^5}$
$a = 4$	$\left(-\frac{469}{96\pi^2} + \frac{341\sqrt{3}}{16\pi^3} - \frac{351}{4\pi^4} + \frac{81\sqrt{3}}{2\pi^5}\right) \left(\gamma + \frac{1}{2}\log 48\right)$ $+ \frac{1019}{144\sqrt{3}\pi} - \frac{5425}{384\pi^2} - \frac{2127\sqrt{3}}{64\pi^3} + \frac{4473}{16\pi^4} - \frac{1323\sqrt{3}}{8\pi^5}$	$-\frac{469}{96\pi^2} + \frac{341\sqrt{3}}{16\pi^3} - \frac{351}{4\pi^4} + \frac{81\sqrt{3}}{2\pi^5}$
$a = 5$	$\left(\frac{167}{48\pi^2} - \frac{235\sqrt{3}}{16\pi^3} + \frac{243}{4\pi^4} - \frac{27\sqrt{3}}{\pi^5}\right) \left(\gamma + \frac{1}{2}\log 48\right)$ $- \frac{671}{144\sqrt{3}\pi} + \frac{2227}{192\pi^2} + \frac{753\sqrt{3}}{64\pi^3} - \frac{2349}{16\pi^4} + \frac{351\sqrt{3}}{4\pi^5}$	$\frac{167}{48\pi^2} - \frac{235\sqrt{3}}{16\pi^3} + \frac{243}{4\pi^4} - \frac{27\sqrt{3}}{\pi^5}$
$a = 6$	$\left(-\frac{119}{96\pi^2} + \frac{29\sqrt{3}}{8\pi^3} - \frac{63}{4\pi^4} + \frac{27\sqrt{3}}{4\pi^5}\right) \left(\gamma + \frac{1}{2}\log 48\right)$ $+ \frac{319}{288\sqrt{3}\pi} - \frac{369}{128\pi^2} - \frac{29\sqrt{3}}{32\pi^3} + \frac{495}{16\pi^4} - \frac{297\sqrt{3}}{16\pi^5}$	$-\frac{119}{96\pi^2} + \frac{29\sqrt{3}}{8\pi^3} - \frac{63}{4\pi^4} + \frac{27\sqrt{3}}{4\pi^5}$

Table 2.3: Numerical coefficients of one-site probabilities on the triangular upper half-plane.

### 2.6.1 On the plane

The standard graph Laplacian on  $\mathcal{G} = \mathcal{L}_H$  is defined by

$$\Delta_{u,v} = \begin{cases} 3 & \text{if } u = v, \\ -1 & \text{if } u \text{ and } v \text{ are neighbors,} \\ 0 & \text{otherwise.} \end{cases} \quad (2.99)$$

A more appropriate way of writing  $\Delta$  to compute its inverse  $G$  is obtained by decomposing the lattice into unit cells [149]. Let  $a(\vec{r}_1, \vec{r}_2) \equiv a(\vec{r}_2 - \vec{r}_1)$  be the  $2 \times 2$  adjacency matrix for the vertices of the unit cells located at  $\vec{r}_1$  and  $\vec{r}_2$ , that is,

$$a_{\alpha_1, \alpha_2}(\vec{r}_2 - \vec{r}_1) = \begin{cases} 1 & \text{if the vertex } \alpha_1 \text{ of the cell } \vec{r}_1 \text{ is a neighbor} \\ & \text{of the vertex } \alpha_2 \text{ of the cell } \vec{r}_2, \\ 0 & \text{otherwise.} \end{cases} \quad (2.100)$$

The only nonzero matrices  $a(\vec{r})$  are therefore

$$\begin{aligned} a(0,0) &= \begin{pmatrix} 0 & 1 \\ 1 & 0 \end{pmatrix}, & a(1,0) &= a(1,1) = \begin{pmatrix} 0 & 0 \\ 1 & 0 \end{pmatrix}, \\ a(-1,0) &= a(-1,-1) = \begin{pmatrix} 0 & 1 \\ 0 & 0 \end{pmatrix}. \end{aligned} \quad (2.101)$$

The  $2 \times 2$  block entry of the Laplacian indexed by  $\vec{r}_1, \vec{r}_2$  (with  $\alpha_1, \alpha_2 = A, B$ ) can then be written as follows,

$$\begin{aligned} \Delta_{(\vec{r}_1; \alpha_1), (\vec{r}_2; \alpha_2)} &= \{3 \mathbb{I}_2 - a(0,0)\} \otimes \delta_{\vec{r}_1, \vec{r}_2} - a(1,0) \otimes \delta_{\vec{r}_1, \vec{r}_2 - \vec{e}_1} \\ &\quad - a(1,1) \otimes \delta_{\vec{r}_1, \vec{r}_2 - \vec{e}_1 - \vec{e}_2} - a(-1,0) \otimes \delta_{\vec{r}_1, \vec{r}_2 + \vec{e}_1} \\ &\quad - a(-1,-1) \otimes \delta_{\vec{r}_1, \vec{r}_2 + \vec{e}_1 + \vec{e}_2}. \end{aligned} \quad (2.102)$$

Its inverse  $G$  depends only on the difference  $\vec{r} \equiv \vec{r}_2 - \vec{r}_1 = (x, y)$ , and is given [4] by

$$\begin{aligned} G_{\alpha_1, \alpha_2}(x, y) &= \int_{-\pi}^{\pi} \frac{d\theta_1}{2\pi} \int_{-\pi}^{\pi} \frac{d\theta_2}{2\pi} \frac{e^{ix\theta_1 + iy\theta_2}}{6 - 2\cos\theta_1 - 2\cos\theta_2 - 2\cos(\theta_1 + \theta_2)} \\ &\quad \times \begin{pmatrix} 3 & 1 + e^{i\theta_1} + e^{i(\theta_1 + \theta_2)} \\ 1 + e^{-i\theta_1} + e^{-i(\theta_1 + \theta_2)} & 3 \end{pmatrix}. \end{aligned} \quad (2.103)$$

It readily follows that  $G_{AA}(x, y) = G_{BB}(x, y)$  and  $G_{AB}(-x, -y) = G_{BA}(x, y)$ . Moreover,

$$G_{AB}(x, y) = \frac{1}{3} \left\{ G_{AA}(x, y) + G_{AA}(x+1, y) + G_{AA}(x+1, y+1) \right\}, \quad (2.104)$$

$$G_{BA}(x, y) = \frac{1}{3} \left\{ G_{AA}(x, y) + G_{AA}(x-1, y) + G_{AA}(x-1, y-1) \right\}. \quad (2.105)$$

Moreover, we observe that  $G_{AA}$  is directly related to the Green function on the triangular lattice (2.85):

$$G_{AA}^H(x, y) = 3G^T(x, y), \quad (2.106)$$

although the variables  $(x, y)$  on both sides refer to different coordinate systems (this is expected since the sublattice of  $A$  vertices is triangular). For one-site sandpile probabilities on the plane, we choose the origin  $i = (0, 0; A)$  and its three neighbors  $(0, 0; B)$ ,  $(-1, 0; B)$ ,  $(-1, -1; B)$  as nodes, and a vertical zipper anchored at the face whose lower left corner is the origin (see Fig. 2.19). In order to evaluate spanning tree probabilities, we define the graph  $\bar{\mathcal{G}}$  by removing the edge  $((0, 0; A), (-1, 0; B))$  from  $\mathcal{G}$ , so that nodes 1 to 4 lie around a single face in counterclockwise order.

Since every site on the hexagonal lattice has three neighbors, the heights  $h_i$  take values in  $\{1, 2, 3\}$  for any recurrent sandpile configuration. The height-one probability is the easiest to compute, since it can be expressed in terms of the standard Green function only [4]. Higher-height probabilities are given as linear combinations of spanning tree probabilities through Eq.(2.87), which we evaluate using the same technique as for the triangular lattice. The explicit values of  $\mathbb{P}_a(i)$  on  $\mathcal{G} = \mathcal{L}_H$  are all rational numbers, equal to

$$\mathbb{P}_1(i) = \frac{1}{12} \simeq 0.083, \quad \mathbb{P}_2(i) = \frac{7}{24} \simeq 0.292, \quad \mathbb{P}_3(i) = \frac{5}{8} \simeq 0.625, \quad (2.107)$$

yielding the mean height  $\langle h \rangle = 61/24$  on the hexagonal lattice, in agreement with  $\mathbb{P}_{\text{ret}} = 13/36$  [84, 91] via Eq. (2.36).

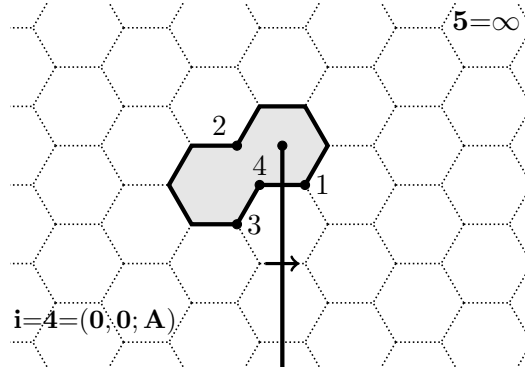


Figure 2.19: The modified graph  $\bar{\mathcal{G}}$  obtained by cutting the edge between nodes 2 and 4. Node 5 corresponds to the sink/root, and will eventually be sent to infinity in sandpile computations. The zipper extends down to infinity.

## 2.6.2 On upper half-planes

In addition to the lattice  $\mathcal{L}_H$ , we consider half-lattices with two kinds of boundaries: one parallel to the  $x$  axis, and a horizontal one (see Fig. 2.20). For both half-planes, which, following [4], we refer respectively to as *principal* and *horizontal*, we choose the reference site  $i = (0, p; A)$  with  $p \gg 1$ . As for the full lattice, we select  $i$ , its three neighbors and the sink as nodes on a modified graph, here obtained by cutting the edge between  $i$  and its neighbor  $(-1, p; B)$ . For simplicity, the zipper is taken as a path on the dual graph starting on a face adjacent to  $i$  and extending up to infinity. The edges with a nontrivial parallel transport  $z \in \mathbb{C}^*$  are the following:  $((0, k; B), (0, k; A))$  for  $k \geq p + 1$ . The same arguments as in Section 2.6.1 are used to write the fractions of spanning trees  $X_q(i)$  in terms of the Green function  $G$  of the half-lattice of interest and the Green function derivative  $G'$  associated with the zipper.

Let us first look at the principal half-plane, whose boundary consists in vertices of the form  $(x, y=1; A)$ , as depicted in the left panel of Fig. 2.20. The corresponding Green function can be written in terms of the full-plane Green function, for either closed or open boundary conditions, using the image method. For the closed boundary, each site is mirrored

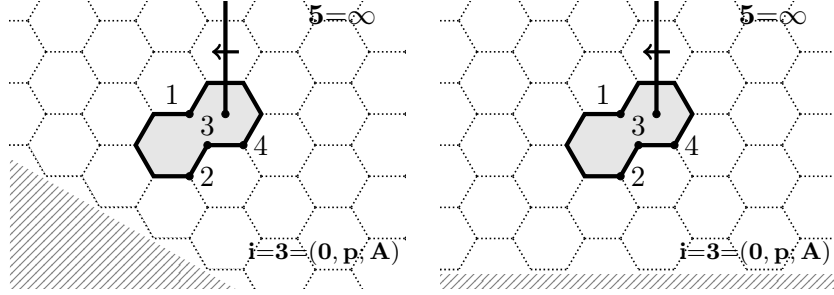


Figure 2.20: The modified graph  $\bar{\mathcal{G}}$  obtained by cutting the edge between nodes 1 and 3 on half-lattices with a principal boundary (at the top) and a horizontal boundary (at the bottom). The sink corresponds to node 5 and is sent to infinity. The zipper extends up to infinity.

through the reflection axis  $y = 2/3$ , so the Green function reads [4]

$$\begin{aligned} G_{(x_1, y_1; \alpha_1), (x_2, y_2; A)}^{\text{cl}} &= G_{(x_1, y_1; \alpha_1), (x_2, y_2; A)} + G_{(x_1, y_1; \alpha_1), (x_2 - y_2, 1 - y_2; B)}, \\ G_{(x_1, y_1; \alpha_1), (x_2, y_2; B)}^{\text{cl}} &= G_{(x_1, y_1; \alpha_1), (x_2, y_2; B)} + G_{(x_1, y_1; \alpha_1), (x_2 - y_2 + 1, 1 - y_2; A)}. \end{aligned} \quad (2.108)$$

Proceeding as in (2.97), we may write the Green function derivative with respect to the zipper represented in Fig. 2.19 in terms of that on the full lattice. For instance if  $\alpha_1 = \alpha_2 = A$ , we find the relation

$$\begin{aligned} G'_{(x_1, y_1; A), (x_2, y_2; A)}^{\text{cl}} &= G'_{(-x_1, p+1-y_1; B), (-x_2, p+1-y_2; B)} \\ &\quad - G'_{(-x_1, p+1-y_1; B), (y_2 - x_2, p+y_2; A)} \\ &\quad - G'_{(y_1 - x_1, p+y_1; A), (-x_2, p+1-y_2; B)} \\ &\quad + G'_{(y_1 - x_1, p+y_1; A), (y_2 - x_2, p+y_2; A)}. \end{aligned} \quad (2.109)$$

The open case is subtler, as the mirror image of a vertex of type  $A$  with respect to the natural reflection line  $y = 1/3$  does not belong to the lattice. However, one can use the Poisson equation to get a suitable

expression for the Green function [4]:

$$\begin{aligned}
G_{(x_1, y_1; \alpha_1), (x_2, y_2; A)}^{\text{op}} &= G_{(x_1, y_1; \alpha_1), (x_2, y_2; A)} - \frac{1}{3} \left[ G_{(x_1, y_1; \alpha_1), (x_2 - y_2, -y_2; B)} \right. \\
&\quad + G_{(x_1, y_1; \alpha_1), (x_2 - y_2 - 1, -y_2; B)} \\
&\quad \left. + G_{(x_1, y_1; \alpha_1), (x_2 - y_2, 1 - y_2; B)} \right], \\
G_{(x_1, y_1; \alpha_1), (x_2, y_2; B)}^{\text{op}} &= G_{(x_1, y_1; \alpha_1), (x_2, y_2; B)} - G_{(x_1, y_1; \alpha_1), (x_2 - y_2, -y_2; B)}.
\end{aligned} \tag{2.110}$$

Here the Green function derivatives on the half-lattice and on the full lattice are connected through

$$\begin{aligned}
G'_{(x_1, y_1; B), (x_2, y_2; B)}^{\text{op}} &= G'_{(-x_1, p+1-y_1; A), (-x_2, p+1-y_2; A)} \\
&\quad + G'_{(-x_1, p+1-y_1; A), (y_2 - x_2, p+1+y_2; A)} \\
&\quad + G'_{(y_1 - x_1, p+1+y_1; A), (-x_2, p+1-y_2; A)} \\
&\quad + G'_{(y_1 - x_1, p+1+y_1; A), (y_2 - x_2, p+1+y_2; A)}
\end{aligned} \tag{2.111}$$

for  $\alpha_1 = \alpha_2 = B$ . Similar relations hold for other values of  $\alpha_1, \alpha_2$ .

We use these formulas together with the integral representation of the Green function on the full lattice (2.103) to compute  $G^{\text{cl,op}}$  and  $G'^{\text{cl,op}}$  as series expansions in  $1/p$  (this is discussed in Appendix A for the triangular lattice; the treatment of the hexagonal lattice is very similar). We find that one-site probabilities on the principal half-plane take the form

$$\sigma_a^{\text{princ}}(r) \equiv \mathbb{P}_a^{\text{princ}}(r) - \mathbb{P}_a = \frac{1}{r^2} (c_a^{\text{princ}} + d_a^{\text{princ}} \log r) + \mathcal{O}(r^{-3} \log r), \tag{2.112}$$

where  $\mathbb{P}_a$  denotes the one-site probability on the full lattice, and  $r$  is the Euclidean distance between the reference site  $i = (0, p; A)$  and the reflection axis used in the image method, namely

$$r = \frac{\sqrt{3}}{2}p - \frac{1}{\sqrt{3}} \quad (\text{closed b.c.}), \quad r = \frac{\sqrt{3}}{2}p - \frac{1}{2\sqrt{3}} \quad (\text{open b.c.}). \tag{2.113}$$

The numerical values of the coefficients  $c_a^{\text{princ}}, d_a^{\text{princ}}$  for both types of boundary conditions are collected in Table 2.4. We note the distinctive change of sign between the two boundary conditions in the most dominant terms (rational for the height 1, logarithmic for the higher heights), as encountered on the square half-lattice [81].

	$c_a^{\text{princ,cl}}$	$d_a^{\text{princ,cl}}$
$a = 1$	$-\frac{1}{16\sqrt{3}\pi}$	0
$a = 2$	$-\frac{3}{16\pi^2} \left( \gamma + \frac{1}{2} \log 48 \right) + \frac{15}{64\pi^2}$	$-\frac{3}{16\pi^2}$
$a = 3$	$\frac{3}{16\pi^2} \left( \gamma + \frac{1}{2} \log 48 \right) - \frac{45-4\sqrt{3}\pi}{192\pi^2}$	$\frac{3}{16\pi^2}$

	$c_a^{\text{princ,op}}$	$d_a^{\text{princ,op}}$
$a = 1$	$\frac{1}{16\sqrt{3}\pi}$	0
$a = 2$	$\frac{3}{16\pi^2} \left( \gamma + \frac{1}{2} \log 48 \right) - \frac{9}{64\pi^2}$	$\frac{3}{16\pi^2}$
$a = 3$	$-\frac{3}{16\pi^2} \left( \gamma + \frac{1}{2} \log 48 \right) + \frac{27-4\sqrt{3}\pi}{192\pi^2}$	$-\frac{3}{16\pi^2}$

Table 2.4: Coefficients for one-site probabilities on the hexagonal half-lattice with a principal boundary.

Let us now turn to the horizontal half-plane (drawn on the right panel of Fig. 2.20), whose boundary sites  $(x, y; \alpha)$  satisfy the equality  $x = 2y - 2$ . For an open boundary, the image method allows one to write the Green function as [4]

$$G_{(x_1, y_1; \alpha_1), (x_2, y_2; \alpha_2)}^{\text{op}} = G_{(x_1, y_1; \alpha_1), (x_2, y_2; \alpha_2)} - G_{(x_1, y_1; \alpha_1), (x_2, x_2 - y_2 + 1; \alpha_2)}. \quad (2.114)$$

With respect to the zipper pictured in Fig. 2.20, the Green function derivative reads:

$$\begin{aligned} G'_{(x_1, y_1; \alpha_1), (x_2, y_2; \alpha_2)}^{\text{op}} &= G'_{(-x_1, p+1-y_1; \bar{\alpha}_1), (-x_2, p+1-y_2; \bar{\alpha}_2)} \\ &\quad - G'_{(-x_1, p+1-y_1; \bar{\alpha}_1), (-x_2, p-x_2+y_2; \bar{\alpha}_2)} \\ &\quad - G'_{(-x_1, p-x_1+y_1; \bar{\alpha}_1), (-x_2, p+1-y_2; \bar{\alpha}_2)} \\ &\quad + G'_{(-x_1, p-x_1+y_1; \bar{\alpha}_1), (-x_2, p-x_2+y_2; \bar{\alpha}_2)}, \end{aligned} \quad (2.115)$$

where  $G'$  is the derivative on the full lattice with a zipper going down to infinity (see Fig. 2.19), and  $\bar{\alpha} = B$  (resp.  $A$ ) if  $\alpha = A$  (resp.  $B$ ). For a

closed boundary, we have not been able to find a suitable reflection axis for the image method, so we only give results for the open half-plane.

Let us define  $r$  as the distance between the reference site  $i = (0, p; A)$  and the reflection axis used in the image method  $y = (x + 1)/2$ , i.e.  $r = p - 1/2$ . Up to third-order terms, one-site probabilities on the open horizontal half-plane are given by

$$\sigma_a^{\text{hor,op}}(r) \equiv \mathbb{P}_a^{\text{hor,op}}(r) - \mathbb{P}_a = \frac{1}{r^2} \left( c_a^{\text{hor,op}} + d_a^{\text{hor,op}} \log r \right) + \mathcal{O}(r^{-3} \log r), \quad (2.116)$$

with coefficients  $c_a^{\text{hor,op}}, d_a^{\text{hor,op}}$  given in Table 2.5. As expected, one-site probabilities on the principal and horizontal half-planes with open boundary conditions coincide at order  $1/r^2$ , namely  $c^{\text{hor,op}} = c^{\text{princ,op}}$  and  $d^{\text{hor,op}} = d^{\text{princ,op}}$ .

	$c_a^{\text{hor,op}}$	$d_a^{\text{hor,op}}$
$a = 1$	$\frac{1}{16\sqrt{3}\pi}$	0
$a = 2$	$\frac{3}{16\pi^2} \left( \gamma + \frac{1}{2} \log 48 \right) - \frac{9}{64\pi^2}$	$\frac{3}{16\pi^2}$
$a = 3$	$-\frac{3}{16\pi^2} \left( \gamma + \frac{1}{2} \log 48 \right) + \frac{27-4\sqrt{3}\pi}{192\pi^2}$	$-\frac{3}{16\pi^2}$

Table 2.5: Coefficients for one-site probabilities on the hexagonal half-lattice with a horizontal open boundary.

### 2.6.3 On boundaries

In this subsection, we consider probabilities involving vertices located on the boundary of the two hexagonal upper half-planes described in the previous subsection. Due to the small number of admissible heights (two on a closed boundary, three on an open one), the calculations are quite straightforward, as they do not require the use of a nontrivial connection on the graph. Indeed, height-one probabilities can be computed in terms of the standard Green function only. The same is true for height-three probabilities on an open boundary, see below, yielding height-two probabilities by subtraction.

We shall compute one-site and two-site probabilities on the boundary of the two half-lattices described above. The simplest case is the principal boundary with closed boundary conditions, since the height of a closed boundary site takes on the values 1 or 2. Therefore, height-two probabilities can be obtained by subtraction from height-one probabilities, which can be computed via defect matrices. This has been done in [4] with the following results,

$$\mathbb{P}_1^{\text{princ,cl}} = \frac{\sqrt{3}}{\pi} - \frac{1}{3}, \quad \mathbb{P}_2^{\text{princ,cl}} = \frac{4}{3} - \frac{\sqrt{3}}{\pi}, \quad (2.117)$$

$$\mathbb{P}_{1,1}^{\text{princ,cl}}(i, j) - \mathbb{P}_1^{\text{princ,cl}} \mathbb{P}_1^{\text{princ,cl}} = -\frac{3}{16\pi^2 x^4} + \dots, \quad (2.118)$$

where  $x = |x_2 - x_1|$  denotes the Euclidean distance between sites  $i = (x_1, 1; A)$  and  $j = (x_2, 1; A)$ .

For open boundary conditions on the principal half-plane, boundary heights  $h_i$  take their value in  $\{1, 2, 3\}$ . The height-three probability at site  $i$  can be evaluated as follows [128]: define a new Laplacian  $\tilde{\Delta}$  such that  $\tilde{\Delta}_{i,i} = \Delta_{i,i} - 1$ , with  $\tilde{\Delta}$  and  $\Delta$  coinciding everywhere else. The burning algorithm [112] gives a bijection between recurrent configurations with  $h_i = 3$  and spanning trees that use the edge between  $i$  and the sink  $s$ . As  $\det \tilde{\Delta}$  counts precisely the number of spanning trees that do not use that particular edge, it follows that

$$\mathbb{P}_3(i) = 1 - \frac{\det \tilde{\Delta}}{\det \Delta} = (\Delta^{-1})_{i,i}. \quad (2.119)$$

The remaining height probability  $\mathbb{P}_2(i)$  can be obtained from the relation  $\sum_{a=1}^3 \mathbb{P}_a(i) = 1$ . With the appropriate Green function (2.110), we find the following one-site and two-site probabilities for the open boundary conditions<sup>4</sup>:

$$\begin{aligned} \mathbb{P}_1^{\text{princ,op}} &= \frac{11}{36} + \frac{4}{\sqrt{3}\pi} - \frac{9}{\pi^2}, & \mathbb{P}_2^{\text{princ,op}} &= -\frac{7}{36} - \frac{2}{\sqrt{3}\pi} + \frac{9}{\pi^2}, \\ \mathbb{P}_3^{\text{princ,op}} &= \frac{8}{9} - \frac{2}{\sqrt{3}\pi}, \end{aligned} \quad (2.120)$$

$$\mathbb{P}_{a,b}^{\text{princ,op}}(i, j) - \mathbb{P}_a^{\text{princ,op}} \mathbb{P}_b^{\text{princ,op}} = -\frac{\alpha_a^{\text{princ,op}} \alpha_b^{\text{princ,op}}}{4x^4} + \dots, \quad (2.121)$$

<sup>4</sup>Only height-one probabilities were given in [4].

for  $a, b = 1, 2, 3$ , with  $\alpha_1^{\text{princ,op}} = \frac{11}{2\sqrt{3}\pi} - \frac{9}{\pi^2}$ ,  $\alpha_2^{\text{princ,op}} = -\frac{7}{2\sqrt{3}\pi} + \frac{9}{\pi^2}$ ,  $\alpha_3^{\text{princ,op}} = -\frac{2}{\sqrt{3}\pi}$  (up to a global sign).

On the horizontal half-plane with open boundary conditions, we obtain similar results using the Green function (2.114):

$$\begin{aligned} \mathbb{P}_1^{\text{hor,op}}(i) &= -\frac{37}{36} + \frac{8}{\sqrt{3}\pi} - \frac{3}{\pi^2}, & \mathbb{P}_2^{\text{hor,op}}(i) &= \frac{55}{36} - \frac{8}{\sqrt{3}\pi} + \frac{3}{\pi^2}, \\ \mathbb{P}_3^{\text{hor,op}}(i) &= \frac{1}{2}, \end{aligned} \quad (2.122)$$

$$\mathbb{P}_{a,b}^{\text{hor,op}}(i, j) - \mathbb{P}_a^{\text{hor,op}} \mathbb{P}_b^{\text{hor,op}} = -\frac{\alpha_a^{\text{hor,op}} \alpha_b^{\text{hor,op}}}{4x^4} + \dots, \quad (2.123)$$

for  $a, b = 1, 2, 3$ , with  $\alpha_1^{\text{hor,op}} = -\frac{1}{3\sqrt{3}\pi} + \frac{1}{\pi^2}$ ,  $\alpha_2^{\text{hor,op}} = \frac{5}{6\sqrt{3}\pi} - \frac{1}{\pi^2}$  and  $\alpha_3^{\text{hor,op}} = -\frac{1}{2\sqrt{3}\pi}$  (again up to a global sign).

More generally, multisite boundary probabilities on both hexagonal half-lattices could easily be computed, as one can enforce a height 1 or 3 (for open b.c.) at a given boundary site using local defect matrices. For the triangular half-plane with an open boundary, the situation is more complicated, as there are three nontrivial probabilities to evaluate separately, namely 2, 3 and 4 (heights 5 and 6 can be handled in the same way as height 3 on the hexagonal lattice).

## 2.7 Conformal field theory

The Abelian sandpile model is believed to be described in the scaling limit by a conformal field theory. The reference [112] was the first one to suggest the value of its central charge, namely  $c = -2$ . Since then, this value as well as many more refined aspects have been examined, largely confirming the validity of the conformal point of view. A recent review devoted to this question can be found in [143].

According to this view, the various degrees of freedom of the discrete model go over to specific conformal fields in such a way that the continuum limit of the discrete correlations yield the corresponding field-theoretical correlations. In the favorable cases, the fundamental or most natural microscopic variables of the discrete model are associated with primary conformal fields. A number of identifications of this type have

been proposed for the sandpile model, mainly on the square lattice, and these include the height variables, relevant for the lattice correlations computed in the previous sections.

On the square lattice, the height variable at every nonboundary site is a microscopic random variable taking the four integer values from 1 to 4. As suggested by the calculations of the previous sections, one does not consider the random height variables themselves, but, at each site, the indicator functions  $\delta_{h(i),a}$ ,  $a = 1, 2, 3, 4$ , of the four fixed-height events. For reasons explained above, one subtracts by their own expectation value on the infinite discrete plane, and therefore one considers

$$h_a(i) \equiv \delta_{h(i),a} - \mathbb{P}_a \quad \text{for } a = 1, 2, 3, 4. \quad (2.124)$$

On the lattice, they define four “fixed-height variables”, not all independent since they satisfy the obvious linear relation  $\sum_a h_a(i) = 0$  at each site. This decomposition into fixed values is not usual in lattice models, but in the present case, it reveals components of fundamentally different nature and therefore provides an enriched perspective. The various correlators computed in previous sections are simply equal to the expectation values of products of fixed-height variables,  $\sigma_{a_1, a_2, \dots}(i_1, i_2, \dots) = \mathbb{E}[h_{a_1}(i_1) h_{a_2}(i_2) \dots]$ .

The basic definition (2.124) of the fixed-height variables can easily be adapted to boundary sites (with specific boundary conditions). It turns out that the bulk conformal fields  $h_a(z, \bar{z})$  associated with the height variables  $h_a(i)$  far from boundaries are more complicated (reflecting in a way the difficulty of computing their joint probabilities on the lattice). In light of the results for one-point functions on the upper half-plane, the nature of the four fields was first conjectured in [129], and then completed in [81]; this conjecture has been found to be consistent with all subsequent calculations. It can be formulated as follows.

*The bulk fixed-height fields  $h_a(z, \bar{z})$  can be identified with specific fields in a nonchiral indecomposable staggered Virasoro module at  $c = -2$ , containing a logarithmic (Jordan) pair of conformal fields  $(\phi, \psi)$  of weights  $(1, 1)$ . The field  $\phi$  is primary and left- and right-degenerate at level 2, while its logarithmic partner  $\psi$  has the following infinitesimal conformal*

transformations, which involve two additional fields  $\rho$  and  $\bar{\rho}$ ,

$$\begin{aligned} L_0\psi &= \bar{L}_0\psi = \psi + \lambda\phi, & L_1\psi &= \rho, & \bar{L}_1\psi &= \bar{\rho}, \\ L_{n>1}\psi &= \bar{L}_{n>1}\psi = 0. \end{aligned} \quad (2.125a)$$

The fields  $\rho$  and  $\bar{\rho}$  are respectively left-primary and right-primary of weights  $(0,1)$  and  $(1,0)$ ,

$$\begin{aligned} L_{n\geq 0}\rho &= \bar{L}_{n\geq 0}\bar{\rho} = 0, & \bar{L}_0\rho &= \rho, & L_0\bar{\rho} &= \bar{\rho}, \\ \bar{L}_{n\geq 1}\rho &= L_{n\geq 1}\bar{\rho} = \kappa\mathbb{I}\delta_{n,1}. \end{aligned} \quad (2.125b)$$

Two additional relations further characterize the module:

$$L_{-1}\rho = \bar{L}_{-1}\bar{\rho} = \beta\lambda\phi, \quad \beta = \frac{1}{2}. \quad (2.125c)$$

Up to normalizations, the height-one field  $h_1$  can be identified with  $\phi$ , each of the other three  $h_2, h_3, h_4$  with (a specific choice of)  $\psi$ .

The constants  $\lambda$  and  $\kappa$  are related to the normalizations of  $\phi$  and  $\psi$ . The nature of the parameter  $\beta$ , however, is quite different, see below. Beyond the choice of normalization of  $\phi$  and  $\psi$ , one has the freedom to redefine  $\psi$  by adding to it an arbitrary multiple of  $\phi$ , since the above structural relations will be preserved. It is in this sense that the last statement in the conjecture should be understood:  $h_2, h_3, h_4$  are proportional to each other up to a multiple of  $\phi$ .

In the following, we use the notation  $h_a(z, \bar{z})$  for the *normalized* fields arising from the scaling limit of the lattice height variables  $h_a(i)$ , their normalizations being directly inherited from those of the lattice variables. To relate them to the fields belonging to the representation described above, we arbitrarily fix the normalizations of  $\phi$  and  $\psi$  by requiring the strict identities

$$\phi(z, \bar{z}) \equiv h_1(z, \bar{z}), \quad \psi(z, \bar{z}) \equiv h_2(z, \bar{z}), \quad (2.126a)$$

which also fix the values of  $\lambda$  and  $\kappa$  to

$$\lambda = -\frac{1}{2} \quad \kappa = -\frac{\mathbb{P}_1}{4}. \quad (2.126b)$$

The other two height variables are then (conjecturally) given by the following combinations [81],

$$h_3(z, \bar{z}) = \frac{8-\pi}{2(\pi-2)} \psi(z, \bar{z}) + \frac{\pi^3-5\pi^2+12\pi-48}{4(\pi-2)^2} \phi(z, \bar{z}), \quad (2.126c)$$

$$h_4(z, \bar{z}) = -\frac{\pi+4}{2(\pi-2)} \psi(z, \bar{z}) + \frac{32+4\pi+\pi^2-\pi^3}{4(\pi-2)^2} \phi(z, \bar{z}). \quad (2.126d)$$

Let us note that the values of these coefficients imply that the height field, defined as the scaling limit of the random height variable, and equal to  $h(z, \bar{z}) = h_1 + 2h_2 + 3h_3 + 4h_4 = h_2 + 2h_3 + 3h_4$ , is itself a logarithmic field of type  $\psi$ .

We see that the fixed-height variables belong to the conformal representation that contains the identity. It was shown [127] that the identity in the bulk has itself a logarithmic partner  $\omega$ , satisfying

$$L_{n \geq 1} \omega = \bar{L}_{n \geq 1} \omega = 0, \quad L_0 \omega = \bar{L}_0 \omega = -\frac{1}{4\pi} \mathbb{I}. \quad (2.127)$$

It is normalized by requiring that  $\langle \omega(z, \bar{z}) \rangle = 1$ . On the lattice,  $\omega(z, \bar{z})$  was identified as corresponding to the insertion of dissipation at  $z$ ; in fact, as we shall briefly recall, it plays a central role in the understanding of fixed-height correlators. More details (multisite correlators of  $\omega$ , fusion and dissipation field  $\omega_b$  at a closed boundary site) can be found in [127].

In turn  $\omega$  is related to the fields discussed above; indeed, one might suspect that  $\rho$  and  $\bar{\rho}$  are actually its two descendants at level 1. Earlier calculations on the lattice [127] are consistent with the following relations,

$$\begin{aligned} \rho &= \delta \bar{L}_{-1} \omega, & \bar{\rho} &= \delta L_{-1} \omega, & \phi &= -4\delta L_{-1} \bar{L}_{-1} \omega, \\ \delta &= \frac{\pi-2}{\pi^2} = \frac{\pi}{2} \mathbb{P}_1. \end{aligned} \quad (2.128)$$

Therefore, the height-one field  $h_1(z, \bar{z})$  would be a level-2 descendant of the dissipation field,  $h_1 = -4\delta \partial \bar{\partial} \omega$ . Some of the lattice calculations of two-point correlators presented in Section 2.4 confirm these relations.

*Chiral* staggered modules of the kind discussed above were studied in [57], where it was noted that different values of  $\beta$  correspond to different equivalence classes of such modules (see [96] for a mathematical

analysis attempting a classification of staggered modules). For nonchiral modules, no classification result is known; one however knows that the bosonic sector of the free symplectic fermions [58] realizes a nonchiral representation<sup>5</sup> satisfying the same structural relations (2.125) but with a different value of  $\beta$ , namely  $\beta = -1$  ([81] to see the explicit realization). Since the chiral restrictions of the symplectic representation and of the module discussed in the above conjecture are not isomorphic, it is expected that they are not isomorphic either as nonchiral modules.

The scaling limit of fixed-height variables on a boundary has also been discussed. In this case, it depends on the boundary condition and was studied in [80, 128] for the open and closed boundary conditions. The results are simpler than in the bulk. It was found that in the continuum limit, the boundary fixed-height fields are chiral fields of scaling dimension 2, which are neither logarithmic nor primary. In particular, the height-one field, which is the only one involved in the calculations of Section 2.4.3, is proportional to the stress-energy tensor for either boundary condition,

$$h_1^{\text{op}}(x) = \frac{(16 - 3\pi)(32 - 9\pi)}{9\pi^3} T(x), \quad h_1^{\text{cl}}(x) = -\frac{3\pi - 8}{\pi^2} T(x). \quad (2.129)$$

Moreover, the other height fields  $h_a^{\text{op}}(x)$ ,  $a > 1$ , are also proportional to  $T(x)$  on an open boundary, whereas the  $h_a^{\text{cl}}(x)$ 's on a closed boundary are not. We refer to [128] for more details about these identifications.

What we want to do in the rest of this section is to focus on the bulk height fields to see whether the new correlations functions computed in Section 2.4 are consistent with the conjectured identifications stated in (2.126).

One part of the conjecture can be easily verified, namely the fact that the field  $h_3$  is a linear combination of  $h_1$  and  $h_2$  (the same then follows for  $h_4$  in view of the relation  $\sum_a h_a = 0$ ). Indeed, it is a simple matter to see by inspection that the correlators that involve the height 3 satisfy

<sup>5</sup>That representation is in fact a module for a W-algebra, and as such, is larger. For instance, it contains four logarithmic pairs of fields with weights  $(1, 1)$ , whereas here only one has been identified so far (of course, this does not rule out the possibility to find more). However, if one restricts to the action of the Virasoro modes only, one finds the relations (2.125).

this linear relation *at dominant order*. This can be explicitly checked on the two-site and three-site correlators on the plane in Section 2.3, and on the one-site and two-site correlators on the upper half-plane in Section 2.4. The lattice one-site functions on the upper half-plane, given in (2.60), make it clear that the linear relation does not hold beyond the dominant order.

The part of the conjecture concerned with the conformal transformations of the fields  $\phi$  and  $\psi$  is much deeper and implies strong constraints on the functional form of the lattice correlators that involve the heights 1 and 2. The one-point functions  $\sigma_a^{\text{op,cl}}(y)$  on the upper half-plane were at the basis of the conjecture. For each boundary condition taken separately, these functions are clearly consistent with  $\psi$  and  $\phi$  being a logarithmic pair. However, the specific way  $\sigma_a^{\text{op}}(y)$  and  $\sigma_a^{\text{cl}}(y)$  are related at dominant order—they depend on the same coefficients, see (2.60a) and (2.60b)—can actually be computed from conformal field theory, by using the field switching between the open and closed boundary conditions, identified as a primary field of weight  $-1/8$  [141]. It was done in [81] and provides a highly nontrivial and convincing check of the conjecture. Explicitly, the one-point functions on the upper half-plane are given in the continuum limit by

$$\langle h_a(z, \bar{z}) \rangle_{\text{op,cl}} = -\frac{1}{(z - \bar{z})^2} \left( c_a^{\text{op,cl}} + d_a^{\text{op,cl}} \log \left| \frac{z - \bar{z}}{2} \right| \right) \quad (2.130)$$

for  $1 \leq a \leq 4$ , where the coefficients  $c_a^{\text{cl}}, d_a^{\text{cl}}$  are the  $c_a$ 's and  $d_a$ 's given in Table 2.1. The coefficients for an open boundary are related to their analogues for a closed boundary by

$$c_a^{\text{op}} = -c_a^{\text{cl}} - \frac{1}{2}d_a^{\text{cl}}, \quad d_a^{\text{op}} = -d_a^{\text{cl}}. \quad (2.131)$$

The two-point correlators  $\sigma_{1,1}(\vec{r})$  and  $\sigma_{2,1}(\vec{r})$  on the plane were discussed in [130,131] and, in the scaling limit, confirm the logarithmic partnership of  $\phi$  and  $\psi$ . We shall briefly rediscuss these two-point functions to understand how their form should be understood, on the conformal side, not as two- but as three-point correlators where the extra background field  $\omega(\infty)$  is to be inserted. This feature will be crucial to understand the rather unusual form of the lattice three-point correlator  $\sigma_{2,1,1}(\vec{r}_{12}, \vec{r}_{13})$ . Interpreted as a conformal nonchiral four-point function, we shall show

that its unexpected functional form follows naturally from the above conjecture *and* the logarithmic nature of the background field  $\omega(\infty)$ .

Being related to chiral four-point functions, the lattice two-point correlators  $\sigma_{a,1}^{\text{op,cl}}(y)$  on the upper half-plane computed in Section 2.4 offer further opportunities to verify the consistency of the conformal framework provided by the conjecture.

### 2.7.1 Correlations on the plane

At dominant order, the lattice two-point correlators on the plane reported in Section 2.3,

$$\sigma_{1,1}(\vec{r}) = \frac{a}{r^4} + \dots, \quad \sigma_{2,1}(\vec{r}) = \frac{1}{r^4} (a \log r + b) + \dots \quad (2.132)$$

look familiar, including the distinctive presence of the same coefficient  $a$  in the two correlators. It is however well known [50] that the self-correlations of the primary field of a logarithmic pair are all identically zero, implying in particular  $\langle \phi(1)\phi(2) \rangle \equiv 0$ . As the coefficient  $a$  computed on the lattice is not zero ( $a = -\mathbb{P}_1^2/2$ ), the correlators  $\sigma_{1,1}$  and  $\sigma_{2,1}$  cannot correspond to conformal two-point functions.

The way out was discussed in [127] and has a clear physical interpretation. The probabilities computed on the infinite lattice are limits of similar quantities formulated at finite volume. The formulation of the sandpile dynamics is well defined at finite volume provided it involves dissipation of sand (to the sink), here chosen to be located on the boundaries of the grid (the dissipative sites). The infinite volume limit of multisite probabilities remains well defined, but the dissipation is sent off to infinity. On the other hand, the conformal field theory is defined right away on the infinite plane, and has no trace of the necessary dissipation. Therefore, dissipation has to be inserted at infinity by hand, in the form of a background insertion  $\omega(\infty)$ . Its conformal weights  $(0,0)$  do not alter the dimensions of the correlators.

Therefore, the lattice correlators in (2.132) should correspond respectively to the following three-point functions,

$$\langle \phi(z_1, \bar{z}_1)\phi(z_2, \bar{z}_2)\omega(\infty) \rangle \quad \text{and} \quad \langle \psi(z_1, \bar{z}_1)\phi(z_2, \bar{z}_2)\omega(\infty) \rangle.$$

Indeed, one finds that these three-point functions reproduce the form given in (2.132) provided the two-point functions  $\langle \phi(z_1, \bar{z}_1)\phi(z_2, \bar{z}_2) \rangle$  and  $\langle \psi(z_1, \bar{z}_1)\phi(z_2, \bar{z}_2) \rangle$  vanish identically [129]. This is again very natural from the sandpile point of view, since these two-point functions would correspond to fractions of recurrent configurations with fixed heights at sites 1 and 2 in a model with no dissipation; such models are known to have no recurrent configurations at all [40]. In what follows, we use this argument to set all correlations involving only  $\phi$ 's and  $\psi$ 's to zero.

Let us now come to the three-point correlators. When the three insertion points are aligned (horizontally or vertically), we recall that these are given at dominant order (terms of dimension 6) by

$$\sigma_{1,1,1}(\vec{r}_{12}, \vec{r}_{13}) = 0 + \dots, \quad \sigma_{2,1,1}(\vec{r}_{12}, \vec{r}_{13}) = \frac{(\pi - 2)^3}{\pi^9} \frac{1}{r_{12}^3 r_{13}^3} + \dots \quad (2.133)$$

It is surprising, in the sandpile model, that the correlator of three heights 1 vanishes (at dominant order). To a large extent, this can be understood in the conformal picture.

The four-point function  $\langle \phi(z_1, \bar{z}_1)\phi(z_2, \bar{z}_2)\phi(z_3, \bar{z}_3)\omega(\infty) \rangle$  should be associated with the scaling limit of the correlator  $\sigma_{1,1,1}$ . From the vanishing of  $\langle \phi(z_1, \bar{z}_1)\phi(z_2, \bar{z}_2)\phi(z_3, \bar{z}_3) \rangle$ , the four-point function can be computed as if  $\omega$  is primary of weights (0,0) (not assumed to be degenerate at level 1 though, like the identity). However, together the Ward identities and the degeneracy conditions of  $\phi$  at level 2 in the theory with central charge  $c = -2$ , namely  $(L_{-1}^2 - 2L_{-2})\phi = (\bar{L}_{-1}^2 - 2\bar{L}_{-2})\phi = 0$ , offer no solution that is fully symmetric under the permutations of sites 1, 2 and 3.

Let us now examine the other three-point correlator  $\sigma_{2,1,1}$  in light of the nonchiral four-point function  $\langle \psi(z_1, \bar{z}_1)\phi(z_2, \bar{z}_2)\phi(z_3, \bar{z}_3)\omega(\infty) \rangle$ . As is usually the case for a correlation involving logarithmic fields, the calculation proceeds in several steps [50]. Finite regular conformal transformations of  $\omega$  involve  $\omega$  itself and the identity, whereas those of  $\psi$  involve  $\psi$  itself,  $\phi$ ,  $\rho$ ,  $\bar{\rho}$  and the identity. This makes a total of 9 four-point functions to be computed before the last one  $\langle \psi(1)\phi(2)\phi(3)\omega(\infty) \rangle$  can be obtained. However, many of them either vanish or are already

known:

$$\begin{aligned} \langle \psi(1)\phi(2)\phi(3) \rangle &= \langle \phi(1)\phi(2)\phi(3) \rangle = \langle \rho(1)\phi(2)\phi(3) \rangle \\ &= \langle \bar{\rho}(1)\phi(2)\phi(3) \rangle = \langle \phi(2)\phi(3) \rangle = 0, \end{aligned} \quad (2.134a)$$

$$\langle \phi(1)\phi(2)\phi(3)\omega(\infty) \rangle = 0, \quad (2.134b)$$

$$\langle \phi(2)\phi(3)\omega(\infty) \rangle = \frac{C_{\phi\phi}}{|z_2 - z_3|^4}, \quad C_{\phi\phi} = -\frac{\mathbb{P}_1^2}{2}. \quad (2.134c)$$

In what follows, we summarize the calculations of the remaining three correlations

$$\langle \rho(1)\phi(2)\phi(3)\omega(4) \rangle, \quad \langle \bar{\rho}(1)\phi(2)\phi(3)\omega(4) \rangle \quad \text{and} \quad \langle \psi(1)\phi(2)\phi(3)\omega(4) \rangle$$

for general positions. To simplify the analysis, we retain only the most general solutions that are symmetric under the exchange of sites 2 and 3 *in the limit where the site 4 goes to infinity*.

The integration of the infinitesimal transformations given in (2.125a) and (2.125b) yields the following transformation rules of  $\rho, \phi$  and  $\omega$  under  $w \rightarrow z(w), \bar{w} \rightarrow \bar{z}(\bar{w})$  [81],

$$\omega(z, \bar{z}) = \omega(w, \bar{w}) - \frac{1}{4\pi} \log \left| \frac{dw}{dz} \right|^2, \quad (2.135a)$$

$$\phi(z, \bar{z}) = \left| \frac{dw}{dz} \right|^2 \phi(w, \bar{w}), \quad (2.135b)$$

$$\rho(z, \bar{z}) = \frac{d\bar{w}}{d\bar{z}} \rho(w, \bar{w}) + \frac{\kappa}{2} \left( \frac{d^2\bar{w}}{d\bar{z}^2} / \frac{d\bar{w}}{d\bar{z}} \right). \quad (2.135c)$$

The Möbius transformations (with  $z_{ij} \equiv z_i - z_j$ )

$$w(z) = \frac{(z_1 - z)z_{34}}{z_{13}(z - z_4)}, \quad \bar{w}(\bar{z}) = \frac{(\bar{z}_1 - \bar{z})\bar{z}_{34}}{\bar{z}_{13}(\bar{z} - \bar{z}_4)}, \quad (2.136)$$

map the four points  $z_1, z_2, z_3$  and  $z_4$  to  $0, x = (z_{12}z_{34})/(z_{13}z_{24}), 1$  and  $\infty$  respectively (and likewise for the conjugate variables). The above transformation rules yield the following form:

$$\langle \rho(1)\phi(2)\phi(3)\omega(4) \rangle = -\frac{\bar{z}_{34}}{\bar{z}_{13}\bar{z}_{14}} \frac{1}{|z_{23}|^4} \left\{ F(x, \bar{x}) + \kappa C_{\phi\phi} \frac{\bar{z}_{13}}{\bar{z}_{34}} \right\}, \quad (2.137)$$

with  $F(x, \bar{x}) = |1 - x|^4 \langle \rho(0, 0)\phi(x, \bar{x})\phi(1, 1)\omega(\infty) \rangle$ .

Further constraints on  $F(x, \bar{x})$  come from the left and right degeneracy conditions of  $\phi$  at level 2. The left degeneracy condition of  $\phi(2)$  (or of  $\phi(3)$ ) yields a homogeneous differential equation in  $x$ , namely

$$x(1-x)\partial^2 F + 2\partial F = 0. \quad (2.138)$$

It can be strengthened in the following way. The following correlator,  $\langle (L_{-1}\rho)(1)\phi(2)\phi(3)\omega(4) \rangle$ , is proportional to  $\langle \phi(1)\phi(2)\phi(3)\omega(4) \rangle$ , which is identically zero. Therefore,  $\langle \rho(1)\phi(2)\phi(3)\omega(4) \rangle$  cannot depend on  $z_1$ , and so  $F(x, \bar{x})$  cannot depend on  $x$ ,  $\partial F = 0$ .

The right degeneracy of  $\phi$  actually delivers two independent, inhomogeneous equations, depending on whether we write it for  $\phi(2)$  or for  $\phi(3)$ . They combine to give a first-order equation,

$$\bar{\mathcal{D}}F(x, \bar{x}) = -\kappa C_{\phi\phi} \frac{1-\bar{x}}{\bar{x}^2}, \quad \bar{\mathcal{D}} \equiv \bar{\partial} + \frac{\bar{x}+2}{\bar{x}(1-\bar{x})}. \quad (2.139)$$

The general solution is obtained from a particular solution of the inhomogeneous equation, for instance  $-\kappa C_{\phi\phi}(1-\bar{x})^2/\bar{x}^2$ , and an arbitrary element of  $\ker \bar{\mathcal{D}}$ , given by  $A(1-\bar{x})^3/\bar{x}^2$ . Inserting this general form into (2.137), taking the limit  $z_4, \bar{z}_4 \rightarrow \infty$  and requiring that the result be symmetric under  $2 \leftrightarrow 3$  fix  $A = \kappa C_{\phi\phi}/2$  and lead to the unique solution,

$$F(x, \bar{x}) = -\kappa C_{\phi\phi} \frac{(1+\bar{x})(1-\bar{x})^2}{2\bar{x}^2}. \quad (2.140)$$

The correlation involving  $\bar{\rho}$  instead of  $\rho$  is similar since the transformations of  $\bar{\rho}$  are those of  $\rho$  with left and right exchanged. The corresponding correlation is simply obtained by exchanging the variables with their conjugates,

$$\langle \bar{\rho}(1)\phi(2)\phi(3)\omega(4) \rangle = \kappa C_{\phi\phi} \frac{z_{34}}{z_{13}z_{14}|z_{23}|^4} \left\{ \frac{(1+x)(1-x)^2}{2x^2} - \frac{z_{13}}{z_{34}} \right\}. \quad (2.141)$$

Finally, the same procedure may be used to compute the last correlator. To do this, we use the finite transformation law of  $\psi$  under  $w \rightarrow z(w)$ ,

$\bar{w} \rightarrow \bar{z}(\bar{w})$  [81],

$$\begin{aligned} \psi(z, \bar{z}) &= \left| \frac{dw}{dz} \right|^2 \left[ \psi(w, \bar{w}) + \log \left| \frac{dw}{dz} \right|^2 \phi(w, \bar{w}) \right] \\ &+ \frac{1}{2} \left( \frac{d^2 w}{dz^2} / \frac{dw}{dz} \right) \frac{d\bar{w}}{d\bar{z}} \rho(w, \bar{w}) \\ &+ \frac{1}{2} \frac{dw}{dz} \left( \frac{d^2 \bar{w}}{d\bar{z}^2} / \frac{d\bar{w}}{d\bar{z}} \right) \bar{\rho}(w, \bar{w}) \\ &+ \frac{\kappa}{4} \left( \frac{d^2 w}{dz^2} / \frac{dw}{dz} \right) \left( \frac{d^2 \bar{w}}{d\bar{z}^2} / \frac{d\bar{w}}{d\bar{z}} \right). \end{aligned} \quad (2.142)$$

The same Möbius transformation as before yields

$$\begin{aligned} \langle \psi(1)\phi(2)\phi(3)\omega(4) \rangle &= \frac{1}{|z_{14}z_{23}^2|^2} \left\{ \left| \frac{z_{34}}{z_{13}} \right|^2 G(x, \bar{x}) + \frac{\bar{z}_{34}}{\bar{z}_{13}} F(x, \bar{x}) \right. \\ &\quad \left. + \frac{z_{34}}{z_{13}} F(\bar{x}, x) + \kappa C_{\phi\phi} \right\}, \end{aligned} \quad (2.143)$$

with  $G(x, \bar{x}) = |1-x|^4 \langle \psi(0,0)\phi(x, \bar{x})\phi(1,1)\omega(\infty) \rangle$  and for the function  $F(x, \bar{x})$  given in (2.140).

The left and right degeneracy conditions of  $\phi(2)$  and  $\phi(3)$  each give two differential equations for  $G(x, \bar{x})$ ; so four equations in total, two in  $x$  and two in  $\bar{x}$ . They combine to give two first-order equations, very close to the one encountered above, as they involve the same differential operator (in  $x$  or  $\bar{x}$ ),

$$\mathcal{D}G(x, \bar{x}) = -\frac{1-x}{x^2} F(x, \bar{x}), \quad (2.144a)$$

$$\bar{\mathcal{D}}G(x, \bar{x}) = -\frac{1-\bar{x}}{\bar{x}^2} F(\bar{x}, x), \quad (2.144b)$$

Their compatibility is readily established on account of the right equation (2.139) satisfied by  $F(x, \bar{x})$ .

The general solution depends on a free parameter  $B$ , related to the choice of an arbitrary element in  $\ker\{\mathcal{D}, \bar{\mathcal{D}}\}$ ,

$$G(x, \bar{x}) = \frac{1}{2} \kappa C_{\phi\phi} (x + \bar{x}) \left| \frac{1-x}{x} \right|^4 + B \left| \frac{(1-x)^3}{x^2} \right|^2. \quad (2.145)$$

Inserted in (2.143), the limit  $z_4, \bar{z}_4 \rightarrow \infty$  yields a result that is symmetric in  $2 \leftrightarrow 3$ , for any value of  $B$ ,

$$\begin{aligned} \langle \psi(1)\phi(2)\phi(3)\omega(\infty) \rangle &= \frac{1}{2} \kappa C_{\phi\phi} \frac{1}{|z_{12}z_{13}|^2} \left[ \frac{1}{z_{13}\bar{z}_{12}} + \frac{1}{z_{12}\bar{z}_{13}} \right] \\ &+ B \left| \frac{z_{23}}{z_{12}^2 z_{13}^2} \right|^2. \end{aligned} \quad (2.146)$$

We note that the term proportional to  $B$  has a singularity in  $|z_{12}|^{-4}$ , namely the most singular term possible in the fusion  $\psi(1)\phi(2)$ . The only fields that can enter the fusion at this order are the identity and  $\omega$ . The vanishing of  $\langle\psi(1)\phi(2)\rangle$  forbids the presence of  $\omega$ , while the correlator  $\langle\psi(1)\phi(2)\omega(\infty)\rangle = (a \log |z_{12}| + b)/|z_{12}|^4$  shows that the identity enters the fusion with a logarithmic term. Since the last term in (2.146) contains no logarithm, we conclude that  $B = 0$ .

When the three fields are aligned horizontally, the variables  $z_{ij}$  are real, so that the previous correlator reduces to

$$\langle h_2(\vec{r}_1) h_1(\vec{r}_2) h_1(\vec{r}_3) \omega(\infty) \rangle = \kappa C_{\phi\phi} \frac{1}{r_{12}^3 r_{13}^3}. \quad (2.147)$$

With  $\kappa = -\mathbb{P}_1/4$  and  $C_{\phi\phi} = -\mathbb{P}_1^2/2$  (see above), we obtain  $\kappa C_{\phi\phi} = \mathbb{P}_1^3/8 = (\pi - 2)^3/\pi^9$ , which exactly reproduces the dominant order of  $\sigma_{2,1,1}(\vec{r}_{12}, \vec{r}_{13})$ , given in (2.51).

### 2.7.2 Bulk-boundary correlations

Section 2.4.3 gave the results of our lattice computations of the two-point correlations  $\sigma_{a,1}^{\text{op,cl}}$  of two heights, the height  $a$  being in the bulk of the upper half-plane, the height 1 on the boundary, taken to be either open or closed. For simplicity, the height  $a$  was located right above the height 1, at a distance  $y$  from the boundary.

For general positions  $x$  (real) and  $z$ , these mixed bulk-boundary correlators should correspond to the following conformal correlators, at dominant order,

$$\begin{aligned} \sigma_{a,1}^{\text{op}}(z, \bar{z}; x) &= \langle h_a(z, \bar{z}) h_1^{\text{op}}(x) \rangle_{\text{op}} + \dots, \\ \sigma_{a,1}^{\text{cl}}(z, \bar{z}; x) &= \langle h_a(z, \bar{z}) h_1^{\text{cl}}(x) \omega(\infty) \rangle_{\text{cl}} + \dots \end{aligned} \quad (2.148)$$

Dissipation at infinity has been inserted in the second correlator; no such insertion is needed when the boundary is open, since each boundary site is dissipative. As before, one may concentrate on  $a = 1, 2$ .

The boundary height-one field being proportional to the stress-energy tensor, the correlators  $\sigma_{a,1}^{\text{op,cl}}(z, \bar{z}; x)$  are related to the one-point functions  $\sigma_a^{\text{op,cl}}(z, \bar{z})$ . These are known from [81] and have been recalled in

(the dominant terms of) (2.60a) and (2.60b). When the boundary is open, the UHP stress-energy tensor can be thought of as the sum of the left and right chiral tensors [27]. Using this property together with the chiral conformal transformations in (2.125), we find that for  $a = 1, 2$ ,

$$\begin{aligned} \langle T(x) h_a(z, \bar{z}) \rangle_{\text{op}} &= \left\{ \frac{1}{(x-z)^2} + \frac{1}{x-z} \partial_z + \frac{1}{(x-\bar{z})^2} + \frac{1}{x-\bar{z}} \partial_{\bar{z}} \right\} \langle h_a(z, \bar{z}) \rangle_{\text{op}} \\ &+ \left\{ \frac{\langle \rho(z, \bar{z}) \rangle_{\text{op}}}{(x-z)^3} + \frac{\langle \bar{\rho}(z, \bar{z}) \rangle_{\text{op}}}{(x-\bar{z})^3} - \frac{\langle h_1(z, \bar{z}) \rangle_{\text{op}}}{2(x-z)^2} - \frac{\langle h_1(z, \bar{z}) \rangle_{\text{op}}}{2(x-\bar{z})^2} \right\} \delta_{a,2}. \end{aligned} \quad (2.149)$$

To complete the calculation, we need to evaluate the one-point correlators  $\langle \rho(z, \bar{z}) \rangle_{\text{op}}$  and  $\langle \bar{\rho}(z, \bar{z}) \rangle_{\text{op}}$ . The quickest way to compute them is by using the relations  $\rho = \delta \bar{L}_{-1} \omega$ ,  $\bar{\rho} = \delta L_{-1} \omega$  as well as

$$\langle \omega(z, \bar{z}) \rangle_{\text{op}} = \frac{1}{2\pi} \log |z - \bar{z}| + \gamma_0, \quad (2.150)$$

with  $\gamma_0 = \frac{1}{2\pi}(\gamma + \frac{3}{2} \log 2) + 1$  and  $\gamma = 0.577216\dots$  the Euler constant [127]. Hence, we have

$$\langle \rho(z, \bar{z}) \rangle_{\text{op}} = -\frac{d_2}{z - \bar{z}}, \quad \langle \bar{\rho}(z, \bar{z}) \rangle_{\text{op}} = \frac{d_2}{z - \bar{z}}, \quad (2.151a)$$

$$\langle h_1(z, \bar{z}) \rangle_{\text{op}} = -\frac{4d_2}{(z - \bar{z})^2}, \quad (2.151b)$$

$$\langle h_2(z, \bar{z}) \rangle_{\text{op}} = -\frac{4}{(z - \bar{z})^2} \left\{ c_2 + \frac{d_2}{2} + d_2 \log \left| \frac{z - \bar{z}}{2} \right| \right\}, \quad (2.151c)$$

where the coefficients  $c_2, d_2$  have been given explicitly in Section 2.4. Plugging these in (2.149) yields

$$\langle T(x) h_1(z, \bar{z}) \rangle_{\text{op}} = -\frac{4d_2}{|x - z|^4}, \quad (2.152a)$$

$$\langle T(x) h_2(z, \bar{z}) \rangle_{\text{op}} = -\frac{4}{|x - z|^4} \left\{ c_2 + \frac{3d_2}{4} + \frac{d_2}{4} \frac{(z - \bar{z})^2}{|x - z|^2} + d_2 \log \left| \frac{z - \bar{z}}{2} \right| \right\}. \quad (2.152b)$$

When the boundary is closed, one has, from (2.127),

$$\begin{aligned}
\langle T(x) h_a(z, \bar{z}) \omega(\infty) \rangle_{\text{cl}} &= \left\{ \frac{1}{(x-z)^2} + \frac{1}{x-z} \partial_z + \frac{1}{(x-\bar{z})^2} + \frac{1}{x-\bar{z}} \partial_{\bar{z}} \right\} \\
&\times \langle h_a(z, \bar{z}) \omega(\infty) \rangle_{\text{cl}} + \left\{ \frac{\langle \rho(z, \bar{z}) \omega(\infty) \rangle_{\text{cl}}}{(x-z)^3} + \frac{\langle \bar{\rho}(z, \bar{z}) \omega(\infty) \rangle_{\text{cl}}}{(x-\bar{z})^3} \right. \\
&\quad \left. - \frac{\langle h_1(z, \bar{z}) \omega(\infty) \rangle_{\text{cl}}}{2(x-z)^2} - \frac{\langle h_1(z, \bar{z}) \omega(\infty) \rangle_{\text{cl}}}{2(x-\bar{z})^2} \right\} \delta_{a,2} \\
&+ \lim_{w, \bar{w} \rightarrow \infty} \left[ \left\{ \frac{1}{x-w} \partial_w + \frac{1}{x-\bar{w}} \partial_{\bar{w}} \right\} \langle h_a(z, \bar{z}) \omega(w, \bar{w}) \rangle_{\text{cl}} \right. \\
&\quad \left. - \frac{\langle h_a(z, \bar{z}) \rangle_{\text{cl}}}{4\pi(x-w)^2} - \frac{\langle h_a(z, \bar{z}) \rangle_{\text{cl}}}{4\pi(x-\bar{w})^2} \right].
\end{aligned} \tag{2.153}$$

The terms on the last line give however no contribution:  $\langle h_a(z, \bar{z}) \rangle_{\text{cl}}$  vanishes identically (no dissipation), and  $\langle h_a(z, \bar{z}) \omega(w, \bar{w}) \rangle_{\text{cl}}$  does not depend on  $w, \bar{w}$  (the precise location of the dissipation is immaterial for this two-point function).

Repeating the same steps as before, this time using [127]

$$\langle \omega(z_1, \bar{z}_1) \omega(z_2, \bar{z}_2) \rangle_{\text{cl}} = \frac{1}{\pi} \log |z_{12}| + 2\gamma_0 + \frac{1}{2\pi} \log \frac{|z_1 - \bar{z}_2|^2}{|z_1 - \bar{z}_1| |z_2 - \bar{z}_2|}, \tag{2.154}$$

we obtain the following two-point correlators:

$$\langle \rho(z, \bar{z}) \omega(\infty) \rangle_{\text{cl}} = \frac{d_2}{z - \bar{z}}, \quad \langle \bar{\rho}(z, \bar{z}) \omega(\infty) \rangle_{\text{cl}} = -\frac{d_2}{z - \bar{z}}, \tag{2.155a}$$

$$\langle h_1(z, \bar{z}) \omega(\infty) \rangle_{\text{cl}} = \frac{4d_2}{(z - \bar{z})^2}, \tag{2.155b}$$

$$\langle h_2(z, \bar{z}) \omega(\infty) \rangle_{\text{cl}} = \frac{4}{(z - \bar{z})^2} \left\{ c_2 + d_2 \log \left| \frac{z - \bar{z}}{2} \right| \right\}, \tag{2.155c}$$

with the same coefficients  $c_2, d_2$ . In turn, this leads to

$$\langle T(x) h_1(z, \bar{z}) \omega(\infty) \rangle_{\text{cl}} = \frac{4d_2}{|x-z|^4}, \tag{2.156a}$$

$$\langle T(x) h_2(z, \bar{z}) \omega(\infty) \rangle_{\text{cl}} = \frac{4}{|x-z|^4} \left\{ c_2 + \frac{d_2}{4} \right. \tag{2.156b}$$

$$\left. + \frac{d_2}{4} \frac{(z - \bar{z})^2}{|x-z|^2} + d_2 \log \left| \frac{z - \bar{z}}{2} \right| \right\}. \tag{2.156c}$$

The correlators (2.152) and (2.156), evaluated when the height  $a$  is right above the boundary height 1, namely for  $x - z = -iy$ , simplify to give

$$\langle T(x) h_1(z, \bar{z}) \rangle_{\text{op}} = -\frac{4d_2}{y^4}, \quad (2.157a)$$

$$\langle T(x) h_2(z, \bar{z}) \rangle_{\text{op}} = -\frac{4}{y^4} \left\{ c_2 - \frac{d_2}{4} + d_2 \log y \right\}, \quad (2.157b)$$

$$\langle T(x) h_1(z, \bar{z}) \omega(\infty) \rangle_{\text{cl}} = \frac{4d_2}{y^4}, \quad (2.157c)$$

$$\langle T(x) h_2(z, \bar{z}) \omega(\infty) \rangle_{\text{cl}} = \frac{4}{y^4} \left\{ c_2 - \frac{3d_2}{4} + d_2 \log y \right\}. \quad (2.157d)$$

Inserting the explicit values of  $c_2, d_2$  and the proportionality constants between  $h_1^{\text{op,cl}}(x)$  and  $T(x)$ , given in (2.129), exactly yields the dominant orders of the lattice correlators  $\sigma_{a,1}^{\text{op,cl}}(y)$  computed in Section 2.4.3.

### 2.7.3 Two-point bulk correlations on the upper half-plane

The last case concerns the lattice correlators  $\sigma_{a,1}^{\text{op,cl}}$  for two heights vertically aligned in the bulk of the upper half-plane. As before, we focus on  $a = 1, 2$  and compute the corresponding conformal correlation function for arbitrary positions, expected to describe the dominant order of the lattice correlators,

$$\begin{aligned} \sigma_{a,1}^{\text{op}}(\vec{r}_1, \vec{r}_2) &= \langle h_a(z_1, \bar{z}_1) h_1(z_2, \bar{z}_2) \rangle_{\text{op}} + \dots, \\ \sigma_{a,1}^{\text{cl}}(\vec{r}_1, \vec{r}_2) &= \langle h_a(z_1, \bar{z}_1) h_1(z_2, \bar{z}_2) \omega(\infty) \rangle_{\text{cl}} + \dots \end{aligned} \quad (2.158)$$

Since the field  $h_1 = \phi$  is degenerate at level 2, the previous correlators satisfy second-order differential equations for  $a = 1$  and for  $a = 2$ . However, for  $a = 1$ , it is much quicker to start from the self-correlators of  $\omega$  and use the relations giving the nonchiral fields  $\rho, \bar{\rho}$  and  $\phi$  in terms of  $\omega$ . This avoids the solving of differential equations and circumvents the problem of fixing the integration constants. In addition, it yields the correlators involving  $\rho$  and  $\bar{\rho}$ , which are in any case required for the case  $a = 2$ , at least for the open boundary condition. We start with  $a = 1$ .

The correlators with two (resp. three) dissipation fields in presence of an open (resp. closed) boundary are easily computed (they are given by

$2 \times 2$  (resp.  $3 \times 3$ ) determinants [127]),

$$\begin{aligned} \langle \omega(z_1, \bar{z}_1) \omega(z_2, \bar{z}_2) \rangle_{\text{op}} &= -\frac{1}{4\pi^2} \log^2 \left| \frac{z_1 - z_2}{z_1 - \bar{z}_2} \right| + \left( \frac{1}{2\pi} \log |z_1 - \bar{z}_1| + \gamma_0 \right) \\ &\quad \times \left( \frac{1}{2\pi} \log |z_2 - \bar{z}_2| + \gamma_0 \right), \end{aligned} \quad (2.159a)$$

$$\begin{aligned} \langle \omega(z_1, \bar{z}_1) \omega(z_2, \bar{z}_2) \omega(z_3, \bar{z}_3) \rangle_{\text{cl}} &= -\frac{1}{4\pi^2} \log |(z_1 - z_2)(z_1 - \bar{z}_2)| \\ &\quad \times \log \frac{|(z_1 - z_2)(z_1 - \bar{z}_2)|}{|(z_2 - z_3)(z_2 - \bar{z}_3)|^2} + \left( \gamma_0 - \frac{1}{2\pi} \log |z_1 - \bar{z}_1| \right) \\ &\quad \times \left( \gamma_0 - \frac{1}{2\pi} \log \frac{|z_3 - \bar{z}_3|}{|(z_2 - z_3)(z_2 - \bar{z}_3)|^2} \right) + \text{cyclic}. \end{aligned} \quad (2.159b)$$

Upon derivation, one easily gets the correlators involving  $\rho$ ,  $\bar{\rho}$  and  $\phi$ . For the open boundary condition, they can be written in the following way:

$$\begin{aligned} \langle \rho(1) \phi(2) \rangle_{\text{op}} &= -\frac{\mathbb{P}_1^2}{8} \left\{ \frac{1}{(z_1 - \bar{z}_2)(\bar{z}_1 - z_2)^2} - \frac{2}{(z_1 - \bar{z}_1)(z_2 - \bar{z}_2)^2} \right. \\ &\quad \left. + \frac{(z_1 - \bar{z}_1)^2 - (z_1 - z_2)(z_1 - \bar{z}_2)}{(z_1 - z_2)(\bar{z}_1 - z_2)^2(\bar{z}_1 - \bar{z}_2)^2} \right\}, \end{aligned} \quad (2.160a)$$

$$\begin{aligned} \langle \bar{\rho}(1) \phi(2) \rangle_{\text{op}} &= -\frac{\mathbb{P}_1^2}{8} \left\{ \frac{1}{(z_1 - \bar{z}_2)^2(\bar{z}_1 - z_2)} + \frac{2}{(z_1 - \bar{z}_1)(z_2 - \bar{z}_2)^2} \right. \\ &\quad \left. + \frac{(z_1 - \bar{z}_1)^2 - (\bar{z}_1 - z_2)(\bar{z}_1 - \bar{z}_2)}{(z_1 - z_2)^2(z_1 - \bar{z}_2)^2(\bar{z}_1 - \bar{z}_2)} \right\}, \end{aligned} \quad (2.160b)$$

$$\langle \phi(1) \phi(2) \rangle_{\text{op}} = \frac{\mathbb{P}_1^2}{2} \left\{ \frac{2}{(z_1 - \bar{z}_1)^2(z_2 - \bar{z}_2)^2} - \frac{1}{|z_1 - z_2|^4} - \frac{1}{|z_1 - \bar{z}_2|^4} \right\}. \quad (2.160c)$$

The third equation in particular, evaluated when  $z_1 = x + iy_1$  and  $z_2 = x + iy_2$  are vertically aligned, reproduces exactly the dominant terms of  $\sigma_{1,1}^{\text{op}}(y_1, y_2)$  reported in Section 2.4.4.

Similar calculations when the boundary is closed leads to slightly different results:

$$\langle \rho(1) \phi(2) \omega(\infty) \rangle_{\text{cl}} = \langle \rho(1) \phi(2) \rangle_{\text{op}} - \frac{\mathbb{P}_1^2}{4} \frac{(\bar{z}_1 - z_2) + (\bar{z}_1 - \bar{z}_2)}{(\bar{z}_1 - z_2)^2(\bar{z}_1 - \bar{z}_2)^2}, \quad (2.161a)$$

$$\langle \bar{\rho}(1) \phi(2) \omega(\infty) \rangle_{\text{cl}} = \langle \bar{\rho}(1) \phi(2) \rangle_{\text{op}} - \frac{\mathbb{P}_1^2}{4} \frac{(z_1 - z_2) + (z_1 - \bar{z}_2)}{(z_1 - z_2)^2(z_1 - \bar{z}_2)^2}, \quad (2.161b)$$

$$\langle \phi(1) \phi(2) \omega(\infty) \rangle_{\text{cl}} = \langle \phi(1) \phi(2) \rangle_{\text{op}}. \quad (2.161c)$$

The correlators involving  $\rho$  and  $\bar{\rho}$  for the closed boundary differ from their open analogues by terms independent of  $z_1$  and  $\bar{z}_1$  respectively, with the consequence that the closed correlator with two  $\phi$ 's in general positions is exactly equal to the one corresponding to the open boundary, in agreement with the lattice results (2.79) and (2.82) when the two insertion points are vertically aligned.

The case  $a = 2$  for the open boundary condition requires to compute the nonchiral two point-function  $\langle \psi(1)\phi(2) \rangle_{\text{op}}$ . We first perform a Möbius transformation, taken to be real to preserve the boundary, so as to bring the two insertion points to positions that only depend on the anharmonic ratio of  $z_1, \bar{z}_1, z_2, \bar{z}_2$  given by

$$x = \frac{(z_1 - \bar{z}_1)(z_2 - \bar{z}_2)}{(z_1 - z_2)(\bar{z}_1 - \bar{z}_2)} = -\frac{4y_1y_2}{|z_1 - z_2|^2}, \quad (\text{real negative}) \quad (2.162)$$

where  $y_1, y_2 > 0$  are the imaginary parts of  $z_1, z_2$ . A convenient choice is to map the two points  $z_1, z_2$  onto respectively  $w_1 = it$  and  $w_2 = 2 + it$  with  $t = \sqrt{-x} > 0$ . The proper map takes the usual form  $w(z) = (az + b)/(cz + d)$  with the following values of the parameters,

$$\begin{aligned} a &= t(x_1 - x_2) - 2y_2, & b &= 2x_1y_2 - t(x_1^2 - x_1x_2 + y_1^2 - y_1y_2), \\ c &= y_1 - y_2, & d &= x_1y_2 - x_2y_1 - 2\frac{y_1y_2}{t}, \end{aligned} \quad (2.163)$$

where  $x_1, x_2$  are the real parts of  $z_1, z_2$ .

The transformation law (2.142) of  $\psi$  yields the following identity,

$$\begin{aligned} \langle \psi(z_1, \bar{z}_1)\phi(z_2, \bar{z}_2) \rangle_{\text{op}} &= \frac{x^2}{y_1^2y_2^2} \left\{ \langle \psi(w_1, \bar{w}_1)\phi(w_2, \bar{w}_2) \rangle_{\text{op}} \right. \\ &\quad \left. + \lambda \log \left( \frac{-x}{y_1^2} \right) \langle \phi(w_1, \bar{w}_1)\phi(w_2, \bar{w}_2) \rangle_{\text{op}} \right\} \\ &\quad - \frac{x^2(y_1 - y_2)}{y_1^2y_2^2} \left\{ \frac{\langle \rho(w_1, \bar{w}_1)\phi(w_2, \bar{w}_2) \rangle_{\text{op}}}{t(\bar{z}_1 - \bar{z}_2) - 2y_2} + \frac{\langle \bar{\rho}(w_1, \bar{w}_1)\phi(w_2, \bar{w}_2) \rangle_{\text{op}}}{t(z_1 - z_2) - 2y_2} \right. \\ &\quad \left. - \frac{\kappa(y_1 - y_2)}{4y_2} \frac{\langle \phi(w_2, \bar{w}_2) \rangle_{\text{op}}}{y_1 + y_2 - t(x_1 - x_2)} \right\}. \end{aligned} \quad (2.164)$$

Of the five correlators appearing on the right-hand side, the last four are known functions of  $x$ , and given in (2.151) and (2.160). Further using

$\lambda = -\frac{1}{2}$  and  $\kappa = -\frac{\mathbb{P}_1}{4}$ , one may simplify the previous expression to

$$\begin{aligned} \langle \psi(z_1, \bar{z}_1) \phi(z_2, \bar{z}_2) \rangle_{\text{op}} &= \frac{x^2}{y_1^2 y_2^2} \left[ H(x) + \frac{\mathbb{P}_1^2}{64} \frac{x^4 - 2x^3 + 4x - 2}{(1-x)^2} \log\left(\frac{-x}{y_1^2}\right) \right] \\ &+ \frac{\mathbb{P}_1^2}{128} \frac{y_1 - y_2}{y_1^2 y_2^3} \frac{x^3(x-2)}{(1-x)^2}, \end{aligned} \quad (2.165)$$

where  $H(x) = \langle \psi(w_1, \bar{w}_1) \phi(w_2, \bar{w}_2) \rangle_{\text{op}}$ . The degeneracy of  $\phi$  implies that the function  $H(x)$  satisfies the following differential equation,

$$\begin{aligned} x(1-x)H''(x) + 2(1-2x)H'(x) - \frac{2H(x)}{x(1-x)} \\ = -\frac{\mathbb{P}_1^2}{64} \frac{x^4 - 14x^3 + 24x^2 - 20x + 6}{x^3(1-x)^3}. \end{aligned} \quad (2.166)$$

The general solution depends on two integration constants, which can be easily fixed by considering two limiting cases. Indeed, for a large horizontal separation of  $\psi$  and  $\phi$  (i.e.  $|x_1 - x_2| \rightarrow \infty$  and  $y_1, y_2$  finite), and for a large distance to the boundary (i.e.  $y_1, y_2 \rightarrow \infty$  and  $|z_1 - z_2|$  finite), the correlator  $\langle \psi(z_1, \bar{z}_1) \phi(z_2, \bar{z}_2) \rangle_{\text{op}}$  must go respectively to the product  $\langle \psi(z_1, \bar{z}_1) \rangle_{\text{op}} \langle \phi(z_2, \bar{z}_2) \rangle_{\text{op}}$  and to the bulk correlator  $\langle \psi(z_1, \bar{z}_1) \phi(z_2, \bar{z}_2) \rangle$  on the full plane.

The final result reads

$$\begin{aligned} \langle \psi(z_1, \bar{z}_1) \phi(z_2, \bar{z}_2) \rangle_{\text{op}} &= \frac{\mathbb{P}_1}{32y_1^2 y_2^2} \frac{x^4 - 2x^3 + 4x - 2}{(1-x)^2} \left[ \frac{3(3\pi - 10)}{2\pi^3} \right. \\ &\left. - \mathbb{P}_1 \left( \log y_1 + \gamma + \frac{5}{2} \log 2 \right) \right] \\ &+ \frac{\mathbb{P}_1^2}{64y_1^2 y_2^2} \left[ \frac{x^3(x-2)}{(1-x)^2} \left( \log(1-x) + \frac{y_1}{2y_2} \right) - \frac{x^2}{1-x} \right]. \end{aligned} \quad (2.167)$$

As a first check, one can verify that when the two fields are vertically aligned,  $x_1 = x_2$ , the previous form exactly reproduces the dominant term of the lattice correlator  $\sigma_{2,1}^{\text{op}}(y_1, y_2)$  given in (2.80). A second and independent check concerns the limit  $y_2 \rightarrow 0$ , which brings the height-one field  $\phi$  to the boundary. In this limit, the bulk  $\phi$  is expected to

expand on open-boundary fields of its own conformal family, to which the identity and the stress-energy tensor (the open-boundary height-one field) belong, namely

$$\phi(z_2, z_2^*) \simeq \frac{C_{-2}}{y_2^2} \mathbb{I} + C_0 T(x_2) + \dots \quad (2.168)$$

The expansion of the correlator (2.167) should then reproduce, up to constants, the correlators  $\langle \psi(z_1, \bar{z}_1) \rangle_{\text{op}}$  and  $\langle \psi(z_1, \bar{z}_1) T(x_2) \rangle_{\text{op}}$  at order  $y_2^{-2}$  and  $y_2^0$  respectively, and give a vanishing term at order  $y_2^{-1}$ . This is exactly what we find; in addition, the two fusion coefficients read  $C_{-2} = \mathbb{P}_1/4$  and  $C_0 = -4\mathbb{P}_1$ .

Although the lattice result for  $\sigma_{2,1}^{\text{cl}}(y_1, y_2)$ , given in (2.83), is very close to  $\sigma_{2,1}^{\text{op}}(y_1, y_2)$ , the situation is more complicated on the conformal side. It requires to compute the equivalent of a chiral six-point correlator, due to the extra background field  $\omega$  (a chiral five-point function if one uses the boundary dissipation field). So a satisfactory argument to write the functional form of  $\sigma_{2,1}^{\text{cl}}(y_1, y_2)$  for general positions is still lacking at the moment.

#### 2.7.4 Other lattices

As discussed in Section 2.1, the Abelian sandpile model can be defined on any connected graph  $\mathcal{G}$ . Most of the analytical and numerical results have been obtained on the simplest two-dimensional regular graph, namely the square lattice, and have led to the conjectural relations (2.125) in the continuum limit. To check the universality of the logarithmic conformal field theory in play, we have computed several height probabilities and correlations on the triangular and hexagonal lattices in Sections 2.5 and 2.6.

On both lattices, our results (2.98), (2.112) and (2.116) for the subtracted one-point probabilities  $\sigma_a(r)$  yield functions of leading order 2 in the inverse distance  $r$  to the boundary of the upper half-plane. Moreover, the  $\sigma_1(r)$ 's are rational functions of  $r$  (as already noted in [4] for the hexagonal lattice), whereas the  $\sigma_{a>1}(r)$ 's contain logarithmic terms, as on the square lattice. The identification of the height-one field as a primary field  $\phi$  of weight  $(1, 1)$  and of the higher-height fields as the

logarithmic partner  $\psi$  of  $\phi$  (up to a normalization and to a multiple of  $\phi$ ) is therefore perfectly consistent with our results on both the triangular and hexagonal lattices

A further check of universality is given by Eq. (2.131), which relates the coefficients of one-point probabilities on upper half-planes with open and closed boundaries. We find these relations to be in full agreement with the coefficients in Table 2.4 for the principal hexagonal half-plane. Unfortunately, we cannot make the comparison for the other two half-lattices, namely the triangular half-plane and the horizontal hexagonal half-plane, as we have not been able to compute the Green function for a closed boundary.

Furthermore, for both hexagonal half-planes (principal and horizontal), we find two-point boundary correlations to be proportional to  $x^{-4}$  at leading order, where  $x$  is the separation between the prescribed heights along the boundary. For open boundary conditions, Eqs. (2.121) and (2.123) show in addition that all boundary height fields are proportional, as for the square lattice.



## Chapter 3

# Loop-erased random walks

The concept of *self-avoiding walk* (SAW) first emerged during the 1950s in physical chemistry [51, 122], as a simple model for the behavior in dilute solutions of chain-like polymers, whose physical extension prohibits multiple occupations of a same point in space. Formally, a self-avoiding walk is a random discrete growth process that does not intersect itself, with a uniform probability measure on all simple paths of fixed length. From a mathematical perspective, little is known rigorously about the self-avoiding walk<sup>1</sup>. In 1980, Lawler defined the *loop-erased random walk* (LERW) in an attempt to better understand the self-avoiding walk [98]. The loop-erasure procedure consists in erasing all loops appearing along a path in chronological order, thus yielding a simple path. The LERW probability measure is then inherited from that of the standard random walk.

Although Lawler soon found the SAW and LERW processes to be different, he discovered that the latter possesses many attributes of other models in critical phenomena, such as the existence of an upper critical dimension and (conjecturally) conformal invariance in two dimensions. In the 1990s, the discovery of the relationship between the uniform spanning tree (UST) and the LERW [115, 126, 157] led to increased interest in the latter (in particular due to the connection between the UST and other models, e.g. dimers [155] and the  $q \rightarrow 0$  Potts model [112]).

---

<sup>1</sup>A recent result one should mention is the proof that the connective constant of the hexagonal lattice is  $\sqrt{2 + \sqrt{2}}$  [47], derived nonrigorously earlier in [119, 120].

Among the results obtained over the years concerning the LERW—mainly in two dimensions—are its reversibility [99], its growth exponent and fractal dimension [48, 86, 100], the return probability [134] and the edge intensity [14, 86, 91, 103] (see [104] for a recent review).

Most notably, the study of the scaling limit of the planar LERW led Schramm to develop *Schramm-Loewner evolutions* (SLEs) [144]. One of the simplest results in the SLE framework is *Schramm’s formula*, which gives the probability that a point  $z$  lies to the left (or right) of an  $\text{SLE}_\kappa$  curve between fixed boundary points in a simply connected domain [145]. Its explicit form on the upper half-plane for a curve  $\gamma$  starting at 0 and growing toward infinity is given by

$$\mathbb{P}[z \text{ lies to the left of } \gamma] = \frac{1}{2} - \frac{\Gamma(4/\kappa)}{\sqrt{\pi} \Gamma(\frac{8-\kappa}{2\kappa})} \frac{x}{y} {}_2F_1\left(\frac{1}{2}, \frac{4}{\kappa}; \frac{3}{2}; -\frac{x^2}{y^2}\right), \quad (3.1)$$

where  $z = x + iy$  and  ${}_2F_1$  is the ordinary hypergeometric function.

Our goal is to derive a discrete version of this formula for the loop-erased random walk and for paths in spanning forests, on a generic planar graph with arbitrary positive edge weights. Using the techniques pertaining to complex connections recalled in Chapter 1, we establish in Section 3.1 the equivalent of Eq. (3.1) for simple paths in spanning forests in terms of the Green function of the graph, generalizing preliminary results given in [88, 91]. We compute several explicit expressions in the scaling limit for various domains and boundary conditions in Section 3.2, and compare some of our results to known  $\text{SLE}_2$  calculations. In Section 3.3, we generalize Schramm’s formula for multiple paths on a planar graph, for all possible connectivities between the marked boundary points. We define in Section 3.4 a natural measure for multiple loop-erased random walks, and show its explicit correspondence with the spanning forest measure on paths used in the preceding sections. Finally, we recall in Section 3.5 the interpretation of partition functions for LERWs (or for paths in spanning forests) as conformal correlators in the scaling limit, via the SLE/CFT correspondence [8, 56]. We find our results on the upper half-plane to be fully consistent with the CFT picture.

### 3.1 Paths in spanning forests and Schramm's formula

In this section, we first define a measure on chemical paths in spanning forests between two fixed vertices  $u_1, u_2$  of an unoriented connected graph, and then extend it to paths in oriented cycle-rooted groves. For  $u_1, u_2$  located on the boundary of the graph, we study the following question about a random simple path from  $u_1$  to  $u_2$  with respect to the measure on forests: What is the probability that such a path leaves a marked face  $f$  to its left, as illustrated in Fig. 3.1? In what follows, we give an explicit combinatorial expression for this probability, called Schramm's formula, by taking the limit  $\Phi \rightarrow \mathbb{I}$  of the corresponding probability in the grove model, in a nontrivial way. Our formula depends only on the standard Green function, which is well known for regular graphs such as those we shall consider in Section 3.2.

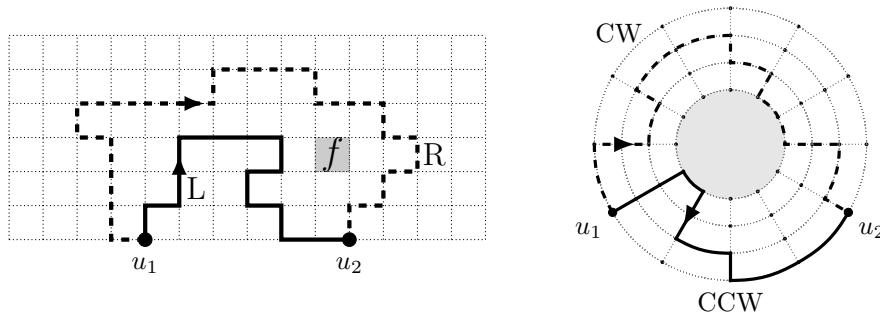


Figure 3.1: On the left are two simple paths on a rectangular grid between two boundary vertices, from  $u_1$  to  $u_2$ ; the solid (resp. dashed) path leaving the marked face  $f$  to its left (resp. right). On the right is a counterclockwise (resp. clockwise) path on an annulus, which can be viewed as leaving the central circular face to its left (resp. right).

#### 3.1.1 Measures on paths in forests and groves

Let  $\mathcal{G}_s = \mathcal{G} \cup \{s\}$  be an unoriented connected graph with a root  $s$  and let  $u_1, u_2 \neq s$  be two of its vertices. We consider the set of all simple unoriented paths on  $\mathcal{G}$  between  $u_1$  and  $u_2$  (a path is simple if it has no self-intersection). We define the weight of such a path  $\gamma : u_1 \leftrightarrow u_2$  as

the weighted sum of two-component spanning forests on  $\mathcal{G}_s$  in which the entire path  $\gamma$  belongs to one tree, and the vertex  $s$  to the other:

$$w_{\text{SF}}(\gamma) = \sum_{2\text{SFs } \mathcal{F} \supset \gamma} w(\mathcal{F}) = C(\gamma) \det \Delta^{(\gamma)}, \quad (3.2)$$

where  $C(\gamma)$  is the product of all the conductances along  $\gamma$ . Here  $\Delta^{(\gamma)}$  is the submatrix of the Dirichlet Laplacian  $\Delta = \Delta_{\mathcal{G}_s}^{(s)}$ , in which the rows and columns indexed by the vertices of  $\gamma$  have been removed. The second equality in (3.2) stems from the fact that 2-component spanning forests on  $\mathcal{G}_s$  that contain a fixed path  $\gamma : u_1 \leftrightarrow u_2$  of length  $n$  are in one-to-one correspondence with  $(n+2)$ -component spanning forests on  $\mathcal{G}_{s,\gamma}$ , in which all the vertices of  $\gamma$  are chosen as roots alongside  $s$  (see Fig. 3.2). The partition function for all paths between  $u_1$  and  $u_2$  in two-component spanning forests is denoted by  $Z[12|s] \equiv Z[u_1 u_2 | s]$ , and is given by Theorem 1.2:

$$Z[12|s] = \sum_{\gamma:u_1 \leftrightarrow u_2} w_{\text{SF}}(\gamma) = G_{1,2} \det \Delta, \quad (3.3)$$

where  $G_{1,2} \equiv G_{u_1, u_2} = (\Delta^{-1})_{u_1, u_2}$ . As a matter of notation, we shall drop the reference to the root  $s$  in the partition function, i.e. write  $Z[12]$  for  $Z[12|s]$ , for the rest of this chapter. Indeed, we shall only be interested in spanning forests in which the root  $s$  is isolated on its own tree (with respect to the other nodes), so it has more of a spectator role than in Chapter 2. The probability distribution on simple paths in two-component spanning forests is given by

$$\mathbb{P}_{\text{SF}}(\gamma : u_1 \leftrightarrow u_2) = \frac{w_{\text{SF}}(\gamma)}{\sum_{\gamma:u_1 \leftrightarrow u_2} w_{\text{SF}}(\gamma)} = \frac{C(\gamma) \det \Delta^{(\gamma)}}{G_{1,2} \det \Delta}. \quad (3.4)$$

In what follows, we shall consider *oriented* simple paths on  $\mathcal{G}$  from  $u_1$  to  $u_2$ . It is therefore natural to define a probability measure on such paths as follows:

$$\mathbb{P}_{\text{SF}}(\gamma : u_1 \rightarrow u_2) = \mathbb{P}_{\text{SF}}(\gamma^* : u_1 \leftrightarrow u_2), \quad (3.5)$$

where  $\gamma$  is obtained from  $\gamma^*$  by orienting all of its edges toward  $u_2$ . Note that this implies that an oriented path  $\gamma$  and the reverse path  $\gamma^{-1}$  have the same probability.

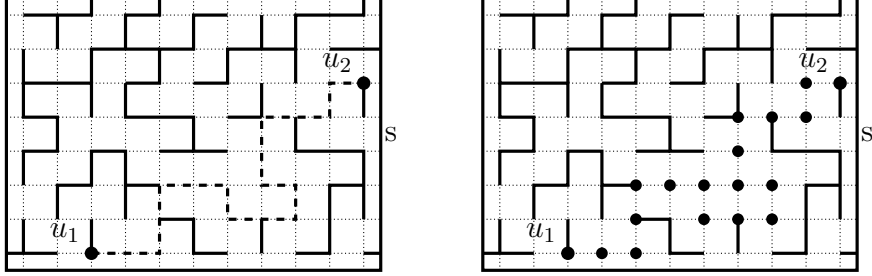


Figure 3.2: On the left is a two-component spanning forest on a wired grid. Two selected vertices  $u_1, u_2$  belong to a tree distinct from the one that includes the root  $s$  (represented by the box surrounding the grid). The dashed line highlights the path  $\gamma$  between  $u_1$  and  $u_2$ , which contains  $n+1$  vertices. On the right is the associated  $(n+2)$ -component spanning forest in which each vertex of  $\gamma$  is the root of a (possibly degenerate) tree, in addition to  $s$ .

Let us now turn to paths in oriented cycle-rooted groves (OCRGs), for which we define the weight of the oriented simple path  $\gamma : u_1 \rightarrow u_2$  as

$$w_{\text{CRG}}(\gamma) = \sum_{\text{OCRGs } \Gamma_{\vec{\sigma}} \supset \gamma} w(\Gamma_{\vec{\sigma}}) = C(\gamma) \phi(\gamma)^{-1} \det \mathbf{\Delta}^{(\gamma)}, \quad (3.6)$$

where  $\vec{\sigma} = \begin{smallmatrix} 2 \\ 1 \end{smallmatrix}$ ,  $w(\Gamma_{\vec{\sigma}})$  is given by Eq. (1.15) and  $\phi(\gamma) = \phi_{u_1 \rightarrow u_2}$  is the product of all parallel transports along  $\gamma$ . Explicitly, if  $\gamma = (v_i)_{0 \leq i \leq n}$  with  $v_0 \equiv u_1$  and  $v_n \equiv u_2$ ,

$$\phi(\gamma) = \phi_{u_1 \rightarrow u_2} = \prod_{i=0}^{n-1} \phi_{v_i, v_{i+1}}. \quad (3.7)$$

Here  $\det \mathbf{\Delta}^{(\gamma)}$  is the weighted sum of OCRGs consisting in  $n+2$  rooted trees, each including a unique vertex of  $\gamma$  or  $s$ , and cycle-rooted trees not intersecting  $\gamma \cup \{s\}$ . Using Theorem 1.5, we find that the partition function for all paths from  $u_1$  to  $u_2$  is  $\mathbf{Z}_{[1]}^2 = \mathbf{G}_{1,2} \det \mathbf{\Delta}$ , where  $\mathbf{G}_{1,2} \equiv \mathbf{G}_{u_1, u_2} = (\mathbf{\Delta}^{-1})_{u_1, u_2}$ . The normalized distribution yields

$$\mathbb{P}_{\text{CRG}}(\gamma : u_1 \rightarrow u_2) = \frac{w_{\text{CRG}}(\gamma)}{\sum_{\gamma: u_1 \rightarrow u_2} w_{\text{CRG}}(\gamma)} = \frac{C(\gamma) \phi(\gamma)^{-1} \det \mathbf{\Delta}^{(\gamma)}}{\mathbf{G}_{1,2} \det \mathbf{\Delta}}. \quad (3.8)$$

It should be noted that  $\mathbb{P}_{\text{CRG}}$  is *not* a probability distribution for a generic connection, as it can take complex or negative values. Furthermore, the distribution of a path  $\gamma$  and its reverse  $\gamma^{-1}$  do not coincide,

$\mathbb{P}_{\text{CRG}}(\gamma) \neq \mathbb{P}_{\text{CRG}}(\gamma^{-1})$ , since  $\phi(\gamma) \neq \phi(\gamma^{-1})$  and  $\mathbf{G}_{1,2} \neq \mathbf{G}_{2,1}$  in general. It is straightforward to establish the relation between Eqs. (3.4) and (3.8) by taking the limit of a trivial connection, i.e.  $\Phi \rightarrow \mathbb{I}$ :

$$\mathbb{P}_{\text{SF}}(\gamma : u_1 \rightarrow u_2) = \lim_{\Phi \rightarrow \mathbb{I}} \mathbb{P}_{\text{CRG}}(\gamma : u_1 \rightarrow u_2). \quad (3.9)$$

Similar formulas hold for a graph  $\mathcal{G}$  with free boundary conditions, as discussed in Section 1.5. In that case, the Dirichlet Laplacians  $\Delta$  and  $\mathbf{\Delta}$  are replaced with the Laplacians  $\Delta_0$  and  $\mathbf{\Delta}_0$ , and the partition functions are given by

$$\mathbf{Z}[1]_1^2 = \lim_{q \rightarrow 0} (\mathbf{G}_q)_{1,2} \det(\mathbf{\Delta}_0 + q\mathcal{P}_0), \quad Z[12] = \frac{1}{N} \det \Delta'. \quad (3.10)$$

### 3.1.2 Schramm's formula

Let us now address the first objective of this chapter, namely writing a discrete version of Schramm's formula for paths in spanning forests on a graph with respect to a marked face  $f$ , in terms of the standard Green function of the graph. Such a formula was first given in [88,91] for graphs with free boundary conditions. We extend it here for graphs connected to a root, using the same technique as in [88,91]. We shall follow similar steps when discussing multiple paths later on in Section 3.3.

In what follows, we consider a graph  $\mathcal{G} = (\mathcal{V}, \mathcal{E})$  embedded on a surface  $\Sigma$  such that the edges in  $\mathcal{E}$  do not intersect each other (except possibly at the vertices in  $\mathcal{V}$ ). We connect a subset  $\mathcal{D}$  of its boundary vertices to a root  $s$  with a set of edges  $\mathcal{E}_s$  to form the extended graph  $\mathcal{G}_s$ . Note that we do not require that  $s$  or the edges in  $\mathcal{E}_s$  belong to  $\Sigma$ . We select two boundary vertices (possibly in  $\mathcal{D}$ ) as the nodes  $u_1, u_2$  and a face  $f$  of the graph<sup>2</sup>. If  $\Sigma$  is orientable, the discrete analogue of Schramm's formula

<sup>2</sup>The reason we consider paths between boundary vertices is twofold. First, this situation is the discrete analogue of *chordal* SLEs, for which explicit results for Schramm's formula have been computed. To our knowledge, the equivalent formula for radial or whole-plane SLEs is not currently known. Second, there are (infinitely) many inequivalent classes of paths between two bulk vertices with respect to a face, instead of just two when  $u_1, u_2$  are on the boundary. Computing their respective probabilities using a connection as presented below would require knowledge of the full line bundle Green function, as opposed to the perturbative expansion used in most of this work.

(3.1) for paths in spanning forests reads

$$\mathbb{P}_L(u_1, u_2; f) = \sum_{\gamma: u_1 \rightarrow u_2} \chi_L(\gamma; f) \mathbb{P}_{\text{SF}}(\gamma : u_1 \rightarrow u_2), \quad (3.11)$$

where  $\chi_L(\gamma; f) = 1$  (resp. 0) if  $\gamma$  leaves  $f$  to its left (resp. right), and  $\mathbb{P}_{\text{SF}}(\gamma : u_1 \rightarrow u_2)$  is given by Eq. (3.4). Alternatively, if we denote by  $Z_L[12]$  (resp.  $Z_R[12]$ ) the weighted sum of two-component spanning forests on  $\mathcal{G}_s$  in which the path from  $u_1$  to  $u_2$  leaves  $f$  to its left (resp. right), the preceding equation may be rewritten as

$$\mathbb{P}_L(u_1, u_2; f) = \frac{Z_L[12]}{Z[12]}. \quad (3.12)$$

While the denominator is already known (3.3), a subtler approach is required to extract  $Z_L[12]$  from  $Z[12] = Z_L[12] + Z_R[12]$  [88]. To do so, let us equip  $\mathcal{G}_s$  with a connection that is trivial everywhere except on a collection of edges  $\{k, \ell\}$  crossed by a *zipper*, that is, a path from  $f$  to the outer face of  $\mathcal{G}$  on the dual graph. We impose for convenience that the zipper intersects the clockwise boundary path from  $u_1$  to  $u_2$  (see Fig. 3.3). We put a constant parallel transport  $\phi_{k, \ell} = z \in \mathbb{C}^*$  on the oriented edges  $(k, \ell)$ —and  $\phi_{\ell, k} = z^{-1}$  in the opposite direction—in such a way that a counterclockwise cycle circling  $f$  has monodromy  $z$ .

This specific choice of a connection allows one to distinguish between paths from  $u_1$  to  $u_2$  that leave  $f$  to their left and to their right. Indeed, the product of parallel transports from  $u_1$  to  $u_2$  appearing in Eq. (3.6) is  $\phi_{1 \rightarrow 2} = 1$  for the former, while  $\phi_{1 \rightarrow 2} = z^{-1}$  for the latter. We can therefore decompose the full partition function for groves with a path from  $u_1$  to  $u_2$  as follows:

$$\mathbf{Z} \begin{bmatrix} 2 \\ 1 \end{bmatrix} = \mathbf{Z}_L \begin{bmatrix} 2 \\ 1 \end{bmatrix} + \mathbf{Z}_R \begin{bmatrix} 2 \\ 1 \end{bmatrix}, \quad (3.13)$$

where  $\phi_{1 \rightarrow 2}$  is constant over the paths of each class, left and right.

If we consider instead paths in the opposite direction, we have  $\phi_{2 \rightarrow 1} = 1$  (resp.  $\phi_{2 \rightarrow 1} = z$ ) for paths from  $u_2$  to  $u_1$  that leave the face  $f$  to their right (resp. left). Similarly to Eq. (3.13), we write

$$\mathbf{Z} \begin{bmatrix} 1 \\ 2 \end{bmatrix} = \mathbf{Z}_L \begin{bmatrix} 1 \\ 2 \end{bmatrix} + \mathbf{Z}_R \begin{bmatrix} 1 \\ 2 \end{bmatrix} \quad (3.14)$$

for paths from  $u_2$  to  $u_1$ , where the indices L, R refer to the left- or right-passage with respect to  $f$  in the original direction, i.e. *from  $u_1$  to  $u_2$* .

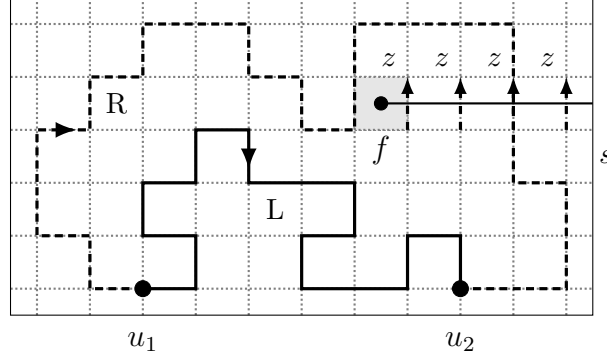


Figure 3.3: Wired rectangular grid with two marked boundary vertices  $u_1, u_2$  and a marked face  $f$ . The solid line from  $f$  to the outer face represents the zipper. The edges crossed by the zipper possess a parallel transport  $z$  from the bottom up (and  $z^{-1}$  from the top down). The path labeled L (resp. R) from  $u_1$  to  $u_2$  leaves  $f$  to its left (resp. right).

Looking at Eqs. (1.15) and (3.6), we see that the weight of a path  $\gamma$  in OCRGs is related to that of its reverse by

$$\text{w}_{\text{CRG}}(\gamma) \phi(\gamma) = \text{w}_{\text{CRG}}(\gamma^{-1}) \phi(\gamma^{-1}). \quad (3.15)$$

As the product of parallel transports along the path from  $u_1$  to  $u_2$  is constant over the left and right classes separately, we find the relations

$$\mathbf{Z}_{\text{L}[2]} = \mathbf{Z}_{\text{L}[1]}, \quad \mathbf{Z}_{\text{R}[2]} = z^{-2} \mathbf{Z}_{\text{R}[1]}, \quad (3.16)$$

which allow us to write and solve the following system for  $\mathbf{Z}_{\text{L,R}[1]}^{[2]}$ :

$$\begin{aligned} \mathbf{G}_{1,2} \det \Delta &= \mathbf{Z}_{[1]}^{[2]} = \mathbf{Z}_{\text{L}[1]}^{[2]} + \mathbf{Z}_{\text{R}[1]}^{[2]}, \\ \mathbf{G}_{2,1} \det \Delta &= \mathbf{Z}_{[2]}^{[1]} = \mathbf{Z}_{\text{L}[1]}^{[2]} + z^{-2} \mathbf{Z}_{\text{R}[1]}^{[2]}. \end{aligned} \quad (3.17)$$

The solution reads

$$\mathbf{Z}_{\text{L}[1]}^{[2]} = \frac{(\mathbf{G}_{2,1} - z^{-2} \mathbf{G}_{1,2}) \det \Delta}{1 - z^{-2}}, \quad \mathbf{Z}_{\text{R}[1]}^{[2]} = \frac{(\mathbf{G}_{1,2} - \mathbf{G}_{2,1}) \det \Delta}{1 - z^{-2}}. \quad (3.18)$$

Since the normalized measure  $\mathbb{P}_{\text{CRG}}$  converges to  $\mathbb{P}_{\text{SF}}$  in the limit of a trivial connection (3.9), that is, when  $z \rightarrow 1$ , one obtains the following combinatorial result for Schramm's formula (3.12):

$$\mathbb{P}_{\text{L}}(u_1, u_2; f) = \lim_{z \rightarrow 1} \frac{(\mathbf{G}_{2,1} - z^{-2} \mathbf{G}_{1,2}) \det \Delta}{1 - z^{-2}} \times \frac{1}{\mathbf{G}_{1,2} \det \Delta} = 1 - \frac{G'_{1,2}}{G_{1,2}}, \quad (3.19)$$

where we have used the antisymmetry of the derivative of the Green function  $G'$  defined in (1.28).

The corresponding formula for graphs with free boundary conditions was given in [88], where Cramer's rule was used to write

$$(\mathbf{G}_0)_{1,2} = \frac{\kappa}{\det \mathbf{\Delta}_0} \left\{ 1 + (z-1) \tilde{G}'_{1,2} \dots \right\}, \quad (3.20)$$

where  $\tilde{G}'$  is defined in (1.38) and  $\kappa = Z[12]$  is the weighted sum of spanning trees on  $\mathcal{G}$ . We present here an alternative derivation using the modified line bundle Green function  $\mathbf{G}_q = (\mathbf{\Delta}_0 + q\mathcal{P}_0)^{-1}$  instead of  $\mathbf{G}_0 = (\mathbf{\Delta}_0)^{-1}$ :

$$\begin{aligned} \mathbb{P}_L(u_1, u_2; f) &= \lim_{q \rightarrow 0} \lim_{z \rightarrow 1} \frac{((\mathbf{G}_q)_{2,1} - z^{-2}(\mathbf{G}_q)_{1,2}) \det(\mathbf{\Delta}_0 + q\mathcal{P}_0)}{1 - z^{-2}} \\ &\quad \times \frac{1}{(\mathbf{G}_q)_{1,2} \det(\mathbf{\Delta}_0 + q\mathcal{P}_0)} \\ &= 1 - \lim_{q \rightarrow 0} \frac{G'_{1,2} + q^{-1}N^{-1}\tilde{G}'_{1,2}}{G_{1,2} + q^{-1}N^{-1}} = 1 - \tilde{G}'_{1,2}, \end{aligned} \quad (3.21)$$

where the properties  $G'_{v,u} = -G'_{u,v}$  and  $\tilde{G}'_{v,u} = -\tilde{G}'_{u,v}$  follow from Eq. (1.38). A third way of obtaining Eq. (3.21) consists in connecting  $u_2$  to the root  $s$ , that is, defining a graph  $\bar{\mathcal{G}}$  such that  $\bar{\mathbf{\Delta}}_{u,v} = (\mathbf{\Delta}_0)_{u,v} + \delta_{u,2} \delta_{2,v}$ . The OCRGs with a path from  $u_1$  to  $u_2$  on  $\mathcal{G}$  are in one-to-one correspondence with those on  $\bar{\mathcal{G}}$  (in which the tree rooted at  $s$  is degenerate, since it cannot contain  $u_2$ ). Moreover, the inverse  $\bar{G} = \bar{\mathbf{\Delta}}^{-1}$  is well defined (due to the connection between  $u_2$  and the root  $s$ ), so Schramm's formula is given by Eq. (3.19):

$$\mathbb{P}_L(u_1, u_2; f) = 1 - \frac{\bar{G}'_{1,2}}{\bar{G}_{1,2}}, \quad (3.22)$$

with  $\bar{G}'$  defined in (1.28) (in terms of  $\bar{G}$  instead of  $G$ ). Writing the Green function  $\bar{G}$  in terms of the regularized Green function  $G$  (1.33) on  $\mathcal{G}$  yields

$$\bar{G}_{u,v} = 1 + G_{u,v} + G_{2,2} - G_{u,2} - G_{2,v}. \quad (3.23)$$

One recovers Eq. (3.21) by plugging this relation into the preceding equation.

## 3.2 Explicit results for passage probabilities

In this section, we consider rectangular grids embedded on surfaces, with unit conductances:  $c_{u,v} = 1$  for any  $\{u, v\} \in \mathcal{E}$ , for various combinations of wired and free boundary conditions. We compute the discrete Green function  $G$  of the graph, and show that it converges in the scaling limit to the continuum Green function (up to a constant normalization factor), which we use to give an explicit expression for (the scaling limit of)  $\mathbb{P}_L(u_1, u_2; f)$ . For the upper half-plane and the cylinder, we compare our results with known  $\text{SLE}_2$  probabilities.

### 3.2.1 The upper half-plane

Let us first compute Schramm's formula on the discrete upper half-plane (UHP)  $\mathcal{G} = \mathbb{Z} \times \mathbb{N}^*$ , whose boundary consists in vertices of the form  $(x, y=1)$ ,  $x \in \mathbb{Z}$ . We shall consider uniform boundary conditions on such a graph, either wired or free. In the former case, all boundary vertices  $(x, 1)$  are connected by an edge to a root  $s$ , so their degree in  $\mathcal{G}_s$  is 4 like the bulk vertices; while in the latter case, the boundary vertices have only degree 3.

Anticipating a bit, we denote by  $G_{u,v}^D$  and  $G_{u,v}^N$  the discrete Green functions of the UHP with wired and free boundary conditions, respectively. Both can be expressed in terms of the Green function  $G$  of the full plane  $\mathbb{Z}^2$ , via the method of images:

$$G_{(x_1, y_1), (x_2, y_2)}^D = G_{(x_1, y_1), (x_2, y_2)} - G_{(x_1, y_1), (x_2, -y_2)}, \quad (3.24)$$

$$G_{(x_1, y_1), (x_2, y_2)}^N = G_{(x_1, y_1), (x_2, y_2)} + G_{(x_1, y_1), (x_2, 1-y_2)}. \quad (3.25)$$

As  $\mathbb{Z}^2$  is invariant under translations, the function  $G_{u,v}$  only depends on the difference  $v - u = (x, y)$ , and possesses the following integral representation:

$$G_{u,v} = G(v - u) = \int_{-\pi}^{\pi} \frac{d\theta_1}{2\pi} \int_{-\pi}^{\pi} \frac{d\theta_2}{2\pi} \frac{e^{ix\theta_1 + iy\theta_2}}{4 - 2\cos\theta_1 - 2\cos\theta_2}. \quad (3.26)$$

Due to the singularity of the integrand at the origin, the function  $G(x, y)$  diverges. However, the difference  $G(x, y) - G(0, 0)$  is finite, and can be

computed asymptotically for large values of  $x^2 + y^2$ :

$$\begin{aligned} G(x, y) - G(0, 0) = & -\frac{1}{4\pi} \{ \log(x^2 + y^2) + 2\gamma + 3 \log 2 \} \\ & + \frac{x^4 - 6x^2y^2 + y^4}{24\pi(x^2 + y^2)^3} + \dots, \end{aligned} \quad (3.27)$$

up to fourth-order terms in  $x, y$ , with  $\gamma = 0.577216\dots$  being the Euler constant.

In order to compute Schramm's formula (3.19), we select two boundary vertices  $u_i = (x_i, 1)$ ,  $i = 1, 2$ , with  $x_1 < x_2$ , and the face  $f$  whose lower left corner is  $(x_*, y_*)$ . As we are interested in taking the scaling limit of this formula, we assume that  $u_1, u_2, f$  are separated from each other by large distances. Furthermore, we suppose for simplicity that  $x_1 < x_2 < x_*$ , and equip  $\mathcal{G}$  with the vertical zipper depicted in the left panel of Fig. 3.4, namely, we put a nontrivial parallel transport  $z \in \mathbb{C}^*$  on the oriented edges  $(k, k+(1, 0))$  for  $k = (x_*, s)$ ,  $1 \leq s \leq y_*$ .

Note that imposing that  $x_* > x_2$  and taking a vertical zipper is simply a matter of convenience, to make the computation of  $G'$  as easy as possible. If rather  $x_1 < x_* < x_2$  or  $x_* < x_1 < x_2$ , one may use a more complicated zipper that touches the boundary to the right of  $u_2$ , or equivalently, work with the vertical zipper and adapt the combinatorics involved in establishing Eq. (3.19) (see the right panel of Fig. 3.4). Both choices are equally valid, and yield the same explicit form for the left-passage probability, which holds for any value of  $x_*$ .

To obtain a continuum version of Schramm's formula, let us introduce new variables  $x, y \in \varepsilon\mathbb{Z}^2$  ( $\varepsilon > 0$ ), defined by  $x = \varepsilon x$ ,  $y = \varepsilon y$ . We shall take the scaling limit by letting  $\varepsilon \rightarrow 0^+$  and  $x, y \rightarrow \infty$  such that  $x, y$  stay finite. From Laplace's equation

$$\begin{aligned} \delta_{(x_1, y_1), (x_2, y_2)} = (\Delta G)_{(x_1, y_1), (x_2, y_2)} = & 4G_{(x_1, y_1), (x_2, y_2)} - G_{(x_1+1, y_1), (x_2, y_2)} \\ & - G_{(x_1-1, y_1), (x_2, y_2)} - G_{(x_1, y_1+1), (x_2, y_2)} - G_{(x_1, y_1-1), (x_2, y_2)}, \end{aligned} \quad (3.28)$$

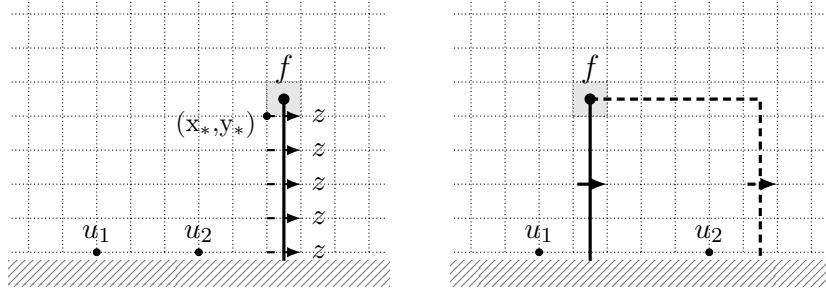


Figure 3.4: On the left are the relative positions on the upper half-plane of the boundary vertices  $u_1, u_2$  and of the face  $f$  whose lower left corner is the vertex  $(x_*, y_*)$ . The zipper edges are equipped with a parallel transport  $z$  in the direction of their arrow (and  $z^{-1}$  in the opposite direction). On the right are two possible choices of zippers for the case  $x_1 < x_* < x_2$  (the arrow indicates the direction of the zipper edges with parallel transport  $z$ ). Both yield different combinatorial expressions for Schramm's formula in terms of  $G, G'$ , but lead to the same explicit result.

it follows readily that

$$\begin{aligned} \mathfrak{G}(x_1, y_1; x_2, y_2) &= \lim_{\varepsilon \rightarrow 0^+} \left( G_{(x_1/\varepsilon, y_1/\varepsilon), (x_2/\varepsilon, y_2/\varepsilon)} - G(0, 0) \right. \\ &\quad \left. - \frac{1}{2\pi} \log \varepsilon + \frac{2\gamma + 3 \log 2}{4\pi} \right) \quad (3.29) \\ &= -\frac{1}{4\pi} \log [(x_1 - x_2)^2 + (y_1 - y_2)^2]. \end{aligned}$$

Similarly, the Green functions  $G^D$  and  $G^N$  converge to the usual (continuum) Green functions  $\mathfrak{G}^D, \mathfrak{G}^N$  with Dirichlet and Neumann boundary conditions, respectively:

$$\begin{aligned} \mathfrak{G}^{D,N}(x_1, y_1; x_2, y_2) &= -\frac{1}{4\pi} \log [(x_1 - x_2)^2 + (y_1 - y_2)^2] \\ &\quad \pm \frac{1}{4\pi} \log [(x_1 - x_2)^2 + (y_1 + y_2)^2]. \quad (3.30) \end{aligned}$$

The same formulas holds if one or both the arguments of the discrete Green function  $G^N$  lie on the boundary of the UHP, i.e. the Green function converges to  $\mathfrak{G}^N(x_1, y_1; x_2, 0)$  or  $\mathfrak{G}^N(x_1, 0; x_2, 0)$ , respectively. A bit more care is required for  $G^D$ , as the continuum Green function

$\mathfrak{G}^D$  vanishes on the boundary. One finds at the lowest order in  $\varepsilon$  that

$$\begin{aligned} G_{(x_1/\varepsilon, y_1/\varepsilon), (x_2/\varepsilon, 1)}^D &= P_1(x_1, y_1; x_2) \varepsilon + \mathcal{O}(\varepsilon^2), \\ G_{(x_1/\varepsilon, 1), (x_2/\varepsilon, 1)}^D &= P(x_1, x_2) \varepsilon^2 + \mathcal{O}(\varepsilon^3), \end{aligned} \quad (3.31)$$

where  $P_1$  and  $P$  are respectively the *Poisson kernel* and the *excursion Poisson kernel*, defined in terms of the continuum Green function by

$$\begin{aligned} P_1(x_1, y_1; x_2) &= \partial_{y_2} \mathfrak{G}^D(x_1, y_1; x_2, y_2) \Big|_{y_2=0}, \\ P(x_1, x_2) &= \partial_{y_1} \partial_{y_2} \mathfrak{G}^D(x_1, y_1; x_2, y_2) \Big|_{y_1=y_2=0}. \end{aligned} \quad (3.32)$$

Using Eqs. (3.30) and (3.31), one may write the Green function and its derivative (1.28) for  $\varepsilon \sim 0^+$  as follows:

$$G_{(x_1/\varepsilon, 1), (x_2/\varepsilon, 1)}^D = \varepsilon^2 P(x_1, x_2) + \dots, \quad (3.33)$$

$$\begin{aligned} G'_{(x_1/\varepsilon, 1), (x_2/\varepsilon, 1)}^D &= \varepsilon^2 \int_0^{y_*} ds (\partial_{x_*} P_1(x_*, s; x_1) P_1(x_*, s; x_2) \\ &\quad - \partial_{x_*} P_1(x_*, s; x_2) P_1(x_*, s; x_1)) + \dots, \end{aligned} \quad (3.34)$$

$$G_{(x_1/\varepsilon, 1), (x_2/\varepsilon, 1)}^N = \left( 2G(0, 0) + \frac{1}{\pi} \log \varepsilon \right) + \mathfrak{G}^N(x_1, 0; x_2, 0) + \dots, \quad (3.35)$$

$$\begin{aligned} G'_{(x_1/\varepsilon, 1), (x_2/\varepsilon, 1)}^N &= \left( 2G(0, 0) + \frac{1}{\pi} \log \varepsilon \right) \int_0^{y_*} ds (\partial_{x_*} \mathfrak{G}^N(x_*, s; x_1, 0) \\ &\quad - \partial_{x_*} \mathfrak{G}^N(x_*, s; x_2, 0)) + \dots \end{aligned} \quad (3.36)$$

The integrals for both derivatives of the Green function can be carried out explicitly, and yield the following left-passage probabilities in the scaling limit:

$$\begin{aligned} \mathbb{P}_L^D(x_1, x_2; z_*) &= 1 + \frac{1}{\pi} (\arg(z_* - x_1) - \arg(z_* - x_2)) \\ &\quad - \frac{1}{\pi} \frac{\operatorname{Re}[(z_* - x_1)(\bar{z}_* - x_2)] \operatorname{Im}[(z_* - x_1)(\bar{z}_* - x_2)]}{|z_* - x_1|^2 |z_* - x_2|^2}, \end{aligned} \quad (3.37)$$

$$\mathbb{P}_L^N(x_1, x_2; z_*) = 1 + \frac{1}{\pi} (\arg(z_* - x_1) - \arg(z_* - x_2)), \quad (3.38)$$

which are illustrated in Fig. 3.5. In particular, if we take  $x_1 = 0$  and  $x_2 \rightarrow \infty$ , Eqs. (3.37) and (3.38) simplify to

$$\mathbb{P}_L^D(z_*) = \frac{\arg z_*}{\pi} - \frac{\operatorname{Re}[z_*] \operatorname{Im}[z_*]}{\pi |z_*|^2}, \quad \mathbb{P}_L^N(z_*) = \frac{\arg z_*}{\pi}. \quad (3.39)$$

The former is in agreement with the original SLE<sub>2</sub> result of Schramm [145]. For the latter, the right-passage probability  $\mathbb{P}_R^N = 1 - \mathbb{P}_L^N$  is simply the harmonic measure of the segment  $[x_1, x_2]$  as seen from  $z_*$ , as observed in [88].

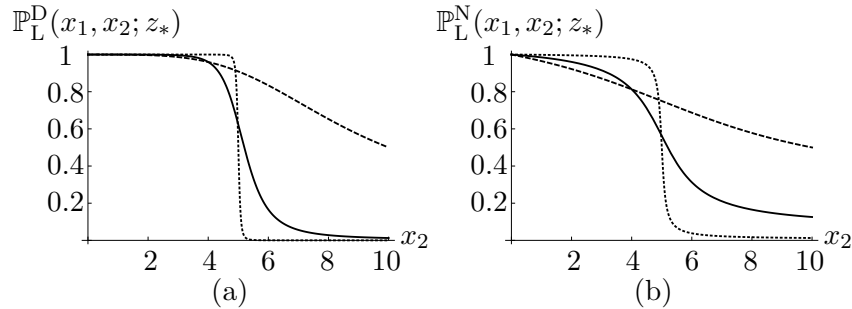


Figure 3.5: Illustration of the left-passage probability on the upper half-plane with (a) Dirichlet or (b) Neumann boundary conditions, for  $x_1 = 0$ ,  $x_* = 5$ , and  $y_* = 1/10$  (dotted),  $y_* = 1$  (solid) or  $y_* = 5$  (dashed).

### 3.2.2 The cylinder

The second application consists in a cylinder graph, namely, a rectangular grid of length  $N$  and height  $M$  with periodic conditions in the horizontal direction. If we denote by  $(x, y)$  the coordinates of the vertices of the grid,  $1 \leq x \leq N$ ,  $1 \leq y \leq M$ , then periodicity in the  $x$  direction implies that  $(N, y)$  and  $(1, y)$  are connected by an edge for  $1 \leq y \leq M$ .

As in Section 3.2.1, we select two vertices  $u_i = (x_i, 1)$ ,  $i = 1, 2$ , with  $x_1 < x_2$ , and a marked face  $f$ , whose lower left corner is  $(x_*, y_*)$ , such that  $x_* > x_2$ . In what follows, we shall consider either wired or free conditions on each boundary component, yielding four cases in total. We shall distinguish between them by using the superscripts NN, DD, DN, ND, where the first (resp. second) letter refers to the type of conditions on the bottom (resp. top) boundary, with N standing for Neumann (free) and D for Dirichlet (wired). For each case, one could compute the discrete Green function in terms of the eigenfunctions  $|f_{m,n}\rangle$  and eigenvalues  $\lambda_{m,n}$  of the Laplacian (which are well known), and then use Eqs. (1.28) and (3.19) to obtain Schramm's formula on the cylinder.

The calculation of  $G'$  through Eq. (1.28) is however tedious, and yields long and cumbersome (explicit) expressions, which we have not been able to simplify when at least one boundary is wired (i.e. DD, DN, ND). We shall therefore omit the results and concentrate on the cylinder with free conditions on both boundaries (NN), for which we have obtained a simple formula.

Next we shall discuss a particular case of the left-passage probability, namely, when the marked face  $f$  is the one at the top of the cylinder (or at the center of an annulus, as depicted in the right panel of Fig. 3.1). Schramm's formula (3.19) therefore gives the probability that a random path from  $u_1$  to  $u_2$  winds counterclockwise around the cylinder; which we shall refer to as the *positive winding probability*.

To compute it, we put a parallel transport  $z = e^{i\theta}$ ,  $\theta \in \mathbb{R}$ , on the oriented edges  $((N, y), (1, y))$  for  $1 \leq y \leq M$ . For such a zipper, the eigenfunctions  $|\mathbf{f}_{m,n}\rangle = |\mathbf{f}_{m,n}(\theta)\rangle$  and eigenvalues  $\lambda_{m,n} = \lambda_{m,n}(\theta)$  of the line bundle Laplacian  $\Delta$  can be evaluated exactly, *for any value of  $\theta$* . Since  $\Delta^\dagger = \Delta$ , the line bundle Green function is given by the familiar formula

$$\mathbf{G} = \mathbf{G}(e^{i\theta}) = \sum_{m,n} \frac{|\mathbf{f}_{m,n}\rangle \langle \mathbf{f}_{m,n}|}{\lambda_{m,n}}. \quad (3.40)$$

It is then easier to compute the derivative of the Green function through

$$G' = \partial_z \mathbf{G}(z) \Big|_{z=1} = -i \partial_\theta \mathbf{G}(e^{i\theta}) \Big|_{\theta=0} \quad (3.41)$$

than via Eq. (1.28). We shall therefore favor the first approach to compute winding probabilities in what follows.

### Free boundaries

We first consider the cylinder graph with free boundary conditions, on which we compute the left-passage probability for a random simple path from  $u_1$  to  $u_2$  with respect to a face  $f$ , using Eqs. (1.38) and (3.21). We take here a vertical zipper going from  $f$  to the bottom boundary, with parallel transport  $z \in \mathbb{C}^*$ . An illustration of the two classes of paths is provided in Fig. 3.6.

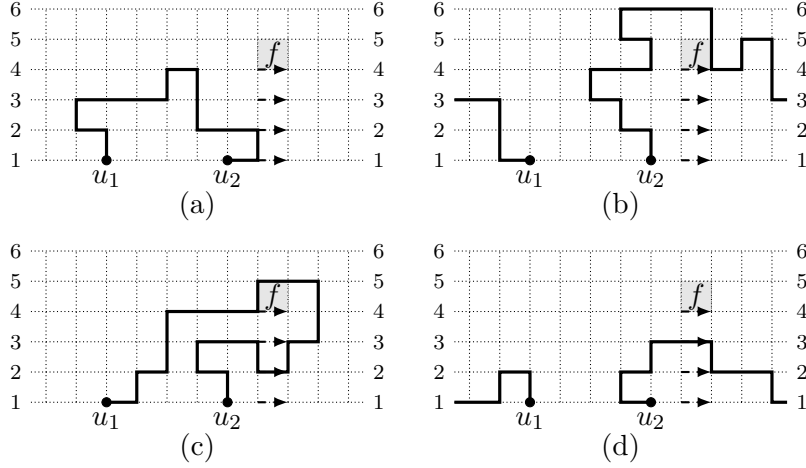


Figure 3.6: Simple paths from  $u_1$  to  $u_2$  on a cylinder graph  $\mathcal{G}$  realized as a rectangular grid with its left and right sides connected (the numbers on the half-edges indicate how they should be glued together to obtain  $\mathcal{G}$ ). The edges with dashed arrows between the marked face  $f$  and the lower boundary are equipped with a parallel transport  $z$  (resp.  $z^{-1}$ ) in the direction (resp. opposite direction) of the arrows. The paths are divided into two classes, according to whether they leave  $f$  to their left as in panels (a) and (b), or to their right as in panels (c) and (d).

The eigenvalues and eigenfunctions of the standard Laplacian  $\Delta_0$  read

$$\lambda_{m,n} = 4 - 2 \cos\left(\frac{\pi m}{M+1}\right) - 2 \cos\left(\frac{2\pi n}{N}\right), \quad (3.42)$$

$$f_{m,n}(x,y) = \left(\frac{2 - \delta_{m,0}}{MN}\right)^{1/2} e^{i(2\pi n)x/N} \cos\left[\frac{\pi m}{M}\left(y - \frac{1}{2}\right)\right], \quad (3.43)$$

for  $0 \leq m \leq M-1$  and  $0 \leq n \leq N-1$ . In particular,  $\lambda_{0,0} = 0$ , meaning  $\Delta_0$  is singular. The regularized Green function, introduced in Section 1.5, takes the form of (1.33).

As on the upper half-plane, we define new coordinates  $x = \varepsilon x$  and  $y = \varepsilon y$  living on the lattice  $\varepsilon\mathbb{Z}^2$ . We take the scaling limit  $\varepsilon \rightarrow 0^+$ ,  $M, N \rightarrow \infty$  such that  $M\varepsilon \rightarrow p$  and  $N\varepsilon \rightarrow 2\pi$ , and compute the Green function  $\mathfrak{G}$

and its derivative  $\tilde{\mathfrak{G}}'$  directly in the continuum. They read respectively

$$\mathfrak{G}(x_1, y_1; x_2, y_2) = \frac{1}{2\pi p} \sum_{\substack{m, n \in \mathbb{Z} \\ (m, n) \neq (0, 0)}} \frac{e^{in(x_1 - x_2)} \cos\left(\frac{\pi m y_1}{p}\right) \cos\left(\frac{\pi m y_2}{p}\right)}{n^2 + \left(\frac{\pi m}{p}\right)^2}, \quad (3.44)$$

$$\tilde{\mathfrak{G}}'(x_1, y_1; x_2, y_2) = \int_0^{y_*} ds (\partial_{x_*} \mathfrak{G}(x_*, s; x_1, y_1) - \partial_{x_*} \mathfrak{G}(x_*, s; x_2, y_2)). \quad (3.45)$$

For boundary points  $u_i = (x_i, 0)$ , we use the Poisson summation formula to write the derivative with respect to  $x_*$  as

$$\partial_{x_*} \mathfrak{G}(x_*, s; x_i, 0) = -\frac{1}{\pi} \sum_{k \in \mathbb{Z}} \sum_{n=1}^{\infty} \sin[n(x_* - x_i)] e^{-n|2kp - s|}. \quad (3.46)$$

The integration over  $s$  is straightforward, and yields

$$\begin{aligned} \int_0^{y_*} ds \partial_{x_*} \mathfrak{G}(x_*, s; x_i, 0) &= -\frac{1}{2} + \frac{x_* - x_i}{2\pi} \\ &+ \frac{1}{\pi} \sum_{n=1}^{\infty} \frac{\sin[n(x_* - x_i)]}{n} \frac{e^{n(p-y_*)} - e^{-n(p-y_*)}}{e^{np} - e^{-np}}. \end{aligned} \quad (3.47)$$

We are now in position to write explicitly Schramm's formula (3.21) for a path on the cylinder with Neumann boundary conditions, in the scaling limit:

$$\begin{aligned} \mathbb{P}_L^{\text{NN}}(x_1, x_2, p; z_*) &= 1 - \frac{x_2 - x_1}{2\pi} \\ &- \frac{1}{\pi} \sum_{n=1}^{\infty} \frac{\sin[n(x_* - x_1)] - \sin[n(x_* - x_2)]}{n} \frac{e^{n(p-y_*)} - e^{-n(p-y_*)}}{e^{np} - e^{-np}}, \end{aligned} \quad (3.48)$$

where  $z_* = x_* + iy_*$ . We illustrate this probability in Fig. 3.7. Taking the limit  $y_* \rightarrow p$  yields the positive winding probability, simply given by

$$\lim_{y_* \rightarrow p} \mathbb{P}_L^{\text{NN}}(x_1, x_2, p; z_*) = \mathbb{P}_+^{\text{NN}}(x_2 - x_1) = 1 - \frac{x_2 - x_1}{2\pi}. \quad (3.49)$$

Surprisingly, this winding probability does *not* depend on the height  $p$  of the cylinder. The corresponding probabilities for other combinations of boundary conditions, on the other hand, *do* depend on  $p$ , as we shall see in Sections 3.2.2 and 3.2.2. We have not found an explanation for this property so far.

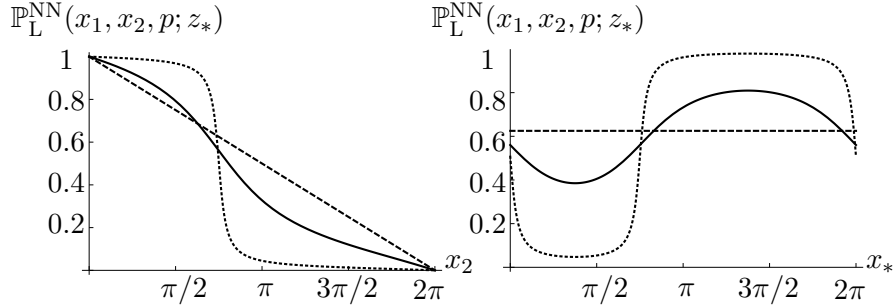


Figure 3.7: Illustration of the left-passage probability on a cylinder of perimeter  $2\pi$  and height  $p = 10$  with Neumann conditions on both boundaries. We assume the random paths to start at  $x_1 = 0$ , and consider three distinct values for the vertical coordinate of the marked point  $z_*$ :  $y_* = 1/10$  (dotted),  $y_* = 1$  (solid) and  $y_* = 10$  (dashed). On the left is the left-passage probability as a function of the position of the endpoint  $x_2$  of the paths, for  $x_* = 3\pi/4$ . On the right is the same probability as a function of the horizontal coordinate  $x_*$  of  $z_*$ , for  $x_2 = 3\pi/4$ .

### Wired boundaries

As a second calculation on the cylinder, let us now determine the positive winding probability (i.e. the left-passage probability with  $y_* = p$ ) when both the top and bottom boundaries of the cylinder are wired to the root  $s$ . We proceed here differently from in Section 3.2.2, in the sense that we compute the line bundle Green function  $\mathbf{G} = \mathbf{G}(e^{i\theta})$  directly, for any value of  $\theta$  (a feat we have not been able to reproduce for a zipper connected to a generic face  $f$  of the graph). We choose here a zipper with parameter  $z = e^{i\theta}$  crossing the edges of the form  $((N, y), (1, y))$  for  $1 \leq y \leq M$ .

The eigenvalue equation for the line bundle Laplacian  $\Delta$  reads

$$\begin{aligned} \Delta \mathbf{f}(x, y) &= 4\mathbf{f}(x, y) - \mathbf{f}(x-1, y) - \mathbf{f}(x+1, y) - \mathbf{f}(x, y-1) - \mathbf{f}(x, y+1) \\ &= \lambda \mathbf{f}(x, y) \end{aligned} \tag{3.50}$$

for  $1 \leq x \leq N$ ,  $1 \leq y \leq M$ . The eigenfunctions must further satisfy the following boundary conditions:

$$\begin{aligned} \mathbf{f}(x, 0) = 0 = \mathbf{f}(x, M + 1), \quad \mathbf{f}(0, y) = e^{i\theta} \mathbf{f}(N, y), \\ \mathbf{f}(N + 1, y) = e^{-i\theta} \mathbf{f}(1, y). \end{aligned} \quad (3.51)$$

One readily finds that the eigenvalues and normalized eigenfunctions are given by

$$\lambda_{m,n} = 4 - 2 \cos \left( \frac{\pi m}{M + 1} \right) - 2 \cos \left( \frac{2\pi n - \theta}{N} \right), \quad (3.52)$$

$$\mathbf{f}_{m,n}(x, y) = \left( \frac{2}{(M + 1)N} \right)^{1/2} e^{i(2\pi n - \theta)x/N} \sin \left( \frac{\pi m y}{M + 1} \right), \quad (3.53)$$

for  $1 \leq m \leq M$  and  $0 \leq n \leq N - 1$ . In the same scaling limit as in Section 3.2.2, the line bundle Green function  $\mathbf{G}$  converges to the continuum Green function  $\mathfrak{G}$  of a cylinder of perimeter  $2\pi$  and height  $p$  with Dirichlet conditions on both boundaries,

$$\mathfrak{G}(x_1, y_1; x_2, y_2; \theta) = \frac{1}{2\pi p} \sum_{\substack{m \in \mathbb{Z}^* \\ n \in \mathbb{Z}}} \frac{e^{i(n - \frac{\theta}{2\pi})(x_1 - x_2)} \sin \left( \frac{\pi m y_1}{p} \right) \sin \left( \frac{\pi m y_2}{p} \right)}{\left( n - \frac{\theta}{2\pi} \right)^2 + \left( \frac{\pi m}{p} \right)^2}. \quad (3.54)$$

For boundary points  $u_i = (x_i, 0)$ ,  $i = 1, 2$ , Schramm's formula may be written in terms of the excursion Poisson kernel  $P(x, p; \theta)$  (see Section 3.2.1 on the UHP) in the scaling limit as

$$\mathbb{P}_+^{\text{DD}}(x, p) = 1 + i \frac{1}{P(x, p; \theta)} \frac{dP(x, p; \theta)}{d\theta} \Big|_{\theta=0}, \quad (3.55)$$

where  $x = x_2 - x_1$ , the subscript  $+$  refers to the positive (counterclockwise) winding, and the superscripts stand for the type of boundary conditions on the bottom and top of the cylinder, respectively.

Recall that the excursion Poisson kernel is given by the normal derivative of the Green function  $\mathfrak{G}$  at the boundary points  $(x_1, 0)$  and  $(x_2, 0)$ . It reads here

$$\begin{aligned} P(x, p; \theta) &\equiv \lim_{\delta_1, \delta_2 \rightarrow 0^+} \frac{1}{\delta_1 \delta_2} \mathfrak{G}(x_1, \delta_1; x_2, \delta_2; \theta) \\ &= \frac{\pi}{4p^2} \sum_{k \in \mathbb{Z}} \frac{e^{ik\theta}}{\sinh^2 \left[ \left( 2\pi k - x \right) \frac{\pi}{2p} \right]}, \end{aligned} \quad (3.56)$$

where we used the Poisson summation formula to write the last equality. Its zeroth and first orders in  $\theta$  can be written in terms of Jacobi's theta functions (which we recall in Appendix C) and yield the following winding probability:

$$\mathbb{P}_+^{\text{DD}}(x, p) = 1 - \frac{1}{2\pi} \frac{1}{\partial_x F_1(x, p)} (x \partial_x + p \partial_p) F_1(x, p), \quad (3.57)$$

in agreement with the  $\text{SLE}_2$  computation of [64, 65]. Here  $F_1(x, p)$  is given by

$$F_1(x, p) = x + p \frac{\vartheta'_1(x/2, e^{-p})}{\vartheta_1(x/2, e^{-p})} = x + p \cot\left(\frac{x}{2}\right) + 4p \sum_{n=1}^{\infty} \frac{\sin(nx)}{e^{2np} - 1}. \quad (3.58)$$

We refer to Fig. 3.8 for an illustration of this winding probability for different moduli  $p$ .

In the limit of long cylinders  $p \rightarrow \infty$ , one recovers the equivalent of Schramm's formula for  $\kappa = 2$  [145] in our geometry,

$$\mathbb{P}_+^{\text{DD}}(x, p) \simeq 1 - \frac{x - \sin x}{2\pi} + \frac{1}{\pi p} \sin x \sin^2(x/2). \quad (3.59)$$

For very thin cylinders, i.e. for  $p \sim 0^+$ , one obtains, using the modular properties of theta functions (recalled in Appendix C),

$$\mathbb{P}_+^{\text{DD}}(x, p) \simeq \frac{e^{-\pi(2\pi-x)/p}}{e^{-\pi x/p} + e^{-\pi(2\pi-x)/p}} \simeq \begin{cases} 1 - e^{-2\pi(\pi-x)/p} & \text{if } 0 < x < \pi, \\ \frac{1}{2} & \text{if } x = \pi, \\ e^{-2\pi(x-\pi)/p} & \text{if } \pi < x < 2\pi. \end{cases} \quad (3.60)$$

which converges to the Heaviside step function. An intuitive explanation for this fact was given in [64], using the correspondence between paths in spanning forests and loop-erased random walks [126]: for very thin cylinders, the loop erasure of walks may be neglected at leading order, and the Heaviside function can be obtained by a simple Brownian motion calculation in the scaling limit.

### Mixed boundaries

The calculation of the positive winding probability on a cylinder with wired and free conditions on its bottom and top boundaries, respectively,

is very similar to that of  $\mathbb{P}_+^{\text{DD}}$ . Therefore, we merely state the result in the scaling limit [65]:

$$\mathbb{P}_+^{\text{DN}}(x, p) = 1 - \frac{1}{2\pi} \frac{1}{\partial_x F_2(x, p)} (x \partial_x + p \partial_p) F_2(x, p), \quad (3.61)$$

with the function  $F_2(x, p)$  defined in terms of Jacobi's theta and elliptic functions by

$$F_2(x, p) = p \vartheta_3^2 \text{cs}(\vartheta_3^2 x/2, \vartheta_2^2/\vartheta_3^2) = p \cot\left(\frac{x}{2}\right) - 4p \sum_{n=1}^{\infty} \frac{\sin(nx)}{e^{2np} + 1}, \quad (3.62)$$

where  $\vartheta_a \equiv \vartheta_a(0, e^{-p})$  for  $a = 2, 3$ . For large cylinders, we find

$$\mathbb{P}_+^{\text{DN}}(x, p) \simeq 1 - \frac{x - \sin x}{2\pi} + \frac{8}{\pi} \sin x \sin^2(x/2) p e^{-2p}, \quad (3.63)$$

which yields the same result as Eq. (3.59) in the limit  $p \rightarrow \infty$ . Interestingly, the first correction is exponential here, as opposed to the  $1/p$  correction computed above for the pure Dirichlet case. When  $p \rightarrow 0^+$ , the winding probability converges to the Heaviside function as follows:

$$\mathbb{P}_+^{\text{DN}}(x, p) \simeq 1 - \left(1 + e^{\pi(\pi-x)/p}\right)^{-1} \simeq \begin{cases} 1 - e^{-\pi(\pi-x)/p} & \text{if } 0 < x < \pi, \\ \frac{1}{2} & \text{if } x = \pi, \\ e^{-\pi(x-\pi)/p} & \text{if } \pi < x < 2\pi. \end{cases} \quad (3.64)$$

Both asymptotic limits of  $\mathbb{P}_+^{\text{DN}}$  are represented in Fig. 3.8.

For the opposite choice of boundary conditions, namely free and wired on the bottom and top boundaries, respectively, we obtain the following Green function in the scaling limit,

$$\mathfrak{G}(x_1, 0; x_2, 0; \theta) = \frac{1}{2\pi} \sum_{n \in \mathbb{Z}} \frac{e^{i(n - \frac{\theta}{2\pi})(x_1 - x_2)}}{n - \frac{\theta}{2\pi}} \tanh \left[ \left( n - \frac{\theta}{2\pi} \right) p \right]. \quad (3.65)$$

Its leading order for  $\theta \sim 0^+$  yields, with  $x = x_2 - x_1$ ,

$$\begin{aligned} \mathfrak{G}(x, p) &\equiv \mathfrak{G}(x_1, 0; x_2, 0; \theta)|_{\theta=0} = \frac{p}{2\pi} + \frac{1}{\pi} \sum_{n=1}^{\infty} \frac{\cos(nx) \tanh(np)}{n} \\ &= \frac{1}{\pi} \log \left( \frac{2 \vartheta_4^2(x/2, e^{-2p})}{\vartheta_1(x/2, e^{-p}) \vartheta_2(0, e^{-p})} \right). \end{aligned} \quad (3.66)$$

The derivative of the Green function can, upon visual inspection, be rewritten as

$$\begin{aligned}\mathfrak{G}'(x, p) &\equiv -i \partial_\theta \mathfrak{G}(x_1, 0; x_2; 0; \theta) \Big|_{\theta=0} \\ &= \frac{x}{2\pi} \mathfrak{G}(x, p) + \frac{1}{2\pi} (p \partial_p - 1) \int_0^x dt \mathfrak{G}(t, p).\end{aligned}\quad (3.67)$$

It follows that Schramm's formula for the Neumann-Dirichlet case reads, in the scaling limit,

$$\mathbb{P}_+^{\text{ND}}(x, p) = 1 - \frac{1}{2\pi} \frac{1}{\partial_x F_3(x, p)} (x \partial_x + p \partial_p - 1) F_3(x, p), \quad (3.68)$$

where  $F_3(x, p)$  is defined by

$$F_3(x, p) = \int_0^x dt \mathfrak{G}(t, p). \quad (3.69)$$

We may compute the large- and small- $p$  expansions as above, using the approximations

$$\mathfrak{G}(x, p) \simeq \frac{p}{2\pi} - \frac{1}{\pi} \log[2 \sin(x/2)] - \frac{2}{\pi} \cos x e^{-2p} \quad \text{for } p \gg 1, \quad (3.70)$$

$$\mathfrak{G}(x, p) \simeq \frac{2}{\pi} e^{-\pi x/(2p)} + \frac{2}{\pi} e^{-\pi(2\pi-x)/(2p)} \quad \text{for } p \ll 1. \quad (3.71)$$

In the limits  $p \rightarrow \infty$  and  $p \rightarrow 0^+$ , the winding probability converges to  $1 - x/(2\pi)$  and to the Heaviside function  $1 - \Theta(x - \pi)$ , respectively (see Fig. 3.8 below).

### 3.2.3 The Möbius strip

Our next example for Schramm's formula consists in a grid embedded on a Möbius strip. The nonorientability of the surface brings out two complications. First, the concepts of "left-passage" and "counterclockwise" are ill defined on such a surface. Second, simple paths between two boundary vertices on a Möbius strip are distributed into not *two* but *three* distinct topological classes, as illustrated in Fig. 3.9. An adaptation of Eq. (3.19) is therefore needed to compute their respective winding probabilities.

The graph  $\mathcal{G}$  we consider here is an  $N \times M$  rectangle, with vertex coordinates  $(x, y)$  for  $1 \leq x \leq N$  and  $1 \leq y \leq M$ . We choose wired

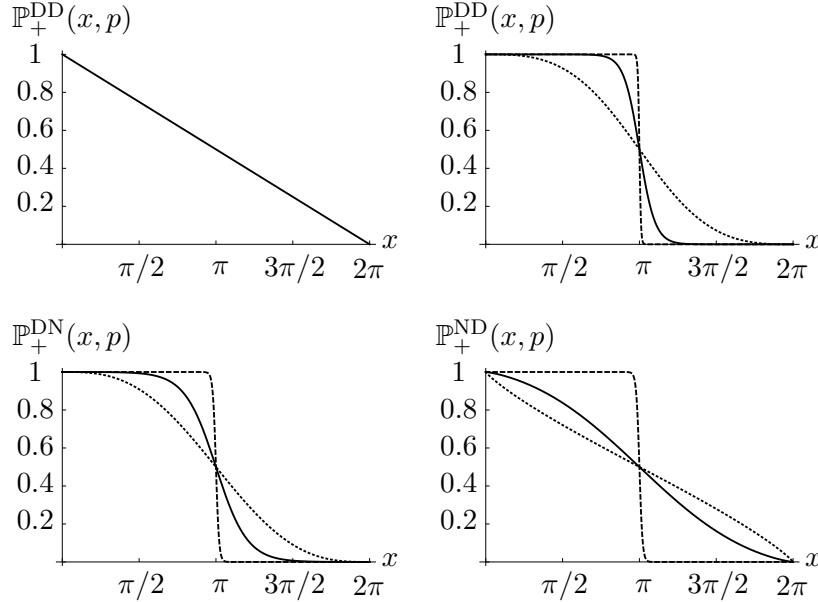


Figure 3.8: Illustration of the four positive winding probability on the cylinder with Dirichlet and/or Neumann conditions on its lower and upper boundaries, for  $p = 1/10$  (dashed),  $p = 1$  (solid) and  $p = 10$  (dotted).

or free conditions on both the top ( $y = M$ ) and bottom ( $y = 1$ ) sides of the rectangle, and twisted periodic conditions in the horizontal direction, namely,  $(x+N, y) \sim (x, M+1-y)$ . The latter are implemented by connecting each vertex  $(N, y)$  of the rectangle to  $(1, M+1-y)$  by an edge, for  $1 \leq y \leq M$ . Furthermore, we equip these edges with a parallel transport  $\phi_{(N+1,y),(1,M+1-y)} = e^{i\theta}$ , with  $\theta \in \mathbb{R}$ .

With respect to the zipper, there are four possible ways to select two boundary vertices  $u_i = (x_i, y_i)$ , with  $1 \leq x_i \leq N$  and  $i = 1, 2$ , as each  $y_i$  may take the value 1 or  $M$ . It is easy to see that choosing  $y_1 = y_2 = 1$  is equivalent to  $y_1 = y_2 = M$ , and that  $y_1 = 1, y_2 = M$  is equivalent to  $y_1 = M, y_2 = 1$ . Let us therefore pick  $u_1 = (x_1, 1)$ , and discuss the two cases  $u_2 = (x_2, 1)$  (with  $x_1 < x_2$ ) and  $u_2 = (x_2, M) \simeq (x_2 + N, 1)$  with  $1 \leq x_2 \leq N$ . We start with the former, and consider oriented cycle-rooted groves on the graph that contain a path from  $u_1$  to  $u_2$ . In such groves, the path from  $u_1$  to  $u_2$  winds around the strip zero, one or

two times, yielding a product of parallel transports  $\phi_{1 \rightarrow 2} = 1, e^{-i\theta}, e^{-2i\theta}$ , respectively (see Fig. 3.9). The noncontractible cycles  $\alpha$  appearing in such groves are of two types, winding once or twice around the strip, and therefore pick up a monodromy factor  $\varpi_\alpha = e^{i\theta}, e^{2i\theta}$  or their inverses (depending on the orientation of the cycles). The contractible cycles, on the other hand, have a trivial monodromy, and so do not appear in OCRGs counted by the partition function  $\mathbf{Z}_1^{[2]}$ .

More precisely, let us observe that an OCRG in the first or third class (i.e. with  $\phi_{1 \rightarrow 2} = 1, e^{-2i\theta}$ ) contains at most one cycle winding once around the strip, and any number of cycles winding twice. On the other hand, the OCRGs in the second class (with  $\phi_{1 \rightarrow 2} = e^{-i\theta}$ ) are quite peculiar, as the existence of the path from  $u_1$  to  $u_2$  forbids any noncontractible cycle. This crucial observation allows one to write the partition function explicitly for all paths in groves from  $u_1$  to  $u_2$  as

$$\begin{aligned} \mathbf{Z}_1^{[2]} &= \mathbf{G}_{1,2} \det \Delta = \sum_{\text{OCRGs } \Gamma_{\vec{\sigma}}} \prod_{\text{cycles } \alpha \in \Gamma_{\vec{\sigma}}} (1 - \varpi_\alpha) \times \phi_{1 \rightarrow 2}^{-1} \\ &= \sum_{k=0}^{\infty} (2 - 2 \cos 2\theta)^k \left\{ N_k^{(1)} + N_k^{(3)} e^{2i\theta} \right. \\ &\quad \left. + \left( \tilde{N}_k^{(1)} + \tilde{N}_k^{(3)} e^{2i\theta} \right) (2 - 2 \cos \theta) \right\} + N_0^{(2)} e^{i\theta}, \end{aligned} \quad (3.72)$$

where  $\vec{\sigma} = \begin{smallmatrix} 2 \\ 1 \end{smallmatrix}$ , and  $N_k^{(j)}$  (resp.  $\tilde{N}_k^{(j)}$ ) denotes the number of unoriented CRGs in class  $j$  with  $k$  cycles winding twice around the strip and no cycle (resp. one cycle) winding once. In the limit  $\theta \rightarrow 0$ , Eq. (3.72) yields

$$Z[12] = \lim_{\theta \rightarrow 0} \mathbf{Z}_1^{[2]} = N_0^{(1)} + N_0^{(2)} + N_0^{(3)}, \quad (3.73)$$

where  $N_0^{(j)}$  is the number of spanning forests on  $\mathcal{G}$  in class  $j$ , whose knowledge is required to compute winding probabilities on the Möbius strip:

$$\begin{aligned} &\mathbb{P}_{\text{SF}}(\text{a random simple path from } u_1 \text{ to } u_2 \text{ is in class } j) \\ &\equiv \mathbb{P}_j(u_1, u_2) = \frac{N_0^{(j)}}{N_0^{(1)} + N_0^{(2)} + N_0^{(3)}}. \end{aligned} \quad (3.74)$$

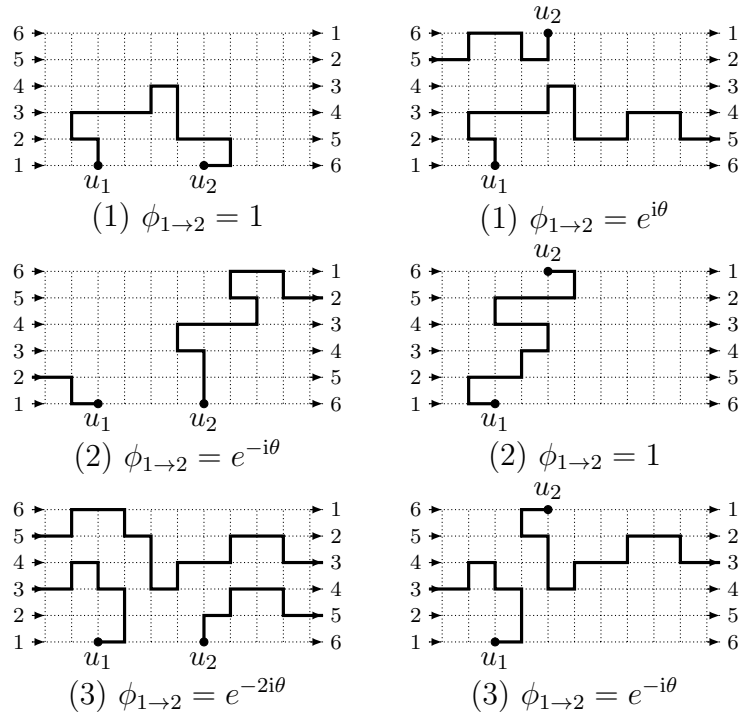


Figure 3.9: Möbius graph  $\mathcal{G}$  drawn as a rectangular grid with twisted periodic boundary conditions in the horizontal direction (the numbers on the half-edges indicate how they should be glued together to obtain the graph  $\mathcal{G}$ ). The oriented edges equipped with a nontrivial parallel transport  $e^{i\theta}$  are drawn with an arrow. Each panel depicts a representative of each class of simple paths between two boundary vertices  $u_1, u_2$ . There are three distinct classes of paths, whether  $u_2$  is located on the bottom boundary of the rectangle (in the left column) or on the top boundary (in the right column).

In order to extract the values of  $N_0^{(j)}$  from Eq. (3.72), we first use the zeroth- and first-order terms in  $\theta$  (as on the cylinder), which yield

$$\mathbf{Z}_{[1]}^{[2]}|_{\theta=0} = N_0^{(1)} + N_0^{(2)} + N_0^{(3)}, \quad \partial_\theta \mathbf{Z}_{[1]}^{[2]}|_{\theta=0} = i N_0^{(2)} + 2i N_0^{(3)}, \quad (3.75)$$

respectively. To write a third independent equation, we evaluate (3.72) at  $\theta=\pi/2$ :

$$\text{Im } \mathbf{Z}_{[1]}^{[2]}|_{\theta=\pi/2} = N_0^{(2)}. \quad (3.76)$$

Using Eqs. (3.75) and (3.76), we find the following combinatorial expressions for winding probabilities on the Möbius strip:

$$\begin{aligned} \mathbb{P}_1(u_1, u_2) &= 1 + \frac{i}{2} \partial_\theta \log \mathbf{Z}_{[1]}^{[2]}|_{\theta=0} - \frac{1}{2} \frac{\text{Im } \mathbf{Z}_{[1]}^{[2]}|_{\theta=\pi/2}}{\mathbf{Z}_{[1]}^{[2]}|_{\theta=0}}, \\ \mathbb{P}_2(u_1, u_2) &= \frac{\text{Im } \mathbf{Z}_{[1]}^{[2]}|_{\theta=\pi/2}}{\mathbf{Z}_{[1]}^{[2]}|_{\theta=0}}, \\ \mathbb{P}_3(u_1, u_2) &= -\frac{i}{2} \partial_\theta \log \mathbf{Z}_{[1]}^{[2]}|_{\theta=0} - \frac{1}{2} \frac{\text{Im } \mathbf{Z}_{[1]}^{[2]}|_{\theta=\pi/2}}{\mathbf{Z}_{[1]}^{[2]}|_{\theta=0}}, \end{aligned} \quad (3.77)$$

where  $\mathbf{Z}_{[1]}^{[2]} = \mathbf{G}_{1,2} \det \mathbf{\Delta}$  can be computed in terms of the eigenvalues and eigenfunctions of  $\mathbf{\Delta} = \mathbf{\Delta}(\theta)$ , which we give below for the Möbius graph with either wired or free boundary conditions.

If instead we take the endpoint of the path on the top boundary of the rectangle,  $u_2 = (x_2, M)$ , the product of parallel transports along the path from  $u_1$  to  $u_2$  (with respect to the same zipper) reads  $\phi_{1 \rightarrow 2} = e^{i\theta}, 1, e^{-i\theta}$  for the first, second and third classes of paths, respectively (see the bottom row of Fig. 3.9). Consequently, the winding probabilities are given by

$$\begin{aligned} \widehat{\mathbb{P}}_1(u_1, u_2) &= \frac{1}{2} + \frac{i}{2} \partial_\theta \log \mathbf{Z}_{[1]}^{[2]}|_{\theta=0} - \frac{1}{2} \frac{\text{Re } \mathbf{Z}_{[1]}^{[2]}|_{\theta=\pi/2}}{\mathbf{Z}_{[1]}^{[2]}|_{\theta=0}}, \\ \widehat{\mathbb{P}}_2(u_1, u_2) &= \frac{\text{Re } \mathbf{Z}_{[1]}^{[2]}|_{\theta=\pi/2}}{\mathbf{Z}_{[1]}^{[2]}|_{\theta=0}}, \\ \widehat{\mathbb{P}}_3(u_1, u_2) &= \frac{1}{2} - \frac{i}{2} \partial_\theta \log \mathbf{Z}_{[1]}^{[2]}|_{\theta=0} - \frac{1}{2} \frac{\text{Re } \mathbf{Z}_{[1]}^{[2]}|_{\theta=\pi/2}}{\mathbf{Z}_{[1]}^{[2]}|_{\theta=0}}, \end{aligned} \quad (3.78)$$

where the hat serves as a reminder that the endpoint  $u_2$  is located on the top boundary of the rectangle. Although the combinatorial forms

(3.77) and (3.78) of the  $\mathbb{P}_j$ 's and the  $\widehat{\mathbb{P}}_j$ 's differ depending on the position of  $u_2$ , we shall show explicitly that they are related to one another by  $x_2 \rightarrow x_2 + N$  for both choices of boundary conditions (wired or free), reflecting the periodicity of the Möbius strip.

### Wired boundary

Let us start with a Möbius graph in which all boundary vertices are wired to the root  $s$ . Its Dirichlet line bundle Laplacian  $\Delta$  has the following eigenvalues and eigenfunctions:

$$\lambda_{m,n} = 4 - 2 \cos \left( \frac{\pi m}{M+1} \right) - 2 \cos \left( \frac{2\pi n + \pi(m+1) - \theta}{N} \right), \quad (3.79)$$

$$\mathbf{f}_{m,n}(x, y) = \left( \frac{2}{MN} \right)^{1/2} e^{i(2\pi n + \pi(m+1) - \theta)x/N} \sin \left( \frac{\pi m y}{M+1} \right), \quad (3.80)$$

for  $1 \leq m \leq M$  and  $0 \leq n \leq N-1$ . As in Section 3.2.2 (for the cylinder), we introduce the variables  $x = \varepsilon x$  and  $y = \varepsilon y$  on the lattice  $\varepsilon\mathbb{Z}^2$ . We take the scaling limit  $\varepsilon \rightarrow 0^+$  and  $M, N \rightarrow \infty$  such that  $M\varepsilon \rightarrow p$  and  $N\varepsilon \rightarrow 2\pi$ . In that limit, the discrete Green function converges to the continuum Green function of a Möbius strip of width  $p$  and perimeter  $4\pi$ , given by

$$\mathfrak{G}(x_1, y_1; x_2, y_2; \theta) = \frac{1}{2\pi p} \sum_{\substack{m \in \mathbb{Z}^* \\ n \in \mathbb{Z}}} \frac{e^{i(n + \frac{m+1}{2} - \frac{\theta}{2\pi})(x_1 - x_2)} \sin \left( \frac{\pi m y_1}{p} \right) \sin \left( \frac{\pi m y_2}{p} \right)}{\left( n + \frac{m+1}{2} - \frac{\theta}{2\pi} \right)^2 + \left( \frac{\pi m}{p} \right)^2}. \quad (3.81)$$

It is useful to separate the series over  $m$  into two parts, according to the parity of  $m$ , to compute the associated excursion Poisson kernel, which reads at  $(x_1, 0), (x_2, 0)$ :

$$\begin{aligned} P(x, p; \theta) &= \lim_{\delta, \varepsilon \rightarrow 0^+} \frac{1}{\delta \varepsilon} \mathfrak{G}(x_1, \delta; x_2, \varepsilon; \theta) \\ &= \frac{\pi}{2p^2} \sum_{k \in \mathbb{Z}} \frac{e^{ik\theta} \{(-1)^k + \cosh [(2\pi k - x)\pi/p]\}}{\sinh^2 [(2\pi k - x)\pi/p]}, \end{aligned} \quad (3.82)$$

where  $x = x_2 - x_1$ . If on the other hand  $u_2 = (x_2, p)$ , we find the excursion Poisson kernel

$$\begin{aligned}\widehat{P}(x, p; \theta) &= \lim_{\delta, \varepsilon \rightarrow 0^+} \frac{1}{\delta \varepsilon} \mathfrak{G}(x_1, \delta; x_2, p - \varepsilon; \theta) \\ &= \frac{\pi}{2p^2} \sum_{k \in \mathbb{Z}} \frac{e^{ik\theta} \{(-1)^k - \cosh[(2\pi k - x)\pi/p]\}}{\sinh^2[(2\pi k - x)\pi/p]}.\end{aligned}\quad (3.83)$$

In the continuum, one finds the following expressions for the winding probabilities on the strip:

$$\begin{aligned}\mathbb{P}_1^D(x, p) &= 1 + \frac{i}{2} \frac{\partial_\theta P(x, p; 0)}{P(x, p; 0)} - \frac{1}{2} \frac{\det \mathbf{\Delta}(\pi/2)}{\det \mathbf{\Delta}(0)} \frac{\operatorname{Im} P(x, p; \pi/2)}{P(x, p; 0)}, \\ \mathbb{P}_2^D(x, p) &= \frac{\det \mathbf{\Delta}(\pi/2)}{\det \mathbf{\Delta}(0)} \frac{\operatorname{Im} P(x, p; \pi/2)}{P(x, p; 0)}, \\ \mathbb{P}_3^D(x, p) &= -\frac{i}{2} \frac{\partial_\theta P(x, p; 0)}{P(x, p; 0)} - \frac{1}{2} \frac{\det \mathbf{\Delta}(\pi/2)}{\det \mathbf{\Delta}(0)} \frac{\operatorname{Im} P(x, p; \pi/2)}{P(x, p; 0)},\end{aligned}\quad (3.84)$$

when  $u_2 = (x_2, 0)$  is on the bottom boundary (similar formulas hold when  $u_2 = (x_2, p)$ ). Comparing Eqs. (3.82) and (3.83), we find that  $P(x+2\pi, p; \theta) = -e^{i\theta} \widehat{P}(x, p; \theta)$ , from which the relations

$$\widehat{\mathbb{P}}_j^D(x, p) = \mathbb{P}_j^D(x + 2\pi, p) \quad (3.85)$$

follow. It is worth noting that the excursion Poisson kernel also satisfies the identity  $P(4\pi - x, p; \theta) = e^{2i\theta} P(x, p; -\theta)$ , implying that

$$\mathbb{P}_j^D(4\pi - x, p) = \mathbb{P}_{4-j}^D(x, p) \quad (3.86)$$

for  $1 \leq j \leq 3$ . It suffices therefore to compute the winding probabilities for  $0 \leq x \leq 2\pi$ , which we assume is the case for the rest of this section.

Let us now come back the excursion Poisson kernel (3.82). Its zeroth and first orders in  $\theta$  can be written in terms of Jacobi's theta and elliptic functions (whose definitions are recalled in the Appendix C) as follows, provided  $0 \leq x \leq 2\pi$ :

$$\begin{aligned}P(x, p; 0) &= -\frac{1}{2\pi p} \partial_x F(x, p), \\ \partial_\theta P(x, p; 0) &= -\frac{i}{4\pi^2 p} (x \partial_x + p \partial_p) F(x, p),\end{aligned}\quad (3.87)$$

with the function  $F(x, p)$  given by

$$\begin{aligned}
F(x, p) &= \frac{p}{2} \vartheta_3^2 (\operatorname{ns}(\vartheta_3^2 x/2, \vartheta_2^2/\vartheta_3^2) + \operatorname{cs}(\vartheta_3^2 x/2, \vartheta_2^2/\vartheta_3^2)) \\
&= \frac{p}{2} \cot(x/4) - 2p \sum_{n=1}^{\infty} \frac{\sin(nx/2)}{(-1)^n e^{np/2} + 1} \\
&= \pi \coth(\pi x/(2p)) + 4\pi \sum_{n=1}^{\infty} \frac{\sinh(n\pi x/p)}{(-1)^n e^{2\pi^2 n/p} + 1},
\end{aligned} \tag{3.88}$$

with  $\vartheta_a \equiv \vartheta_a(0, e^{-p/2})$  for  $a = 2, 3$ , and where we used the modular properties of Jacobi's theta and elliptic functions to write the last equality. The two series representations of  $F(x, p)$  will be used below to compute the asymptotics of  $\mathbb{P}_j^D(x, p)$  for  $p \rightarrow \infty$  and  $p \rightarrow 0^+$ .

Similarly, the imaginary part of the excursion Poisson kernel at  $\theta = \pi/2$  can be recast into the form

$$\operatorname{Im} P(x, p; \pi/2) = -\frac{1}{2\pi p} \partial_x \tilde{F}(x, p), \tag{3.89}$$

with the auxiliary function  $\tilde{F}(x, p)$  defined as

$$\begin{aligned}
\tilde{F}(x, p) &= \frac{p}{2} \vartheta_2^2 \operatorname{cd}(\vartheta_3^2 x/4, \vartheta_2^2/\vartheta_3^2) \\
&= 2p \sum_{n=0}^{\infty} \frac{(-1)^n e^{(2n+1)p/4} \cos[(2n+1)x/4]}{e^{(2n+1)p/2} - 1} \\
&= \pi + 4\pi \sum_{n=1}^{\infty} \frac{(-1)^n e^{2\pi^2 n/p} \cosh(n\pi x/p)}{e^{4\pi^2 n/p} + 1}.
\end{aligned} \tag{3.90}$$

In addition to the excursion Poisson kernel, knowledge of the determinant of the Laplacian is also required to compute winding probabilities on the Möbius strip using (3.84). For the discrete graph  $\mathcal{G}$ , it reads

$$\det \Delta(\theta) = \prod_{m=1}^M \prod_{n=0}^{N-1} \left[ 4 - 2 \cos\left(\frac{\pi m}{M+1}\right) - 2 \cos\left(\frac{2\pi n + \pi(m+1) - \theta}{N}\right) \right]. \tag{3.91}$$

A similar determinant was computed in [64] for  $\theta = 0$ ; we follow essentially the same procedure here. We start by introducing the variable  $t_m$  defined by the relation  $\cosh t_m = 2 - \cos(\pi m/(M+1))$ . For  $m \ll M$ ,

$t_m = \pi m/(M+1) + \dots$  at leading order. This new variable enables us to compute the product over  $n$ :

$$\begin{aligned}
& \prod_{n=0}^{N-1} \left( 2 \cosh t_m - 2 \cos \left( \frac{2\pi n + \pi(m+1) - \theta}{N} \right) \right) \\
&= \prod_{n=0}^{N-1} e^{t_m} \left( 1 - e^{-t_m + i(2\pi n + \pi(m+1) - \theta)/N} \right) \left( 1 - e^{-t_m - i(2\pi n + \pi(m+1) - \theta)/N} \right) \\
&= e^{Nt_m} \left( 1 - e^{-Nt_m + i\pi(m+1) + i\theta} \right) \left( 1 - e^{-Nt_m + i\pi(m+1) - i\theta} \right),
\end{aligned} \tag{3.92}$$

where the second equality comes from the factorization

$$q^N - 1 = \prod_{j=0}^{N-1} (q - e^{i2\pi j/N}). \tag{3.93}$$

The logarithm of the determinant therefore reads

$$\begin{aligned}
\log \det \mathbf{\Delta}(\theta) &= \log(4 \sin^2(\theta/2)) + \sum_{m=1}^{M-1} N t_m \\
&+ \sum_{m=1}^{M-1} \log \left[ \left( 1 - e^{-Nt_m + i\pi(m+1) + i\theta} \right) \left( 1 - e^{-Nt_m + i\pi(m+1) - i\theta} \right) \right],
\end{aligned} \tag{3.94}$$

where the first term on the right-hand side comes from the contribution  $m = 0$  in  $\det \mathbf{\Delta}(\theta)$ . The second term may be evaluated perturbatively by applying the Euler-Maclaurin formula:

$$\sum_{m=1}^M t_m = \frac{4G}{\pi}(M+1) - \frac{1}{2} \log(3 + 2\sqrt{2}) - \frac{\pi}{12M} + \dots \tag{3.95}$$

up to corrections of order  $1/M^2$ . Here  $G = 0.915966\dots$  is Catalan's constant. In the last term of Eq. (3.94), the main contribution to the sum comes from the values of  $m \ll M$ , so we can replace  $t_m$  with  $\pi m/M$ . We may therefore express the determinant of the Laplacian as follows in the scaling limit:

$$\begin{aligned}
\det \mathbf{\Delta}(\theta) &\simeq \exp \left( \frac{4G}{\pi}(M+1)N - \frac{1}{2} \log(3 + 2\sqrt{2})N \right) \\
&\times e^{-\pi N/(12M)} \times 4 \sin^2(\theta/2) \\
&\times \prod_{m=1}^{\infty} \left( 1 - e^{-N\pi m/M + i\pi(m+1) + i\theta} \right) \left( 1 - e^{-N\pi m/M + i\pi(m+1) - i\theta} \right).
\end{aligned} \tag{3.96}$$

It should be noted that the first exponential factor diverges as  $M, N \rightarrow \infty$ . However, since it is a mere constant and Eq. (3.84) only involves ratios of this determinant, we may discard it to define a *regularized* determinant, which we can write in terms of Dedekind's eta function  $\eta(q)$  and Jacobi's theta function  $\vartheta_2(z, q)$  as

$$(\det \Delta(\theta))_{\text{reg}} = \frac{\vartheta_2(\theta/2, i e^{-\pi^2/p})}{2 \cos(\theta/2) \eta(-i e^{-\pi^2/p})}. \quad (3.97)$$

To calculate explicitly the winding probabilities (3.77), we need to compute both its logarithmic derivative at  $\theta = 0$  and the ratio of determinants evaluated at  $\pi/2$  and 0. It is straightforward to see that the former vanishes, while the latter is equal to

$$\begin{aligned} \frac{(\det \Delta(\pi/2))_{\text{reg}}}{(\det \Delta(0))_{\text{reg}}} &= \sqrt{2} \frac{\vartheta_2(\pi/4, e^{-2\pi^2/p}) \vartheta_4(\pi/4, e^{-2\pi^2/p})}{\vartheta_2(0, e^{-2\pi^2/p}) \vartheta_4(0, e^{-2\pi^2/p})} \\ &= \sqrt{2} e^{-p/16} \frac{\vartheta_2(ip/8, e^{-p/2}) \vartheta_4(ip/8, e^{-p/2})}{\vartheta_2(0, e^{-p/2}) \vartheta_4(0, e^{-p/2})} \\ &\equiv \sqrt{2} \Theta_{2,4}(p). \end{aligned} \quad (3.98)$$

Putting all the pieces together yields the following formulas for winding probabilities on the Möbius strip with Dirichlet boundary conditions:

$$\begin{aligned} \mathbb{P}_1^D(x, p) &= 1 - \frac{1}{4\pi} \frac{(x \partial_x + p \partial_p) F(x, p)}{\partial_x F(x, p)} - \frac{1}{\sqrt{2}} \Theta_{2,4}(p) \frac{\partial_x \tilde{F}(x, p)}{\partial_x F(x, p)}, \\ \mathbb{P}_2^D(x, p) &= \sqrt{2} \Theta_{2,4}(p) \frac{\partial_x \tilde{F}(x, p)}{\partial_x F(x, p)}, \quad \mathbb{P}_3^D(x, p) = 1 - \mathbb{P}_1^D(x, p) - \mathbb{P}_2^D(x, p), \end{aligned} \quad (3.99)$$

with  $F, \tilde{F}, \Theta_{2,4}$  defined by Eqs. (3.88), (3.90) and (3.98), respectively. These probabilities are illustrated in Fig. 3.10, in the asymptotic cases  $p \rightarrow \infty$  and  $p \rightarrow 0^+$ . For the former limit, we find for  $p \gg 1$  that

$$\begin{aligned} \frac{(x \partial_x + p \partial_p) F(x, p)}{\partial_x F(x, p)} &\simeq x - 2 \sin(x/2) + 8 \sin(x/2) \sin^2(x/4) p e^{-p/2}, \\ \Theta_{2,4}(p) &\simeq \frac{1}{2} e^{p/16} + \frac{1}{2} e^{-7p/16}, \\ \frac{\partial_x \tilde{F}(x, p)}{\partial_x F(x, p)} &\simeq 4 \sin^3(x/4) e^{-p/4} - 8(2 + \cos(x/2) + \cos x) \\ &\quad \times \sin^3(x/4) e^{-3p/4}. \end{aligned} \quad (3.100)$$

For large strips, the winding probabilities therefore read

$$\begin{aligned}\mathbb{P}_1^D(x, p) &\simeq 1 - \frac{x - 2\sin(x/2)}{4\pi} - \sqrt{2}\sin^3(x/4)e^{-3p/16}, \\ \mathbb{P}_2^D(x, p) &\simeq 2\sqrt{2}\sin^3(x/4)e^{-3p/16}, \\ \mathbb{P}_3^D(x, p) &= 1 - \mathbb{P}_1^D(x, p) - \mathbb{P}_2^D(x, p).\end{aligned}\tag{3.101}$$

In contrast, we also consider the case  $p \ll 1$  of very thin strips, for which we use the modular properties of Jacobi's theta and elliptic functions to obtain the expansions

$$\begin{aligned}\frac{(x\partial_x + p\partial_p)F(x, p)}{\partial_x F(x, p)} &\simeq 2\pi\frac{\partial_x \tilde{F}(x, p)}{\partial_x F(x, p)} \simeq \frac{2\pi e^{-\pi(2\pi-x)/p}}{e^{-\pi x/p} + e^{-\pi(2\pi-x)/p}}, \\ \Theta_{2,4}(p) &\simeq \frac{1}{\sqrt{2}} + \sqrt{2}e^{-2\pi^2/p}.\end{aligned}\tag{3.102}$$

We discuss these asymptotic results for  $p \rightarrow \infty$  and  $p \rightarrow 0^+$  below.

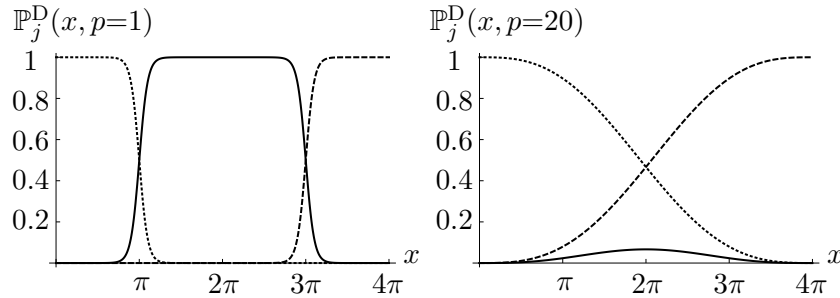


Figure 3.10: Winding probabilities of a random simple path from  $u_1 = (x_1, 0)$  to  $u_2 = (x_2, 0)$  on a Möbius strip with Dirichlet boundary conditions, as functions of the separation  $x = x_2 - x_1$ . The probabilities for the three winding classes ( $1 \leq j \leq 3$ ) are drawn with a dotted, solid, and dashed line, respectively.

### Free boundary

We proceed similarly for the Möbius strip with free boundary conditions. Using the same zipper as for the wired strip, we find the eigenvalues and

eigenfunctions of  $\Delta = \Delta(\theta)$  to be given by

$$\lambda_{m,n} = 4 - 2 \cos\left(\frac{\pi m}{M}\right) - 2 \cos\left(\frac{2\pi n + \pi m - \theta}{N}\right), \quad (3.103)$$

$$\mathbf{f}_{m,n}(x,y) = \left(\frac{2 - \delta_{m,0}}{MN}\right)^{1/2} e^{i(2\pi n + \pi m - \theta)x/N} \cos\left[\frac{\pi m}{M}\left(y - \frac{1}{2}\right)\right], \quad (3.104)$$

for  $0 \leq m \leq M-1$  and  $0 \leq n \leq N-1$ . The corresponding Green function in the scaling limit satisfies Neumann boundary conditions at  $y = 0$  and  $y = p$ , and reads

$$\mathfrak{G}(x_1, y_1; x_2, y_2; \theta) = \frac{1}{2\pi p} \sum_{m,n \in \mathbb{Z}} \frac{e^{i(n + \frac{m}{2} - \frac{\theta}{2\pi})(x_1 - x_2)} \cos\left(\frac{\pi m y_1}{p}\right) \cos\left(\frac{\pi m y_2}{p}\right)}{\left(n + \frac{m}{2} - \frac{\theta}{2\pi}\right)^2 + \left(\frac{\pi m}{p}\right)^2}. \quad (3.105)$$

For boundary points, i.e.  $y_1 = y_2 = 0$ , the Green function simplifies to

$$\begin{aligned} \mathfrak{G}(x, p; \theta) &= \frac{1}{4\pi} \sum_{n \in \mathbb{Z}} \frac{e^{-i(n - \frac{\theta}{2\pi})x} \coth\left[\left(n - \frac{\theta}{2\pi}\right)\frac{p}{2}\right]}{n - \frac{\theta}{2\pi}} \\ &+ \frac{1}{4\pi} \sum_{n \in \mathbb{Z}} \frac{e^{-i(n + \frac{1}{2} - \frac{\theta}{2\pi})x} \tanh\left[\left(n + \frac{1}{2} - \frac{\theta}{2\pi}\right)\frac{p}{2}\right]}{n + \frac{1}{2} - \frac{\theta}{2\pi}}, \end{aligned} \quad (3.106)$$

where  $x = x_2 - x_1$ . For  $\theta \rightarrow 0^+$ , the Green function is singular because  $\det \Delta(\theta) \rightarrow 0$ . More precisely, its Laurent series reads, up to regular terms,

$$\mathfrak{G}(x, p; \theta) = \frac{2\pi}{p\theta^2} + \frac{ix}{p\theta} + \dots \quad (3.107)$$

As for the strip with Dirichlet boundary conditions, it suffices to study the winding probabilities for  $0 \leq x \leq 2\pi$ . Indeed, the Green function satisfies the relations

$$\operatorname{Im} \mathfrak{G}(4\pi - x, p; \pi/2) = \operatorname{Im} \mathfrak{G}(x, p; \pi/2), \quad (3.108)$$

$$\mathfrak{G}(4\pi - x, p; \theta) = \mathfrak{G}(x, p; \theta) + \frac{2i(2\pi - x)}{p\theta} + \dots, \quad (3.109)$$

implying that  $\mathbb{P}_j^N(x) = \mathbb{P}_{4-j}^N(4\pi - x)$  for any  $x$  between  $2\pi$  and  $4\pi$ , for  $1 \leq j \leq 3$ .

The regularized determinant is obtained by taking the same steps as in Section 3.2.2 and yields

$$(\det \Delta(\theta))_{\text{reg}} = \frac{2 \sin(\theta/2) \vartheta_1(\theta/2, i e^{-\pi^2/p})}{\eta(i e^{-\pi^2/p})}. \quad (3.110)$$

Using Eqs. (3.106) and (3.110), we find after some algebra the following winding probabilities on the Möbius strip with Neumann boundary conditions, in the scaling limit:

$$\begin{aligned}\mathbb{P}_1^N(x, p) &= 1 - \frac{x}{4\pi} - H(x, p), & \mathbb{P}_2^N(x, p) &= 2H(x, p), \\ \mathbb{P}_3^N(x, p) &= \frac{x}{4\pi} - H(x, p),\end{aligned}\tag{3.111}$$

where the auxiliary function  $H(x, p)$  is defined by

$$\begin{aligned}H(x, p) &= -\frac{i}{\sqrt{2\pi}} e^{-p/16} \frac{\vartheta_1(ip/8, e^{-p/2})\vartheta_3(ip/8, e^{-p/2})}{\vartheta_1'(0, e^{-p/2})\vartheta_3(0, e^{-p/2})} \\ &\times \sum_{n \in \mathbb{Z}} \frac{\sin[(n + \frac{1}{4})x]}{(n + \frac{1}{4}) \sinh[(n + \frac{1}{4})p]}.\end{aligned}\tag{3.112}$$

In the limit of large and thin strips, we find respectively for  $0 \leq x \leq 2\pi$ :

$$H(x, p) \simeq \frac{2\sqrt{2}}{\pi} \sin(x/4) e^{-3p/16},\tag{3.113}$$

$$H(x, p) \simeq \frac{x}{4\pi} - \frac{p}{2\pi^2} e^{-\pi(2\pi-x)/p}.\tag{3.114}$$

An illustration of winding probabilities on the Möbius strip with Neumann boundary conditions is provided in Fig. 3.11.

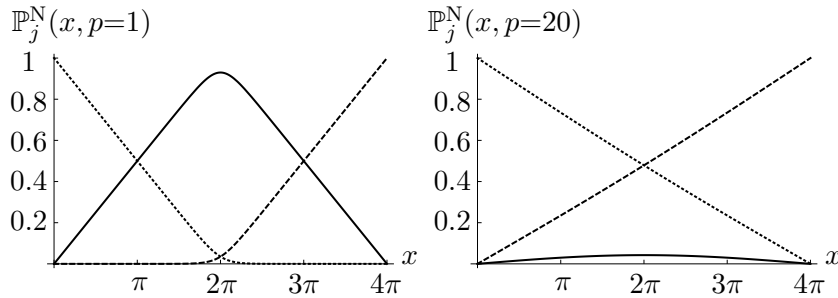


Figure 3.11: Winding probabilities of a random simple path from  $u_1 = (x_1, 0)$  to  $u_2 = (x_2, 0)$  on a Möbius strip with Neumann boundary conditions, as functions of the separation  $x = x_2 - x_1$ . The probabilities for the three winding classes ( $1 \leq j \leq 3$ ) are drawn with a dotted, solid, and dashed line, respectively.

### Asymptotics

For both types of boundary conditions, Dirichlet or Neumann, we have computed the winding probabilities in the limit of very large ( $p \rightarrow \infty$ ) or very thin ( $p \rightarrow 0^+$ ) strips. In the former case, we find that  $\mathbb{P}_2(x, p) \rightarrow 0$  as  $p \rightarrow \infty$ , for  $0 < x < 4\pi$ . The intuitive interpretation is the following: all paths in the second class must cross the strip along its width  $p$ , whereas the paths in the first and third classes do not. As there are many more (typically shorter) paths in the first and third classes than in the second one, the winding probability  $\mathbb{P}_2$  is suppressed in the limit  $p \rightarrow \infty$ . The two remaining probabilities can then be thought of as counterclockwise (class 1) and clockwise (class 3) probabilities. Indeed, we find precisely the same formulas for the Möbius strip and for the cylinder (see Eqs. (3.49) and (3.59)), up to the rescaling  $x \rightarrow 2x$  (for both boundary conditions):

$$\begin{aligned} \mathbb{P}_1^D(x, \infty) &= 1 - \frac{x/2 - \sin(x/2)}{2\pi}, & \mathbb{P}_3^D(x, \infty) &= 1 - \mathbb{P}_1^D(x, \infty), \\ \mathbb{P}_1^N(x, \infty) &= 1 - \frac{x/2}{2\pi}, & \mathbb{P}_3^N(x, \infty) &= 1 - \mathbb{P}_1^N(x, \infty). \end{aligned} \quad (3.115)$$

In the limit of thin strips  $p \rightarrow 0^+$ , we argue once again that shorter paths are favored over longer ones, which implies in particular that  $\mathbb{P}_1(x, 0) = 0$  for  $0 < x < 2\pi$  and  $\mathbb{P}_3(x, 0) = 0$  for  $2\pi < x < 4\pi$ . All winding probabilities converge to the same functions as on the cylinder, namely Heaviside functions (resp. piecewise linear functions) for Dirichlet (resp. Neumann) boundary conditions.

### 3.3 Passage probabilities for multiple paths

In Section 3.1, we have defined a measure on simple paths in spanning forests, extended it to oriented cycle-rooted groves, and computed the marginal probability associated with the left- or right-passage of a random path with respect to a marked face of a graph  $\mathcal{G}$  embedded on an orientable surface, i.e. Schramm's formula. The resulting probability (3.19) is expressed in terms of the standard Green function of the graph, whose explicit expression is well known for regular graphs such as the upper half-plane or the cylinder, considered in Section 3.2.

Let us now generalize this formula to multiple nonintersecting simple paths between  $2n$  nodes located on the boundary of the outer face of a planar graph  $\mathcal{G}$  (not including the root  $s$ , whose only role here is to enforce wired boundary conditions at some of the boundary vertices). We denote the collection of these special vertices by  $\mathcal{N} = \{u_1, \dots, u_{2n}\}$  or simply  $\{1, \dots, 2n\}$ , and label them in counterclockwise order. Let  $\sigma = r_1 s_1 | \dots | r_n s_n$  be a fixed (unoriented) pairing of the nodes, with  $R = \{r_1, \dots, r_n\}$  and  $S = \{s_1, \dots, s_n\}$  partitioning  $\mathcal{N}$ . We consider the set of all spanning forests on  $\mathcal{G}_s = \mathcal{G} \cup \{s\}$  consisting in  $n+1$  trees, each of which containing a single pair of nodes  $\{r_i, s_i\}$  or the root  $s$  (note that some pairings cannot be realized due to the planarity of  $\mathcal{G}$ ). The measure (3.2) on single paths in two-component spanning forests generalizes naturally to multiple unoriented paths  $\gamma_i : r_i \leftrightarrow s_i$ ,  $1 \leq i \leq n$ , in  $(n+1)$ -component spanning forests as follows:

$$\begin{aligned} \text{w}_{\text{SF}}(\gamma_1, \dots, \gamma_n) &= \sum_{(n+1)\text{SFs } \mathcal{F} \supset \bigcup_i \gamma_i} \text{w}(\mathcal{F}) \\ &= \prod_{i=1}^n C(\gamma_i) \times \det \Delta^{(\gamma_1, \dots, \gamma_n)}, \end{aligned} \quad (3.116)$$

where  $\Delta^{(\gamma_1, \dots, \gamma_n)}$  is the restriction of the standard Laplacian to rows and columns indexed by vertices not in  $\bigcup_i \gamma_i \cup \{s\}$ . Similarly, the weight on multiple oriented paths  $\gamma_i : r_i \rightarrow s_i$  in oriented cycle-rooted groves, defined in (3.6) for a single path, is given by

$$\begin{aligned} \text{w}_{\text{CRG}}(\gamma_1, \dots, \gamma_n) &= \sum_{\text{OCRGs } \Gamma_{\vec{\sigma}} \supset \bigcup_i \gamma_i} \text{w}(\Gamma_{\vec{\sigma}}) \\ &= \prod_{i=1}^n C(\gamma_i) \phi(\gamma_i)^{-1} \times \det \Delta^{(\gamma_1, \dots, \gamma_n)}, \end{aligned} \quad (3.117)$$

where  $\vec{\sigma} = \begin{smallmatrix} s_1 \\ r_1 \end{smallmatrix} | \dots | \begin{smallmatrix} s_n \\ r_n \end{smallmatrix}$  and  $\Delta$  is the line bundle Laplacian of  $\mathcal{G}_s$  with Dirichlet boundary conditions at  $s$ . Here the sum is over oriented cycle-rooted groves consisting in  $n+1$  trees and any number of cycle-rooted trees (the latter do not contain any nodes).

Let  $f$  be a face of the graph  $\mathcal{G}$  and  $\vec{\sigma}$  be an oriented pairing of the  $2n$  nodes. The OCRGs  $\Gamma_{\vec{\sigma}}$  can be sorted into  $n+1$  *winding classes*, according to the way the  $n$  paths wind around the face  $f$  (i.e. if they leave  $f$  to their right or to their left). As a matter of convention, we

shall assume all paths to be oriented toward the node with the highest label in each pair when we refer to the oriented pairing  $\vec{\sigma}$ , and call this the canonical orientation. To distinguish between the different winding classes, we introduce a zipper as in Section 3.1.2, going from  $f$  to the outer face of  $\mathcal{G}$  and intercepting the boundary path between nodes  $u_{2n}$  and  $u_1$ . As can be seen for the case  $n = 3$  illustrated in Fig. 3.12, two complications arise when considering multiple paths (as opposed to single paths):

- (i)  $n$ -tuples of paths belonging to distinct winding classes may have the same product of parallel transports  $\prod_{i=1}^n \phi(\gamma_i)$  (which is constant over each class, as for the case  $n = 1$ ). For instance, triplets of paths in the second and third classes of Fig. 3.12 are weighted by a global factor  $\phi_{1 \rightarrow 4} \phi_{2 \rightarrow 3} \phi_{5 \rightarrow 6} = z^{-1}$  in both cases.
- (ii) For a generic oriented pairing  $\vec{\sigma}$ , Theorem 1.5 does not yield the partition function  $\mathbf{Z}[\vec{\sigma}]$  directly. Instead, it only allows one to write a system of linear equations relating partition functions for distinct pairings to minors of the line bundle Green function, which is computable for most regular graphs (perturbatively around  $\Phi = \mathbb{I}$ , at least).

Due to these obstacles, writing an explicit form for Schramm's formulas for multiple paths in terms of the Green function proves to be substantially more complicated than for a single path. In what follows, we first discuss the easiest case, namely pairs of paths, using the same formalism as in Section 3.1.2, and give explicit formulas for the three distinct winding probabilities in terms of the Green function  $G$  and its derivative  $G'$ , defined in (1.28). As we shall see, obtaining such formulas a la Schramm is already cumbersome for only two paths, so a more systematic, combinatorial approach is required for  $n > 2$  paths. Such a technique will be provided in Section 3.3.2, and relies on so-called *cyclic Dyck paths* and *cover-inclusive Dyck tilings*, introduced respectively in [91] and [90, 148].

### 3.3.1 Two paths

Let us first compute Schramm's formulas for two paths between four boundary nodes, denoted by  $\mathcal{N} = \{u_1, u_2, u_3, u_4\} \equiv \{1, 2, 3, 4\}$ , with respect to a given face  $f$ . There are two ways to connect these nodes in

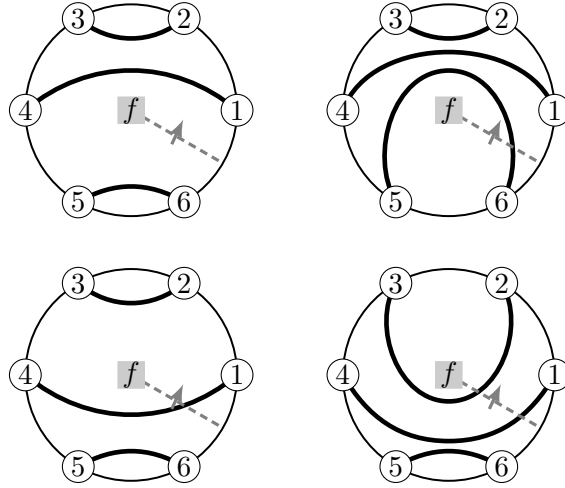


Figure 3.12: Schematic representation of the four distinct winding classes for triplets of paths corresponding to the pairing  $\vec{\sigma} = \begin{smallmatrix} 4 & 3 & 6 \\ 1 & 2 & 5 \end{smallmatrix}$ . The zipper is drawn as the dashed line from the marked face  $f$  to the outer boundary. The oriented edges crossed by the zipper have a parallel transport  $z$  in the direction of the arrow, and  $z^{-1}$  in the opposite direction.

pairs by nonintersecting paths in OCRGs, corresponding to the partitions  $12|34$  and  $14|23$ . The paths are further divided into three winding classes according to whether they leave  $f$  to their left or to their right (recall that the paths are oriented toward the node with the higher index in each pair). We denote the partition functions associated with each of the six subclasses as follows:

$$\mathbf{Z}_{LL} \left[ \begin{smallmatrix} 2 & 4 \\ 1 & 3 \end{smallmatrix} \right], \mathbf{Z}_{LR} \left[ \begin{smallmatrix} 2 & 4 \\ 1 & 3 \end{smallmatrix} \right], \mathbf{Z}_{RL} \left[ \begin{smallmatrix} 2 & 4 \\ 1 & 3 \end{smallmatrix} \right], \mathbf{Z}_{LL} \left[ \begin{smallmatrix} 4 & 3 \\ 1 & 2 \end{smallmatrix} \right], \mathbf{Z}_{RL} \left[ \begin{smallmatrix} 4 & 3 \\ 1 & 2 \end{smallmatrix} \right], \mathbf{Z}_{RR} \left[ \begin{smallmatrix} 4 & 3 \\ 1 & 2 \end{smallmatrix} \right],$$

where the indices refer to the left- or right-passage of the first and second paths with respect to  $f$ , respectively (some pairs of indices are not realizable on a planar graph, e.g. paths in the pairing  $12|34$  cannot both leave  $f$  to their right). We give an illustration of these six classes in Fig. 3.13.

The number of winding classes for pairs of paths corresponds exactly to the number of partitions of  $\mathcal{N} = \{u_1, u_2, u_3, u_4\}$  into two disjoint subsets of order two,  $R$  and  $S = \mathcal{N} \setminus R$ , that we can select in Theorem 1.5. For

instance, if  $R = \{2, 4\}$  and  $S = \{1, 3\}$ , the theorem reads

$$\begin{aligned} \det \Delta \det \mathbf{G}_{2,4}^{1,3} &= \mathbf{Z}_{[2|4]}^1 - \mathbf{Z}_{[2|4]}^3 \\ &= (\mathbf{Z}_{\text{LL}}[2|4]^1 + \mathbf{Z}_{\text{LR}}[2|4]^1 + \mathbf{Z}_{\text{RL}}[2|4]^1) \\ &\quad - (\mathbf{Z}_{\text{LL}}[2|4]^3 + \mathbf{Z}_{\text{RL}}[2|4]^3 + \mathbf{Z}_{\text{RR}}[2|4]^3), \end{aligned} \quad (3.118)$$

where the indices refer to the left- or right-passage with respect to  $f$  for paths with the canonical orientation (from the lower to the higher node index). As the product of parallel transports along the paths between the nodes is constant over each class separately, we may rewrite the preceding equation in terms of partition functions for paths with the canonical orientation:

$$\begin{aligned} \det \Delta \det \mathbf{G}_{2,4}^{1,3} &= \mathbf{Z}_{\text{LL}}[1|3]^2 + z^{-2} \mathbf{Z}_{\text{LR}}[1|3]^2 + z^{-2} \mathbf{Z}_{\text{RL}}[1|3]^2 \\ &\quad - \mathbf{Z}_{\text{LL}}[1|2]^4 - z^{-2} \mathbf{Z}_{\text{RL}}[1|2]^4 - z^{-2} \mathbf{Z}_{\text{RR}}[1|2]^4. \end{aligned} \quad (3.119)$$

Anticipating the general discussion for  $n > 2$  paths, we shall rather use another choice of orientation, which consists in taking the canonical orientation on paths that do not cross the zipper (L paths), and the reverse on paths that do (R paths). We shall explain the motivation behind this convention in Section 3.3.2. With respect to this new orientation, one finds the equation

$$\begin{aligned} \det \Delta \det \mathbf{G}_{2,4}^{1,3} &= \mathbf{Z}_{\text{LL}}[1|3]^2 + \mathbf{Z}_{\text{LR}}[1|4]^2 + \mathbf{Z}_{\text{RL}}[2|3]^1 \\ &\quad - \mathbf{Z}_{\text{LL}}[1|2]^4 - \mathbf{Z}_{\text{RL}}[4|2]^3 - z^2 \mathbf{Z}_{\text{RR}}[4|3]^1 \end{aligned} \quad (3.120)$$

for  $R = \{2, 4\}$  and  $S = \{1, 3\}$ . Doing so for the five other subsets  $R \subset \mathcal{N}$  of order two yields a system of equations represented by a matrix  $\mathbf{A}_2$  given by

$$\begin{array}{l} \mathbf{Z}_{\text{LL}}[1|3]^2 \\ \mathbf{Z}_{\text{LR}}[1|4]^2 \\ \mathbf{Z}_{\text{RL}}[2|3]^1 \\ \mathbf{Z}_{\text{LL}}[4|2]^3 \\ \mathbf{Z}_{\text{RL}}[1|4]^3 \\ \mathbf{Z}_{\text{RR}}[4|3]^1 \end{array} \begin{pmatrix} \det \Delta \det \mathbf{G}_{1,2}^{3,4} & 0 & 0 & 0 & -1 & -w & -w^2 \\ \det \Delta \det \mathbf{G}_{1,3}^{2,4} & 1 & w & w & -1 & -w & -w \\ \det \Delta \det \mathbf{G}_{1,4}^{2,3} & 1 & 1 & w & 0 & 0 & 0 \\ \det \Delta \det \mathbf{G}_{2,3}^{1,4} & 1 & w & 1 & 0 & 0 & 0 \\ \det \Delta \det \mathbf{G}_{2,4}^{1,3} & 1 & 1 & 1 & -1 & -1 & -w \\ \det \Delta \det \mathbf{G}_{3,4}^{1,2} & 0 & 0 & 0 & -1 & -1 & -1 \end{pmatrix},$$

where  $w \equiv z^2$ .  $\mathbf{A}_2$  is invertible for  $z \neq \pm 1$ , as its determinant is equal to  $(1-w)^5$ . Explicitly, one obtains the inverse

$$\mathbf{A}_2^{-1} = \frac{1}{(1-w)^2} \begin{pmatrix} -(1+w) & 1+w & -2w & -2w & w+w^2 & -(w+w^2) \\ 1 & -1 & 1 & w & -w & w \\ 1 & -1 & w & 1 & -w & w \\ -1 & w & -w & -w & w & -w^2 \\ 2 & -(1+w) & 1+w & 1+w & -(1+w) & 2w \\ -1 & 1 & -1 & -1 & 1 & -1 \end{pmatrix}, \quad (3.121)$$

from which the partition functions of interest can be extracted. For example, we have

$$\begin{aligned} Z_{\text{LR}}[12|34] &= \lim_{z \rightarrow 1} \mathbf{Z}_{\text{LR}} \begin{bmatrix} 2 & 3 \\ 1 & 4 \end{bmatrix} \\ &= \lim_{z \rightarrow 1} \frac{\det \Delta}{(1-z^2)^2} \left\{ \det \mathbf{G}_{1,2}^{3,4} - \det \mathbf{G}_{1,3}^{2,4} + \det \mathbf{G}_{1,4}^{2,3} \right. \\ &\quad \left. + z^2 \det \mathbf{G}_{2,3}^{1,4} - z^2 \det \mathbf{G}_{2,4}^{1,3} + z^2 \det \mathbf{G}_{3,4}^{1,2} \right\} \quad (3.122) \\ &= \det \Delta \{ G_{1,2} G'_{3,4} - G_{1,3} G'_{2,4} + G_{1,4} G'_{2,3} \\ &\quad - G'_{1,2} G'_{3,4} + G'_{1,3} G'_{2,4} - G'_{1,4} G'_{2,3} \}, \end{aligned}$$

where  $G'$  is the derivative of the Green function defined in (1.28). The total partition function  $Z[12|34]$  can be obtained by summing the partition functions for all winding classes LL, LR, RL of the pairing 12|34, or computed directly from Theorem 1.2, which yields

$$Z[12|34] = \det \Delta \det G_{1,4}^{2,3} = \det \Delta \{ G_{1,2} G_{3,4} - G_{1,3} G_{2,4} \}, \quad (3.123)$$

as the pairing 13|24 cannot be realized on a planar graph, implying  $Z[13|24] = 0$ . After some algebra, one finds that the probability that a pair of paths in 12|34 belongs in each of three winding classes reads

$$\begin{aligned} \mathbb{P}_{\text{LL}}(12|34) &= 1 - \mathbb{P}_{\text{LR}}(12|34) - \mathbb{P}_{\text{RL}}(12|34), \\ \mathbb{P}_{\text{LR}}(12|34) &= \frac{G_{1,2} G'_{3,4} - G_{1,3} G'_{2,4} + G_{1,4} G'_{2,3}}{G_{1,2} G_{3,4} - G_{1,3} G_{2,4}} \\ &\quad + \frac{-G'_{1,2} G'_{3,4} + G'_{1,3} G'_{2,4} - G'_{1,4} G'_{2,3}}{G_{1,2} G_{3,4} - G_{1,3} G_{2,4}}, \quad (3.124) \\ \mathbb{P}_{\text{RL}}(12|34) &= \frac{G_{1,4} G'_{2,3} - G_{2,4} G'_{1,3} + G_{3,4} G'_{1,2}}{G_{1,2} G_{3,4} - G_{1,3} G_{2,4}} \\ &\quad + \frac{-G'_{1,2} G'_{3,4} + G'_{1,3} G'_{2,4} - G'_{1,4} G'_{2,3}}{G_{1,2} G_{3,4} - G_{1,3} G_{2,4}}. \end{aligned}$$

The probabilities for the classes of paths in 14|23, on the other hand, are given by

$$\begin{aligned}
 \mathbb{P}_{LL}(14|23) &= 1 - \mathbb{P}_{RL}(14|23) - \mathbb{P}_{RR}(14|23), \\
 \mathbb{P}_{RL}(14|23) &= \frac{G_{1,3} G'_{2,4} + G'_{1,3} G_{2,4} - G_{1,4} G'_{2,3} - G'_{1,4} G_{2,3}}{G_{1,3} G_{2,4} - G_{1,4} G_{2,3}} - 2\mathbb{P}_{RR}(14|23), \\
 \mathbb{P}_{RR}(14|23) &= \frac{-G'_{1,2} G'_{3,4} + G'_{1,3} G'_{2,4} - G'_{1,4} G'_{2,3}}{G_{1,3} G_{2,4} - G_{1,4} G_{2,3}}.
 \end{aligned}
 \tag{3.125}$$

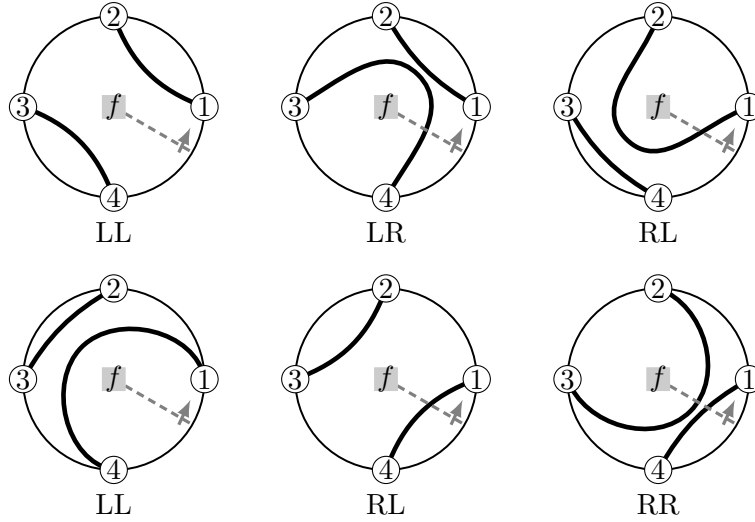


Figure 3.13: Illustration of the six different ways two paths between four nodes can wind around a marked face  $f$ . In the first (resp. second) row, the nodes are paired according to 12|34 (resp. 14|23). The indices L, R indicate whether the first and second paths leave  $f$  to their left or right (for the canonical orientation). The dashed gray line represents the zipper, whose arrow indicates the orientation of the edges with parallel transport  $z$ .

### 3.3.2 More than two paths

Let us now compute the winding probabilities for  $n > 2$  paths between  $2n$  fixed boundary vertices in the same manner as for two paths using Theorem 1.5. To do so, we define a correspondence between winding

classes and combinatorial objects called *cyclic Dyck paths* [91], and give an explicit expression of the matrix  $\mathbf{A}_n$  provided by Theorem 1.5 as well as its inverse  $\mathbf{A}_n^{-1}$ . This will in turn allow us to write a combinatorial expression for winding partition functions of spanning forests, from which Schramm's formulas follow.

Let us first recall the definition of a standard<sup>3</sup> Dyck path of length  $2n$ . It is a lattice path going from  $(0, 0)$  to  $(2n, 0)$  consisting in *up* steps  $(1, 1)$  and *down* steps  $(1, -1)$  that never passes below the  $x$  axis (such a path must therefore have an equal number of up and down steps). Equivalently, a Dyck path can be seen as a collection of heights  $h_i \in \mathbb{N}$ ,  $0 \leq i \leq 2n$ , with  $|h_i - h_{i-1}| = 1$  and  $h_0 = h_{2n} = 0$ ; an up (resp. down) step at position  $i$  corresponding to a pair of adjacent heights  $(h_{i-1}, h_i)$  such that  $h_i - h_{i-1} = +1$  (resp.  $-1$ ). In such a path, drawn as a mountain range as in Fig. 3.14, each up step is paired with the closest down step to its right located at the same height; the pair being called a *chord*. A third characterization of a Dyck path is given by the oriented pairing of the elements in  $\mathcal{N} = \{1, 2, \dots, 2n\}$  according to the chords below the path (from the up to the down step). The bijection between standard Dyck paths of length  $2n$  and planar pairings of  $2n$  nodes is well known (see e.g. [154]): each chord of a standard Dyck path pairs two labeled steps, thus defining a natural planar pairing of the nodes. This one-to-one correspondence has been used in particular to give a formula for all partition functions  $Z[\sigma]$  of  $(n+1)$ -component spanning forests in terms of the Green function of the graph, where  $\sigma$  is a planar pairing of boundary vertices [90] (see also Corollary 3.6 below).

Since there are  $(n+1)$  times more winding classes than standard Dyck paths, it is clear that the latter do not suffice to take into account the position of paths with respect to the face  $f$  in each winding class. Following [91], we extend the definition of a Dyck path by allowing cyclic permutations of the labels associated with the steps, as well as of the labels of the heights (we choose as a convention the index 0 for the starting point of the step with the label 1). Such paths with numbered steps in cyclic order are called *cyclic Dyck paths*<sup>4</sup> (there are therefore

<sup>3</sup>We use the adjective “standard” for such Dyck paths to distinguish them from cyclic Dyck paths, which will be introduced below.

<sup>4</sup>This definition differs slightly from the one of [91], in that we do not consider paths with a single “flat” step  $(1, 0)$  here.

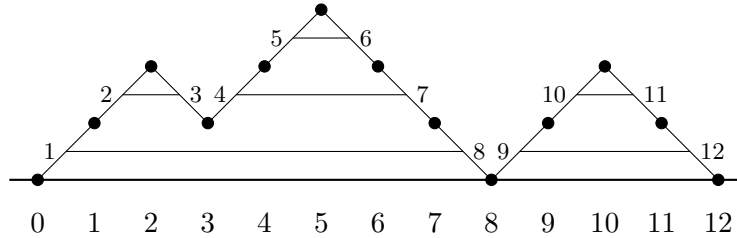


Figure 3.14: Standard Dyck path  $\sigma$  of length 12, which can be defined as a sequence of 6 up and 6 down steps, as a collection of 13 heights, or as a set of 6 chords:  $\sigma = \text{UUDUDDDUUDD} = \{0, 1, 2, 1, 2, 3, 2, 1, 0, 1, 2, 1, 0\} = \{(1, 8), (2, 3), (4, 7), (5, 6), (9, 12), (10, 11)\}$ .

$2n$  cyclic Dyck paths corresponding to a given mountain range). As a matter of notation, we shall denote such paths as vectors (e.g.  $\vec{\sigma}$ ), as opposed to standard Dyck paths, written as scalars (e.g.  $\sigma$ ).

Consider now a particular winding class of a pairing of  $\mathcal{N}$ , with  $k$  paths crossing the zipper. We choose the canonical orientation (from lower to higher node index) for the  $n-k$  paths that do not intersect the zipper, and the opposite for the  $k$  paths that do. We call this particular way of orienting paths a *cyclic orientation*. The resulting oriented pairing  $\vec{\sigma}$  corresponds to the chords of a cyclic Dyck path, whose first step is labeled by the lowest index among the starting points of these  $k$  paths. We provide an illustration of this correspondence in Fig. 3.15. It should be noted that it is not surjective, as certain cyclic Dyck paths cannot be obtained in this manner. Namely, those that include a down step touching the  $x$  axis to the left of the step with the label 1. Such paths are however equivalent to obtainable ones up to cyclic permutations of mountaintops together with their step and height labels (an example is given in the bottom panel of Fig. 3.15).

The main benefit of choosing the cyclic orientation over the canonical one is notational. Indeed, the way the paths of a winding class wind around the face  $f$  is directly encoded in a cyclic Dyck path  $\vec{\sigma}$  (or equivalently, in a cyclically oriented pairing  $\vec{\sigma}$ ). The corresponding winding partition functions in spanning forests and OCRGs will be denoted from now on by  $Z[\vec{\sigma}]$  and  $\mathbf{Z}[\vec{\sigma}]$ , respectively (dropping the cumbersome sub-

scripts L, R used in Sections 3.1.2 and 3.3.1). In doing so, however, one finds a conflict of notation for standard Dyck paths  $\sigma$ , which correspond to winding classes in which no path crosses the zipper. Indeed, the notation  $Z[\sigma]$  has until now been reserved for the total partition function of spanning forests in which the nodes are paired according to the unoriented pairing  $\sigma$ . To avoid any confusion in what follows, we shall denote from now on the winding partition function and the total partition by  $Z[\sigma]$  and  $Z_t[\sigma]$ , respectively.

Before we use this correspondence between winding classes and cyclic Dyck paths, let us introduce several definitions and notations associated with cyclic Dyck paths, some of which were given in [91]:

**Definition 3.1.** *Let  $\vec{\sigma}, \vec{\tau}$  be two cyclic Dyck paths of length  $2n$ , and  $R \subset \mathcal{N} = \{1, 2, \dots, 2n\}$  a subset of indices of order  $n$ . Then*

- $\mathcal{A}(\vec{\sigma}) = \sum_{i=0}^{2n} h_i(\vec{\sigma})$  denotes the area between  $\vec{\sigma}$  and the  $x$  axis, where the  $h_i$ 's are the heights of  $\vec{\sigma}$ .
- $W(\vec{\sigma}) = h_0(\vec{\sigma})$  is the number of chords of  $\vec{\sigma}$  for which the index of the up step is higher than the one of the down step (in which case the chord is said to be wrapped).
- $R \cap \vec{\sigma}$  means that  $R$  intersects each chord of  $\vec{\sigma}$  exactly once, that is,  $R$  contains the index of one of the two steps belonging to each chord.
- $R \cdot \vec{\sigma}$  stands for the number of up steps of  $\vec{\sigma}$  whose indices lie in  $R$ .
- $R : \vec{\sigma}$  is the number of up steps of  $\vec{\sigma}$  with indices in  $R$  that belong to wrapped chords.
- $R|\vec{\sigma}_{\ell(1)}$  counts the steps of  $\vec{\sigma}$  that appear to the left of the step 1 (excluded) and whose indices appear in  $R$ .
- $U^{\vec{\sigma}}$  (resp.  $D^{\vec{\sigma}}$ ) denotes the set of up (resp. down) steps of  $\vec{\sigma}$ .
- $U_{r(1)}^{\vec{\sigma}}$  is the set of up steps of  $\vec{\sigma}$  that appear to the right of the step 1 (included).

- $D_{\ell(1)}^{\vec{\sigma}}$  denotes the set of down steps of  $\vec{\sigma}$  that appear to the left of the step 1 (excluded).
- $D_{\ell(1,\vec{\sigma})}^{\vec{\tau}}$  is the set of down steps of  $\vec{\tau}$  whose indices appear to the left of the step 1 in  $\vec{\sigma}$  (excluded).

As an example, let us consider the cyclic Dyck path illustrated in the top right panel of Fig. 3.15, given by  $\vec{\sigma} = \{(5, 2), (6, 7), (8, 1), (3, 4)\} = \{2, 1, 0, 1, 0, 0, 1, 2, 1\}$ , which yields  $W(\vec{\sigma}) = 2$  (due to the chords  $(5, 2)$  and  $(8, 1)$ ). If  $R = \{1, 4, 5, 6\}$ , then  $R \cap \vec{\sigma}, R \cdot \vec{\sigma} = |\{5, 6\}| = 2, R : \vec{\sigma} = |\{5\}| = 1$  and  $R|\vec{\sigma}_{\ell(1)} = |\{5, 6\}| = 2$ .

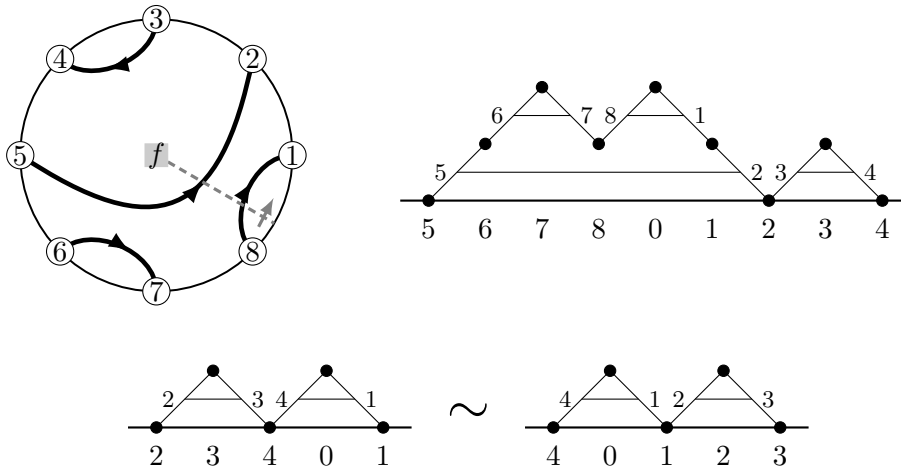


Figure 3.15: On the top left is a schematic representation of a winding class of quadruples of paths in spanning forests. The paths  $5 \rightarrow 2$  and  $8 \rightarrow 1$  cross the zipper, and are therefore oriented from the higher to the lower index, as opposed to the paths  $3 \rightarrow 4$  and  $6 \rightarrow 7$ . On the top right is the corresponding cyclic Dyck path, whose first step label is  $\min\{5, 8\} = 5$ . At the bottom lies a cyclic Dyck path that cannot be realized as a winding class of paths. The path obtained by cyclically rotating its two mountaintops, however, corresponds to the winding class RL of the pairing  $14|23$ , pictured in Fig. 3.13.

Let us now show how to write linear relations between winding partition functions using Theorem 1.5. There are  $C_n = \frac{1}{n+1} \binom{2n}{n}$  planar pairings of  $2n$  nodes on the boundary of a planar graph, each of which containing  $n+1$  winding classes of paths with respect to the marked face  $f$ ; thus

yielding a total of  $\binom{2n}{n}$  winding classes, and as many inequivalent cyclic Dyck paths. As there are as many distinct subsets  $R \subset \mathcal{N}$  of order  $n$ , the linear equations provided by Theorem 1.5 relating winding partition functions to minors of the line bundle Green function  $\mathbf{G}$  can be encoded in the square matrix  $\mathbf{A}_n$  defined by

$$\det \Delta \det \mathbf{G}_R^S = \sum_{\vec{\sigma}} (\mathbf{A}_n)_{R, \vec{\sigma}} \mathbf{Z}[\vec{\sigma}], \quad (3.126)$$

where the sum is over all cyclic Dyck paths of length  $2n$ . The entries of this matrix are given by

**Proposition 3.2.** *Let  $\vec{\sigma}$  be a pairing of  $2n$  nodes with the cyclic orientation along each path, seen as a cyclic Dyck path of length  $2n$ . Let  $R \subset \mathcal{N} = \{1, 2, \dots, 2n\}$  with  $|R| = n$ . If we define the new variable  $w \equiv z^2$ , then*

$$(\mathbf{A}_n)_{R, \vec{\sigma}} = \begin{cases} (-1)^{\frac{1}{2}(\mathcal{A}(\vec{\sigma})-n)+(n+1)W(\vec{\sigma})} w^{W(\vec{\sigma})-R:\vec{\sigma}} & \text{if } R \cap \vec{\sigma}, \\ 0 & \text{if } R \not\cap \vec{\sigma}. \end{cases} \quad (3.127)$$

As an example, consider for instance the cyclic Dyck path depicted in the top right panel of Fig. 3.15,  $\vec{\sigma} = \{(5, 2), (6, 7), (8, 1), (3, 4)\}$ , and the subset of indices  $R = \{1, 4, 5, 6\}$ . As explained above,  $R$  contains a index of each chord of  $\vec{\sigma}$  (i.e.  $R \cap \vec{\sigma}$ ), and  $W(\vec{\sigma}) = 2$ ,  $R : \vec{\sigma} = 1$ . Moreover the area between  $\vec{\sigma}$  and the horizontal axis is  $\mathcal{A}(\vec{\sigma}) = 8$ , so

$$(\mathbf{A}_4)_{R, \vec{\sigma}} = (-1)^{\frac{1}{2}(8-4)+(4+1)2} w^{2-1} = w. \quad (3.128)$$

The proof of Proposition 3.2 is a bit technical, and is left to Appendix D. A similar matrix was considered in [91], in which all but one node are located around a single marked face, the remaining one lying on the boundary of the outer face. The authors gave a formula for the inverse in terms of combinatorial objects called *cover-inclusive Dyck tilings*, introduced in [90, 148]. We recall their definition here, as they shall be needed to write the inverse of  $\mathbf{A}_n$ .

A *Dyck tile* is obtained from a Dyck path by replacing each vertex of the path with a  $\sqrt{2} \times \sqrt{2}$  square rotated by  $45^\circ$ , and by gluing all the squares together to form a single ribbon (see for instance the first two

panels at the top of Fig. 3.16). In particular, the simplest Dyck tile is a single square, associated with the degenerate Dyck path of length zero.

Let  $\vec{\mu}, \vec{\sigma}$  be two cyclic Dyck paths of length  $2n$  with the same positions of indices, and let  $h_i(\vec{\mu}), h_i(\vec{\sigma})$  be the heights of their vertices. The cyclic Dyck path  $\vec{\mu}$  is said to dominate  $\vec{\sigma}$  if  $h_i(\vec{\mu}) \geq h_i(\vec{\sigma})$  for  $0 \leq i \leq 2n$ ; which is denoted by  $\vec{\mu} \geq \vec{\sigma}$ . A *Dyck tiling* of the shape  $\vec{\sigma}/\vec{\mu}$  between two paths  $\vec{\mu}, \vec{\sigma}$  such that  $\vec{\mu} \geq \vec{\sigma}$  is then obtained by filling the surface between  $\vec{\mu}$  and  $\vec{\sigma}$  with Dyck tiles. Furthermore, a Dyck tiling is said to be *cover-inclusive* if, for any two tiles right above one another, the top one does not stick out horizontally with respect to the bottom one. We illustrate all cover-inclusive Dyck tilings of a given shape in the bottom panel of Fig. 3.16.

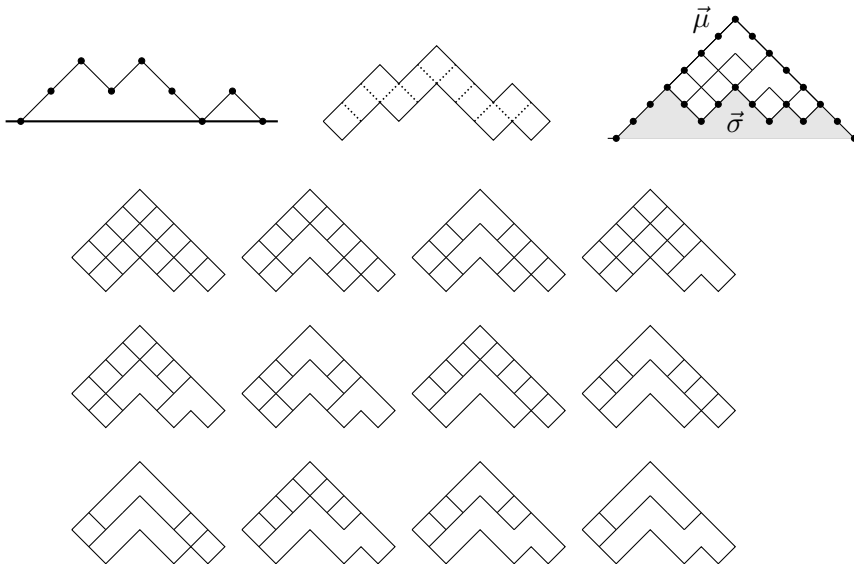


Figure 3.16: On the left is a Dyck path, together with the associated Dyck tile (in the middle). On the right is a Dyck tiling of the shape  $\vec{\sigma}/\vec{\mu}$  between the paths  $\vec{\mu}$  and  $\vec{\sigma}$ , which is *not* cover-inclusive (the two L shapes both cover a single square). At the bottom lie all cover-inclusive Dyck tilings of  $\vec{\sigma}/\vec{\mu}$ .

Let us now give a formula for the inverse of the matrix  $\mathbf{A}_n$  defined in Proposition 3.2. In terms of the quantities introduced in Definition 3.1, we have

**Proposition 3.3.** *Let  $\mathbf{B}_n$  be the square matrix defined by*

$$(\mathbf{B}_n)_{\vec{\sigma}, R} = (-1)^{\Sigma R + W(\vec{\sigma}) + n} \sum_{\vec{\mu} \geq \vec{\sigma}} \text{ci}(\vec{\sigma}/\vec{\mu}) w^{n - W(\vec{\sigma}) - R \cdot \vec{\mu} + R|\vec{\sigma}_{\ell(1)} - |D_{\ell(1)}^{\vec{\sigma}}|}, \quad (3.129)$$

for all cyclic Dyck paths  $\vec{\sigma}$  of length  $2n$  and for all subsets  $R \subset \mathcal{N}$  of order  $n$ , where  $\text{ci}(\vec{\sigma}/\vec{\mu})$  denotes the number of cover-inclusive Dyck tilings of the shape between  $\vec{\mu}$  and  $\vec{\sigma}$ . Then for any two cyclic Dyck paths  $\vec{\sigma}, \vec{\tau}$  of length  $2n$

$$\sum_{R \subset \mathcal{N}: |R|=n} (\mathbf{B}_n)_{\vec{\sigma}, R} (\mathbf{A}_n)_{R, \vec{\tau}} = (1 - w)^n \delta_{\vec{\sigma}, \vec{\tau}}. \quad (3.130)$$

Again we refer to Appendix D for the proof. This proposition allows one to write winding partition functions for paths in OCRGs as

$$\mathbf{Z}[\vec{\sigma}] = \frac{\det \Delta}{(1 - w)^n} \sum_{R \subset \mathcal{N}: |R|=n} (\mathbf{B}_n)_{\vec{\sigma}, R} \det \mathbf{G}_R^S, \quad (3.131)$$

where  $S = \mathcal{N} \setminus R$  and  $\mathbf{G} = \Delta^{-1}$  is the line bundle Green function of the graph. Corresponding partition functions  $Z[\vec{\sigma}]$  for paths in spanning forests can be obtained by taking the limit  $z \rightarrow 1$  (or equivalently  $w \rightarrow 1$ ) of  $\mathbf{Z}[\vec{\sigma}]$ . The result is given by

**Theorem 3.4.** *Let  $\vec{\sigma}$  be a cyclic Dyck path of length  $2n$ . Then*

$$Z[\vec{\sigma}] = (-1)^{W(\vec{\sigma})} \det \Delta \sum_{\vec{\mu} \geq \vec{\sigma}} \text{ci}(\vec{\sigma}/\vec{\mu}) \text{pf} \mathcal{M}_{\vec{\mu}}, \quad (3.132)$$

where the matrix  $\mathcal{M}_{\vec{\mu}}$  is defined as follows for  $1 \leq i, j \leq 2n$ :

$$(\mathcal{M}_{\vec{\mu}})_{i,j} = -G'_{i,j} + G_{i,j} \left( \mathbf{1}_{i \in U_{r(1)}^{\vec{\mu}}} - \mathbf{1}_{i \in D_{\ell(1)}^{\vec{\mu}}} - \mathbf{1}_{j \in U_{r(1)}^{\vec{\mu}}} + \mathbf{1}_{j \in D_{\ell(1)}^{\vec{\mu}}} \right). \quad (3.133)$$

Here  $\mathbf{1}$  is the indicator function and  $U_{\ell, r(1)}^{\vec{\sigma}}, D_{\ell, r(1)}^{\vec{\sigma}}$  are given in Definition 3.1.

*Proof.* Taking the limit  $w \rightarrow 1$  of Eq. (3.131) leads to

$$\begin{aligned} Z[\vec{\sigma}] &= (-1)^{W(\vec{\sigma})} \det \Delta \sum_{\vec{\mu} \geq \vec{\sigma}} \text{ci}(\vec{\sigma}/\vec{\mu}) \lim_{w \rightarrow 1} \frac{w^{n - W(\vec{\sigma}) - |D_{\ell(1)}^{\vec{\sigma}}|}}{(1 - w)^n} \\ &\quad \times \sum_{\substack{R \subset \mathcal{N} \\ |R|=n}} (-1)^{n + \Sigma R} w^{-R \cdot \vec{\mu} + R|\vec{\sigma}_{\ell(1)}} \det \mathbf{G}_R^S, \end{aligned} \quad (3.134)$$

where we used the explicit expression of  $\mathbf{B}_n$  given by Proposition 3.3. The first sum is over cyclic Dyck paths  $\vec{\mu} \geq \vec{\sigma}$ , so  $R|\vec{\sigma}_{\ell(1)} = R|\vec{\mu}_{\ell(1)}$ , as the step indices of  $\vec{\mu}, \vec{\sigma}$  appear in the same order. Moreover

$$-R \cdot \vec{\mu} + R|\vec{\mu}_{\ell(1)} = \left| R \cap D_{\ell(1)}^{\vec{\mu}} \right| - \left| R \cap U_{r(1)}^{\vec{\mu}} \right|, \quad (3.135)$$

since  $R \cdot \vec{\mu}$  counts the up steps of  $\vec{\mu}$  in  $R$  and  $R|\vec{\mu}_{\ell(1)}$  the steps of  $\vec{\mu}$  to the left of the step 1 that belong to  $R$ . Substituting this relation in Eq. (3.134) allows one to compute the sum over  $R$  via the following

**Lemma 3.5** ([123]). *For any matrix  $A$  of order  $2n$  and any two subsets  $X, Y \subset \mathcal{N}$  with  $X \cap Y = \emptyset$ ,*

$$\sum_{\substack{R \subset \mathcal{N} \\ |R|=n}} (-1)^{n+\Sigma R} x^{2(|R \cap X| - |R \cap Y|)} \det A_R^S = x^{|X| - |Y|} \text{pf} \left( \tilde{A} - \tilde{A}^t \right), \quad (3.136)$$

where  $S = \mathcal{N} \setminus R$  and  $R$  are both ordered, and the matrix  $\tilde{A}$  is defined as follows:

$$\tilde{A}_{i,j} = A_{i,j} x^{\mathbf{1}_{i \in X} + \mathbf{1}_{j \in Y} - \mathbf{1}_{i \in Y} - \mathbf{1}_{j \in X}}. \quad (3.137)$$

Picking  $A = \mathbf{G}$ ,  $w = x^{1/2}$ ,  $X = D_{\ell(1)}^{\vec{\mu}}$  and  $Y = U_{r(1)}^{\vec{\mu}}$  in the lemma allows one to rewrite Eq. (3.134) as

$$\begin{aligned} Z[\vec{\sigma}] &= (-1)^{W(\vec{\sigma})} \det \Delta \sum_{\vec{\mu} \geq \vec{\sigma}} \text{ci}(\vec{\sigma}/\vec{\mu}) \lim_{w \rightarrow 1} w^{n - W(\vec{\sigma}) - |D_{\ell(1)}^{\vec{\sigma}}| + \frac{1}{2}|D_{\ell(1)}^{\vec{\mu}}| - \frac{1}{2}|U_{r(1)}^{\vec{\mu}}|} \\ &\quad \times \text{pf} \left( \frac{\tilde{\mathbf{G}} - \tilde{\mathbf{G}}^t}{1 - w} \right) \\ &= (-1)^{W(\vec{\sigma})} \det \Delta \sum_{\vec{\mu} \geq \vec{\sigma}} \text{ci}(\vec{\sigma}/\vec{\mu}) \lim_{w \rightarrow 1} \text{pf} \left( \frac{\tilde{\mathbf{G}} - \tilde{\mathbf{G}}^t}{1 - w} \right), \end{aligned} \quad (3.138)$$

where the derivative of the matrix  $\tilde{\mathbf{G}}$  reads

$$\begin{aligned} \partial_w \tilde{\mathbf{G}}_{i,j} \Big|_{w=1} &= \partial_w \mathbf{G}_{i,j} \Big|_{w=1} - \frac{1}{2} \mathbf{G}_{i,j} \Big|_{w=1} \\ &\quad \times \left\{ \mathbf{1}_{i \in U_{r(1)}^{\vec{\mu}}} - \mathbf{1}_{i \in D_{\ell(1)}^{\vec{\mu}}} - \mathbf{1}_{j \in U_{r(1)}^{\vec{\mu}}} + \mathbf{1}_{j \in D_{\ell(1)}^{\vec{\mu}}} \right\} \\ &= -\frac{1}{2} (\mathcal{M}_{\vec{\mu}})_{i,j}. \end{aligned} \quad (3.139)$$

The result of the preceding equation relies on the definition of  $G, G'$  as the zeroth- and first-order derivative of the line bundle Green function  $\mathbf{G}$  evaluated at  $z = 1$ :

$$G = \lim_{z \rightarrow 1} \mathbf{G} = \lim_{w \rightarrow 1} \mathbf{G}, \quad G' = \lim_{z \rightarrow 1} \partial_z \mathbf{G} = \lim_{w \rightarrow 1} 2 \partial_w \mathbf{G} \quad (3.140)$$

for  $w = z^2$ . Similarly we find  $\partial_w \tilde{\mathbf{G}}_{i,j}^t|_{w=1} = \frac{1}{2} (\mathcal{M}_{\vec{\mu}})_{i,j}$ , which concludes the proof of Theorem 3.4.  $\square$

A particular case of Theorem 3.4 arises for cyclic Dyck paths  $\vec{\sigma}$  of length  $2n$  that correspond to a single mountaintop of maximal height  $n$  at its peak. Indeed, the sum over cyclic Dyck paths  $\vec{\mu}$  that dominate  $\vec{\sigma}$  includes only a single term, namely  $\vec{\mu} = \vec{\sigma}$ . Consequently the winding partition function  $Z[\vec{\sigma}]$  is given (up to a multiplicative constant) by a single Pfaffian,  $\text{pf} \mathcal{M}_{\vec{\sigma}}$ . Among such cyclic Dyck paths is the one defined by  $\vec{\sigma}_R = \{(2n, 1), (2n-1, 2), \dots, (n+1, n)\}$ , which corresponds to  $n$ -tuples of paths that all leave the marked face  $f$  to their right when canonically oriented (from lower to higher node index). It turns out that  $Z[\vec{\sigma}_R]$  has an exceptionally simple form, as all of its up steps appear to the left of the step 1. Indeed, this implies that  $U_{r(1)}^{\vec{\sigma}_R} = \emptyset = D_{\ell(1)}^{\vec{\sigma}_R}$ , so the matrix  $\mathcal{M}_{\vec{\sigma}_R}$  is equal to  $-G'|_{\mathcal{N}}$ , and  $W(\vec{\sigma}_R) = n$  (all chords have an up step with a higher index than the corresponding down step). The theorem therefore yields

$$Z[\vec{\sigma}_R] = \det \Delta \times \text{pf} (G'|_{\mathcal{N}}). \quad (3.141)$$

As an immediate corollary of Theorem 3.4, we may write an explicit expression for the *total* partition function  $Z_t[\sigma]$  of all paths between  $2n$  nodes paired according to the pairing  $\sigma$  (which we also see as a standard Dyck path), corresponding to the sum of the  $n+1$  winding partition functions for the pairing  $\sigma$ . The result is as follows:

**Corollary 3.6** ([90]). *Let  $\sigma$  be a standard Dyck path of length  $2n$ . Then*

$$Z_t[\sigma] = \det \Delta \sum_{\mu \geq \sigma} (-1)^{\frac{1}{2}(\mathcal{A}(\mu) - n)} \text{ci}(\sigma/\mu) \det G_{U^\mu}^{D^\mu}, \quad (3.142)$$

where the sets of up and down steps of  $\mu$ ,  $U^\mu$  and  $D^\mu$ , are sorted in ascending order.

*Proof.* To compute the total partition function indexed by  $\sigma$ , it suffices to take the reference face  $f$  as the outer face of the graph. This amounts to setting  $G' = 0$ , so that Theorem 3.4 yields

$$Z_t[\sigma] = \det \Delta \sum_{\mu \geq \sigma} \text{ci}(\lambda/\mu) \text{pf} \mathcal{M}_\mu, \quad (3.143)$$

where  $(\mathcal{M}_\mu)_{i,j} = G_{i,j} (\mathbf{1}_{i \in U^\mu} - \mathbf{1}_{j \in U^\mu})$ . In other words,  $(\mathcal{M}_\mu)_{i,j}$  is equal to  $+G_{i,j}$  (resp.  $-G_{i,j}$ ) if  $i$  is an up (resp. down) step and  $j$  a down (resp. up) step of  $\mu$  and 0 otherwise. Let us then define the matrix  $\mathcal{M}_{\pi(\mu)}$  obtained by permuting the rows and columns of  $\mathcal{M}_\mu$  such that the indices in  $U^\mu$  appear first and those in  $D^\mu$  come second:

$$\mathcal{M}_\mu = P_{\pi(\mu)} \mathcal{M}_{\pi(\mu)} P_{\pi(\mu)}^t, \quad (3.144)$$

where  $\pi(\mu)$  denotes the appropriate permutation of the indices of  $\mathcal{N} = \{1, 2, \dots, 2n\}$  and  $P_{\pi(\mu)}$  the corresponding permutation matrix. Since  $\mathcal{M}_{\pi(\mu)}$  is an antidiagonal block matrix, its Pfaffian can be written as

$$\text{pf} \mathcal{M}_{\pi(\mu)} = (-1)^{\frac{1}{2}n(n-1)} \det G_{U^\mu}^{D^\mu}. \quad (3.145)$$

To determine the signature of the permutation  $\pi(\mu)$ , consider first the maximal standard Dyck path  $\mu_{\max}$  whose chords are given by

$$(1, 2n), (2, 2n-1), \dots, (n, n+1). \quad (3.146)$$

The permutation  $\pi(\mu_{\max})$  is simply the identity. Assume next that  $\mu, \mu'$  are two standard Dyck paths such that  $\mu'$  is obtained from  $\mu$  by turning an up step  $k$  into a down step of  $\mu'$ , and the adjacent down step  $k+1$  into an up step of  $\mu'$  (note that all Dyck paths contain at least one chord between two adjacent steps). It follows that  $\pi(\mu)$  and  $\pi(\mu')$  have opposite signatures, and  $\mathcal{A}(\mu') = \mathcal{A}(\mu) - 2$ .

Let then  $\mu$  be a standard Dyck path. It is clear that it can be obtained from  $\mu_{\max}$  by  $N$  elementary reversal operations of the type described above. Using  $\mathcal{A}(\mu) = \mathcal{A}(\mu_{\max}) - 2N = n^2 - 2N$ , one finds the relation

$$\det P_{\pi(\mu)} = (-1)^N \det P_{\pi(\mu_{\max})} = (-1)^{\frac{1}{2}(n^2 - \mathcal{A}(\mu))}, \quad (3.147)$$

from which the result of the corollary follows.  $\square$

Finally, it should be noted that Theorem 3.4 can be adapted to graphs with free boundary conditions (i.e. in which the root  $s$  is isolated, or equivalently, absent), as discussed in Section 1.5. Using Proposition 1.7, one may compute the winding partitions  $Z[\vec{\sigma}]$  on such graphs simply by substituting

$$G_{i,j} \rightarrow G_{i,j} + q^{-1}N^{-1}, \quad G'_{i,j} \rightarrow G'_{i,j} + q^{-1}N^{-1}\tilde{G}'_{i,j},$$

in Theorem 3.4, where the functions  $G'$  and  $\tilde{G}'$  on the right-hand side are defined in Eq. (1.38), and then by taking the limit  $q \rightarrow 0$ .

### 3.4 Correspondence with loop-erased random walks

In this section, we recall the definitions of the standard random walk (SRW) and the loop-erased random walk (LERW) on an unoriented connected graph  $\mathcal{G}_s$ . The connection between the latter and the random spanning tree has been known for many years ([126] for the uniform distribution, [157] for a generic weighted one): for any two vertices  $u, v$  of the graph, the distribution of the LERW started at  $u$  and stopped at  $v$  is the same as the distribution of the unique chemical path between these two vertices in the random spanning tree. This correspondence is especially apparent through Wilson's algorithm:

**Theorem 3.7** ([157]). *Let  $\mathcal{G}_s$  be an unoriented connected graph, and let  $s, v_1, v_2, \dots, v_{|\mathcal{V}|}$  be an enumeration of its vertices. Define  $\mathcal{T}_0$  as the degenerate tree consisting in the vertex  $s$ , and  $\mathcal{T}_j$  as the tree obtained as the union of  $\mathcal{T}_{j-1}$  and the loop erasure of a SRW from  $v_j$  to  $\mathcal{T}_{j-1}$ , for  $1 \leq j \leq |\mathcal{V}|$ . Then  $\mathcal{T}_{|\mathcal{V}|}$  is a spanning tree on  $\mathcal{G}_s$ , occurring with the probability induced by (1.1).*

We provide here an alternative proof based on explicit formulas for the probability measures for the LERW [7, 116] and for paths in spanning forests, given by Eq. (3.4). This derivation allows one to generalize in a straightforward manner the correspondence for multiple walks, whose joint probability measure was given in [65].

### 3.4.1 Single walks

Let us consider an unoriented connected graph  $\mathcal{G}$  with vertices  $\mathcal{V}$  and edges  $\mathcal{E}$ . Let  $s$  be an additional vertex connected by a set of edges  $\mathcal{E}_s$  to a subset of vertices  $\mathcal{D} \subset \mathcal{V}$  in the extended graph  $\mathcal{G}_s$ . We assume for now that  $\mathcal{D}$  is nonempty, and discuss the case  $\mathcal{D} = \emptyset$  below (see Eq. (3.167)). Let  $A_s$  be a transition matrix for  $\mathcal{G}_s$  with a root  $s$ , i.e. such that

- $(A_s)_{u,v} \geq 0$  for any  $u \in \mathcal{V}$ ,  $v \in \mathcal{V} \cup \{s\}$ , with  $(A_s)_{u,v} > 0$  if and only if  $\{u, v\} \in \mathcal{E} \cup \mathcal{E}_s$ ;
- $(A_s)_{s,v} = 0$  for any  $v \in \mathcal{V} \cup \{s\}$ ;
- $\sum_v (A_s)_{u,v} = 1$  for any  $u \in \mathcal{V}$ , where the sum is over all vertices of  $\mathcal{G}_s$ , including  $s$ .

The probabilistic interpretation of the SRW is the following: starting at  $v_0$ , a walker moving on the edges of the graph goes toward one of the neighbors  $v_1$  of  $v_0$ , with probability  $(A_s)_{v_0,v_1}$ . The walker continues moving from  $v_1$  to one of its neighbors  $v_2$  with probability  $(A_s)_{v_1,v_2}$ . The process is iterated until the walker reaches the root  $s$  and remains there forever, since  $(A_s)_{s,v} = 0$  for any  $v \in \mathcal{V}$ .

A *walk* or *path*  $\omega_s$  on  $\mathcal{G}_s$  starting from a vertex  $v_0 \neq s$  and ending at  $s$  is defined as a collection of vertices  $(v_0, v_1, \dots, v_n=s)$  such that  $(v_i, v_{i+1}) \in \mathcal{E}$  for  $0 \leq i \leq n-2$ , and  $(v_{n-1}, v_n) \in \mathcal{E}_s$ . Its SRW weight is defined by

$$w_{\text{SRW}}(\omega_s) = \prod_{i=0}^{n-1} (A_s)_{v_i, v_{i+1}}. \tag{3.148}$$

In what follows, we shall consider a SRW starting at a given vertex  $u_1$  and reaching  $s$  through a fixed edge  $(u_2, s) \in \mathcal{E}_s$ , with  $u_2 \in \mathcal{D}$ . The partition function can be computed by summing first over all walks of length  $n$ , and then summing over all positive integers  $n$ . Its result reads

$$\begin{aligned} \sum_{\substack{\omega_s: u_1 \rightarrow s \\ \text{with } (u_2, s) \in \omega_s}} w_{\text{SRW}}(\omega_s) &= \sum_{n=0}^{\infty} (A_s^n)_{u_1, u_2} (A_s)_{u_2, s} \\ &= [(\mathbb{I} - A_s)^{-1}]_{u_1, u_2} \times (A_s)_{u_2, s}. \end{aligned} \tag{3.149}$$

The convergence of the geometric series follows from the fact that the spectral radius  $\rho(A)$  is strictly less than one, where  $A$  is the submatrix

of  $A_s$  with the row and column indexed by  $s$  removed. Indeed,  $A$  is positive and irreducible (since  $\mathcal{G}$  is connected and unoriented). Due to the Perron-Frobenius theorem,  $A$  has an eigenvalue  $r = \rho(A)$  associated with a left-eigenvector  $\mathbf{p}$  whose entries are strictly positive. We can assume without loss of generality that  $|\mathbf{p}|_1 = \sum_u p_u = 1$ . It follows that

$$\begin{aligned} r &= |r\mathbf{p}|_1 = |\mathbf{p}A|_1 = \sum_u \sum_{v \neq s} p_u A_{u,v} = \sum_u \sum_{v \neq s} p_u (A_s)_{u,v} \\ &= \sum_u p_u \sum_v (A_s)_{u,v} - \sum_u p_u (A_s)_{u,s} = 1 - \sum_u p_u (A_s)_{u,s} < 1, \end{aligned} \quad (3.150)$$

since  $p_u > 0$  and there exists at least one  $u$  such that  $(A_s)_{u,s} > 0$ . It is then straightforward to see that  $\rho(A) < 1$  is equivalent to  $\sum_{n \geq 0} A_s^n < \infty$  using the Jordan canonical form of  $A_s$ .

The *loop-erased random walk* (LERW) was introduced in [98] as an example of a random process that produces simple walks (i.e. with no self-intersection) and that is easier to treat analytically than the canonical self-avoiding walk; the difference between the two residing in their respective probability measures. The loop erasure of a walk  $\omega_s$  is obtained by chronologically erasing loops along  $\omega_s$ , thus yielding a simple path. This procedure is equivalent to the following (shorter) algorithm. Let  $\omega_s = (v_0, v_1, \dots, v_n=s)$  be a walk on the graph  $\mathcal{G}_s$ . The loop erasure of  $\omega_s$ , denoted by  $\gamma_s = \text{LE}(\omega_s) = (v_{i_0}, v_{i_1}, \dots, v_{i_J})$ , is defined inductively by

$$i_0 = 0, \quad i_{j+1} = \max_{0 \leq k \leq n} \{k : v_k = v_{i_j}\} + 1, \quad (3.151)$$

which stops at  $j = J$  such that  $v_{i_J} = s$ . An illustration of the loop erasure procedure is provided in Fig. 3.17. The LERW weight of a simple path  $\gamma_s$  is defined as the sum of the weights of all walks  $\omega_s$  whose loop erasure yields  $\gamma_s$ :

$$\text{wLERW}(\gamma_s) = \sum_{\omega_s: \text{LE}(\omega_s) = \gamma_s} \text{wSRW}(\omega_s). \quad (3.152)$$

To compute an explicit form for the LERW weight in terms of the matrix  $A_s$ , one may use the algorithm defined in Eq. (3.151) to decompose a walk  $\omega_s$  such that  $\text{LE}(\omega_s) = \gamma_s = (v_0, v_1, \dots, v_n=s)$  as follows. If we define  $\mathcal{G}_s^{(j)} \equiv \mathcal{G}_s \setminus \{v_0, v_1, \dots, v_j\}$ , then  $\omega_s$  can be seen as a (possibly trivial) loop attached to  $v_0$  on  $\mathcal{G}_s$ , followed by the edge  $(v_0, v_1)$ ; a loop

attached to  $v_1$  on  $\mathcal{G}_s^{(0)}$  comes next, followed by the edge  $(v_1, v_2)$ ; and so on. The process is iterated until the edge  $(v_{n-1}, v_n=s)$  is used, at which point the walk is stopped. If  $A_s^{(j)}$  denotes the restriction of the weight matrix  $A_s$  to the vertices of  $\mathcal{G}_s^{(j)}$ , then

$$\sum_{\substack{\omega_j: v_j \rightarrow v_j \\ \text{on } \mathcal{G}_s^{(j-1)}}} \text{wSRW}(\omega_j) = \left[ \left( \mathbb{I} - A_s^{(j-1)} \right)^{-1} \right]_{v_j, v_j}, \quad (3.153)$$

where the sum is over all loops attached to  $v_j$  conditioned to not intersect  $\{v_0, v_1, \dots, v_{j-1}\}$ . The preceding equation allows one to express Eq. (3.152) as

$$\begin{aligned} \text{wLERW}(\gamma_s) &= \left[ \left( \mathbb{I} - A_s \right)^{-1} \right]_{v_0, v_0} (A_s)_{v_0, v_1} \left[ \left( \mathbb{I} - A_s^{(0)} \right)^{-1} \right]_{v_1, v_1} \\ &\quad \times (A_s)_{v_1, v_2} \left[ \left( \mathbb{I} - A_s^{(1)} \right)^{-1} \right]_{v_2, v_2} \\ &\quad \times \dots \times \left[ \left( \mathbb{I} - A_s^{(n-2)} \right)^{-1} \right]_{v_{n-1}, v_{n-1}} (A_s)_{v_{n-1}, v_n}. \end{aligned} \quad (3.154)$$

Using Cramer’s formula for the inverse of a matrix yields telescopic cancellations, and the result simplifies to [7, 116]

$$\begin{aligned} \text{wLERW}(\gamma_s) &= \prod_{i=0}^{n-1} (A_s)_{v_i, v_{i+1}} \times \frac{\det \left( \mathbb{I} - A_s^{(0)} \right)}{\det \left( \mathbb{I} - A_s \right)} \\ &\quad \times \frac{\det \left( \mathbb{I} - A_s^{(1)} \right)}{\det \left( \mathbb{I} - A_s^{(0)} \right)} \times \dots \times \frac{\det \left( \mathbb{I} - A_s^{(n-1)} \right)}{\det \left( \mathbb{I} - A_s^{(n-2)} \right)} \\ &= \text{wSRW}(\gamma_s) \times \frac{\det \left( \mathbb{I} - A_s^{(n-1)} \right)}{\det \left( \mathbb{I} - A_s \right)}. \end{aligned} \quad (3.155)$$

Let us now consider a loop-erased random walk on  $\mathcal{G}_s$  starting at a fixed vertex  $u_1 \in \mathcal{G}$ , and reaching  $s$  through a specified edge  $(u_2, s)$ . We denote the corresponding simple paths by  $u_1 \rightarrow u_2 \rightarrow s$ . The partition function reads

$$\begin{aligned} \sum_{\gamma_s: u_1 \rightarrow u_2 \rightarrow s} \text{wLERW}(\gamma_s) &= \sum_{\gamma_s: u_1 \rightarrow u_2 \rightarrow s} \sum_{\omega_s: \text{LE}(\omega_s) = \gamma_s} \text{wSRW}(\omega_s) \\ &= \sum_{\omega_s: u_1 \rightarrow u_2 \rightarrow s} \text{wSRW}(\omega_s), \end{aligned} \quad (3.156)$$



With Eq. (3.159), one has a probability measure on simple paths on the graph  $\mathcal{G}$  from  $u_1$  to  $u_2$ , in which any explicit reference to the root  $s$  has been eliminated. While it is often more convenient to use this equation rather than Eq. (3.157) for what follows, one should remember that the presence of  $s$  translates into  $A$  being substochastic, i.e its rows indexed by vertices  $u \in \mathcal{D}$  (the neighbors of  $s$  on  $\mathcal{G}_s$ ) sum to strictly less than one (which ensures in particular the invertibility of  $\mathbb{I} - A$ ).

Let us now show that Eq. (3.159) coincides with the measure on paths in two-component spanning forests, defined in (3.4).

**Proposition 3.8.** *Let  $\gamma = (v_0=u_1, v_1, \dots, v_{n-1}, v_n=u_2)$  be a simple path on  $\mathcal{G}$ , and  $A$  be the transition matrix defined by*

$$A_{u,v} = \frac{c_{u,v}}{\deg_s(u)} \tag{3.160}$$

*if  $(u, v) \in \mathcal{E}$  and 0 otherwise. Here  $\deg_s(u) = \sum_{w \sim u} c_{u,w}$  is the degree of  $u$  in  $\mathcal{G}_s$ , where the sum is over all neighbors of  $u$  in  $\mathcal{G}_s$ . Then*

$$\mathbb{P}_{\text{LERW}}(\gamma) = \mathbb{P}_{\text{SF}}(\gamma). \tag{3.161}$$

*As a consequence, any simple path  $\gamma$  and the reverse path  $\gamma^{-1}$  occur with the same probability with respect to the LERW measure.*

*Proof.* Let us define the matrix  $M_{u,v} = \deg_s(u) \delta_{u,v}$  for  $u, v \in \mathcal{V}$ . It is straightforward to check that the Dirichlet Laplacian on  $\mathcal{G}_s$  reads  $\Delta = M(\mathbb{I} - A)$ , which implies that  $\det(\mathbb{I} - A) = \det \Delta / \det M$  and

$$\begin{aligned} \det(\mathbb{I} - A^{(\gamma)}) &= \det \Delta^{(\gamma)} / \det M^{(\gamma)}, \\ \text{with } \det M &= \det M^{(\gamma)} \times \prod_{i=0}^n \deg_s(v_i). \end{aligned} \tag{3.162}$$

The SRW weight of the path  $\gamma$  and the  $(u_1, u_2)$  entry of the matrix  $(\mathbb{I} - A)^{-1}$  are given by

$$\begin{aligned} w_{\text{SRW}}(\gamma) &= C(\gamma) \deg_s(u_2) \prod_{i=0}^n \frac{1}{\deg_s(v_i)}, \\ [(\mathbb{I} - A)^{-1}]_{u_1, u_2} &= \deg_s(u_2) G_{u_1, u_2}. \end{aligned} \tag{3.163}$$

Substituting the preceding equations into Eq. (3.159) yields the result of the proposition. □

Before we turn to multiple walks, note that we have assumed the endpoint  $u_2$  to be connected to the root  $s$  for random walks (i.e.  $u_2 \in \mathcal{D}$ ), so that the walker stops moving once he reaches the root  $s$  through the edge  $(u_2, s)$ . The probability (3.159) may however be extended for simple paths  $\gamma : u_1 \rightarrow u_2$  such that  $u_2 \notin \mathcal{D}$ . To see this, let us denote by  $\mathcal{G}_s^\varepsilon$  the graph obtained by adding an extra edge  $(u_2, s)$  to  $\mathcal{G}_s$  such that the corresponding transition matrix  $A_s^\varepsilon$  coincides with  $A_s$  everywhere except on the row indexed by  $u_2$ , with

$$(A_s^\varepsilon)_{u_2, v} = (1 - \varepsilon) \times (A_s)_{u_2, v} \text{ for } v \neq s, \quad (A_s^\varepsilon)_{u_2, s} = \varepsilon. \quad (3.164)$$

The weight of a simple path  $\gamma_s^\varepsilon = \gamma \cup \{s\} : u_1 \rightarrow u_2 \rightarrow s$  on  $\mathcal{G}_s^\varepsilon$  is then given by Eq. (3.155):

$$\begin{aligned} \text{wLERW}(\gamma_s^\varepsilon) &= \text{wSRW}(\gamma_s^\varepsilon) \frac{\det(\mathbb{I} - (A_s^\varepsilon)^{(\gamma)})}{\det(\mathbb{I} - A_s^\varepsilon)} \\ &= \varepsilon \text{wSRW}(\gamma) \frac{\det(\mathbb{I} - A^{(\gamma)})}{\det(\mathbb{I} - A)} + \dots \end{aligned} \quad (3.165)$$

at lowest order in  $\varepsilon$ . It is then natural to define the probability associated with a path  $\gamma : u_1 \rightarrow u_2$  on  $\mathcal{G}$  as

$$\mathbb{P}_{\text{LERW}}(\gamma) = \lim_{\varepsilon \rightarrow 0^+} \mathbb{P}_{\text{LERW}}(\gamma_s^\varepsilon). \quad (3.166)$$

The result of Eq. (3.166) is given by Eq. (3.159), which holds therefore whether  $u_2$  is in  $\mathcal{D}$  or not, as does Proposition 3.8.

Finally, the case  $\mathcal{D} = \emptyset$ —i.e. graphs  $\mathcal{G}$  without a root, or equivalently, extended graphs  $\mathcal{G}_s$  in which  $s$  is isolated—can be dealt with in a similar way, namely by adding an extra edge  $(u_2, s)$  with transition probability  $\varepsilon$ , and then taking the limit  $\varepsilon \rightarrow 0^+$  of the probability distribution defined on  $\mathcal{G}_s^\varepsilon$ . The result reads

$$\mathbb{P}_{\text{LERW}}(\gamma) = \text{wSRW}(\gamma) \frac{\det(\mathbb{I} - A^{(\gamma)})}{(-1)^{u_1+u_2} \det(\mathbb{I} - A)_{\mathcal{V} \setminus \{u_1\}}^{\mathcal{V} \setminus \{u_2\}}}. \quad (3.167)$$

It is straightforward to show that Proposition 3.8 is valid in this case as well.

### 3.4.2 Multiple walks

Up to this point we have considered a single LERW on the graph  $\mathcal{G}_s$ , starting at any fixed vertex  $u_1 \in \mathcal{G}$  and ending at  $s$  through a fixed edge  $(u_2, s) \in \mathcal{E}_s$ . We have shown that such paths can be traded for shorter ones from  $u_1$  to  $u_2$ , for which we have established the link with the spanning forest measure. We now generalize this process to multiple simple paths between marked vertices (nodes) that do not intersect each other.

Two definitions of multiple LERWs seem the most natural: either one considers SRWs conditioned to not intersect each other, or one asks only that their loop erasures do not intersect (except at  $s$  in both cases). We shall favor here the second definition, with the additional requirement that the  $j$ th SRW do not intersect the loop erasures of the first  $j-1$  walks on  $\mathcal{G}$ , following [52, 65]. We consider a set of nodes  $\mathcal{N} = \{u_1, u_2, \dots, u_{2n}\} \subset \mathcal{V}$  (not including the root  $s$ ), which we divide into two subsets,  $R = \{r_1, \dots, r_n\}$  and  $S = \mathcal{N} \setminus R = \{s_1, \dots, s_n\}$ . We assume that  $(s_i, s) \in \mathcal{E}_s$  and consider LERWs from  $r_i$  to  $s$  conditioned to exit  $\mathcal{G}$  through  $(s_i, s)$ , for  $1 \leq i \leq n$ . The weight of a given  $n$ -tuple of paths  $\Gamma_s = (\gamma_1^s, \dots, \gamma_n^s)$  is defined as follows [65],

$$\begin{aligned} w_{\text{LERW}}^{\mathcal{G}_s}(\Gamma_s) &= w_{\text{LERW}}^{\mathcal{G}_s}(\gamma_1^s) \times w_{\text{LERW}}^{\mathcal{G}_s}(\gamma_2^s | \gamma_1^s) \times \dots \\ &\quad \times w_{\text{LERW}}^{\mathcal{G}_s}(\gamma_n^s | \gamma_1^s, \dots, \gamma_{n-1}^s), \end{aligned} \tag{3.168}$$

where the factor  $w_{\text{LERW}}^{\mathcal{G}_s}(\gamma_i^s | \gamma_1^s, \dots, \gamma_{i-1}^s)$  on the right-hand side is the sum over all walks  $\omega_i^s : r_i \rightarrow s_i \rightarrow s$  with  $\text{LE}(\omega_i^s) = \gamma_i^s$  that only intersect  $\bigcup_{j=1}^{i-1} \gamma_j^s$  at the root  $s$ . Conditioning  $\omega_i = \omega_i^s \setminus \{s\}$  to not intersect  $\gamma_j = \gamma_j^s \setminus \{s\}$  for  $1 \leq j \leq i-1$  amounts to growing  $\omega_i^s$  on  $\mathcal{G}_s \setminus \bigcup_{j=1}^{i-1} \gamma_j$  (the graph from which the vertices of  $\gamma_1, \dots, \gamma_{i-1}$  have been removed, together with their incident edges). Using Eq. (3.155), one can therefore rewrite the preceding equation as

$$\begin{aligned}
w_{\text{LERW}}^{\mathcal{G}_s}(\Gamma_s) &= w_{\text{LERW}}^{\mathcal{G}_s}(\gamma_1^s) \times \cdots \times w_{\text{LERW}}^{\mathcal{G}_s \setminus \bigcup_{j=1}^{n-1} \gamma_j}(\gamma_n^s) \\
&= w_{\text{SRW}}^{\mathcal{G}_s}(\gamma_1^s) \frac{\det(\mathbb{I} - A_s^{(\gamma_1)})}{\det(\mathbb{I} - A_s)} \times \cdots \\
&\quad \times w_{\text{SRW}}^{\mathcal{G}_s \setminus \bigcup_{j=1}^{n-1} \gamma_j}(\gamma_n^s) \frac{\det(\mathbb{I} - A_s^{(\gamma_1, \dots, \gamma_n)})}{\det(\mathbb{I} - A_s^{(\gamma_1, \dots, \gamma_{n-1})})} \\
&= (A_s)_{s_1, s} w_{\text{SRW}}^{\mathcal{G}}(\gamma_1) \frac{\det(\mathbb{I} - A^{(\gamma_1)})}{\det(\mathbb{I} - A)} \times \cdots \\
&\quad \times (A_s)_{s_n, s} w_{\text{SRW}}^{\mathcal{G}}(\gamma_n) \frac{\det(\mathbb{I} - A^{(\gamma_1, \dots, \gamma_n)})}{\det(\mathbb{I} - A^{(\gamma_1, \dots, \gamma_{n-1})})} \\
&= \prod_{j=1}^n (A_s)_{s_j, s} \times w_{\text{SRW}}^{\mathcal{G}}(\Gamma) \frac{\det(\mathbb{I} - A^{(\Gamma)})}{\det(\mathbb{I} - A)},
\end{aligned} \tag{3.169}$$

where  $w_{\text{SRW}}(\Gamma) = \prod_{i=1}^n w_{\text{SRW}}(\gamma_i)$  and  $A^{(\Gamma)}$  denotes the restriction of  $A$  to vertices not belonging to  $\Gamma = \Gamma_s \setminus \{s\}$ . In particular, it follows from Eq. (3.169) that the joint measure on multiple simple paths does not depend on the order in which the walks are grown. As the product over  $j$  on the right-hand side is constant over all  $n$ -tuples of paths on  $\mathcal{G}_s$ , we may consider simple paths on  $\mathcal{G}$  instead. The weight of an  $n$ -tuple of nonintersecting simple paths  $\Gamma = (\gamma_1, \dots, \gamma_n)$ , with  $\gamma : r_i \rightarrow s_i$  on  $\mathcal{G}$  for  $1 \leq i \leq n$ , is then defined as [65]

$$w_{\text{LERW}}(\Gamma) = w_{\text{SRW}}(\Gamma) \frac{\det(\mathbb{I} - A^{(\Gamma)})}{\det(\mathbb{I} - A)}. \tag{3.170}$$

Let us now show that the SF and LERW weights on  $\Gamma$ , given respectively by Eq. (3.116) and Eq. (3.170), are proportional to each other—thus implying that both normalized measures coincide.

**Proposition 3.9.** *Let  $\mathcal{G}_s = \mathcal{G} \cup \{s\}$  be an unoriented connected graph with a root  $s$  and a set of nodes  $\mathcal{N} = \{u_1, \dots, u_{2n}\} \subset \mathcal{V}$ . Let  $R = \{r_1, \dots, r_n\} \subset \mathcal{N}$  and  $S = \{s_1, \dots, s_n\} = \mathcal{N} \setminus R$  such that  $(s_i, s) \in \mathcal{E}_s$  for  $1 \leq i \leq n$ . Consider  $n$  nonintersecting simple paths  $\gamma_i : r_i \rightarrow s_i$  on  $\mathcal{G}$ , and write  $\Gamma = (\gamma_1, \dots, \gamma_n)$ . If  $A_{u,v} = c_{u,v} / \deg_s(u)$  for  $(u, v) \in \mathcal{E}$  and 0 otherwise, then*

$$w_{\text{LERW}}(\Gamma) = K \times w_{\text{SF}}(\Gamma), \tag{3.171}$$

where  $K = K(\mathcal{G}_s, S)$  is independent of  $\Gamma$ . As a consequence,  $\mathbb{P}_{\text{LERW}}(\Gamma) = \mathbb{P}_{\text{SF}}(\Gamma)$ .

*Proof.* Let  $M$  be the matrix defined by  $M_{u,v} = \deg_s(u) \delta_{u,v}$  for  $u, v \in \mathcal{V}$ . Then  $\Delta = M(\mathbb{I} - A)$  and

$$w_{\text{SRW}}(\Gamma) = \frac{C(\Gamma) \deg_s(S)}{\deg_s(\Gamma)}, \quad \frac{\det(\mathbb{I} - A^{(\Gamma)})}{\det(\mathbb{I} - A)} = \frac{\det \Delta^{(\Gamma)} \deg_s(\Gamma)}{\det \Delta}, \tag{3.172}$$

where  $\deg_s(S)$  and  $\deg_s(\Gamma)$  are the products of the degrees (on  $\mathcal{G}_s$ ) of all vertices belonging to  $S$  and  $\Gamma$ , respectively. Hence we find

$$K = \frac{\deg_s(S)}{\det \Delta}, \tag{3.173}$$

which concludes the proof. □

A less explicit argument for the equality between the LERW and SF measures for multiple paths, based on Wilson’s algorithm (Theorem 3.7), was given in [83]. The idea consists in picking an enumeration of the vertices of  $\mathcal{G}_s$  such that  $s$  and  $R = \{r_1, \dots, r_n\}$  appear first, and then growing a SRW from  $r_1$  to  $s$  exiting  $\mathcal{G}$  through the edge  $(s_1, s)$ , followed by a second SRW from  $r_2$  to  $s$  through  $(s_2, s)$  that does not intersect the loop erasure of the first SRW, and so on, such that the  $j$ th SRW from  $r_j$  to  $s$  through  $(s_j, s)$  does not intersect the loop erasures of the first  $j-1$  SRWs. The algorithm resumes as in Theorem 3.7 when the  $n$  paths from  $R$  to  $S$  have been constructed, and yields a spanning tree associated with a unique spanning forest with  $n+1$  trees (each of which containing a pair  $r_i, s_i$  or the root  $s$ ), obtained by removing the prescribed edges  $(s_1, s), \dots, (s_n, s)$  from the spanning tree.

Finally, note that the requirement that  $s_1, \dots, s_n$  be neighbors of the root may be relaxed, allowing some or all of them to not be connected to  $s$  on  $\mathcal{G}_s$ . If this is the case for  $k$  elements of  $S$ —say  $s_1, \dots, s_k$ —define a modified graph  $\mathcal{G}_s^\varepsilon$  by adding  $k$  edges  $(s_i, s)$  to  $\mathcal{G}_s$  such that

$$(A_s^\varepsilon)_{s_i,v} = (1 - \varepsilon) \times (A_s)_{s_i,v} \text{ for } v \neq s, \quad (A_s^\varepsilon)_{s_i,s} = \varepsilon, \tag{3.174}$$

for  $1 \leq i \leq k$ . The weight of any  $n$ -tuple  $\Gamma_s^\varepsilon$  on  $\mathcal{G}_s^\varepsilon$  then reads

$$w_{\text{LERW}}(\Gamma_s^\varepsilon) = \varepsilon^k w_{\text{LERW}}(\Gamma) + \dots \tag{3.175}$$

at leading order in  $\varepsilon \sim 0^+$ , with  $w_{\text{LERW}}(\Gamma)$  given by Eq. (3.170). Consequently, the result of Proposition 3.9 is valid in this setting as well. A similar argument can be made if  $s$  is entirely disconnected from the rest of the graph.

The equality between  $\mathbb{P}_{\text{LERW}}$  and  $\mathbb{P}_{\text{SF}}$  holds therefore for any positions of the extremities of the paths, on any unoriented connected graph, with or without a root. However, concrete computations of probabilities require knowledge of the explicit expressions of the partition functions for certain classes of walks from  $R$  to  $S$  (see Sections 3.1 and 3.3). The only case for which we have been able to derive such expressions is for paths between boundary vertices of graphs embedded on surfaces (with noncrossing edges), with uniform conductances (see Section 3.2).

### 3.5 Comparison with SLE/CFT results

Let us now discuss how our formulas compare, in the scaling limit, with known results obtained in the framework of Schramm-Loewner evolution (SLE) and conformal field theory (CFT). We concentrate here on the case of the upper half-plane  $\mathbb{H}$  with Dirichlet boundary conditions, which is the canonical setup for both SLE and CFT on domains with a boundary.

The original formula for the left-passage probability for a single  $\text{SLE}_2$  curve is due to Schramm [145]. Its generalization to multiple random curves was first discussed in [60], in which the authors provide explicit formulas for  $n = 2$  curves only and  $\kappa = 0, 2, 8/3, 4, 8$ , using the correspondence between  $\text{SLE}_\kappa$  and a CFT with central charge  $c = (3\kappa - 8)(6 - \kappa)/(2\kappa)$  [8, 56] (a more rigorous SLE approach has recently been developed in [107], again for  $n = 2$  curves). Their computations make use of the fact that conditioning an SLE partition function on the existence of a curve connecting two boundary points  $x_1, x_2$  is equivalent to inserting a boundary operator  $\phi$  at  $x_1, x_2$  in the corresponding CFT correlator [8, 27, 56]. The field  $\phi$  has a weight  $h_\phi = (6 - \kappa)/(2\kappa)$ , and is degenerate at level two; thus yielding a second-order differential

equation for any correlator containing a  $\phi$  [12]:

$$\left( \frac{3}{2(2h_\phi + 1)} \partial_{x_1}^2 - \sum_{i=2}^k \frac{1}{x_1 - z_i} \partial_{z_i} - \sum_{i=2}^k \frac{h_i}{(x_1 - z_i)^2} \right) \langle \phi(x_1) \mathcal{O}_2(z_2) \dots \mathcal{O}_k(z_k) \rangle = 0, \quad (3.176)$$

where  $x_1 \in \partial\mathbb{H}$ ,  $z_i \in \mathbb{H}$  and  $\mathcal{O}_i$  are arbitrary fields of weight  $h_i$ ,  $2 \leq i \leq k$ . The condition that a random curve from  $x_1$  to  $x_2$  leaves a point  $z$  to its left or right is implemented by the insertion of an indicator operator  $\chi(z)$  of weight zero, treated as a local operator [9]. Explicitly, the scaling limit of the probability that a simple path leaves  $z$  to its left (or right) is then given by

$$\mathbb{P}(x_1, x_2; z) = \frac{\langle \chi(z) \phi(x_1) \phi(x_2) \rangle}{\langle \phi(x_1) \phi(x_2) \rangle}. \quad (3.177)$$

The probabilities  $\mathbb{P}_L$  or  $\mathbb{P}_R$  are found by solving Eq. (3.176) and imposing different boundary values for  $\mathbb{P}(x_1, x_2; z)$  as a function of  $z$ . The generalization to multiple curves is straightforward in the CFT framework, and yields

$$\mathbb{P}(\mathbf{x}; z) = \frac{\langle \chi(z) \Phi(\mathbf{x}) \rangle}{\langle \Phi(\mathbf{x}) \rangle}, \quad (3.178)$$

where  $\mathbf{x} = (x_1, x_2, \dots, x_{2n})$  and  $\Phi(\mathbf{x}) = \phi(x_1) \phi(x_2) \dots \phi(x_{2n})$ . Here  $\chi(z)$  is any of the indicator functions that each curve leaves  $z$  to its left or right. As for a single curve, the boundary conditions allow us to determine which case is computed, as well as the way the  $x_i$ 's are paired together. Due to the level-two degeneracy of  $\phi$ , both the numerator and the denominator of Eq. (3.178) satisfy  $2n$  BPZ equations of the form of Eq. (3.176). Particularizing to  $\kappa = 2$  (which implies that  $c = -2$  and  $h_\phi = 1$ ), we find that the equation with respect to  $x_1$  for the numerator reads:

$$\left( \frac{1}{2} \partial_{x_1}^2 - \sum_{i=2}^{2n} \left( \frac{1}{x_1 - x_i} \partial_{x_i} + \frac{1}{(x_1 - x_i)^2} \right) - \frac{1}{x_1 - z} \partial_z - \frac{1}{x_1 - \bar{z}} \partial_{\bar{z}} \right) \langle \chi(z) \Phi(\mathbf{x}) \rangle = 0. \quad (3.179)$$

The corresponding equation for the denominator  $\langle \Phi(\mathbf{x}) \rangle$  is the same except for the last two terms, which are absent. In [60] the authors

noted that solving these coupled equations is already too difficult for  $n = 2$ , even when the endpoints of both curves are sent to infinity. They considered the limit of “fused” curves, namely, when the distance between the starting points of the curves goes to zero, for which they found analytical solutions of the fused BPZ equations. Their results for  $\kappa = 2$  read, with  $z = x + iy$  and  $t = x/y$ ,

$$\begin{aligned}\mathbb{P}_{\text{LL}}(t) &= \frac{1}{4} + \frac{1}{9\pi^2(1+t^2)^3} [(-16 - 9t^2 + 9t^4) - 9\pi(t^3 + t^5) \\ &\quad + 9(1+t^2)\arctan(t)(2t^3 - \pi(1+t^2)^2 + (1+t^2)^2\arctan(t))], \\ \mathbb{P}_{\text{RR}}(t) &= \mathbb{P}_{\text{LL}}(-t), \quad \mathbb{P}_{\text{RL}}(t) = 1 - \mathbb{P}_{\text{LL}}(t) - \mathbb{P}_{\text{RR}}(t).\end{aligned}\tag{3.180}$$

In comparison, note that our results for two curves on the upper half-plane are valid for any positions of the starting and ending points, provided their order is fixed:  $x_1 < x_2 < x_3 < x_4$ . Their explicit expressions can be found using Eqs (3.124) and (3.125), in which the Green function and its derivative are replaced in the scaling limit with the excursion Poisson kernel  $P$  and its derivative  $P'$ , as argued in Section 3.2.1. For instance, if  $x_1, x_2$  are paired with  $x_4, x_3$ , respectively, the winding probabilities read in the scaling limit

$$\begin{aligned}\mathbb{P}_{\text{LL}}(14|23) &= 1 - \mathbb{P}_{\text{RL}}(14|23) - \mathbb{P}_{\text{RR}}(14|23), \\ \mathbb{P}_{\text{RL}}(14|23) &= \frac{P_{1,3}P'_{2,4} + P'_{1,3}P_{2,4} - P_{1,4}P'_{2,3} - P'_{1,4}P_{2,3}}{P_{1,3}P_{2,4} - P_{1,4}P_{2,3}} - 2\mathbb{P}_{\text{RR}}(14|23), \\ \mathbb{P}_{\text{RR}}(14|23) &= \frac{-P'_{1,2}P'_{3,4} + P'_{1,3}P'_{2,4} - P'_{1,4}P'_{2,3}}{P_{1,3}P_{2,4} - P_{1,4}P_{2,3}},\end{aligned}\tag{3.181}$$

where  $P_{i,j} \equiv P(x_i, x_j)$  and  $P'_{i,j} \equiv P'(x_i, x_j; z)$  are given by

$$\begin{aligned}P(x_i, x_j) &= \frac{1}{\pi(x_i - x_j)^2}, \\ P'(x_i, x_j; z) &= -\frac{1}{\pi^2(x_i - x_j)^2} (\arg(z - x_i) - \arg(z - x_j)) \\ &\quad + \frac{1}{\pi^2(x_i - x_j)^2} \frac{\text{Re}[(z - x_i)(\bar{z} - x_j)] \text{Im}[(z - x_i)(\bar{z} - x_j)]}{|z - x_i|^2 |z - x_j|^2}.\end{aligned}\tag{3.182}$$

The probabilities (3.180) are recovered by taking the limit  $x_1, x_2 \rightarrow -\infty$  and  $x_3, x_4 \rightarrow 0$  in Eq.(3.181).

A further consistency check of the CFT interpretation consists in showing that the (scaling limit of) the six distinct winding partition functions

$$\begin{aligned} &Z_{LL}[12|34], Z_{LR}[12|34], Z_{RL}[12|34], \\ &Z_{LL}[14|23], Z_{RL}[14|23], Z_{RR}[14|23] \end{aligned}$$

all satisfy Eq. (3.179). It is indeed the case, and a similar check holds for the total partition functions  $Z_t[12|34]$  and  $Z_t[14|23]$ . More generally, it would be interesting to provide the same validation of the CFT version of Schramm's formulas for any number of curves. While the total partition functions  $Z_t[\sigma]$  have been proved to satisfy the BPZ equation in [83], the analogue check for the winding partitions functions  $Z[\vec{\sigma}]$  is more difficult and remains to be done.



# Conclusion

In this thesis, we have shown how a complex connection on a graph and the associated line bundle Laplacian may be used to compute spanning forest events on certain types of graphs. The main tool is the grove theorem (Theorem 1.5 [91]), which generalizes Kirchhoff's theorem for combinatorial objects resembling spanning forests called (oriented) cycle-rooted groves. Although the quantities of interest in this dissertation—partition functions of spanning forests with fixed topological properties—are defined independently from any connection on the graph, they may be computed by introducing a nontrivial connection  $\Phi$  supported on a zipper, and by taking the limit  $\Phi \rightarrow \mathbb{I}$  in an appropriate manner.

For the Abelian sandpile model (ASM), we have illustrated how this new technique dramatically reduces the complexity of computations compared to standard graph-theoretical methods. We have used this technique to evaluate new lattice correlators, some of which we have been able to compare (successfully) to conformal correlators. While our results strengthen the validity of the current conformal conjectures for the ASM, they have not provided any new insight to better understand the CFT in play. A major step in that direction would consist in the computation of joint probabilities for multiple heights strictly larger than 1 on the lattice(s). The grove theorem, together with the relation between joint height probabilities and fractions of spanning trees given in Section 2.1.3, should in principle be applicable in this case as well. However, as explained at the beginning of Section 2.3, using a single zipper does not suffice for multiple nonunit heights. As the introduction of the zipper is a mere computational trick on annular-one graphs, it is not

clear how (or even if) a connection may be used to compute partition functions for multiple clusters of nodes far away from one another.

The second part of this thesis has dealt with loop-erased random walks (LERW), for which a discrete version of Schramm's formula has been established through the relationship between the LERW and spanning trees. We have given several explicit expressions for this formula in the scaling limit, for various domains and combinations of Dirichlet and Neumann boundary conditions. Relying on the grove theorem once again, we have generalized Schramm's formula for multiple nonintersecting LERWs on a planar graph. Quite remarkably, our result (Theorem 3.4) depends only on the standard Green function of the graph, and holds for any number of paths, positions of the nodes along the boundary, node connectivity, and combination of boundary conditions (Dirichlet and Neumann).

A natural direction to investigate would be the left-passage probability of a single curve with respect to *two* marked faces (or points in the scaling limit). The unique case for which this probability has been computed in the SLE/CFT framework is for  $\kappa = 8/3$  [150] (with a more rigorous proof given later in [13]). For a LERW, using a complex connection supported on two zippers with respective parameters  $z$  and  $w$ , one attached to each marked face, does not suffice to find combinatorial expressions for the partition functions of interest (indeed, the same product of parallel transports would be assigned to topologically distinct classes of paths). A more appropriate approach has been sketched in [91], and requires one to use a matrix-valued  $SL(2, \mathbb{C})$ -connection (for which an equivalent of Theorem 1.4 exists [88]). Knowledge of the associated vector bundle Green function in terms of the standard Green function would however be required for explicit computations, and is still lacking at the moment.

Finally, we mention two lattice models for which the use of a line bundle Laplacian might lead to interesting developments. The first one is the Ising model, whose partition function in the high-temperature representation may be written as (the square root of) the determinant of an adjacency matrix through the Kac-Ward formula [82, 136]. Its recent generalization to graphs on surfaces has yielded an unexpected relation between the Kac-Ward matrix and the determinant of the line bundle Laplacian [33, 34]. Whether this might allow one to make progress to-

ward the derivation of Schramm's formula for the Ising model remains however to be seen. The second model is the so-called *double dimer model*, whose configurations are obtained by superimposing two independent dimer configurations, thus forming cycles and doubled edges. Paths between boundary vertices can be obtained by imposing fixed boundary monomers in one of the two superimposed dimer configurations. Recent results for this model include a generalization of Kasteleyn's theorem for the partition function on graphs equipped with a connection and (a sketch of) Schramm's formula for a single double dimer path [89]. Due to striking similarities between the spanning tree model and the double dimer model, it is reasonable to think that analogues of Theorems 1.5 and 3.4 exist for the latter model as well.



# Appendix A

## Green functions

In this appendix, we briefly review the Green function in presence of a zipper, following [91], and in particular the way the first derivative can be computed. As required by the calculations presented in the text, we consider the Green function and its derivative on the infinite planar graph  $\mathbb{Z}^2$ , the half-infinite planar graph  $\mathbb{Z} \times \mathbb{N}^*$ , the infinite triangular lattice  $\mathcal{L}_T$ , as well as local modifications thereof by which a finite number of edges are removed.

### A.1 Zipper on the plane

The type of spanning tree probabilities we want to compute requires the knowledge of the Green function  $\mathbf{G}_{u,v}(z) = (\mathbf{\Delta}^{-1}(z))_{u,v}$  on the plane, in presence of a (semi-infinite) zipper. The Green function depends on the parameter  $z$  carried by the zipper, however the full dependence on  $z$  is not needed; only its zeroth and first orders around  $z = 1$  are required. By writing the Laplacian  $\mathbf{\Delta}(z)$  with the zipper as a perturbation of the standard Laplacian  $\Delta \equiv \mathbf{\Delta}(1)$ , one obtains [91]

$$\mathbf{G}_{u,v}(z) = G_{u,v} - (z - 1) \sum_{(k,\ell): \phi_{k,\ell}=z} (G_{u,k} G_{\ell,v} - G_{u,\ell} G_{k,v}) + \mathcal{O}(z - 1)^2. \tag{A.1}$$

On the square lattice  $\mathbb{Z}^2$ , the zeroth order  $G_{u,v} = \mathbf{G}_{u,v}(1)$  is the standard Green function, given by

$$\begin{aligned} G(v-u) &\equiv G_{u,v} = \int_{-\pi}^{\pi} \frac{d\alpha d\beta}{8\pi^2} \frac{e^{i(\alpha p + \beta q)}}{2 - \cos \alpha - \cos \beta} \\ &= \int_{-\pi}^{\pi} \frac{d\alpha}{4\pi} \frac{t^{|\alpha|} e^{i\alpha p}}{\sqrt{y^2 - 1}}, \quad v-u = (p, q), \end{aligned} \quad (\text{A.2})$$

with  $y(\alpha) \equiv 2 - \cos \alpha$  and  $t(\alpha) \equiv y(\alpha) - \sqrt{y(\alpha)^2 - 1}$ . Although the integral is divergent, the difference  $G_{u,v} - G_{0,0}$  is finite for any  $u, v$ . The leading asymptotic behavior for large distances  $|u-v|$  as well as finite-distance values are well known [153]. Subleading terms in the large-distance expansion of  $G_{u,v}$  in inverse powers of  $r \equiv |u-v|$  have been computed in [62]. With  $v-u = re^{i\varphi}$ , the first few terms read

$$\begin{aligned} G_{u,v} &= G_{0,0} - \frac{1}{2\pi} \left( \log r + \gamma + \frac{3}{2} \log 2 \right) + \frac{\cos 4\varphi}{24\pi r^2} \\ &+ \frac{1}{r^4} \left( \frac{3 \cos 4\varphi}{80\pi} + \frac{5 \cos 8\varphi}{96\pi} \right) \\ &+ \frac{1}{r^6} \left( \frac{51 \cos 8\varphi}{224\pi} + \frac{35 \cos 12\varphi}{144\pi} \right) \\ &+ \frac{1}{r^8} \left( \frac{217 \cos 8\varphi}{640\pi} + \frac{45 \cos 12\varphi}{16\pi} + \frac{1925 \cos 16\varphi}{768\pi} \right) + \dots \end{aligned} \quad (\text{A.3})$$

From (A.1), the first derivative  $G'_{u,v} \equiv \partial_z \mathbf{G}_{u,v}(z)|_{z=1}$  is given by

$$G'_{u,v} = \sum_{(k,\ell): \phi_{k,\ell}=z} (G_{u,\ell} G_{k,v} - G_{u,k} G_{\ell,v}). \quad (\text{A.4})$$

It satisfies the useful identity

$$(\Delta_0 G')_{u,v} = - (G' \Delta_0)_{v,u} = \sum_{(k,\ell): \phi_{k,\ell}=z} [\delta_{u,\ell} G_{k,v} - \delta_{u,k} G_{\ell,v}]. \quad (\text{A.5})$$

We note that  $G'_{u,v}$  has the same singularity, proportional to  $G_{0,0}$ , as  $G_{u,v}$  itself, with however a main difference: the coefficient of  $G_{0,0}$  is constant for  $G_{u,v}$ , but is a complicated function of  $u, v$  for  $G'_{u,v}$ .

On  $\mathbb{Z}^2$ , the summation in (A.4) is infinite, but can be reduced to a finite sum by combining three ingredients: the antisymmetry of  $G'_{u,v}$ , the rotation and translation invariance, and deformations of the zipper. The symmetry of the Green function implies the antisymmetry of its first

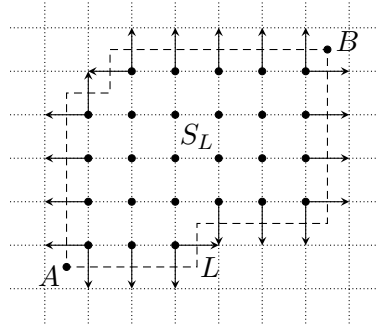


Figure A.1: Zipper forming a closed loop  $L$ . The arrows indicate the oriented edges on which the parallel transport equals  $z$ .

derivative,  $G'_{u,v} = -G'_{v,u}$ . Rotation and translation invariance of  $G'_{u,v}$  are manifest provided  $u, v$  and the zipper are all rotated or translated simultaneously.

Finally, the derivative  $G'_{u,v}$  only depends weakly on the location of the zipper. For fixed  $u, v$ , the zipper can in fact be freely deformed—keeping the endpoints fixed—without changing the value of  $G'_{u,v}$ , except when the zipper line is moved over  $u$  or  $v$ , in which case the move brings an extra contribution.

To show this, we consider the derivative  $G'_{u,v}{}^{\text{loop}}$  as given by (A.4) for a closed zipper loop  $L$  as in Fig. A.1. Let us denote by  $S_L$  the subset of vertices that lie inside the contour  $L$ . Since the contributions of an oriented edge  $(k, \ell)$  and its opposite  $(\ell, k)$  cancel each other out in  $G'$ , one can extend the summation to all edges  $(k, \ell)$  such that  $k$  is in  $S_L$ :

$$\begin{aligned}
 G'_{u,v}{}^{\text{loop}} &= - \sum_{(k,\ell) \in L} \left( G_{u,k} G_{\ell,v} - G_{u,\ell} G_{k,v} \right) \\
 &= - \sum_{(k,\ell): k \in S_L} \left( G_{u,k} G_{\ell,v} - G_{u,\ell} G_{k,v} \right) \\
 &= - \sum_{k \in S_L} \left[ G_{u,k} \left( 4G_{k,v} - (\Delta_0 G)_{k,v} \right) - \left( 4G_{u,k} - (\Delta_0 G)_{u,k} \right) G_{k,v} \right] \\
 &= G_{u,v} \sum_{k \in S_L} (\delta_{k,v} - \delta_{k,u}).
 \end{aligned} \tag{A.6}$$

With respect to a pair of points  $A, B$  on the loop  $L$ , one can compare the values of  $G'_{u,v}$  for the two zippers with endpoints  $A$  and  $B$ , one going through the lower-right of  $S_L$ , the other going through the upper-left of  $S_L$ . The two stretches can be considered as deformations of each other, except for the orientation of the arrows. Since reversing the arrows merely changes the sign of the corresponding  $G'_{u,v}$ , the full loop contribution  $G'_{u,v}{}^{\text{loop}}$  may be written as  $G'_{u,v}{}^{\text{loop}} = G'_{u,v}{}^{\text{new}} - G'_{u,v}{}^{\text{old}}$  for a proper choice of orientation of the arrows. The identity (A.6) then shows that

$$G'_{u,v}{}^{\text{new}} - G'_{u,v}{}^{\text{old}} = \begin{cases} G_{u,v} & \text{if the zipper has crossed } v \text{ only,} \\ -G_{u,v} & \text{if the zipper has crossed } u \text{ only,} \\ 0 & \text{if the zipper has crossed none or} \\ & \text{both of } u, v. \end{cases} \quad (\text{A.7})$$

According to our convention of which is the new zipper and which is the old one, the vertices  $u, v$  are crossed in the direction of the arrows attached to the moving zipper. If they are crossed in the opposite direction, the difference (A.7) changes sign.

Let us illustrate how  $G'_{u,v}$  can be computed in closed form for the particular case of the zipper  $\{(0, m), (1, m)\}_{m \leq 0}$  on the square lattice, using the previous observations [91]. We shall compute the derivative  $G'_{u,v}$  for  $u = (-1, 1)$  and  $v = (5, -2)$ , following the steps pictured in Fig. A.2.

We begin by rigidly rotating the whole lattice (zipper and marked points) by  $180^\circ$  around the black dot to which the zipper is attached. Under this rotation, a vertex  $x$  is mapped to  $x' = (1, 1) - x$ , so the two reference points  $(-1, 1)$  and  $(5, -2)$  are mapped to  $u' = (2, 0)$  and  $v' = (-4, 3)$  respectively, while the zipper is now pointing upward (indicated by an up arrow in the middle equation below). To put the zipper back in the original position, we rotate it by  $180^\circ$  to the left, this time keeping the marked points fixed. In the process, the zipper goes over  $v' = (-4, 3)$  in the direction of the arrows, producing an additional term:

$$G'_{(-1,1),(5,-2)} = G'_{(2,0),(-4,3)}^\uparrow = G'_{(2,0),(-4,3)} - G_{(2,0),(-4,3)}. \quad (\text{A.8})$$

In the next step, we add a finite number of zipper edges so that the endpoint is in the same relative position with respect to  $v'$  as it was with respect to  $u$  in the original configuration. In our example, one

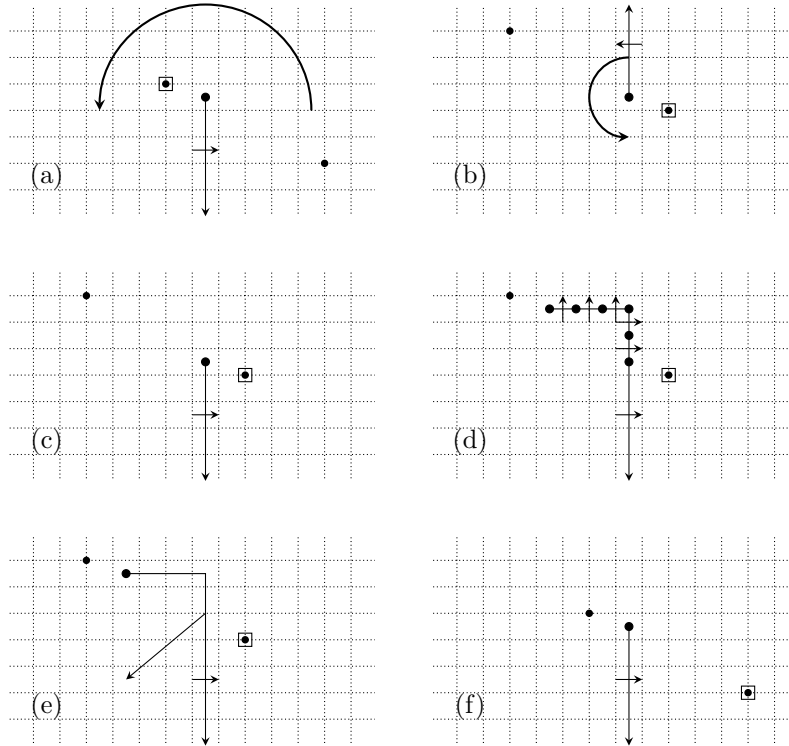


Figure A.2: Computation of  $G'_{u,v}$  for  $u = (-1, 1)$  and  $v = (5, -2)$ . The boxed vertex corresponds to the first argument of the derivative of the Green function  $G'$ . The six panels (a)–(f) illustrate the transformations and deformations explained in the text.

needs to add the following set of five edges:

$$E = \left\{ ((0, 1), (1, 1)), ((0, 2), (1, 2)), ((0, 2), (0, 3)), \right. \\ \left. ((-1, 2), (-1, 3)), ((-2, 2), (-2, 3)) \right\}. \tag{A.9}$$

Deforming the zipper again to make it go straight down, we recover the original relative positions of the vertices with respect to the zipper. A rigid translation puts the whole configuration in the original position except for the inversion of  $u$  and  $v$  (the square box has changed place).

In the example, one finds:

$$\begin{aligned}
G'_{(-1,1),(5,-2)} &= G'_{(2,0),(-4,3)} - G_{(2,0),(-4,3)} \\
&= G'_{(5,-2),(-1,1)} - G_{(2,0),(-4,3)} \\
&\quad + \sum_{(k,\ell) \in E} [G_{(2,0),k} G_{\ell,(-4,3)} - G_{(2,0),\ell} G_{k,(-4,3)}] \\
&= -\frac{1}{2} G_{(2,0),(-4,3)} \\
&\quad + \frac{1}{2} \sum_{(k,\ell) \in E} [G_{(2,0),k} G_{\ell,(-4,3)} - G_{(2,0),\ell} G_{k,(-4,3)}] \\
&= G_{0,0} \left( -\frac{15}{4} + \frac{152}{15\pi} \right) - \frac{677}{32} + \frac{1559}{21\pi} - \frac{1939}{90\pi^2},
\end{aligned} \tag{A.10}$$

where  $G_{0,0}$  is the divergent part of the Green function.

Proceeding this way, one obtains the values of the derivative  $G'_{u,v}$  for the origin and its four nearest neighbors, with the same zipper location as in the previous calculation (see Table A.1). These are the only values of  $G'_{u,v}$  needed to complete the computation of the single-height probabilities of Section 2.2.

## A.2 Zipper on the upper half-plane

On the upper half-plane, a zipper going out from an inner face can be of essentially two different kinds, either going off to infinity or terminating somewhere on the boundary, as illustrated in Fig. A.3. It is semi-infinite in the former case, finite in the latter. Despite this seemingly substantial difference, the derivatives of the Green function associated with them are closely related, as were those associated with two different zippers on the full plane. As shown in Appendix A.1, two zippers on the full plane starting from the same point and going to infinity in different directions are deformable into each other; the associated Green function derivatives are equal or differ by  $\pm G_{u,v}$ . The same relation holds on the UHP.

Let us first consider the zippers  $Z_2$  and  $Z_3$ . Each one involves a nontrivial parallel transport on a boundary edge. According to (A.4), the Green function derivatives  $G_{u,v}^{\text{op/cl}}(Z_2)$  and  $G_{u,v}^{\text{op/cl}}(Z_3)$  are given by finite sums

$G'_{u,v}$	(1, 0)	(0, 1)	(-1, 0)
(1, 0)	0	$\frac{1}{2}G_{0,0} - \frac{1}{2\pi}$	$G_{0,0}(1 - \frac{1}{\pi}) - \frac{5}{8} + \frac{5}{4\pi}$
(0, 1)	$-\frac{1}{2}G_{0,0} + \frac{1}{2\pi}$	0	$G_{0,0}(\frac{1}{2} - \frac{1}{\pi}) - \frac{1}{4\pi}$
(-1, 0)	$G_{0,0}(-1 + \frac{1}{\pi}) + \frac{5}{8} - \frac{5}{4\pi}$	$G_{0,0}(-\frac{1}{2} + \frac{1}{\pi}) + \frac{1}{4\pi}$	0
(0, -1)	$-G_{0,0}(\frac{1}{2} + \frac{1}{\pi}) + \frac{3}{4\pi}$	$-\frac{1}{\pi}G_{0,0} + \frac{3}{8} - \frac{3}{4\pi}$	$G_{0,0}(\frac{1}{2} - \frac{2}{\pi}) - \frac{1}{4} + \frac{1}{\pi}$
(0, 0)	$-\frac{3}{4}G_{0,0} + \frac{5}{32}$	$-\frac{1}{4}G_{0,0} + \frac{3}{32}$	$G_{0,0}(\frac{1}{4} - \frac{1}{\pi}) + \frac{1}{32}$

$G'_{u,v}$	(0, -1)	(0, 0)
(1, 0)	$G_{0,0}(\frac{1}{2} + \frac{1}{\pi}) - \frac{3}{4\pi}$	$\frac{3}{4}G_{0,0} - \frac{5}{32}$
(0, 1)	$\frac{1}{\pi}G_{0,0} - \frac{3}{8} + \frac{3}{4\pi}$	$\frac{1}{4}G_{0,0} - \frac{3}{32}$
(-1, 0)	$G_{0,0}(-\frac{1}{2} + \frac{2}{\pi}) + \frac{1}{4} - \frac{1}{\pi}$	$G_{0,0}(-\frac{1}{4} + \frac{1}{\pi}) - \frac{1}{32}$
(0, -1)	0	$G_{0,0}(\frac{1}{4} - \frac{1}{\pi}) + \frac{1}{32}$
(0, 0)	$G_{0,0}(-\frac{1}{4} + \frac{1}{\pi}) - \frac{1}{32}$	0

Table A.1: Values of the Green function derivative of the square lattice around the origin, with respect to the zipper depicted in Fig. 2.7.

over two different sets of edges, where the Green function  $G$  is to be replaced with the form appropriate to the boundary condition. Let us now observe that either sum may be extended to include all or some of those edges depicted at the bottom of Fig. A.3. Indeed, any of them brings a zero contribution to the sum, since

$$G_{u,(x,1)} G_{(x,0),v} - G_{u,(x,0)} G_{(x,1),v}$$

vanishes identically for both boundary conditions. For the open boundary, the relevant Green function  $G_{u,v}^{\text{op}}$  vanishes when one of its arguments is on the line  $y = 0$ ; while for the closed boundary, it satisfies the identities  $G_{u,(x,1)}^{\text{cl}} = G_{u,(x,0)}^{\text{cl}}$  and  $G_{(x,1),v}^{\text{cl}} = G_{(x,0),v}^{\text{cl}}$  for any sites  $u$  and  $v$ .

Instead of using the zipper  $Z_3$ , we can complement it with the segment lying between the two endpoints of  $Z_2$  and  $Z_3$ . We then see that the so-extended  $Z_3$  line together with the  $Z_2$  line form a closed circuit. The result of Appendix A.1 implies that the Green function derivatives  $G_{u,v}^{\text{op/cl}}(Z_2)$  and  $G_{u,v}^{\text{op/cl}}(Z_3)$  are equal or differ by a factor  $\pm G_{u,v}^{\text{op/cl}}$  depending on whether  $u$  and/or  $v$  are in the region delimited by the zippers  $Z_2$  and  $Z_3$  (including the boundary sites). We note that the fact that the



It is not difficult to see that  $\mathbf{G}^{\text{op}}(z)$  can be related, by the method of images, to an inverse Laplacian on the full plane. Because the method involves a reflection through the real axis, the relevant Laplacian on the full plane must be defined relative to two semi-infinite zippers, namely the original zipper  $Z_1$  in the UHP and its reflected version  $Z_1^*$ , starting on the edge  $((1, -y - 1), (0, -y - 1))$  and going downward. We shall denote by  $\Delta^*(z)$  and  $\mathbf{G}^*(z)$  the corresponding Laplacian and its inverse. The double zipper  $Z_1 \cup Z_1^*$  on the plane ensures the following symmetry  $\mathbf{G}_{u,v}^*(z) = \mathbf{G}_{u,v^*}^*(z)$  whenever  $u = (u_1, 0)$  is on the real axis, where  $v^* = (v_1, -v_2)$  is the reflected site of  $v = (v_1, v_2)$ . It then follows that  $\mathbf{G}^{\text{op}}(z)$  is equal to

$$\mathbf{G}_{u,v}^{\text{op}}(z) = \mathbf{G}_{u,v}^*(z) - \mathbf{G}_{u,v^*}^*(z), \quad u, v \in \text{UHP}. \quad (\text{A.11})$$

At order 0 in  $(1-z)$ , it yields the usual relation (2.54), while at order 1, we obtain,

$$G_{u,v}^{\prime\text{op}} = G_{u,v}^{\prime\uparrow} + G_{u,v}^{\prime\downarrow} - G_{u,v^*}^{\prime\uparrow} - G_{u,v^*}^{\prime\downarrow}, \quad v^* = (v_1, -v_2), \quad (\text{A.12})$$

where the up (resp. down) arrow refers to  $Z_1$  (resp.  $Z_1^*$ ).

A translation and a change of orientation, combined with a reflection for  $Z_1$ , bring the two zippers  $Z_1$  and  $Z_1^*$  onto the zipper we have used on the plane in Sections 2.2 and 2.3 (namely, starting at the edge  $((0, 0), (1, 0))$  and going downward). We therefore find the following relations:

$$\begin{aligned} G_{u,v}^{\prime\uparrow} &= -G'_{u^*+(0,y+1),v^*+(0,y+1)}, \\ G_{u,v}^{\prime\downarrow} &= -G'_{u+(0,y+1),v+(0,y+1)}, \end{aligned} \quad (\text{A.13})$$

where  $G'$  is computed relative to the zipper we used on the plane. Combining the previous two equations, we obtain Eq. (2.56):

$$\begin{aligned} G_{(u_1,u_2),(v_1,v_2)}^{\prime\text{op}} &= -G'_{(u_1,-u_2+y+1),(v_1,-v_2+y+1)} - G'_{(u_1,u_2+y+1),(v_1,v_2+y+1)} \\ &\quad + G'_{(u_1,-u_2+y+1),(v_1,v_2+y+1)} + G'_{(u_1,u_2+y+1),(v_1,-v_2+y+1)}. \end{aligned} \quad (\text{A.14})$$

The arguments are easily adapted to the closed boundary condition by taking into account the appropriate reflection, leading to

$$G_{u,v}^{\prime\text{cl}} = G_{u,v}^{\prime\uparrow} + G_{u,v}^{\prime\downarrow} + G_{u,v^*}^{\prime\uparrow} + G_{u,v^*}^{\prime\downarrow}, \quad v^* = (v_1, 1 - v_2). \quad (\text{A.15})$$

Paying attention to the way the zipper  $Z_1$  must be reflected readily gives the expression quoted in the text, in (2.57). Similarly, one finds that the corresponding derivatives on the diagonal upper half-plane are given by Eqs. (2.63) and (2.64).

### A.3 Modified graphs

Most of the spanning tree computations presented in the text involve the removal of one or more edges from the graph  $\mathcal{G} = \mathbb{Z}^2$  or  $\mathcal{G} = \mathbb{Z} \times \mathbb{N}^*$ . The resulting Laplacian  $\bar{\Delta}(z)$  on the modified graph  $\bar{\mathcal{G}}$  is a local perturbation of the original Laplacian  $\Delta(z)$  on the full graph by a matrix of finite rank. The inverse  $\bar{\mathbf{G}} = [\bar{\Delta}(z)]^{-1}$  and the determinant of  $\bar{\Delta}(z)$  can be computed in terms of the corresponding quantities for  $\Delta(z)$  by making use of the Woodbury formula. As  $\Delta(z)^t = \Delta(z^{-1})$  and  $\bar{\Delta}(z)^t = \bar{\Delta}(z^{-1})$ , the modified Laplacian can be written as  $\bar{\Delta} = \Delta - U^t U$  if the removed edges have a trivial parallel transport. In which case the Woodbury formula implies

$$\bar{\Delta}^{-1} = \Delta^{-1} + [\Delta^{-1} U^t (\mathbb{I} - U \Delta^{-1} U^t)^{-1} U \Delta^{-1}], \quad (\text{A.16})$$

$$\det \bar{\Delta} = \det \Delta \times \det(\mathbb{I} - U \Delta^{-1} U^t). \quad (\text{A.17})$$

When the perturbation  $U^t U$  has finite rank  $r$ , the matrix  $U$  may be taken as an  $r \times \infty$  rectangular matrix. Then the matrix to be inverted,  $\mathbb{I} - U \Delta^{-1} U^t$ , is  $r$ -dimensional, as is the last determinant on the second line. If  $U^t U$  has rank 1, the Woodbury formula reduces to the Sherman-Morrison formula.

Let us first illustrate the use of the Woodbury formula when two edges are removed, as was the case for single-site probabilities on the plane, reviewed in Section 2.2. The computations required to remove the two edges  $\{5, 2\}$  and  $\{5, 3\}$ . The only nonzero entries of the perturbation  $U^t U$  have row and column indices in the set  $\{5, 2, 3\}$ , and are given by

$$U^t U \Big|_{\{5,2,3\}} = \begin{pmatrix} 2 & -1 & -1 \\ -1 & 1 & 0 \\ -1 & 0 & 1 \end{pmatrix}. \quad (\text{A.18})$$

This matrix being of rank 2, a convenient choice is to take

$$U = \begin{pmatrix} \cdots & 1 & -1 & 0 & \cdots \\ \cdots & 1 & 0 & -1 & \cdots \end{pmatrix}, \quad (\text{A.19})$$

where the columns shown are labeled by the vertices 5, 2 and 3, all the others being identically zero.

The matrices  $\overline{\Delta}$  and  $\Delta$  in (A.16) depend on  $z$ , but for the purpose of computing  $\overline{G}$  and  $\overline{G}'$ , only the zeroth and first orders in  $z - 1$  are required. By using the following explicit values of  $G, G'$  on the plane, see Table A.1,

$$\begin{aligned} G_{2,5} &= G_{3,5} = G_{0,0} - \frac{1}{4}, & G_{2,3} &= G_{0,0} - \frac{1}{\pi}, \\ G'_{2,5} &= \frac{1}{4}G_{0,0} - \frac{3}{32}, & G'_{2,3} &= \left(\frac{1}{2} - \frac{1}{\pi}\right)G_{0,0} - \frac{1}{4\pi}, \\ G'_{5,3} &= \left(\frac{1}{4} - \frac{1}{\pi}\right)G_{0,0} + \frac{1}{32}, \end{aligned} \quad (\text{A.20})$$

one finds the expansion of  $(\mathbb{I} - U\Delta^{-1}U^t)^{-1}$  to first order,

$$\begin{aligned} (\mathbb{I} - U\Delta^{-1}U^t)^{-1} &= \frac{\pi}{2(\pi-1)} \begin{pmatrix} \pi & \pi-2 \\ \pi-2 & \pi \end{pmatrix} \\ &+ \frac{\pi(4-\pi)}{16(\pi-1)} \begin{pmatrix} 0 & 1 \\ -1 & 0 \end{pmatrix} (z-1) + \mathcal{O}(z-1)^2. \end{aligned} \quad (\text{A.21})$$

It leads to the following expression for  $\overline{\mathbf{G}}$ , valid to first order,

$$\begin{aligned} \overline{\mathbf{G}}_{u,v} &= \mathbf{G}_{u,v} + \frac{\pi}{2} (2\mathbf{G}_{u,5} - \mathbf{G}_{u,2} - \mathbf{G}_{u,3}) (2\mathbf{G}_{5,v} - \mathbf{G}_{2,v} - \mathbf{G}_{3,v}) \\ &+ \frac{\pi}{2(\pi-1)} (\mathbf{G}_{u,2} - \mathbf{G}_{u,3}) (\mathbf{G}_{2,v} - \mathbf{G}_{3,v}) \\ &+ \frac{\pi(4-\pi)}{32(\pi-1)} (z-1) \left\{ (G_{u,2} - G_{u,3}) (2G_{5,v} - G_{2,v} - G_{3,v}) \right. \\ &\left. - (2G_{u,5} - G_{u,2} - G_{u,3}) (G_{2,v} - G_{3,v}) \right\} + \dots \end{aligned} \quad (\text{A.22})$$

from which the explicit formulas for  $\overline{G}$  and  $\overline{G}'$  needed in Section 2.2 are easily derived. The ratio of partition functions, needed in the same calculations of Section 2.2, is straightforward to compute in the limit  $z \rightarrow 1$ :

$$\frac{\overline{Z}}{Z} = \frac{\det \overline{\Delta}}{\det \Delta} = \det(\mathbb{I} - U\Delta^{-1}U^t) = \frac{\pi-1}{\pi^2}. \quad (\text{A.23})$$

In the calculation of multisite probabilities presented in Section 2.3, extra lattice changes were to be considered, namely the removal of three edges in the neighborhood of each height 1. For simplicity, let us focus on  $\mathbb{P}_{2,1}(\vec{r})$ , which was shown to be given in terms of essentially the same grove fractions as for  $\mathbb{P}_2$ , but on a lattice  $\tilde{\mathcal{G}}$  obtained from  $\mathbb{Z}^2$  by cutting three edges around the height 1. One may therefore proceed in two steps.

The first step relates the Green function  $\overline{\mathbf{G}}(z)$  on the fully modified lattice  $\tilde{\mathcal{G}}$  to the function  $\tilde{\mathbf{G}}(z)$  pertaining to  $\tilde{\mathcal{G}}$ . For this, we use the Woodbury formula (A.16) with the matrix given in (A.19). Because the entries  $\overline{\mathbf{G}}_{u,v}(z)$  are only required for  $u, v$  close to site  $i$  (where the height 2 is located), see the expression (2.43), we similarly need the entries of  $\tilde{\mathbf{G}}(z)$  for sites close to  $i$ .

The second step is to relate  $\tilde{\mathbf{G}}(z)$  to  $\mathbf{G}(z)$ , the  $z$ -dependent Green function on the usual square lattice  $\mathbb{Z}^2$ . For this, we use a second matrix  $V$  implementing the removal of the three edges between site 7 and sites 8, 9 and 10, as pictured in Figure 2.9. Again, a convenient choice is to set

$$V = \begin{pmatrix} 1 & -1 & 0 & 0 \\ \cdots & 1 & 0 & -1 & 0 & \cdots \\ 1 & 0 & 0 & -1 \end{pmatrix}. \quad (\text{A.24})$$

However, since  $V$  is located around the distant site  $j$  (with height 1), the Woodbury identity shows that the calculation of  $\tilde{\mathbf{G}}_{u,v}(z)$  for  $u, v$  close to site  $i$  requires the knowledge of  $\mathbf{G}_{u,v}(z)$  for  $u$  and/or  $v$  close to site  $j$ , namely far from the head of the zipper. The zeroth order in  $z - 1$ , namely  $G_{u,v}$ , is well known and has been recalled in (A.3). To compute the first order  $G'_{u,v}$ , the technique reviewed in Appendix A.1 is no longer helpful, as one would need to add an arbitrarily large number of new zipper edges. Indeed, we found it more convenient to resort to the defining expression (A.4) for  $G'_{u,v}$  in which we use the integral representation (A.2) of  $G_{u,v}$ . In this way, the infinite summation over the edges of the zipper can easily be carried out.

As an illustration, let us review the calculation of  $G'_{u,v}$  where  $u = (0, 0)$  is the origin and  $v = \vec{r} = (p, q)$  is the site 7 (the height 1). As before, the edges crossed by the zipper form the set  $\{(k, \ell) = (k, k + (1, 0))\}$  where  $k$  runs over the sites  $(0, -m)$  with  $m \geq 0$ . For simplicity, we assume  $q$

to be positive and large, and show later on how to deal with other cases, i.e.  $q$  small and/or negative. Since calculations of two-site probabilities in Section 2.3 are carried out to order  $r^{-6}$ , our purpose here is likewise to obtain the asymptotic expansion of  $G'_{0,\vec{r}}$  to that order. According to (A.4), and for  $q$  positive, it is given by

$$\begin{aligned}
G'_{0,\vec{r}} &= \sum_k (G_{0,\ell} G_{k,\vec{r}} - G_{0,k} G_{\ell,\vec{r}}) \\
&= \sum_{m \geq 0} \left( G(1, m) G(p, q+m) - G(0, m) G(p-1, q+m) \right) \\
&= \sum_{m \geq 0} \int_0^\pi \int_0^\pi \frac{d\alpha_1 d\alpha_2}{4\pi^2} \frac{\cos p\alpha_1 \cos \alpha_2 - \cos[(p-1)\alpha_1]}{\sqrt{y_1^2-1}\sqrt{y_2^2-1}} t_1^{q+m} t_2^m \\
&= \int_0^\pi \frac{d\alpha_1}{2\pi} \frac{t_1^q}{\sqrt{y_1^2-1}} \int_0^\pi \frac{d\alpha_2}{2\pi} \frac{\cos p\alpha_1 \cos \alpha_2 - \cos[(p-1)\alpha_1]}{\sqrt{y_2^2-1}} \frac{1}{1-t_1 t_2},
\end{aligned} \tag{A.25}$$

where  $y_i \equiv y(\alpha_i)$  and  $t_i \equiv t(\alpha_i)$ , defined right after (A.2).

The principle underlying the asymptotic evaluation of this double integral is simple [81]. One first observes that the function  $t_1$  of  $\alpha_1$  decreases away from the origin. From  $t_1 \simeq 1 - \alpha_1 + \dots$  for small  $\alpha_1$ , it follows that for large  $q$ ,  $t_1^q \simeq e^{-q\alpha_1}$  decreases exponentially (with polynomial corrections, see below). This suggests to expand the rest of the integrand in powers of  $\alpha_1$  and simply integrate term by term. A simple dimensional analysis shows that the integral of  $e^{-q\alpha_1} \alpha_1^k$  contributes to order  $r^{-(k+1)}$ , so that the expansion of the integrand to order  $\alpha_1^5$  is sufficient. In fact, the only integrals we shall need are the following one,

$$\begin{aligned}
&\int_0^\infty d\alpha_1 e^{-q\alpha_1} \frac{\sin p\alpha_1}{\alpha_1} (A \log \alpha_1 + B) \\
&= \frac{1}{2} \left\{ 2B - A [\log(p^2 + q^2) + 2\gamma] \right\} \arctan \frac{p}{q},
\end{aligned} \tag{A.26}$$

and its  $p$ - and  $q$ -derivatives (in order to bring higher powers of  $\alpha_1$  in the integrand). The extension of the integration domain from  $[0, \pi]$  to  $[0, \infty)$  is valid up to exponentially small corrections.

The idea just explained is simple but requires extra care for two reasons. First, the naive expansion of the integrand in powers of  $\alpha_1$ , before doing the integral over  $\alpha_2$ , is not allowed because it yields increasingly singular

functions of  $\alpha_2$ , which are not integrable. And second, as noted above,  $G'_{0,\vec{r}}$  is expected to contain a divergent piece proportional to  $G_{0,0}$ , which needs to be properly identified.

In order to handle these two difficulties, we split the expression (A.25) into three pieces,

$$G'_{0,\vec{r}} = \int_0^\pi \frac{d\alpha_1}{4\pi^2} \frac{t_1^q}{\sqrt{y_1^2 - 1}} \int_0^\pi d\alpha_2 \frac{\cos p\alpha_1 (\cos \alpha_2 - 1)}{\sqrt{y_2^2 - 1}} \frac{1}{1 - t_1 t_2} \quad (\text{A.27})$$

$$+ \int_0^\pi \frac{d\alpha_1}{4\pi^2} \frac{t_1^q}{\sqrt{y_1^2 - 1}} \int_0^\pi d\alpha_2 \frac{\cos p\alpha_1 - \cos (p-1)\alpha_1}{\sqrt{y_2^2 - 1}} \times \left( \frac{1}{1 - t_1 t_2} - \frac{1}{1 - t_1} \right) \quad (\text{A.28})$$

$$+ \int_0^\pi \frac{d\alpha_1}{4\pi^2} \frac{t_1^q}{\sqrt{y_1^2 - 1}} \int_0^\pi d\alpha_2 \frac{\cos p\alpha_1 - \cos (p-1)\alpha_1}{\sqrt{y_2^2 - 1}} \frac{1}{1 - t_1}, \quad (\text{A.29})$$

which we call respectively  $G_1$ ,  $G_2$  and  $G_3$ .

**First contribution.** We rewrite the function of  $\alpha_2$  involved in  $G_1$  as

$$\left\{ \frac{\cos \alpha_2 - 1}{\sqrt{y_2^2 - 1}(1 - t_1 t_2)} - \frac{\alpha_1 + \frac{\alpha_1^3}{12} + \frac{\alpha_1^5}{120}}{2\sqrt{y_3^2 - 1}} \right\} + \frac{\alpha_1 + \frac{\alpha_1^3}{12} + \frac{\alpha_1^5}{120}}{2\sqrt{y_3^2 - 1}}, \quad (\text{A.30})$$

where  $y_3 \equiv y(\alpha_1 + \alpha_2)$ . In the first term inside the brackets, the subtracted term is such that the expansion in  $\alpha_1$  to order 6 produces coefficients that are regular functions of  $\alpha_2$ , which can be integrated exactly,

$$\int_0^\pi d\alpha_2 \left\{ \frac{\cos \alpha_2 - 1}{\sqrt{y_2^2 - 1}(1 - t_1 t_2)} - \frac{\alpha_1 + \frac{\alpha_1^3}{12} + \frac{\alpha_1^5}{120}}{2\sqrt{y_3^2 - 1}} \right\} \quad (\text{A.31})$$

$$= -\frac{3\pi}{4} - \frac{\alpha_1^2}{4\sqrt{2}} - \frac{7\alpha_1^4}{192\sqrt{2}} - \frac{137\alpha_1^6}{30720\sqrt{2}} + \dots$$

The function in the second term of Eq. (A.30) can also be integrated exactly and then expanded for small  $\alpha_1$ ,

$$\int_0^\pi \frac{d\alpha_2}{\sqrt{y_3^2 - 1}} = \left[ -\operatorname{arcth} \frac{\sqrt{2} \cos \frac{\alpha_2}{2}}{\sqrt{3 - \cos \alpha_2}} \right]_{\alpha_1}^{\pi + \alpha_1}$$

$$= -\log \alpha_1 + \frac{3}{2} \log 2 + \frac{\alpha_1}{2\sqrt{2}} + \frac{\alpha_1^2}{24} + \frac{\alpha_1^3}{32\sqrt{2}} \quad (\text{A.32})$$

$$- \frac{43\alpha_1^4}{5760} + \frac{11\alpha_1^5}{5120\sqrt{2}} + \frac{949\alpha_1^6}{725760} + \dots$$

The two terms together and the further expansion of  $(y_1^2 - 1)^{-1/2}$  yield

$$G_1 = -\frac{3}{8}G_{0,\bar{r}} + \int_0^\pi \frac{d\alpha_1}{8\pi^2} t_1^q \cos p\alpha_1 \left\{ \left( -\log \alpha_1 + \frac{3}{2} \log 2 \right) \right. \\ \left. \times \left( 1 + \frac{\alpha_1^4}{32} \right) + \frac{\alpha_1^2}{24} - \frac{43\alpha_1^4}{5760} + \dots \right\}. \quad (\text{A.33})$$

**Second contribution.** We use the same subtraction trick to rewrite the function in (A.28) as

$$\left\{ \frac{1}{\sqrt{y_2^2 - 1}} \left( \frac{1}{1 - t_1 t_2} - \frac{1}{1 - t_1} \right) + \frac{1 + \frac{\alpha_1^2}{4} + \frac{\alpha_1^4}{96} + \frac{19\alpha_1^6}{5760}}{\sqrt{y_1^2 - 1}\sqrt{y_3^2 - 1}} \right\} \\ - \frac{1 + \frac{\alpha_1^2}{4} + \frac{\alpha_1^4}{96} + \frac{19\alpha_1^6}{5760}}{\sqrt{y_1^2 - 1}\sqrt{y_3^2 - 1}}$$

and apply the same method as for  $G_1$ . The integral of the function in curly brackets yields

$$\int_0^\pi d\alpha_2 \left\{ \frac{1}{\sqrt{y_2^2 - 1}} \left( \frac{1}{1 - t_1 t_2} - \frac{1}{1 - t_1} \right) + \frac{1 + \frac{\alpha_1^2}{4} + \frac{\alpha_1^4}{96} + \frac{19\alpha_1^6}{5760}}{\sqrt{y_1^2 - 1}\sqrt{y_3^2 - 1}} \right\} \\ = \frac{1}{2\sqrt{2}} + \frac{11\alpha_1^2}{96\sqrt{2}} + \frac{787\alpha_1^4}{46080\sqrt{2}} + \dots \quad (\text{A.34})$$

Together with the previous result (A.32), simple trigonometric identities and a few more expansions in  $\alpha_1$ , it leads to the following expression for  $G_2$ ,

$$G_2 = -\int_0^\pi \frac{d\alpha_1}{8\pi^2} t_1^q \cos p\alpha_1 \left\{ \left( -\log \alpha_1 + \frac{3}{2} \log 2 \right) \left( 1 + \frac{\alpha_1^4}{32} \right) + \frac{\alpha_1^2}{24} - \frac{43\alpha_1^4}{5760} + \dots \right\} \\ + \int_0^\pi \frac{d\alpha_1}{8\pi^2} t_1^q \sin p\alpha_1 \left\{ \left( -\log \alpha_1 + \frac{3}{2} \log 2 \right) \left( \frac{2}{\alpha_1} - \frac{\alpha_1}{6} + \frac{43\alpha_1^3}{720} - \frac{949\alpha_1^5}{60480} \right) \right. \\ \left. + \frac{\alpha_1}{12} - \frac{7\alpha_1^3}{320} + \frac{4607\alpha_1^5}{725760} + \dots \right\}. \quad (\text{A.35})$$

Curiously, the first integral is exactly the opposite of that in  $G_1$ , so that the two cancel out.

**Third contribution.** The last contribution (A.29) is the simplest one since the two integrals are decoupled, the one over  $\alpha_2$  simply giving a

multiple of  $G_{0,0}$ . A few expansions yield

$$G_3 = -G_{0,0} \int_0^\pi \frac{d\alpha_1}{2\pi} t_1^q \left\{ \sin p\alpha_1 \left( \frac{1}{\alpha_1} + \frac{1}{2} - \frac{\alpha_1}{12} - \frac{\alpha_1^2}{8} - \frac{\alpha_1^3}{720} \right. \right. \\ \left. \left. + \frac{5\alpha_1^4}{192} - \frac{\alpha_1^5}{30240} + \dots \right) + \cos p\alpha_1 \left( \frac{1}{2} + \frac{\alpha_1}{4} - \frac{\alpha_1^3}{24} + \frac{19\alpha_1^5}{1920} + \dots \right) \right\}. \quad (\text{A.36})$$

The last step before doing the remaining integrals is to recast  $t_1^q$  into a more workable function. The expansion of  $\log t_1$ ,

$$\log t_1 = -\alpha_1 + \frac{\alpha_1^3}{12} - \frac{\alpha_1^5}{96} + \frac{79\alpha_1^7}{40320} + \dots, \quad (\text{A.37})$$

shows that the following expansion is sufficient to finish the calculations to the required order,

$$t_1^q = e^{-q\alpha_1} \left( 1 + \frac{q\alpha_1^3}{12} - \frac{q\alpha_1^5}{96} + \frac{q^2\alpha_1^6}{288} + \frac{79q\alpha_1^7}{40320} - \frac{q^2\alpha_1^8}{1152} + \frac{q^3\alpha_1^9}{10368} + \dots \right). \quad (\text{A.38})$$

By using the integral (A.26), the rest of the computation is straightforward. For completeness, we give the final result, more conveniently expressed in polar coordinates,  $p = r \cos \varphi$ ,  $q = r \sin \varphi$  with  $0 < \varphi < \pi$ , so  $p^2 + q^2 = r^2$  and  $\arctan(p/q) = \pi/2 - \varphi$ :

$$G'_{0,\bar{r}} = G_{0,0} \left( \frac{\varphi}{2\pi} - \frac{5}{8} - \frac{\cos \varphi - \sin \varphi}{4\pi r} - \frac{3 \cos 2\varphi - \sin 4\varphi}{24\pi r^2} \right. \\ - \frac{\cos 3\varphi + \sin 3\varphi + \cos 5\varphi - \sin 5\varphi}{16\pi r^3} \\ - \frac{27 \sin 4\varphi + 60 \cos 6\varphi - 25 \sin 8\varphi}{480 \pi r^4} - \frac{5[\cos 7\varphi + \sin 7\varphi + \cos 9\varphi - \sin 9\varphi]}{32\pi r^5} \\ \left. - \frac{189 \cos 6\varphi + 972 \sin 8\varphi + 2205 \cos 10\varphi - 980 \sin 12\varphi}{4032 \pi r^6} + \dots \right) \\ - (\log r + \gamma + \frac{3}{2} \log 2) \left( -\frac{5\pi - 4\varphi}{16\pi^2} + \frac{\sin 4\varphi}{48\pi^2 r^2} + \frac{18 \sin 4\varphi + 25 \sin 8\varphi}{960 \pi^2 r^4} \right. \\ \left. + \frac{459 \sin 8\varphi + 490 \sin 12\varphi}{4032 \pi^2 r^6} + \dots \right) \\ - \frac{1}{4} (5\pi - 4\varphi) \left( \frac{\cos 4\varphi}{48\pi^2 r^2} + \frac{18 \cos 4\varphi + 25 \cos 8\varphi}{960 \pi^2 r^4} + \frac{459 \cos 8\varphi + 490 \cos 12\varphi}{4032 \pi^2 r^6} + \dots \right) \\ + \frac{\sin 4\varphi}{32\pi^2 r^2} + \frac{90 \sin 4\varphi + 137 \sin 8\varphi}{2304 \pi^2 r^4} + \frac{3483 \sin 8\varphi + 3805 \sin 12\varphi}{11520 \pi^2 r^6} + \dots \quad (\text{A.39})$$

The expression, albeit complicated, remarkably simplifies for diagonal positions  $\vec{r} = (p, p)$  ( $\varphi = \frac{\pi}{4}$ ) and vertical positions  $\vec{r} = (0, q)$  ( $\varphi = \frac{\pi}{2}$ ):

$$G'_{0,(p,p)} = -\frac{1}{2}G_{0,0} + \frac{1}{4\pi}(\log r + \gamma + \frac{3}{2}\log 2) + \frac{1}{48\pi r^2} - \frac{7}{960\pi r^4} + \frac{31}{4032\pi r^6} + \dots \quad (\text{A.40})$$

$$G'_{0,(0,q)} = G_{0,0} \left( -\frac{3}{8} + \frac{1}{4\pi r} + \frac{1}{8\pi r^2} + \frac{1}{8\pi r^3} + \frac{1}{8\pi r^4} + \frac{5}{16\pi r^5} + \frac{19}{32\pi r^6} \right) + \frac{3}{16\pi}(\log r + \gamma + \frac{3}{2}\log 2) - \frac{1}{64\pi r^2} - \frac{43}{1280\pi r^4} - \frac{949}{5376\pi r^6} + \dots \quad (\text{A.41})$$

This is best understood using the technique reviewed in Appendix A.1, which enables us to write  $G'_{0,\vec{r}}$  as a finite sum whose number of terms grows linearly with  $p$  or  $q$ . In case  $p = q$  or  $p = 0$ , huge cancellations happen, and we are left with only a few terms:

$$G'_{0,(p,p)} = -\frac{1}{2}G(p, p), \quad (\text{A.42})$$

$$G'_{0,(0,q)} = -\frac{1}{2}G(0, q) + \frac{1}{2}G(0, 0)G(0, q-1) - \frac{1}{2}G(1, 0)G(0, q). \quad (\text{A.43})$$

Next we discuss the extension of  $G'_{0,\vec{r}}$  with  $r \gg 1$  to  $\pi \leq \varphi \leq 2\pi$ . Remember indeed that the development presented above only holds if  $q = r \sin \varphi \gg 1$ . If  $q$  is small (i.e.  $\varphi$  close to 0,  $\pi$  or  $2\pi$ ),  $G'_{0,\vec{r}}$  can still be evaluated for  $|p| \gg 1$  using transformation properties of  $G'$  under zipper deformations:

$$G'_{0,(p,q)} = G'_{0,(-q,p)} - G(0, 0)G(p-1, q) + G(1, 0)G(p, q), \quad (\text{A.44})$$

$$G'_{0,(p,q)} = G'_{0,(q,-p)} + G(0, 0)G(p, q-1) - G(1, 0)G(p, q), \quad (\text{A.45})$$

for  $p > 0$  and  $p < 0$ , respectively. If rather  $|q| \gg 1$  but  $q < 0$ , the asymptotic expression of the derivative of the Green function may be obtained from the following relation:

$$G'_{0,\vec{r}} = G'_{0,-\vec{r}} + G_{0,0} [G(p, q-1) - 2G(p, q) + G(p+1, q)] - \frac{1}{2}\text{sign}(p - \frac{1}{2}) G(p, q). \quad (\text{A.46})$$

## A.4 Triangular lattice

In this appendix, we first recall some exact values of the Green function of the triangular lattice for small distances, as well as its asymptotic expansion for large distances. Then we discuss the methods we used to compute the Green function derivative on the full plane, with respect to the zipper depicted in Fig. 2.14. We work out an example in details for the short- and large-distance regimes, to illustrate the general principle of computation. The analogous developments for the hexagonal lattice will be skipped (indeed, remember that the Green functions of both lattices are related through Eq. (2.106)).

### A.4.1 Values of Green functions

In the coordinate system of Section 2.5, the Green function of the triangular lattice was given in integral form in (2.85),

$$\begin{aligned} G_{(x_1, y_1), (x_2, y_2)} &= G(x_1 - x_2, y_1 - y_2) \\ &= \int_{-\pi}^{\pi} \frac{d\theta_1}{2\pi} \int_{-\pi}^{\pi} \frac{d\theta_2}{2\pi} \frac{e^{i(x_1 - x_2)\theta_1 + i(y_1 - y_2)\theta_2}}{6 - 2\cos\theta_1 - 2\cos\theta_2 - 2\cos(\theta_1 + \theta_2)}. \end{aligned} \quad (\text{A.47})$$

One of the two integrals can be worked out explicitly, and leads to the following result [3, 37]:

$$G(x, y) = \int_0^{\pi/2} \frac{d\theta}{2\pi} \frac{e^{-|x-y|s(\theta)} \cos[(x+y)\theta]}{\sin\theta\sqrt{4-\cos^2\theta}}, \quad (\text{A.48})$$

where the function  $s(\theta)$  is defined as follows for  $0 \leq \theta \leq \pi/2$ :

$$\begin{aligned} s(\theta) &= \log \left[ \tan\theta\sqrt{4-\cos^2\theta} + \sqrt{4\tan^2\theta + \cos^2\theta} \right] \\ &= \sqrt{3}\theta + \frac{2\theta^5}{15\sqrt{3}} + \frac{2\theta^9}{135\sqrt{3}} + \dots \end{aligned} \quad (\text{A.49})$$

In Table A.2, we list the value of the Green function for small separations [3], where  $G_{0,0} \equiv G(0,0)$  is the divergent part of the integral (A.48). The large-distance expansion of  $G(x, y)$  can be computed from the corresponding result on the hexagonal lattice [4] and is given by

$$G(x, y) = G_{0,0} - \frac{1}{2\sqrt{3}\pi} \left( \log r + \gamma + \frac{1}{2} \log 12 \right) + \frac{\cos 6\varphi}{60\sqrt{3}\pi r^4} + \mathcal{O}(r^{-6}), \quad (\text{A.50})$$

where  $r = \sqrt{x^2 + y^2 - xy} \gg 1$  and  $\varphi$  is the angle between the horizontal axis and  $(x, y)$ , i.e.  $x = r \cos \varphi + \frac{r}{\sqrt{3}} \sin \varphi$  and  $y = \frac{2r}{\sqrt{3}} \sin \varphi$ . Here  $\gamma = 0.577216\dots$  is the Euler constant.

$\phi(x, y)$	$y = -2$	$y = -1$	$y = 0$	$y = 1$	$y = 2$
$x = -2$	$-\frac{4}{3} + \frac{2\sqrt{3}}{\pi}$	$\frac{1}{3} - \frac{\sqrt{3}}{\pi}$	$-\frac{4}{3} + \frac{2\sqrt{3}}{\pi}$	$\frac{5}{2} - \frac{5\sqrt{3}}{\pi}$	$-8 + \frac{14\sqrt{3}}{\pi}$
$x = -1$	$\frac{1}{3} - \frac{\sqrt{3}}{\pi}$	$-\frac{1}{6}$	$-\frac{1}{6}$	$\frac{1}{3} - \frac{\sqrt{3}}{\pi}$	$\frac{5}{2} - \frac{5\sqrt{3}}{\pi}$
$x = 0$	$-\frac{4}{3} + \frac{2\sqrt{3}}{\pi}$	$-\frac{1}{6}$	$0$	$-\frac{1}{6}$	$-\frac{4}{3} + \frac{2\sqrt{3}}{\pi}$
$x = 1$	$\frac{5}{2} - \frac{5\sqrt{3}}{\pi}$	$\frac{1}{3} - \frac{\sqrt{3}}{\pi}$	$-\frac{1}{6}$	$-\frac{1}{6}$	$\frac{1}{3} - \frac{\sqrt{3}}{\pi}$
$x = 2$	$-8 + \frac{14\sqrt{3}}{\pi}$	$\frac{5}{2} - \frac{5\sqrt{3}}{\pi}$	$-\frac{4}{3} + \frac{2\sqrt{3}}{\pi}$	$\frac{1}{3} - \frac{\sqrt{3}}{\pi}$	$-\frac{4}{3} + \frac{2\sqrt{3}}{\pi}$

Table A.2: Values of the Green function of the triangular lattice for small distances, with  $\phi(x, y) = G(x, y) - G_{0,0}$ .

#### A.4.2 Green function derivative for small distances

The definition (1.28) of the Green function derivative  $G'$  with respect to the zipper in Fig. 2.14 yields:

$$\begin{aligned}
 G'_{(x_1, y_1), (x_2, y_2)} = \sum_{k=0}^{\infty} & \left[ G_{(x_1, y_1), (1, -k)} G_{(0, -k), (x_2, y_2)} \right. \\
 & - G_{(x_1, y_1), (0, -k)} G_{(1, -k), (x_2, y_2)} \\
 & + G_{(x_1, y_1), (1, -k)} G_{(0, -k-1), (x_2, y_2)} \\
 & \left. - G_{(x_1, y_1), (0, -k-1)} G_{(1, -k), (x_2, y_2)} \right]. \tag{A.51}
 \end{aligned}$$

For generic vertices  $u_i = (x_i, y_i)$ ,  $G'$  must be computed through an explicit summation over all zipper edges using the integral representation of the Green function (A.48). However, if  $u_1, u_2$  are close to the head of the zipper (i.e. close to the origin of the lattice), we can find the value  $G'$  using its symmetries and transformation properties recalled in Appendix A.1.

Let us illustrate how these properties can be used to obtain an explicit expression for the Green function derivative [91]. Consider for instance the vertices  $u_1 = (0, 0)$  and  $u_2 = (3, 1)$  together with the zipper represented in the first panel of Fig. A.4. We begin by moving the head of the

zipper while keeping  $u_1, u_2$  fixed, that is, we add the following edges to the sum in Eq. (A.51):  $(1, 1) - (1, 0)$ ,  $(2, 1) - (1, 0)$ ,  $(2, 1) - (2, 0)$ . Then we deform and rotate the zipper counterclockwise so that it points upward (see panels (c)-(d) in Fig. A.4). Since in doing so we drag the zipper across  $u_2$ , the derivative picks up an additional term  $+G_{u_1, u_2}$ . Finally, we rotate the whole lattice by  $180^\circ$  to the left, with both  $u_1, u_2$  and the zipper included, and we shift it so that  $u_2$  now lies at the original position of  $u_1$  (and vice versa). The antisymmetry of  $G'_{u_1, u_2}$  allows one to recast  $G'_{(0,0),(3,1)}$  as the sum of a finite number of terms. One finds

$$\begin{aligned}
G'_{(0,0),(3,1)} &= \frac{1}{2} \left\{ G_{(0,0),(1,1)} G_{(1,0),(3,1)} - G_{(0,0),(1,0)} G_{(1,1),(3,1)} \right. \\
&\quad + G_{(0,0),(2,1)} G_{(1,0),(3,1)} - G_{(0,0),(1,0)} G_{(2,1),(3,1)} \\
&\quad \left. + G_{(0,0),(2,1)} G_{(2,0),(3,1)} - G_{(0,0),(2,0)} G_{(2,1),(3,1)} - G_{(0,0),(3,1)} \right\} \\
&= \frac{1}{2} \left\{ G(1, 1)G(2, 1) - G(1, 0)G(2, 0) + G(2, 1)G(2, 1) \right. \\
&\quad - G(1, 0)G(1, 0) + G(2, 1)G(1, 1) \\
&\quad \left. - G(2, 0)G(1, 0) - G(3, 1) \right\} \\
&= G_{0,0} \left( \frac{5}{3} - \frac{4\sqrt{3}}{\pi} \right) - \frac{107}{72} + \frac{8}{\sqrt{3}\pi} + \frac{3}{2\pi^2},
\end{aligned} \tag{A.52}$$

where the values of  $G(x, y)$  given in Table A.2 have been used together with the symmetry relation  $G(3, 1) = G(-2, 1)$ . Proceeding this way, one finds the values of the Green function derivative evaluated at the origin and its six neighbors with respect to this particular zipper, as tabulated in Table A.3.

### A.4.3 Green function derivative for large distances

On the upper half-lattice, the image method allows one to write  $G'^{\text{op}}$  in terms of  $G'$  on the full triangular lattice, with respect to the zippers depicted in Figs. 2.14 and 2.17 for the full lattice and the half-lattice respectively. In particular, for vertices  $u_i$  of the form  $(a_i, p+b_i)$  with

$G'_{u_1, u_2}$	(0, 0)	(1, 0)	(1, 1)	(0, 1)
(0, 0)	0	$-\frac{2}{3}G_{0,0} + \frac{7}{72}$	$-\frac{1}{3}G_{0,0} + \frac{5}{72}$	$-\frac{1}{6}G_{0,0} + \frac{1}{24}$
(1, 0)	$\frac{2}{3}G_{0,0} - \frac{7}{72}$	0	$\frac{1}{3}G_{0,0} - \frac{5}{72}$	$\frac{1}{2}G_{0,0} + \frac{1}{6} - \frac{\sqrt{3}}{2\pi}$
(1, 1)	$\frac{1}{3}G_{0,0} - \frac{5}{72}$	$-\frac{1}{3}G_{0,0} + \frac{5}{72}$	0	$\frac{1}{6}G_{0,0} - \frac{1}{24}$
(0, 1)	$\frac{1}{6}G_{0,0} - \frac{1}{24}$	$-\frac{1}{2}G_{0,0} - \frac{1}{6} + \frac{\sqrt{3}}{2\pi}$	$-\frac{1}{6}G_{0,0} + \frac{1}{24}$	0
(-1, 0)	$G_{0,0} \left( -\frac{1}{2} + \frac{\sqrt{3}}{\pi} \right) - \frac{1}{72}$	$G_{0,0} \left( -\frac{7}{6} + \frac{\sqrt{3}}{\pi} \right) + \frac{7}{9} - \frac{7}{2\sqrt{3}\pi}$	$G_{0,0} \left( -\frac{5}{6} + \frac{\sqrt{3}}{\pi} \right) - \frac{1}{9} + \frac{1}{\sqrt{3}\pi}$	$G_{0,0} \left( -\frac{2}{3} + \frac{\sqrt{3}}{\pi} \right) + \frac{1}{8} - \frac{1}{2\sqrt{3}\pi}$
(-1, -1)	$G_{0,0} \left( \frac{1}{2} - \frac{\sqrt{3}}{\pi} \right) + \frac{1}{72}$	$G_{0,0} \left( -\frac{1}{6} - \frac{\sqrt{3}}{\pi} \right) - \frac{2}{9} + \frac{2}{\sqrt{3}\pi}$	$G_{0,0} \left( \frac{1}{6} - \frac{\sqrt{3}}{\pi} \right) + \frac{5}{9} - \frac{5}{2\sqrt{3}\pi}$	$G_{0,0} \left( \frac{1}{3} - \frac{\sqrt{3}}{\pi} \right) - \frac{11}{36} + \frac{2}{\sqrt{3}\pi}$
(0, -1)	$-\frac{1}{6}G_{0,0} + \frac{1}{24}$	$-\frac{5}{6}G_{0,0} + \frac{1}{8}$	$-\frac{1}{2}G_{0,0} - \frac{1}{6} + \frac{\sqrt{3}}{2\pi}$	$-\frac{1}{3}G_{0,0} + \frac{23}{36} - \frac{\sqrt{3}}{\pi}$

$G'_{u_1, u_2}$	(-1, 0)	(-1, -1)	(0, -1)
(0, 0)	$G_{0,0} \left( \frac{1}{2} - \frac{\sqrt{3}}{\pi} \right) + \frac{1}{72}$	$G_{0,0} \left( -\frac{1}{2} + \frac{\sqrt{3}}{\pi} \right) - \frac{1}{72}$	$\frac{1}{6}G_{0,0} - \frac{1}{24}$
(1, 0)	$G_{0,0} \left( \frac{7}{6} - \frac{\sqrt{3}}{\pi} \right) - \frac{7}{9} + \frac{7}{2\sqrt{3}\pi}$	$G_{0,0} \left( \frac{1}{6} + \frac{\sqrt{3}}{\pi} \right) + \frac{2}{9} - \frac{2}{\sqrt{3}\pi}$	$\frac{5}{6}G_{0,0} - \frac{1}{8}$
(1, 1)	$G_{0,0} \left( \frac{5}{6} - \frac{\sqrt{3}}{\pi} \right) + \frac{1}{9} - \frac{1}{\sqrt{3}\pi}$	$G_{0,0} \left( -\frac{1}{6} + \frac{\sqrt{3}}{\pi} \right) - \frac{5}{9} + \frac{5}{2\sqrt{3}\pi}$	$\frac{1}{2}G_{0,0} + \frac{1}{6} - \frac{\sqrt{3}}{2\pi}$
(0, 1)	$G_{0,0} \left( \frac{2}{3} - \frac{\sqrt{3}}{\pi} \right) - \frac{1}{8} + \frac{1}{2\sqrt{3}\pi}$	$G_{0,0} \left( -\frac{1}{3} + \frac{\sqrt{3}}{\pi} \right) + \frac{11}{36} - \frac{2}{\sqrt{3}\pi}$	$\frac{1}{3}G_{0,0} - \frac{23}{36} + \frac{\sqrt{3}}{\pi}$
(-1, 0)	0	$G_{0,0} \left( -1 + \frac{2\sqrt{3}}{\pi} \right) + \frac{11}{72} - \frac{1}{\sqrt{3}\pi}$	$G_{0,0} \left( -\frac{1}{3} + \frac{\sqrt{3}}{\pi} \right) + \frac{11}{36} - \frac{2}{\sqrt{3}\pi}$
(-1, -1)	$G_{0,0} \left( 1 - \frac{2\sqrt{3}}{\pi} \right) - \frac{11}{72} + \frac{1}{\sqrt{3}\pi}$	0	$G_{0,0} \left( \frac{2}{3} - \frac{\sqrt{3}}{\pi} \right) - \frac{1}{8} + \frac{1}{2\sqrt{3}\pi}$
(0, -1)	$G_{0,0} \left( \frac{1}{3} - \frac{\sqrt{3}}{\pi} \right) - \frac{11}{36} + \frac{2}{\sqrt{3}\pi}$	$G_{0,0} \left( -\frac{2}{3} + \frac{\sqrt{3}}{\pi} \right) + \frac{1}{8} - \frac{1}{2\sqrt{3}\pi}$	0

Table A.3: Values of the Green function derivative of the triangular lattice around the origin, with respect to the zipper shown in panel (a) of Fig. A.4.

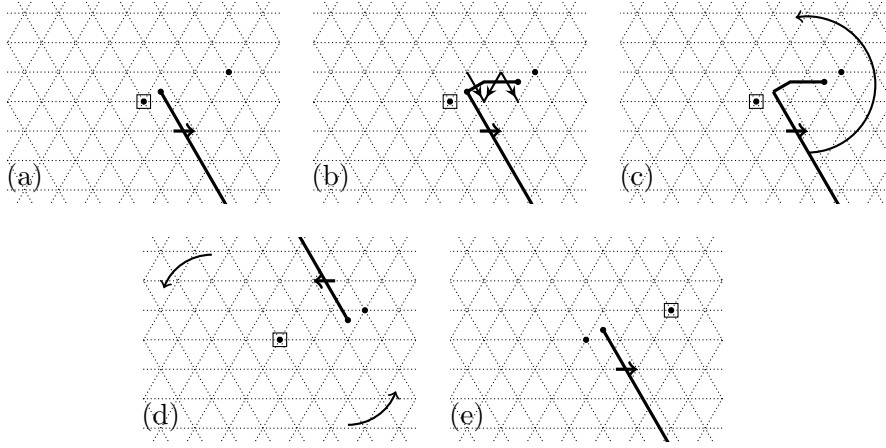


Figure A.4: Computation of  $G'_{(0,0),(3,1)}$  for the triangular lattice. The boxed vertex corresponds to the first argument of the derivative  $G'$ . The panels (a)-(e) illustrate the transformations explained in the text.

$a_i, b_i = o(1)$ , Eq. (2.97) yields

$$\begin{aligned}
 G'_{(a_1, p+b_1), (a_2, p+b_2)}^{\text{op}} &= G'_{(-a_1, -b_1), (-a_2, -b_2)} - G'_{(-a_1, -b_1), (p-a_2+b_2, 2p+b_2)} \\
 &\quad - G'_{(p-a_1+b_1, 2p+b_1), (-a_2, -b_2)} \\
 &\quad + G'_{(p-a_1+b_1, 2p+b_1), (p-a_2+b_2, 2p+b_2)}.
 \end{aligned}
 \tag{A.53}$$

In Appendix A.4.2, we have shown how to compute the first term on the right-hand side, using the transformation properties of the Green function derivative  $G'$ . The remaining terms can in principle be evaluated in the same fashion. However, it would require the addition of  $\mathcal{O}(p)$  extra edges to move the head of the zipper, and then evaluating the resulting sum for large  $p$ . Instead we found it more convenient to start from (1.28) and the integral representation (A.48) of the Green function. As an example, we compute the asymptotic expansion of  $G'_{u_1, u_2}$  for  $u_1 = (0, 0)$ ,

$u_2 = (p, 2p+1)$  in powers of  $1/p$ :

$$\begin{aligned}
G'_{(0,0),(p,2p+1)} &= \sum_{k=0}^{\infty} \left[ G_{(0,0),(1,-k)} G_{(0,-k),(p,2p+1)} \right. \\
&\quad - G_{(0,0),(0,-k)} G_{(1,-k),(p,2p+1)} \\
&\quad + G_{(0,0),(1,-k)} G_{(0,-k-1),(p,2p+1)} \\
&\quad \left. - G_{(0,0),(0,-k-1)} G_{(1,-k),(p,2p+1)} \right] \\
&= \sum_{k=0}^{\infty} \left[ G(k, -1) G(2p+k+1, p) - G(k, 0) G(2p+k+1, p-1) \right. \\
&\quad \left. + G(k, -1) G(2p+k+2, p) - G(k+1, 0) G(2p+k+1, p-1) \right] \\
&= \sum_{k=0}^{\infty} \int_0^{\pi/2} \frac{d\theta_1}{2\pi} \int_0^{\pi/2} \frac{d\theta_2}{2\pi} \frac{e^{-k s_1} e^{-(p+k+1) s_2}}{\sin \theta_1 \sin \theta_2 \sqrt{4 - \cos^2 \theta_1} \sqrt{4 - \cos^2 \theta_2}} \\
&\quad \times \left\{ e^{-s_1} \cos[(k-1)\theta_1] \cos[(3p+k+1)\theta_2] - e^{-s_2} \cos[k\theta_1] \cos[(3p+k)\theta_2] \right. \\
&\quad + e^{-(s_1+s_2)} \cos[(k-1)\theta_1] \cos[(3p+k+2)\theta_2] \\
&\quad \left. - e^{-(s_1+s_2)} \cos[(k+1)\theta_1] \cos[(3p+k)\theta_2] \right\}, \tag{A.54}
\end{aligned}$$

where  $s_i \equiv s(\theta_i) = \log \left[ \tan \theta_i \sqrt{4 - \cos^2 \theta_i} + \sqrt{4 \tan^2 \theta_i + \cos^2 \theta_i} \right]$  for  $i = 1, 2$ . The summation over  $k$  can be computed exactly and yields

$$\begin{aligned}
G'_{(0,0),(p,2p+1)} &= \frac{1}{4\pi^2} \int_0^{\pi/2} d\theta_1 \int_0^{\pi/2} d\theta_2 e^{-p s_2} \cos[3p\theta_2] f_1(\theta_1, \theta_2) \\
&\quad + \frac{1}{4\pi^2} \int_0^{\pi/2} d\theta_1 \int_0^{\pi/2} d\theta_2 e^{-p s_2} \sin[3p\theta_2] f_2(\theta_1, \theta_2), \tag{A.55}
\end{aligned}$$

where  $f_1, f_2$  are explicitly known functions of  $\theta_1, \theta_2$  that do not depend on  $p$ . For large values of the distance  $p$ ,  $e^{-p s_2} \simeq e^{-\sqrt{3} p \theta_2}$  (A.49), so the main contribution to the integral over  $\theta_2$  comes from the region  $\theta_2 \sim 0$ .

From the integrals

$$\begin{aligned} \int_0^{\pi/2} d\theta_2 e^{-p s_2} \cos(3p\theta_2) &\simeq \int_0^\infty d\theta_2 e^{-\sqrt{3}p\theta_2} \cos(3p\theta_2) + \mathcal{O}(p^{-5}) \\ &= \frac{1}{4\sqrt{3}p} + \mathcal{O}(p^{-5}), \end{aligned} \quad (\text{A.56})$$

$$\begin{aligned} \int_0^{\pi/2} d\theta_2 e^{-p s_2} \sin(3p\theta_2) &\simeq \int_0^\infty d\theta_2 e^{-\sqrt{3}p\theta_2} \sin(3p\theta_2) + \mathcal{O}(p^{-5}) \\ &= \frac{1}{4p} + \mathcal{O}(p^{-5}), \end{aligned} \quad (\text{A.57})$$

where we have neglected exponentially small terms, it follows that

$$\begin{aligned} \int_0^{\pi/2} d\theta_2 e^{-p s_2} \cos(3p\theta_2) \theta_2^k &\simeq \mathcal{O}(p^{-k-1}), \\ \int_0^{\pi/2} d\theta_2 e^{-p s_2} \sin(3p\theta_2) \theta_2^k &\simeq \mathcal{O}(p^{-k-1}). \end{aligned} \quad (\text{A.58})$$

A power expansion of  $f_i(\theta_1, \theta_2)$  ( $i=1, 2$ ) up to order  $\theta_2$  would therefore be enough to obtain  $G'_{(0,0),(p,2p+1)}$  up to order  $1/p^2$ , which is expected to be the leading (nonconstant) order contributing to  $\mathbb{P}_a^{\text{OP}}(i)$  on the half-lattice. However, a naive expansion in  $\theta_2$  of  $f_i(\theta_1, \theta_2)$  ( $i=1, 2$ ) yields nonintegrable coefficients. To avoid this, we split both integrands in Eq. (A.55) into two and three pieces respectively:

$$\begin{aligned} &\left\{ f_1(\theta_1, \theta_2) - \frac{1 - \sqrt{3}\theta_2}{\sin(\theta_1 + \theta_2)\sqrt{4 - \cos^2(\theta_1 + \theta_2)}} \right\} \\ &+ \frac{1 - \sqrt{3}\theta_2}{\sin(\theta_1 + \theta_2)\sqrt{4 - \cos^2(\theta_1 + \theta_2)}}, \end{aligned} \quad (\text{A.59})$$

$$\begin{aligned} &\left\{ f_2(\theta_1, \theta_2) - \frac{\frac{1}{\theta_2} - \sqrt{3} + \theta_2}{\sin(\theta_1 + \theta_2)\sqrt{4 - \cos^2(\theta_1 + \theta_2)}} - \frac{-\frac{1}{\theta_2} + \frac{4}{\sqrt{3}} - \frac{8\theta_2}{3}}{\sin\theta_1\sqrt{4 - \cos^2\theta_1}} \right\} \\ &+ \frac{\frac{1}{\theta_2} - \sqrt{3} + \theta_2}{\sin(\theta_1 + \theta_2)\sqrt{4 - \cos^2(\theta_1 + \theta_2)}} + \frac{-\frac{1}{\theta_2} + \frac{4}{\sqrt{3}} - \frac{8\theta_2}{3}}{\sin\theta_1\sqrt{4 - \cos^2\theta_1}}. \end{aligned} \quad (\text{A.60})$$

By construction, the terms between brackets can be expanded in powers of  $\theta_2$  up to first order and then be integrated over  $\theta_1$ . Their integrals

read:

$$\int_0^{\pi/2} d\theta_1 \left\{ f_1(\theta_1, \theta_2) - \frac{1 - \sqrt{3}\theta_2}{\sin(\theta_1 + \theta_2)\sqrt{4 - \cos^2(\theta_1 + \theta_2)}} \right\} \\ = -\frac{\pi}{3\sqrt{3}\theta_2} + \frac{\pi}{3} - \left( \frac{1}{2} + \frac{\pi}{3\sqrt{3}} \right) \theta_2 + \mathcal{O}(\theta_2^2), \quad (\text{A.61})$$

$$\int_0^{\pi/2} d\theta_1 \left\{ f_2(\theta_1, \theta_2) - \frac{\frac{1}{\theta_2} - \sqrt{3} + \theta_2}{\sin(\theta_1 + \theta_2)\sqrt{4 - \cos^2(\theta_1 + \theta_2)}} \right. \\ \left. - \frac{-\frac{1}{\theta_2} + \frac{4}{\sqrt{3}} - \frac{8\theta_2}{3}}{\sin\theta_1\sqrt{4 - \cos^2\theta_1}} \right\} \\ = -\frac{1}{2} + \frac{\pi}{3\sqrt{3}} + \left( \frac{\sqrt{3}}{2} - \frac{\pi}{3} \right) \theta_2 + \mathcal{O}(\theta_2^2). \quad (\text{A.62})$$

The first counterterm in Eqs. (A.59) and (A.60) can be integrated exactly over  $\theta_1$ , and then expanded in powers of  $\theta_2$ :

$$\int_0^{\pi/2} d\theta_1 \frac{1}{\sin(\theta_1 + \theta_2)\sqrt{4 - \cos^2(\theta_1 + \theta_2)}} \\ = \frac{\log 3 - 2 \log \theta_2}{2\sqrt{3}} + \frac{\theta_2}{2} + \frac{5\theta_2^3}{48} - \frac{\theta_2^4}{45\sqrt{3}} + \mathcal{O}(\theta_2^5). \quad (\text{A.63})$$

The second counterterm in Eq. (A.60) is divergent, and is proportional to the divergent part of the Green function (A.48):

$$\int_0^{\pi/2} d\theta_1 \frac{1}{\sin\theta_1\sqrt{4 - \cos^2\theta_1}} = 2\pi G_{0,0}. \quad (\text{A.64})$$

Finally, we can carry out the integral over  $\theta_2$  using Eqs. (A.56),(A.57) in addition to the following results (and their derivatives with respect to  $p$ ):

$$\int_0^{\pi/2} d\theta_2 e^{-p s_2} \cos(3p\theta_2) \frac{1}{\theta_2} \simeq 2\sqrt{3}\pi G_{0,0} - (\log p + \gamma + \log 6) \\ + \mathcal{O}(p^{-4}), \quad (\text{A.65})$$

$$\int_0^{\pi/2} d\theta_2 e^{-p s_2} \sin(3p\theta_2) \frac{1}{\theta_2} \simeq \frac{\pi}{3} + \mathcal{O}(p^{-4}), \quad (\text{A.66})$$

$$\int_0^{\pi/2} d\theta_2 e^{-p s_2} \sin(3p\theta_2) \frac{\log \theta_2}{\theta_2} \simeq -\frac{\pi}{3} \left( \log p + \gamma + \frac{1}{2} \log 12 \right) \\ + \mathcal{O}(p^{-4} \log p), \quad (\text{A.67})$$

where we have dropped exponentially small terms. Up to order  $1/p^2$ , we find that  $G'_{(0,0),(p,2p+1)}$  reads:

$$\begin{aligned}
G'_{(0,0),(p,2p+1)} &= G_{0,0} \left( -\frac{1}{3} + \frac{1}{2\sqrt{3}\pi p} - \frac{1}{6\sqrt{3}\pi p^2} \right) + (\log p + \gamma + \log 6) \\
&\quad \times \left( \frac{1}{6\sqrt{3}\pi} - \frac{1}{24\pi^2 p} + \frac{1}{48\pi^2 p^2} \right) \\
&\quad + \frac{1}{12\sqrt{3}\pi p} - \frac{9 + 2\sqrt{3}\pi}{432\pi^2 p^2} + \mathcal{O}(p^{-3} \log p).
\end{aligned} \tag{A.68}$$

The development presented above allows one to compute the asymptotic expansion for the second and third terms of Eq. (A.53), that is, for  $G'_{u_1, u_2}$  when only one of its arguments is close to the head of the zipper. The fourth term however corresponds to a derivative  $G'_{u_1, u_2}$  where both  $u_i = (p+a_i, 2p+b_i)$  ( $i = 1, 2$ ) are far away from the zipper. In that case, the arguments of the Green functions appearing on the right-hand side of Eq. (A.51) are large. Hence, we can use the asymptotic expansion (A.50) before summing over  $k$  to get the power expansion of  $G'_{u_1, u_2}$  through the Euler-Maclaurin formula. For example, for  $a_1 = b_1 = 0$ ,  $a_2 = b_2 = -1$ , the derivative of the Green function reads

$$\begin{aligned}
G'_{(p,2p),(p-1,2p-1)} &= G_{0,0} \left( \frac{1}{4\sqrt{3}\pi p} + \frac{7}{24\sqrt{3}\pi p^2} \right) \\
&\quad + (\log p + \gamma + \log 6) \left( -\frac{1}{24\pi^2 p} - \frac{7}{144\pi^2 p^2} \right) \\
&\quad - \frac{1}{24\pi^2 p} - \frac{1}{32\pi^2 p^2} + \mathcal{O}(p^{-3} \log p).
\end{aligned} \tag{A.69}$$

## Appendix B

# Symmetries and maps between predecessor diagrams on half-planes

In Section 2.4, we computed one-site probabilities  $\mathbb{P}_a(i)$  on (horizontal and diagonal) upper half-planes, and several two-site probabilities  $\mathbb{P}_{a,1}(i, j)$  on the horizontal half-plane. The boundary conditions considered were either fully open or fully closed. Contrary to their full-plane analogues for one-site probabilities, predecessor diagrams on half-planes are not invariant under rotations by  $90^\circ$ . However, the probabilities of occurrence of some diagrams are related to one another through simple transformations. Since all four cases are similar, we provide a detailed discussion only for the upper half-plane  $\mathcal{G} = \mathbb{Z} \times \mathbb{N}^*$  with a horizontal open boundary. For more generality, we discuss the case of an  $n$ -site probability with  $n-1$  heights equal to 1. As explained in Section 1.4, the probabilities associated with predecessor diagrams only depend on the Green function  $G^{\text{op}}$  and its derivative  $G'^{\text{op}}$ . Since we shall not refer to other types of Green functions in this section, we shall drop the superscript “op” for both functions, i.e. write  $G, G'$  for  $G^{\text{op}}, G'^{\text{op}}$ .

Let us consider multisite probabilities  $\mathbb{P}_{a,1,\dots,1}(i_1, \dots, i_n)$  on the upper half-plane  $\mathcal{G} = \mathbb{Z} \times \mathbb{N}^*$  with open boundary conditions, where the height  $a$  is at  $i_1$ . The reference sites  $i_k$  have coordinates  $(x_k, y_k)$  and are assumed

to be far away from one another and from the boundary. For each  $k$ , we denote by  $\mathcal{V}_k = \{i_k, N_k, E_k, S_k, W_k\}$  the close neighborhood of  $i_k$ , containing  $i_k$  and its four nearest neighbors. The actual calculation of  $\mathbb{P}_{a,1,\dots,1}(i_1, \dots, i_n)$  requires that the graph  $\mathcal{G}$  be modified by removing certain edges around the reference sites. The removal of edges around  $i_k$  is implemented by a matrix  $U_k$  so that the Laplacian on the modified graph  $\bar{\mathcal{G}}$  can be written as  $\bar{\Delta} = \Delta - U^t U = \Delta - \sum_{k=1}^n U_k^t U_k$  (see Appendix A.3; the matrix  $U$  here is obtained simply by piling up the rectangular matrices  $U_k$ ). Note that each of the  $U_k$ 's is defined up to a sign.

### Height-one probabilities

We first consider the joint probabilities  $\mathbb{P}_{1,\dots,1}(i_1, \dots, i_n)$  of heights 1. In this case, each  $U_k$  is a rectangular  $3 \times \infty$  matrix, of the form given in (A.24): it is identically zero for column labels outside of  $\mathcal{V}_k$ , the column with entries equal to 1 corresponds to  $i_k$ , while the three columns with one entry equal to  $-1$  are labeled by three neighbors of  $i_k$ . As recalled above, which three neighbors of  $i_k$  are chosen is irrelevant. We can write the multisite probability symmetrically, as a  $3n \times 3n$  determinant,

$$\mathbb{P}_{1,\dots,1}(i_1, \dots, i_n) = \det(\mathbb{I} - UGU^t), \quad (\text{B.1})$$

with  $G = (\Delta_{\mathcal{G}})^{-1}$  is the Green matrix on the (unmodified) upper half-plane with open boundary condition. We want to show that the probability  $\mathbb{P}_{1,\dots,1}(i_1, \dots, i_n)$  is an even function of each of the  $y_k$  variables.

Because of the structure of  $U$ , the determinant involves only the Green matrix entries contained in the blocks  $G_{\mathcal{V}_\ell, \mathcal{V}_{\ell'}}$ , for  $1 \leq \ell, \ell' \leq n$ . The transformation  $y_k \mapsto -y_k$  affects those entries of  $G$  labeled by sites in  $\mathcal{V}_k$ . If one denotes the neighbors of  $i_k$  as  $(x_k + a, y_k + b)$  for some  $a, b = 0, \pm 1$ , then (2.54), or (A.11), implies the following transformations:

$$\begin{aligned} G_{(x_k+a, y_k+b), (x_k+c, y_k+d)} \Big|_{y_k \mapsto -y_k} &= G_{(x_k+a, -y_k+b), (x_k+c, -y_k+d)} \\ &= G_{(x_k+a, y_k-b), (x_k+c, y_k-d)}, \end{aligned} \quad (\text{B.2a})$$

$$G_{(x_k+a, y_k+b), v} \Big|_{y_k \mapsto -y_k} = -G_{(x_k+a, y_k-b), v}, \quad (\text{B.2b})$$

$$G_{u, (x_k+c, y_k+d), v} \Big|_{y_k \mapsto -y_k} = -G_{u, (x_k+c, y_k-d), v}, \quad (\text{B.2c})$$

if  $u$  and  $v$  are far from  $i_k$ . Up to a sign, replacing  $y_k$  with its opposite amounts to exchanging the northern neighbor  $N_k$  of  $i_k$  with its southern neighbor  $S_k$ . This is equivalent to conjugating  $G$  with a matrix  $\Sigma_k$ , equal to the infinite permutation matrix  $\sigma_k$  permuting  $N_k$  and  $S_k$  times a matrix that is minus the identity on the  $5 \times 5$  block labeled by sites of  $\mathcal{V}_k$ , and the identity elsewhere. We write

$$\Sigma_k = \mathbb{I}_{\mathcal{G} \setminus \mathcal{V}_k} \oplus (-\sigma_k) \Big|_{\mathcal{V}_k}, \quad \sigma_k \Big|_{\mathcal{V}_k} = \begin{pmatrix} i_k & N_k & E_k & S_k & W_k \\ 1 & 0 & 0 & 0 & 0 \\ 0 & 0 & 0 & 1 & 0 \\ 0 & 0 & 1 & 0 & 0 \\ 0 & 1 & 0 & 0 & 0 \\ 0 & 0 & 0 & 0 & 1 \end{pmatrix}. \quad (\text{B.3})$$

This leads to the following transformation

$$\mathbb{P}_{1, \dots, 1}(i_1, \dots, i_n) \Big|_{y_k \mapsto -y_k} = \det(\mathbb{I} - U \Sigma_k G \Sigma_k^t U^t). \quad (\text{B.4})$$

It is not difficult to see that the factor  $-\sigma_k$  can be absorbed into a redefinition of  $U_k$  into  $-U_k \sigma_k$  (since  $U_k$  is identically zero for column indices outside of  $\mathcal{V}_k$ ). As observed above, the sign is irrelevant, so we can say that  $U_k$  is simply redefined into  $\hat{U}_k \equiv U_k \sigma_k$ , which means that a different choice is made for the removal of edges around  $i_k$ . Since this probability does not depend on this choice (see Section 2.1.3), we obtain the result as claimed,

$$\mathbb{P}_{1, \dots, 1}(i_1, \dots, i_n) \Big|_{y_k \mapsto -y_k} = \mathbb{P}_{1, \dots, 1}(i_1, \dots, i_n). \quad (\text{B.5})$$

Let us note that the identity is true to all orders in the variables  $y_k$ , and not only at the order relevant for the scaling limit.

## Predecessor diagrams with leaves

Next we look at joint probabilities  $\mathbb{P}_{a, 1, \dots, 1}(i_1, \dots, i_n)$  for which site  $i_1$  has height  $a \geq 2$ . It requires to compute various fractions of spanning trees where  $i_1$  has at least one predecessor among its neighbors while all other reference sites have none. We shall denote by  $X_D^{\mathcal{G}}$  the fraction of spanning trees on  $\mathcal{G}$  corresponding to a given predecessor diagram  $D$

around  $i_1$ . As shown in the text in Section 2.3, it can be done in two steps. The first step considers a modified lattice  $\tilde{\mathcal{G}}$  in order to enforce a height 1 at the sites  $i_k$ , for  $k \geq 2$ . This first modification is controlled by the same rectangular matrices  $U_{k \geq 2}$ , discussed in the previous case. We then obtain

$$X_D^{\mathcal{G}} = X_D^{\tilde{\mathcal{G}}} \times \frac{\det \Delta_{\tilde{\mathcal{G}}}}{\det \Delta_{\mathcal{G}}} = X_D^{\tilde{\mathcal{G}}} \times \mathbb{P}_{1, \dots, 1}^{\mathcal{G}}(i_2, \dots, i_n). \quad (\text{B.6})$$

In the second step, the fraction  $X_D^{\tilde{\mathcal{G}}}$  is computed using the grove theorem (Theorem 1.5), together with the insertion of a zipper anchored at  $i_1$  as well as a further modification of  $\tilde{\mathcal{G}}$  to  $\bar{\mathcal{G}}$ , by which two edges incident to  $i_1$  are removed to form an annular-one graph. It involves a perturbation matrix  $U_1$ , of the form (A.19), with nonzero entries corresponding to sites of  $\mathcal{V}_1$  (see also below). Then  $X_D^{\tilde{\mathcal{G}}}$  can be expressed in terms of  $\bar{\mathcal{G}}, \bar{\mathcal{G}}'$ , evaluated at the nodes lying around the “hole” of the annulus, namely at  $\mathcal{V}_1$ . From the relation  $\bar{\Delta}(z) = \Delta(z) - \sum_{k=1}^n U_k^t U_k$ , namely we include the zipper on both  $\bar{\mathcal{G}}$  and  $\mathcal{G}$ , the entries of  $\bar{\mathcal{G}}, \bar{\mathcal{G}}'$  on sites of  $\mathcal{V}_1$  may be written in terms of entries of  $G$  and  $G'$ . Indeed, the Woodbury formula enables one to relate  $\bar{\mathbf{G}}(z)$  to  $\mathbf{G}(z)$ . An expansion in powers of  $z-1$  then yields

$$\bar{G} = G + GU^t A^{-1} UG, \quad \text{with } A = \mathbb{I} - UGU^t, \quad (\text{B.7})$$

$$\bar{G}' = G' + G'U^t A^{-1} UG + GU^t A^{-1} UG'U^t A^{-1} UG + GU^t A^{-1} UG', \quad (\text{B.8})$$

where  $U$  is the matrix obtained by piling up all  $U_k$ 's, for  $1 \leq k \leq n$ .

Let us now examine the effect on  $X_D^{\mathcal{G}}$  of changing the sign of  $y_k$ . We first discuss the easier case  $k \geq 2$ . We have seen in the previous subsection that the transformation  $y_k \mapsto -y_k$  has the effect of replacing the Green matrix  $G$  with its conjugate  $\Sigma_k G \Sigma_k$ . The conjugation may itself be absorbed in the redefinition of  $U_k$  into  $\hat{U}_k = U_k \sigma_k$  and leaves the factor  $\mathbb{P}_{1, \dots, 1}^{\mathcal{G}}(i_2, \dots, i_n)$  invariant. It is not difficult to see that the transformation has the same effect on  $\bar{G}$ : it replaces  $U_k$  with  $\hat{U}_k$  and conjugates  $\bar{G}$  with  $\Sigma_k$ .

In fact, exactly the same conclusion applies to  $\bar{G}'$  provided the site  $i_k$  is far from the zipper (this restriction is what makes the case  $k = 1$

different). It follows from the relation (A.11), which shows that  $G'$  obeys the same relations (B.2) as  $G$ , implying that it too gets conjugated with  $\Sigma_k$  when one transforms  $y_k$  to  $-y_k$ . The equation (B.8) readily shows that the transformations of  $\bar{G}$  and  $\bar{G}'$  are strictly identical.

We know that  $X_D^{\tilde{\mathcal{G}}}$  may be written in terms of the entries  $\bar{G}_{u,v}$  and  $\bar{G}'_{u,v}$  for  $u, v \in \mathcal{V}_1$ . Because  $\Sigma_k$  is trivial on sites far from  $\mathcal{V}_k$ , the conjugation with  $\Sigma_k$  has no effect at all on sites of  $\mathcal{V}_1$ ,

$$\bar{G}_{u,v} \Big|_{U_k} \longrightarrow (\Sigma_k \bar{G} \Sigma_k)_{u,v} = \bar{G}_{u,v} \Big|_{\hat{U}_k}, \quad u, v \in \mathcal{V}_1, \quad (\text{B.9})$$

and similarly for  $\bar{G}'_{u,v}$ . The notation on the left-hand side (resp. right-hand side) of the equation indicates that the removed edges around  $i_k$  in the modified graph  $\bar{\mathcal{G}}$  are encoded in  $U_k$  (resp.  $\hat{U}_k$ ). It follows that the net effect of the transformation  $y_k \mapsto -y_k$  is to replace  $U_k$  with  $\hat{U}_k$ , and is therefore irrelevant. Hence, we conclude that  $X_D^{\tilde{\mathcal{G}}}$  and  $\mathbb{P}_{a,1,\dots,1}(i_1, \dots, i_n)$  are even functions of  $y_k$  for any  $k \geq 2$ .

The effect of the transformation  $y_1 \mapsto -y_1$  on a fraction  $X_D^{\tilde{\mathcal{G}}}$  is similar to some extent, but differs by the presence of the zipper in the neighborhood of  $i_1$ . The transformation of  $\bar{G}$  can be computed along the same lines as above, but that of  $\bar{G}'$  is tricky to write in general, because the precise location of the zipper depends on the edge cuts necessary to make of  $\tilde{\mathcal{G}}$  an annular-one graph, which themselves depend on the predecessor diagram one considers. So we shall illustrate the computation in a specific example, namely the case of  $\mathbb{P}_2^{\text{op}}(i_1)$  discussed in Section 2.4.1. There we claimed that the transformation  $y_1 \mapsto -y_1$  exchanges the two fractions of spanning trees  $X_1^{\text{S}}(i_1)$  and  $X_1^{\text{N}}(i_1)$ , for which the reference site  $i_1$  has its southern (resp. northern) neighbor as its unique predecessor. As one does not enforce any height 1, there is no first modification to consider, so that  $\tilde{\mathcal{G}} = \mathcal{G}$ .

To compute  $X_1^{\text{S}}(i_1)$ , we define the annular-one graph  $\bar{\mathcal{G}}$  by removing the edges connecting  $i_1$  to its northern and western neighbors, meaning that we choose the matrix  $U_1$  as

$$U_1 = \begin{pmatrix} & i_1 & N_1 & E_1 & S_1 & W_1 & \\ \cdots & 1 & -1 & 0 & 0 & 0 & \cdots \\ \cdots & 1 & 0 & 0 & 0 & -1 & \cdots \end{pmatrix}, \quad (\text{B.10})$$

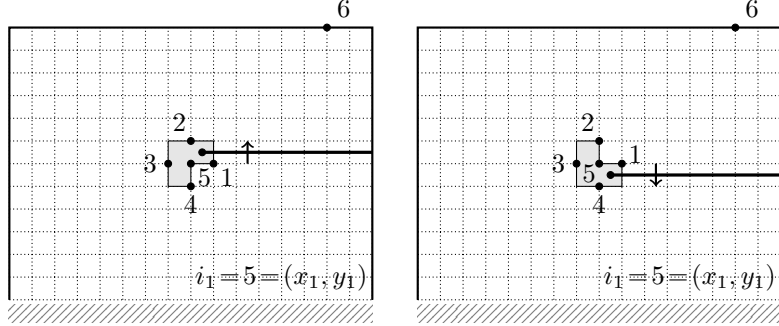


Figure B.1: Schematic representation of the graphs  $\bar{G}$  modified according to  $U_1$  (left) and to  $\hat{U}_1 = U_1\sigma_1$  (right), as used for the computation of  $X_1^S(i_1)$  and  $X_1^N(i_1)$ , together with their nodes and zipper.

The vertices of  $\mathcal{V}_1 = \{i_1, N_1, E_1, S_1, W_1\}$  are nodes, with the sink  $s$  taken as the sixth node as usual. To facilitate the calculations, we choose, as represented on the left panel of Fig. B.1, a semi-infinite zipper going horizontally to the right, with a nontrivial parallel transport  $z \in \mathbb{C}^*$  on the oriented edges  $((x_1+k+1, y_1), (x_1+k+1, y_1+1))$ , for  $k \geq 0$ .

From Section 2.2, the fraction  $X_1^S(i_1)$  is equal to the following ratio:

$$\begin{aligned} X_1^S(i_1) &= 3 \frac{\bar{Z}[4|12356]}{Z} \\ &= 3 \frac{\bar{Z}}{Z} \left[ (\bar{G}_{4,4} - \bar{G}_{4,5}) - (\bar{G}_{3,4} - \bar{G}_{3,5} - \bar{G}'_{3,4} + \bar{G}'_{3,5} - \bar{G}'_{4,5}) \right]. \end{aligned} \quad (\text{B.11})$$

The effect on  $\bar{G}$  of the change  $y_1 \mapsto -y_1$  is exactly the same as the one computed above:  $\bar{G}$  gets conjugated with  $\Sigma_1$  and at the same time, the matrix  $U_1$  is replaced with  $\hat{U}_1 \equiv U_1\sigma_1$ , where  $\sigma_1$  acts on  $\mathcal{V}_1$  by exchanging  $N_1$  and  $S_1$ . However, since  $\bar{G}$  is evaluated at sites in  $\mathcal{V}_1$ , the conjugation is nontrivial, yielding

$$\bar{G}_{u,v} \Big|_{U_1} \longrightarrow (\Sigma_1 \bar{G} \Sigma_1)_{u,v} = \bar{G}_{\sigma_1(u), \sigma_1(v)} \Big|_{\hat{U}_1}, \quad u, v \in \mathcal{V}_1, \quad (\text{B.12})$$

Similarly we find using Eq. (A.17) that

$$\frac{\bar{Z}}{Z} \Big|_{U_1} \longrightarrow \frac{\bar{Z}}{Z} \Big|_{\hat{U}_1}.$$

We compute the change of  $\bar{G}'$  by using its expression in terms of  $\bar{G}$  itself,

$$\bar{G}'_{u,v} = \sum_{k=0}^{\infty} \left( \bar{G}_{u,(x_1+k+1,y_1+1)} \bar{G}_{(x_1+k+1,y_1),v} - \bar{G}_{u,(x_1+k+1,y_1)} \bar{G}_{(x_1+k+1,y_1+1),v} \right). \quad (\text{B.13})$$

For  $u$  and  $v$  in  $\mathcal{V}_1$ , it yields the following transformation

$$\begin{aligned} \bar{G}'_{u,v} \Big|_{U_1} &\longrightarrow \sum_{k=0}^{\infty} \left( \bar{G}_{\sigma_1(u),(x_1+k+1,y_1-1)} \bar{G}_{(x_1+k+1,y_1),\sigma_1(v)} \right. \\ &\quad \left. - \bar{G}_{\sigma_1(u),(x_1+k+1,y_1)} \bar{G}_{(x_1+k+1,y_1-1),\sigma_1(v)} \right) \Big|_{\hat{U}_1} \\ &= \bar{G}_{\sigma_1(u),\sigma_1(v)}^{\text{new}} \Big|_{\hat{U}_1}, \end{aligned} \quad (\text{B.14})$$

where in addition to the action of  $\sigma_1$  as seen before, the derivative  $\bar{G}^{\text{new}}$  is defined with respect to a new zipper, located one lattice spacing below the original one, and with a reversed orientation, now pointing downward, see the right panel of Fig. B.1. Note that the hollow face has also been reversed, since the edge cuts are now prescribed by  $\hat{U}_1$ ; the edges connecting  $i_1$  to its western and southern neighbors are accordingly removed.

Altogether, we obtain

$$\begin{aligned} X_1^{\text{S}}(i_1) \Big|_{y_1 \mapsto -y_1} &= 3 \frac{\bar{Z}}{Z} \left[ (\bar{G}_{2,2} - \bar{G}_{2,5}) \right. \\ &\quad \left. - (\bar{G}_{3,2} - \bar{G}_{3,5} - \bar{G}_{3,2}^{\text{new}} + \bar{G}_{3,5}^{\text{new}} - \bar{G}_{2,5}^{\text{new}}) \right] \Big|_{\hat{U}_1}, \end{aligned} \quad (\text{B.15})$$

where the bar refers to the lattice  $\bar{\mathcal{G}}$  modified according to  $\hat{U}_1 = U_1 \sigma_1$ . It is straightforward to see that the combinatorial expression appearing on the right-hand side is that of  $3\bar{Z}[2|13456]/Z$ , and that it is equal to the fraction of spanning trees on the original graph  $\mathcal{G}$  such that  $i_1$  has its northern neighbor  $N_1$  as its unique predecessor. We therefore find

$$X_1^{\text{S}}(i_1) \Big|_{y_1 \mapsto -y_1} = X_1^{\text{N}}(i_1). \quad (\text{B.16})$$

Using a similar argument, one can show that

$$X_1^{\text{E}}(i_1) \Big|_{y_1 \mapsto -y_1} = X_1^{\text{E}}(i_1), \quad X_1^{\text{W}}(i_1) \Big|_{y_1 \mapsto -y_1} = X_1^{\text{W}}(i_1); \quad (\text{B.17})$$



Figure B.2: Predecessor diagram  $D$  on the upper half-plane contributing to  $X_2$  and its mirror diagram  $D^*$ . The eastern neighbor of  $i_1$ , drawn as an open circle, is *not* a predecessor of  $i_1$ .

the two being actually equal by the obvious left-right symmetry. From these relations, we obtain that the height-two probability

$$\mathbb{P}_2(i_1) = \mathbb{P}_1(i_1) + \frac{1}{3} \{X_1^N(i_1) + X_1^E(i_1) + X_1^S(i_1) + X_1^W(i_1)\} \quad (\text{B.18})$$

is an even function of the variable  $y_1$ .

More generally, let us consider a given predecessor diagram  $D$  for  $i_1$  on  $\mathcal{G}$  and its associated probability  $X_D$ . We define  $D^*$  as the mirror predecessor diagram of  $D$ , such that the roles of  $N_1$  and  $S_1$  are swapped in  $D^*$  with respect to  $D$  (see for instance Fig. B.2). We conjecture the following relation, which we have verified for all diagrams contributing to one- and two-site probabilities on the upper half-plane with open boundary condition:

$$X_D(i_1) \Big|_{y_1 \mapsto -y_1} = X_{D^*}(i_1). \quad (\text{B.19})$$

Moreover, we make the following observation: a predecessor diagram  $D$  and its mirror image  $D^*$  contribute equally to the same fraction  $X_p(i_1)$  of spanning trees with  $p$  predecessors of  $i_1$  among its neighbors. Consequently, if Eq. (B.19) holds, multisite probabilities  $\mathbb{P}_{a,1,\dots,1}$  on the UHP with an open boundary are even functions of  $y_1$  (and hence of each  $y_k$  as shown above).

### Closed boundary conditions and the diagonal upper half-plane

Predecessor diagrams on the upper half-plane  $\mathcal{G} = \mathbb{Z} \times \mathbb{N}^*$  with a closed boundary are also related to one another through a simple transforma-

tion under which the Green function (2.55) is invariant:

$$G_{(a,b),(c,d)}^{\text{cl}} = G_{(a,b),(c,1-d)}^{\text{cl}} = G_{(a,1-b),(c,1-d)}^{\text{cl}}. \quad (\text{B.20})$$

Using similar arguments to those for the open boundary, we argue that a diagram  $D$  and its mirror image  $D^*$  are related through  $y_1 \mapsto 1 - y_1$ , for a reference site  $i_1$  located at  $(x_1, y_1)$ . It follows that joint probabilities of a single height  $h_{i_1} = a \geq 1$  and many unit heights  $h_{i_k} = 1$  for  $2 \leq k \leq n$  are even functions of the variables  $r_k = y_k - 1/2$ .

On the diagonal upper half-plane (DUHP)  $\mathcal{G} = \{(x, y) \in \mathbb{Z}^2 | y > x\}$ , Green functions for open (2.61) and closed (2.62) boundary conditions possess the following symmetries:

$$G_{(a,b),(c,d)}^{\text{op}} = -G_{(a,b),(d,c)}^{\text{op}} = G_{(b,a),(d,c)}^{\text{op}}, \quad (\text{B.21})$$

$$G_{(a,b),(c,d)}^{\text{cl}} = G_{(a,b),(d-1,c+1)}^{\text{cl}} = G_{(b-1,a+1),(d-1,c+1)}^{\text{cl}}, \quad (\text{B.22})$$

so probabilities  $\mathbb{P}_{a,1,\dots,1}(i_1, \dots, i_n)$  on the DUHP are even functions of the variables

$$r_k = \frac{y_k - x_k}{\sqrt{2}} \quad \text{for open b.c. and } r_k = \frac{y_k - x_k - 1}{\sqrt{2}} \quad \text{for closed b.c.} \quad (\text{B.23})$$

Finally, let us note that the existence of such relations between the probabilities of mirror predecessor diagrams is not specific to the square lattice. Indeed, the symmetries of the Green functions on the triangular and hexagonal half-lattices yield relations similar to Eq. (B.19) for predecessor diagrams on these graphs.



## Appendix C

# Jacobi's theta and elliptic functions

In this appendix, we recall the definitions of Jacobi's theta and elliptic functions, give some well-known representations of these functions and list the properties we used in this thesis. In what follows,  $z, \tau \in \mathbb{C}$  with  $\text{Im } \tau > 0$ , where  $\tau$  is called the *lattice parameter* or the *half-period ratio*. The *nome*  $q$  defined by  $q = e^{i\pi\tau}$  is such that  $0 < |q| < 1$ .

### C.1 Jacobi's theta functions

The four theta functions  $\vartheta_a(z, q)$ , with  $1 \leq a \leq 4$ , are  $2\pi$ -periodic functions of  $z$  for fixed  $q$ , defined by their Fourier series

$$\vartheta_1(z, q) = 2 \sum_{n=0}^{\infty} (-1)^n q^{(n+\frac{1}{2})^2} \sin[(2n+1)z], \quad (\text{C.1})$$

$$\vartheta_2(z, q) = 2 \sum_{n=0}^{\infty} q^{(n+\frac{1}{2})^2} \cos[(2n+1)z], \quad (\text{C.2})$$

$$\vartheta_3(z, q) = 1 + 2 \sum_{n=1}^{\infty} q^{n^2} \cos(2nz), \quad (\text{C.3})$$

$$\vartheta_4(z, q) = 1 + 2 \sum_{n=1}^{\infty} (-1)^n q^{n^2} \cos(2nz). \quad (\text{C.4})$$

As a matter of notation, it is common to simply write  $\vartheta_a$  for  $\vartheta_a(0, q)$  and  $\vartheta_a(z)$  for  $\vartheta_a(z, q)$  in equations where a single nome  $q$  appears. Using Jacobi's triple product, one can rewrite these four functions as infinite products:

$$\vartheta_1(z, q) = 2q^{1/4} \sin z \prod_{m=1}^{\infty} (1 - q^{2m})(1 - q^{2m}e^{2iz})(1 - q^{2m}e^{-2iz}), \quad (\text{C.5})$$

$$\vartheta_2(z, q) = 2q^{1/4} \cos z \prod_{m=1}^{\infty} (1 - q^{2m})(1 + q^{2m}e^{2iz})(1 + q^{2m}e^{-2iz}), \quad (\text{C.6})$$

$$\vartheta_3(z, q) = \prod_{m=1}^{\infty} (1 - q^{2m})(1 + q^{2m-1}e^{2iz})(1 + q^{2m-1}e^{-2iz}), \quad (\text{C.7})$$

$$\vartheta_4(z, q) = \prod_{m=1}^{\infty} (1 - q^{2m})(1 - q^{2m-1}e^{2iz})(1 - q^{2m-1}e^{-2iz}). \quad (\text{C.8})$$

Let us recall as well the series representation of their logarithm, which directly follows from the infinite-product formulas:

$$\log \frac{\vartheta_1(z, q)}{2q^{1/6}\eta(q) \sin z} = - \sum_{k=1}^{\infty} \frac{2 \cos(2kz)}{k(q^{-2k} - 1)}, \quad (\text{C.9})$$

$$\log \frac{\vartheta_2(z, q)}{2q^{1/6}\eta(q) \cos z} = - \sum_{k=1}^{\infty} \frac{2(-1)^k \cos(2kz)}{k(q^{-2k} - 1)}, \quad (\text{C.10})$$

$$\log \frac{\vartheta_3(z, q)}{2q^{-1/12}\eta(q)} = - \sum_{k=1}^{\infty} \frac{2(-1)^k q^{-k} \cos(2kz)}{k(q^{-2k} - 1)}, \quad (\text{C.11})$$

$$\log \frac{\vartheta_4(z, q)}{2q^{-1/12}\eta(q)} = - \sum_{k=1}^{\infty} \frac{2q^{-k} \cos(2kz)}{k(q^{-2k} - 1)}, \quad (\text{C.12})$$

where Dedekind's eta function is defined by

$$\eta(q) = q^{1/12} \prod_{m=1}^{\infty} (1 - q^{2m}). \quad (\text{C.13})$$

Jacobi's imaginary transformation  $\tau \rightarrow -1/\tau$  yields the following modular properties,

$$\vartheta_1(z, e^{i\pi\tau}) = -i(-i\tau)^{-1/2} e^{-iz^2/(\pi\tau)} \vartheta_1(-z/\tau, e^{-i\pi/\tau}), \quad (\text{C.14})$$

$$\vartheta_2(z, e^{i\pi\tau}) = (-i\tau)^{-1/2} e^{-iz^2/(\pi\tau)} \vartheta_4(-z/\tau, e^{-i\pi/\tau}), \quad (\text{C.15})$$

$$\vartheta_3(z, e^{i\pi\tau}) = (-i\tau)^{-1/2} e^{-iz^2/(\pi\tau)} \vartheta_3(-z/\tau, e^{-i\pi/\tau}), \quad (\text{C.16})$$

$$\vartheta_4(z, e^{i\pi\tau}) = (-i\tau)^{-1/2} e^{-iz^2/(\pi\tau)} \vartheta_2(-z/\tau, e^{-i\pi/\tau}), \quad (\text{C.17})$$

where  $(-i\tau)^{-1/2}$  is interpreted as satisfying  $|\arg(-i\tau)| < \pi/2$ .

## C.2 Jacobi's elliptic functions

To define Jacobi's twelve elliptic functions, one introduces the *elliptic modulus*  $k$  and  $K = K(k)$  the complete elliptic integral of the first kind, related to the nome  $q$  through

$$k = \vartheta_2^2/\vartheta_3^2, \quad K = \pi\vartheta_3^2/2. \quad (\text{C.18})$$

In addition,  $k' = \sqrt{1 - k^2}$  is called the *complementary elliptic modulus*. There are three principal elliptic functions, defined in terms of theta functions as

$$\begin{aligned} \operatorname{sn}(z, k) &= \frac{\vartheta_3 \vartheta_1(\pi z/(2K), q)}{\vartheta_2 \vartheta_4(\pi z/(2K), q)}, & \operatorname{cn}(z, k) &= \frac{\vartheta_4 \vartheta_2(\pi z/(2K), q)}{\vartheta_2 \vartheta_4(\pi z/(2K), q)}, \\ \operatorname{dn}(z, k) &= \frac{\vartheta_4 \vartheta_3(\pi z/(2K), q)}{\vartheta_3 \vartheta_4(\pi z/(2K), q)}. \end{aligned} \quad (\text{C.19})$$

The modular relations due to Jacobi's imaginary transformation follow from those of the theta functions:

$$\operatorname{sn}(iz, k) = i \operatorname{sc}(z, k'), \quad \operatorname{cn}(iz, k) = \operatorname{nc}(z, k'), \quad \operatorname{dn}(iz, k) = \operatorname{dc}(z, k'). \quad (\text{C.20})$$

The nine auxiliary elliptic functions are obtained from the principal ones using the relations

$$\operatorname{pq}(z, k) = \frac{\operatorname{pr}(z, k)}{\operatorname{qr}(z, k)} = \frac{1}{\operatorname{qp}(z, k)}, \quad (\text{C.21})$$

where  $p, q, r = s, c, d, n$  and with the convention that  $\operatorname{pq}(z, k) \equiv 1$  if  $q = p$ .

Jacobi's elliptic functions possess a Fourier representation only if  $z, q$  satisfy certain inequalities. We only indicate here the Fourier series of

the eight functions used in Chapter 3. When  $q \exp(2|\operatorname{Im} \pi z/(2K)|) < 1$ ,

$$\operatorname{cn}(z, k) = \frac{2\pi}{Kk} \sum_{n=0}^{\infty} \frac{q^{-(n+1/2)} \cos[\pi(2n+1)z/(2K)]}{q^{-(2n+1)} + 1}, \quad (\text{C.22})$$

$$\operatorname{dn}(z, k) = \frac{\pi}{2K} + \frac{2\pi}{K} \sum_{n=1}^{\infty} \frac{q^{-n} \cos(\pi n z/K)}{q^{-2n} + 1}, \quad (\text{C.23})$$

$$\operatorname{cd}(z, k) = \frac{2\pi}{Kk} \sum_{n=0}^{\infty} \frac{(-1)^n q^{-(n+1/2)} \cos[\pi(2n+1)z/(2K)]}{q^{-(2n+1)} - 1}, \quad (\text{C.24})$$

$$\operatorname{nd}(z, k) = \frac{\pi}{2Kk'} + \frac{2\pi}{Kk'} \sum_{n=1}^{\infty} \frac{(-1)^n q^{-n} \cos(\pi n z/K)}{q^{-2n} + 1}. \quad (\text{C.25})$$

In case the weaker condition  $q \exp(|\operatorname{Im} \pi z/(2K)|) < 1$  is satisfied,

$$\operatorname{ns}(z, k) = \frac{\pi}{2K} \frac{1}{\sin[\pi z/(2K)]} + \frac{2\pi}{K} \sum_{n=0}^{\infty} \frac{\sin[\pi(2n+1)z/(2K)]}{q^{-(2n+1)} - 1}, \quad (\text{C.26})$$

$$\operatorname{cs}(z, k) = \frac{\pi}{2K} \cot[\pi z/(2K)] - \frac{2\pi}{K} \sum_{n=1}^{\infty} \frac{\sin(\pi n z/K)}{q^{-2n} + 1}, \quad (\text{C.27})$$

$$\operatorname{dc}(z, k) = \frac{\pi}{2K} \frac{1}{\cos[\pi z/(2K)]} + \frac{2\pi}{K} \sum_{n=0}^{\infty} \frac{(-1)^n \cos[\pi(2n+1)z/(2K)]}{q^{-(2n+1)} - 1}, \quad (\text{C.28})$$

$$\operatorname{nc}(z, k) = \frac{\pi}{2Kk'} \frac{1}{\cos[\pi z/(2K)]} - \frac{2\pi}{Kk'} \sum_{n=0}^{\infty} \frac{(-1)^n \cos[\pi(2n+1)z/(2K)]}{q^{-(2n+1)} + 1}. \quad (\text{C.29})$$

# Appendix D

## Technical proofs

In this fourth appendix, we give the proofs of Propositions 3.2 and 3.3. The latter relies on several technical lemmas, some of which were given in [90, 91].

### Proof of Proposition 3.2:

Due to Theorem 1.5,  $(\mathbf{A}_n)_{R, \vec{\sigma}}$  is nonzero only if each chord of  $\vec{\sigma}$  links an element of  $R$  to one of  $S = \mathcal{N} \setminus R$ , i.e. if every  $r_i$  is connected to  $s_{\rho(i)}$  in  $\vec{\sigma}$  for some permutation  $\rho \in S_n$ . Recall that for the cyclic orientation, all paths are oriented from the up to the down step of the chords of  $\vec{\sigma}$ . All  $r_i$ 's that index up steps therefore contribute a factor 1 to the matrix entry. On the other hand, we have to reverse the orientation of each path  $r_i \rightarrow s_{\rho(i)}$  when  $r_i$  indexes a down step of  $\vec{\sigma}$ . As  $\phi_{r_i \rightarrow s_{\rho(i)}} = z$  (resp. 1) if  $r_i < s_{\rho(i)}$  (resp.  $r_i > s_{\rho(i)}$ ) when  $r_i$  is a down step, we find for  $w = z^2$  that

$$(\mathbf{A}_n)_{R, \vec{\sigma}} = \pm w^{W(\vec{\sigma}) - R \cdot \vec{\sigma}}. \quad (\text{D.1})$$

We now turn to the signs of the entries of  $\mathbf{A}_n$ , which originate from the signature of the permutations  $\rho$  mapping indices of  $S$  to indices of  $R$  in Theorem 1.5. Let  $\lambda$  be a standard (noncyclic) Dyck path with up steps  $U = \{u_1, u_2, \dots, u_n\}$  such that  $u_i < u_j$  if  $i < j$ . We denote by  $D = \{d_1, d_2, \dots, d_n\}$  the collection of down steps of  $\lambda$ , such that  $(u_i, d_i)$  is a chord of  $\lambda$  for  $1 \leq i \leq n$ . Since  $D$  is not ordered in general, there exists a permutation  $\pi$  of the indices  $1, 2, \dots, n$  that sorts  $D$  in ascending order; we write the result  $D_\pi$ . The signature of  $\pi$  is given

by  $\epsilon(\pi) = (-1)^{I(D)}$ , where  $I(D) = |\{(d_i, d_j) | d_i > d_j \text{ and } i < j\}|$  is the inversion number of  $D$ . Observe that the condition  $u_i < u_j < d_j < d_i$  means that the chord  $(u_j, d_j)$  lies above  $(u_i, d_i)$  in  $\lambda$  (represented as a mountain range). It follows that the inversion number can be expressed as

$$I(D) = \sum_{\substack{\text{chords } (u_i, d_i) \\ \text{of } \lambda}} |\{\text{chords } (u_j, d_j) \text{ of } \lambda \text{ above } (u_i, d_i)\}|. \quad (\text{D.2})$$

By tiling the area between  $\lambda$  and the  $x$  axis with  $\sqrt{2} \times \sqrt{2}$  squares as depicted in Fig. D.1, we see that the number of chords of  $\lambda$  above a given chord  $(u_i, d_i)$  is equal to the number of squares intersected by  $(u_i, d_i)$  in their lower half. Each of these squares is intersected in its lower half by exactly one chord of  $\lambda$ , so  $I(D)$  is the number of squares under  $\lambda$  or, equivalently,  $I(D) = \frac{1}{2}(\mathcal{A}(\lambda) - n)$ . The sign associated with  $(\mathbf{A}_n)_{U, \lambda}$  is therefore given by  $\epsilon(\pi^{-1}) = (-1)^{\frac{1}{2}(\mathcal{A}(\lambda) - n)}$ .

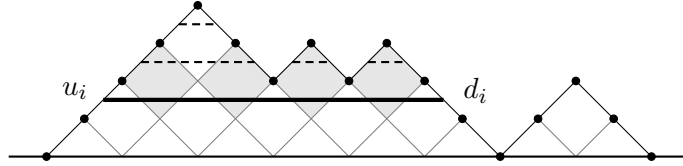


Figure D.1: Standard Dyck path with a marked chord  $(u_i, d_i)$ , which intersects the lower half of four gray squares. The four chords that lie above  $(u_i, d_i)$  are drawn as dashed lines.

The next step of the proof consists in showing that the sign of  $(\mathbf{A}_n)_{R, \lambda}$  does not depend on  $R$ . To do so, let us define  $U, D$  as above as the sets of up and down steps of  $\lambda$ , and let  $R$  be  $U \cup \{d_\ell\} \setminus \{u_\ell\}$  for some index  $\ell$ , i.e.  $R = \{u_1, u_2, \dots, u_{\ell-1}, d_\ell, u_{\ell+1}, \dots, u_n\}$ . The subset  $S$  associated with  $R$  is therefore  $S = \{d_1, d_2, \dots, d_{\ell-1}, u_\ell, d_{\ell+1}, \dots, d_n\}$ . To compute  $I(S) - I(R)$  we need to distinguish between two cases:

- (a) Consider a chord  $(u_j, d_j)$  that lies to the left of  $(u_\ell, d_\ell)$  in  $\lambda$ , that is, such that  $u_j < d_j < u_\ell < d_\ell$ . Since  $u_j < u_\ell, d_\ell$  and  $d_j < u_\ell, d_\ell$ , these two chords do not contribute to  $I(R)$  or  $I(S)$ . Similarly there is no contribution from a chord to the right of  $(u_\ell, d_\ell)$  or below it.
- (b) A chord  $(u_j, d_j)$  above  $(u_\ell, d_\ell)$  is such that  $u_\ell < u_j < d_j < d_\ell$ , so it contributes equally to both  $I(R)$  and  $I(S)$ .

Since  $I(D) - I(U) = I(D) = I(S) - I(R)$ , we see that the signs of  $(\mathbf{A}_n)_{U,\lambda}$  and  $(\mathbf{A}_n)_{R,\lambda}$  are the same. The argument holds if  $R$  is obtained from  $U$  by replacing two or more up steps of  $\lambda$  with the corresponding down steps. The sign is therefore the same for any  $R$  such that  $R \cap \lambda$ .

Finally, we take into account cyclic Dyck paths. Let  $\vec{\sigma}$  be a cyclic Dyck path with up steps  $U$  and down steps  $D$ . We define  $\vec{\sigma}'$  by shifting all step indices of  $\vec{\sigma}$  to the left by one unit, that is  $U' = U + 1 \pmod{2n}$  and  $D' = D + 1 \pmod{2n}$ . Assume first that  $2n \in D$ , then  $I(U') = I(U)$  and  $I(D') - I(D) = n - 1 \pmod{2}$ . If rather  $2n \in U$  then  $I(U') - I(U) = n - 1 \pmod{2}$  and  $I(D') = I(D)$ . In both cases  $(-1)^{I(D') - I(U')} = (-1)^{n+1}(-1)^{I(D) - I(U)}$ . Therefore, if a cyclic Dyck path  $\vec{\sigma}$  is obtained by shifting  $k$  times to the left the indices of a standard Dyck path  $\lambda$ , then the sign of  $(\mathbf{A}_n)_{R,\vec{\sigma}}$  is  $(-1)^{\frac{1}{2}(\mathcal{A}(\lambda) - n) + k(n+1)}$ , with  $\mathcal{A}(\lambda) = \mathcal{A}(\vec{\sigma})$ .

Lastly we make the following observation: a unit shift of the indices of  $\vec{\sigma}$  to the left to define  $\vec{\sigma}'$  implies that  $|W(\vec{\sigma}') - W(\vec{\sigma})| = 1$ , since  $W(\vec{\sigma}) = h_0(\vec{\sigma})$  is the height of the left endpoint of the step indexed by 1 in  $\vec{\sigma}$ . Since the parity of  $W(\vec{\sigma})$  alternates between even and odd for each unit shift of the indices of  $\vec{\sigma}$  to the left, the sign of  $(\mathbf{A}_n)_{R,\vec{\sigma}}$  can be recast as  $(-1)^{\frac{1}{2}(\mathcal{A}(\vec{\sigma}) - n) + (n+1)W(\vec{\sigma})}$ .  $\square$

**Lemma D.1.** *Let  $\vec{\sigma}$  be a cyclic Dyck path and  $R \subset \mathcal{N}$  a subset of order  $n$  such that  $R \cap \vec{\sigma}$ . If we write  $\Sigma R \equiv \sum_{i=1}^n r_i$  then*

$$(-1)^{\Sigma R} = (-1)^{R \cdot \vec{\sigma} + \frac{1}{2}(\mathcal{A}(\vec{\sigma}) - n) + n W(\vec{\sigma})}. \quad (\text{D.3})$$

*Proof.* Let  $R \subset \mathcal{N}$  such that  $R$  intersects each chord of  $\vec{\sigma}$  once. Let  $i, j$  be the indices of a chord of  $\vec{\sigma}$  with  $i \in R$ , and define  $R' \equiv (R \setminus \{i\}) \cup \{j\}$ . Since  $i$  and  $j$  have opposite parity,  $(-1)^{\Sigma R'} = -(-1)^{\Sigma R}$ . Moreover  $R' \cdot \vec{\sigma} = R \cdot \vec{\sigma} - 1$  if  $i$  is an up step, and  $R' \cdot \vec{\sigma} = R \cdot \vec{\sigma} + 1$  if  $i$  is a down step. It follows that  $(-1)^{\Sigma R' - \Sigma R} = (-1)^{R' \cdot \vec{\sigma} - R \cdot \vec{\sigma}}$ . This relation holds more generally for any  $R'$  that intersects once each chord of  $\vec{\sigma}$ .

Consider in particular the set  $R$  of up steps of  $\vec{\sigma}$ , which implies that  $R \cdot \vec{\sigma} = n$ , and assume that the first step of  $\vec{\sigma}$  has the label  $\ell \geq 1$ . Denote by  $s_j$  the value of the step at position  $j$  for  $1 \leq j \leq 2n$ , with

$s_j = +1$  (resp.  $-1$ ) if  $j$  is an up step (resp. down step) of  $\vec{\sigma}$ . The height  $h_j$  for  $0 \leq j \leq 2n$  is given by

$$h_j = \begin{cases} h_{j-1} + s_j = h_0 + \sum_{k=1}^j s_k & \text{if } 1 \leq j \leq \ell - 1, \\ h_{j+1} - s_j = h_0 + \sum_{k=1}^{j-1} s_k & \text{if } \ell + 2 \leq j \leq 2n, \\ 0 & \text{if } j = \ell, \ell + 1, \end{cases} \quad (\text{D.4})$$

where  $h_\ell = h_{\ell+1} = 0$  since they correspond to the first and last vertices of the cyclic Dyck path  $\vec{\sigma}$ . After some algebra, we can express the area  $\mathcal{A}(\vec{\sigma})$  between the Dyck path and the horizontal axis in terms of the  $s_j$ 's as

$$\mathcal{A}(\vec{\sigma}) = \sum_{j=0}^{2n} h_j = 2n h_0 - \sum_{j=1}^{2n} j s_j. \quad (\text{D.5})$$

By separating the last sum in the equation above for positive and negative values of the  $s_j$ 's, one finds

$$\sum_{j=1}^{2n} j s_j = \sum_{j: s_j=+1} j s_j + \sum_{j: s_j=-1} j s_j = \sum_{j: s_j=+1} 2j - n(2n + 1), \quad (\text{D.6})$$

where we used the fact that  $s_1 + s_2 + \dots + s_{2n} = 0$  for a (cyclic) Dyck path. Hence, we obtain the following formula (recall that  $h_0(\vec{\sigma}) = W(\vec{\sigma})$ ):

$$\Sigma R = \sum_{j: s_j=+1} j = n^2 + \frac{1}{2}(n - \mathcal{A}(\vec{\sigma})) + n W(\vec{\sigma}), \quad (\text{D.7})$$

which completes the proof.  $\square$

**Lemma D.2.** *Let  $\lambda$  be a standard, noncyclic, Dyck path with a chord  $(\ell, m)$ . Define  $\lambda'$  as the Dyck path obtained by “pushing down” the chord  $(\ell, m)$  of  $\lambda$ , that is, by replacing the up step  $\ell$  with a down step and the down step  $m$  with an up step (note that not all chords can be pushed down). The areas between the two Dyck paths are related by*

$$\mathcal{A}(\lambda') = \mathcal{A}(\lambda) - 2(m - \ell). \quad (\text{D.8})$$

Moreover, for any subset  $R \subset \mathcal{N}$  such that  $R \cap \lambda$ ,  $(-1)^{R \cdot \lambda' - R \cdot \lambda} = (-1)^{\frac{1}{2}(\mathcal{A}(\lambda') - \mathcal{A}(\lambda))}$ .

*Proof.* Observe that the heights of the vertices  $h'_i$  in  $\lambda'$  are decreased by 2 with respect to their counterparts  $h_i$  in  $\lambda$  for  $\ell \leq i \leq m - 1$ . If the up

step  $\ell$  of  $\lambda$  belongs to  $R$ , then  $R \cdot \lambda' = R \cdot \lambda - 1$  since  $\ell$  is a down step of  $\lambda'$ . Conversely if  $m \in R$ ,  $R \cdot \lambda' = R \cdot \lambda + 1$  since  $m$  is a down step of  $\lambda$  but an up step of  $\lambda'$ . In both cases  $R \cdot \lambda$  and  $R \cdot \lambda'$  differ by one, and  $m - \ell = \frac{1}{2}(\mathcal{A}(\lambda) - \mathcal{A}(\lambda'))$  is odd.  $\square$

**Lemma D.3** (Adapted from [91]). *Let  $\lambda$  and  $\vec{\sigma}$  be a standard and a cyclic Dyck paths, respectively. Then*

$$\sum_{R: R \cap \vec{\sigma}} (-1)^{R \cdot \vec{\sigma}} w^{-R \cdot \lambda - R \cdot \vec{\sigma}} = (-1)^{\frac{1}{2}(\mathcal{A}(\vec{\sigma}) - \mathcal{A}(\lambda))} (1 - w^{-1})^n \quad (\text{D.9})$$

*if it possible to push down some chords of  $\vec{\sigma}$  to obtain  $\lambda$ , and 0 otherwise. In particular the step labels of  $\vec{\sigma}$  and  $\lambda$  must appear in the same order for the sum to be nonzero, i.e.  $\vec{\sigma}$  must be a standard Dyck path.*

*Proof.* Let us assume first that  $\vec{\sigma}$  is a standard Dyck path, which we shall simply write as  $\sigma$ . If we can push down some chords of  $\sigma$  to obtain  $\lambda$ , then each chord of  $\sigma$  connects an up step to a down step of  $\lambda$  (not necessarily belonging to the same chord). For any two subsets  $R, R' \subset \mathcal{N}$  of order  $n$  that intersect each chord of  $\sigma$  exactly once,

$$(-1)^{R \cdot \sigma + R' \cdot \sigma} = (-1)^{R \cdot \lambda + R' \cdot \lambda}. \quad (\text{D.10})$$

Indeed, consider a chord  $(i, j)$  of  $\sigma$  on which  $R$  and  $R'$  differ. Without loss of generality, we can assume that the up step  $i$  belongs to  $R$  and the down step  $j$  to  $R'$ . If  $(i, j)$  was pushed down to obtain  $\lambda$  then  $i$  is a down step of  $\lambda$  in  $R$ , and  $j$  an up step of  $\lambda$  in  $R'$ . Otherwise  $i$  is an up step of  $\lambda$  and  $j$  a down step of  $\lambda$ . In both cases, the chord  $(i, j)$  brings a factor  $-1$  to both  $(-1)^{R \cdot \sigma + R' \cdot \sigma}$  and  $(-1)^{R \cdot \lambda + R' \cdot \lambda}$ . Now denote by  $R_0$  the set of down steps of  $\lambda$ , so  $R_0 \cdot \lambda = 0$ . Then  $R_0 \cdot \sigma$  is the number of chords of  $\sigma$  that are pushed down to obtain  $\lambda$ . Lemma D.2 then yields the equality  $(-1)^{R_0 \cdot \sigma} = (-1)^{\frac{1}{2}(\mathcal{A}(\sigma) - \mathcal{A}(\lambda))}$ . As  $(-1)^{R \cdot \sigma} = (-1)^{R_0 \cdot \sigma + R \cdot \lambda}$ , it follows that

$$\begin{aligned} \sum_{R: R \cap \sigma} (-1)^{R \cdot \sigma} w^{-R \cdot \lambda} &= (-1)^{R_0 \cdot \sigma} \sum_{R: R \cap \sigma} (-w^{-1})^{R \cdot \lambda} \\ &= (-1)^{\frac{1}{2}(\mathcal{A}(\sigma) - \mathcal{A}(\lambda))} (1 - w^{-1})^n, \end{aligned} \quad (\text{D.11})$$

where the last equality is given by the binomial expansion. On the other hand, if  $\lambda$  cannot be obtained by pushing down some chords of  $\sigma$ , there

is a chord  $(i, j)$  of  $\sigma$  such that both  $i$  and  $j$  are up steps of  $\lambda$ . Then for each  $R$  such that  $R \cap \sigma$  in the sum, define  $R'$  as the symmetric difference of  $R$  with  $\{i, j\}$ . Since  $(-1)^{R \cdot \sigma} = -(-1)^{R' \cdot \sigma}$  and  $R \cdot \lambda = R' \cdot \lambda$ , the sum over all  $R$ 's such that  $R \cap \sigma$  is zero.

Let us now discuss the case of a cyclic, nonstandard, Dyck path  $\vec{\sigma}$ , for which there are several subcases:

- (i) If  $(i, j)$  is a chord of  $\vec{\sigma}$  such that  $i < j$  are both up or down steps of  $\lambda$ , the sum is zero. To see this, define for each  $R$  such that  $R \cap \vec{\sigma}$  its symmetric difference with  $\{i, j\}$ , denoted by  $R'$ . Then  $(-1)^{R \cdot \vec{\sigma}} = -(-1)^{R' \cdot \vec{\sigma}}$ ,  $w^{-R \cdot \lambda} = w^{-R' \cdot \lambda}$  and  $w^{-R \cdot \vec{\sigma}} = w^{-R' \cdot \vec{\sigma}}$ , so the contributions of  $R$  and  $R'$  cancel each other out.
- (ii) Suppose  $(2n, j)$  is a chord of  $\vec{\sigma}$  such that  $j$  is an up step of  $\lambda$ . For each  $R$  define  $R'$  as the symmetric difference of  $R$  with  $\{2n, j\}$ . If  $j \in R$  then  $w^{-R \cdot \lambda} = w^{-R' \cdot \lambda - 1}$  and  $w^{-R \cdot \vec{\sigma}} = w^{-R' \cdot \vec{\sigma} + 1}$ . Conversely if  $j \in R'$  then  $w^{-R \cdot \lambda} = w^{-R' \cdot \lambda + 1}$  and  $w^{-R \cdot \vec{\sigma}} = w^{-R' \cdot \vec{\sigma} - 1}$ . Therefore,  $(-1)^{R \cdot \vec{\sigma}} = -(-1)^{R' \cdot \vec{\sigma}}$  and  $w^{-R \cdot \lambda - R \cdot \vec{\sigma}} = w^{-R' \cdot \lambda - R' \cdot \vec{\sigma}}$  in both cases, so the sum is zero.
- (iii) Assume  $(i, 2n)$  is a chord of  $\vec{\sigma}$  such that  $i$  is a down step of  $\lambda$ . Then for  $R'$  the symmetric difference of  $R$  with  $\{i, 2n\}$ , we have  $(-1)^{R \cdot \vec{\sigma}} = -(-1)^{R' \cdot \vec{\sigma}}$ ,  $w^{-R \cdot \lambda} = w^{-R' \cdot \lambda}$  and  $w^{-R \cdot \vec{\sigma}} = w^{-R' \cdot \vec{\sigma}}$ . Therefore,  $R, R'$  give opposite contributions to the sum, which vanishes.
- (iv) Suppose  $(2n, j)$  is a chord of  $\vec{\sigma}$  such that  $j$  is a down step of  $\lambda$ . The subpath of  $\vec{\sigma}$  consisting in steps  $\{1, \dots, j-1\}$  is a standard Dyck path, so it contains the same number of up steps and down steps of  $\vec{\sigma}$ . Consider now the subpath of  $\lambda$  with the same indices. Since both  $j$  and  $2n$  are down steps of  $\lambda$  with opposite parity,  $h_j(\lambda) - h_{2n}(\lambda)$  must be odd, so the step  $j$  lies higher than the step  $2n$  on  $\lambda$ . This implies that the subset  $\{1, \dots, j-1\}$  contains more up steps than down steps of  $\lambda$ . Therefore, there exists a chord  $(\ell, m)$  of  $\vec{\sigma}$  with  $1 \leq \ell < m \leq j-1$  such that both  $\ell$  and  $m$  are up steps of  $\lambda$ , so we can refer to subcase (i).
- (v) If  $(i, 2n)$  is a chord of  $\vec{\sigma}$  with  $i$  an up step of  $\lambda$ , then the subpath of  $\vec{\sigma}$  indexed by the indices  $\{i+1, \dots, 2n-1\}$  is a standard Dyck path.

- a. If  $h_{i-1}(\lambda) > h_{2n}(\lambda) = 0$ , that is if the up step  $i$  is higher than the down step  $2n$  in  $\lambda$ , then the subset  $\{i+1, \dots, 2n-1\}$  contains more down steps than up steps of  $\lambda$ . Therefore, there exists a chord  $(\ell, m)$  of  $\vec{\sigma}$  with  $i < \ell < m < 2n$  such that both  $\ell$  and  $m$  are down steps of  $\lambda$ , which corresponds to subcase (i).
- b. If on the other hand  $h_{i-1}(\lambda) = h_{2n}(\lambda) = 0$ , then the subpath of  $\lambda$  indexed by  $\{1, \dots, i-1\}$  is a Dyck path. In that case, if  $i-1$  is an up step of  $\vec{\sigma}$ , it belongs to a chord  $(i-1, j)$  of  $\vec{\sigma}$  with  $i-1 > j$ .
- If  $j$  is an up step of  $\lambda$ , subcase (ii) occurs;
  - If  $j$  is an down step of  $\lambda$ , subcase (iv) occurs.

If on the contrary  $i-1$  is a down step of  $\vec{\sigma}$ , it belongs to a chord  $(j, i-1)$  of  $\vec{\sigma}$  with  $j < i-1$ .

- If  $j$  is a down step of  $\lambda$ , subcase (iii) occurs;
- If  $j$  is an up step of  $\lambda$  such that  $h_{j-1}(\lambda) > h_{i-1}(\lambda) = 0$ , subcase (v)a. occurs;
- If  $j$  is an up step of  $\lambda$  such that  $h_{j-1}(\lambda) = h_{i-1}(\lambda) = 0$ , then the subpath of  $\lambda$  indexed by  $\{1, \dots, j-1\}$  is a standard Dyck path, so we can consider subcase (v)b. again with  $j-1$  instead of  $i-1$ .

For all cases, we see that the sum in Eq. (D.9) vanishes if  $\vec{\sigma}$  is not a standard Dyck path.  $\square$

**Lemma D.4** ([90]). *Let  $\vec{\mu}, \vec{\sigma}, \vec{\tau}$  be cyclic Dyck paths, and let  $M$  be the matrix defined by  $M_{\vec{\mu}, \vec{\tau}} = 1$  if  $\vec{\mu}$  can be obtained by pushing down some of the chords of  $\vec{\tau}$ , and zero otherwise. Then*

$$\sum_{\vec{\mu} \geq \vec{\sigma}} (-1)^{\frac{1}{2}(\mathcal{A}(\vec{\mu}) - \mathcal{A}(\vec{\sigma}))} \text{ci}(\vec{\sigma}/\vec{\mu}) M_{\vec{\mu}, \vec{\tau}} = \delta_{\vec{\sigma}, \vec{\tau}}. \quad (\text{D.12})$$

### Proof of Proposition 3.3:

Let us first consider a standard Dyck path  $\lambda$ , for which  $W(\lambda) = R|\lambda_{\ell(1)} =$

$|D_{\ell(1)}^\lambda| = 0$ . The product of  $\mathbf{B}_n$  and  $\mathbf{A}_n$  yields

$$\begin{aligned} \sum_{\substack{R \subset \mathcal{N} \\ |R|=n}} (\mathbf{B}_n)_{\lambda,R} (\mathbf{A}_n)_{R,\vec{\tau}} &= \sum_{R: R \cap \vec{\tau}} (-1)^{\Sigma R + n} \sum_{\mu \geq \lambda} \text{ci}(\lambda/\mu) w^{n-R \cdot \mu} \\ &\quad \times (-1)^{\frac{1}{2}(\mathcal{A}(\vec{\tau})-n)+(n+1)W(\vec{\tau})} w^{W(\vec{\tau})-R \cdot \vec{\tau}} \\ &= (-1)^{\frac{1}{2}(\mathcal{A}(\vec{\tau})+n)+(n+1)W(\vec{\tau})} w^{n+W(\vec{\tau})} \\ &\quad \times \sum_{\mu \geq \lambda} \text{ci}(\lambda/\mu) \sum_{R: R \cap \vec{\tau}} (-1)^{\Sigma R} w^{-R \cdot \mu - R \cdot \vec{\tau}}. \end{aligned} \quad (\text{D.13})$$

We use Lemma D.1 to write  $(-1)^{\Sigma R}$  in terms of  $(-1)^{R \cdot \vec{\tau}}$  on the right-hand side, and Lemma D.3 to compute the sum over all  $R$ 's such that  $R \cap \vec{\tau}$ . The result reads

$$(-w)^{n+W(\vec{\tau})} (1-w^{-1})^n \sum_{\mu \geq \lambda} (-1)^{\frac{1}{2}(\mathcal{A}(\vec{\tau})-\mathcal{A}(\mu))} \text{ci}(\lambda/\mu) M_{\mu,\vec{\tau}}.$$

Applying Lemma D.4 to the above expression yields

$$\begin{aligned} \sum_{\substack{R \subset \mathcal{N} \\ |R|=n}} (\mathbf{B}_n)_{\lambda,R} (\mathbf{A}_n)_{R,\vec{\tau}} &= (-1)^{\frac{1}{2}(\mathcal{A}(\vec{\tau})-\mathcal{A}(\lambda))} (-w)^{W(\vec{\tau})} (1-w)^n \delta_{\lambda,\vec{\tau}} \\ &= (1-w)^n \delta_{\lambda,\vec{\tau}}. \end{aligned} \quad (\text{D.14})$$

Consider now two cyclic Dyck paths  $\vec{\sigma}, \vec{\tau}$  such that the first step of  $\vec{\sigma}$  (resp.  $\vec{\tau}$ ) is labeled by the index  $k+1$  (resp.  $\ell+1$ ). Let us define  $\sigma_0$  and  $\vec{\tau}'$  by subtracting  $k \bmod 2n$  to the label of each step of  $\vec{\sigma}$  and  $\vec{\tau}$ , so that  $\sigma_0$  is a standard Dyck path. We define for each  $R$  the subset  $R'$  by subtracting  $k \bmod 2n$  to each index in  $R$ . We further assume that  $R \cap \vec{\tau}$ , as  $(\mathbf{A}_n)_{R,\vec{\tau}}$  vanishes otherwise. Our goal is to rewrite the product  $(\mathbf{B}_n)_{\vec{\sigma},R} (\mathbf{A}_n)_{R,\vec{\tau}}$  in terms of  $(\mathbf{B}_n)_{\sigma_0,R'} (\mathbf{A}_n)_{R',\vec{\tau}'}$ , and then use Eq. (D.14) to get the desired result.

Let us first discuss the signs of both products. Explicitly, their quotient reads

$$\begin{aligned} &\frac{(-1)^{\Sigma R + W(\vec{\sigma}) + n + \frac{1}{2}(\mathcal{A}(\vec{\tau})-n) + (n+1)W(\vec{\tau})}}{(-1)^{\Sigma R' + W(\sigma_0) + n + \frac{1}{2}(\mathcal{A}(\vec{\tau}')-n) + (n+1)W(\vec{\tau}')}} \\ &= (-1)^{kn + W(\vec{\sigma}) + (n+1)(W(\vec{\tau}) - W(\vec{\tau}'))}, \end{aligned} \quad (\text{D.15})$$

since  $\sigma_0$  is a standard Dyck path ( $W(\sigma_0) = 0$ ) and  $\Sigma R = \Sigma R' + kn \pmod{2n}$ . Moreover the permutation of the indices of  $\vec{\tau}$  to form  $\vec{\tau}'$  leaves the area under the path invariant:  $\mathcal{A}(\vec{\tau}) = \mathcal{A}(\vec{\tau}')$ . In addition, observe that rotating the step indices of  $\vec{\tau}$  by one unit to the left changes  $W(\vec{\tau}) = h_0(\vec{\tau})$  by  $\pm 1$ . One may therefore write the equality  $(-1)^{W(\vec{\tau})-W(\vec{\tau}')} = (-1)^k = (-1)^{W(\vec{\sigma})}$ , which implies that Eq. (D.15) is equal to 1.

Applying this result together with the property  $R \cdot \vec{\mu} = R' \cdot \mu_0$  for all cyclic Dyck paths  $\vec{\mu} \geq \vec{\sigma}$  yields the relation

$$\frac{(\mathbf{B}_n)_{\vec{\sigma}, R} (\mathbf{A}_n)_{R, \vec{\tau}}}{(\mathbf{B}_n)_{\sigma_0, R'} (\mathbf{A}_n)_{R', \vec{\tau}'}} = w^{W(\vec{\tau})-W(\vec{\tau}')-W(\vec{\sigma})+R|\vec{\sigma}_{\ell(1)}-|D_{\ell(1)}^{\vec{\sigma}}|-R:\vec{\tau}+R':\vec{\tau}'}. \quad (\text{D.16})$$

To simplify this expression, let us note that for any  $R$  such that  $R \cap \vec{\tau}$ ,  $R : \vec{\tau} = R|\vec{\tau}_{\ell(1)} - |D_{\ell(1)}^{\vec{\tau}}$ . Indeed,  $R|\vec{\tau}_{\ell(1)}$  counts the number of indices  $i \in R$  such that (a) the chord  $(i, j)$  belongs to  $\vec{\tau}$  with  $i$  appearing before the step 1 and  $j$  afterward (i.e.  $i > j$ ), or (b) the chord  $(i, j)$  or the chord  $(j, i)$  belongs to  $\vec{\tau}$  with both  $i, j$  appearing before the step 1 in  $\vec{\tau}$ . Since  $R$  intersects each chord of  $\vec{\tau}$  exactly once, there are as many indices of the second type in  $R$  as there are down steps before the step 1 in  $\vec{\tau}$ .

Let us now use this decomposition to compute the difference  $R' : \vec{\tau}' - R : \vec{\tau}$ . Assume first that the path  $\vec{\tau}$  touches the horizontal axis only at its endpoints. There are two possible cases:

- (a) If  $\ell \leq k$ , the step 1 of  $\vec{\tau}$  is rotated to the left to obtain  $\vec{\tau}'$ . Therefore,  $|D_{\ell(1)}^{\vec{\tau}}| \geq |D_{\ell(1)}^{\vec{\tau}'}$  and  $R|\vec{\tau}_{\ell(1)} \geq R'|\vec{\tau}'_{\ell(1)}$ , since there are more indices before the step 1 of  $\vec{\tau}$  than before that of  $\vec{\tau}'$ . These extra steps before the step 1 of  $\vec{\tau}$  are labeled by  $2n, 2n-1, \dots, 2n-k+1$ : they are precisely the indices of  $\vec{\sigma}$  appearing before its step 1. It follows that  $|D_{\ell(1)}^{\vec{\tau}}| = |D_{\ell(1)}^{\vec{\tau}'}| + |D_{\ell(1, \vec{\sigma})}^{\vec{\tau}}|$  and  $R|\vec{\tau}_{\ell(1)} = R'|\vec{\tau}'_{\ell(1)} + R|\vec{\sigma}_{\ell(1)}$ , where  $D_{\ell(1, \vec{\sigma})}^{\vec{\tau}}$  is given by Definition 3.1. Hence, we find the relation

$$R|\vec{\sigma}_{\ell(1)} - R : \vec{\tau} + R' : \vec{\tau}' = |D_{\ell(1, \vec{\sigma})}^{\vec{\tau}}|, \quad (\text{D.17})$$

which, crucially, is independent from  $R$ .

- (b) If  $\ell > k$ , the step 1 of  $\vec{\tau}$  is rotated to the right to define  $\vec{\tau}'$ . Therefore,  $|D_{\ell(1)}^{\vec{\tau}'}| \geq |D_{\ell(1)}^{\vec{\tau}}|$  and  $R'|\vec{\tau}'_{\ell(1)} \geq R|\vec{\tau}_{\ell(1)}$ , since there are more indices before the step 1 of  $\vec{\tau}'$  than before that of  $\vec{\tau}$ . The extra steps before

the step 1 of  $\vec{\tau}'$  are labeled by  $2n, 2n-1, \dots, 2n-k+1$ . They also correspond to the steps  $1, \dots, k$  in  $\vec{\tau}$ , which are the indices of  $\vec{\sigma}$  after its step 1 (included). Hence, we find that  $\left|D_{\ell(1)}^{\vec{\tau}'}\right| = \left|D_{\ell(1)}^{\vec{\tau}}\right| + n - \left|D_{\ell(1,\vec{\sigma})}^{\vec{\tau}}\right|$  and  $R'|\vec{\tau}'_{\ell(1)} = R|\vec{\tau}_{\ell(1)} + n - R|\vec{\sigma}_{\ell(1)}$ , since any cyclic Dyck path of length  $2n$  has  $n$  down steps and  $|R| = n$ . Equation (D.17) holds as well in this case.

Up to this point, we have not considered cyclic Dyck paths  $\vec{\tau}$  that intersect the horizontal axis at intermediary vertices distinct from its extremities (see for instance Fig. 3.15). As explained at the beginning of Section 3.3.2, certain permutations of the step indices yield “forbidden” paths, in which the step 1 is located to the right of an intersection with the horizontal axis. They can however be transformed into “admissible” cyclic Dyck paths by cyclically rotating connected components such that the step 1 appears in the first one. Doing so changes the number of steps located to the left of the step 1, so the above decomposition of  $R|\vec{\tau}_{\ell(1)}$  and  $\left|D_{\ell(1)}^{\vec{\tau}}\right|$  does not hold. Since  $R \cap \vec{\tau}$ , it should be clear however that the difference of both quantities, which is equal to  $R : \vec{\tau}$ , is left invariant under permutations of connected components of paths. Equation (D.17) is therefore valid for any cyclic Dyck paths  $\vec{\sigma}, \vec{\tau}$ .

Putting all the pieces together yields the following equation,

$$\begin{aligned} \sum_{\substack{R \subset \mathcal{N} \\ |R|=n}} (\mathbf{B}_n)_{\vec{\sigma}, R} (\mathbf{A}_n)_{R, \vec{\tau}} &= \sum_{\substack{R' \subset \mathcal{N} \\ |R'|=n}} (\mathbf{B}_n)_{\sigma_0, R'} (\mathbf{A}_n)_{R', \vec{\tau}'} \\ &\times w^{W(\vec{\tau}) - W(\vec{\tau}') - W(\vec{\sigma}) - \left|D_{\ell(1)}^{\vec{\sigma}}\right| + \left|D_{\ell(1,\vec{\sigma})}^{\vec{\tau}}\right|} \quad (\text{D.18}) \\ &= (1-w)^n w^{W(\vec{\tau}) - W(\vec{\tau}') - W(\vec{\sigma}) - \left|D_{\ell(1)}^{\vec{\sigma}}\right| + \left|D_{\ell(1,\vec{\sigma})}^{\vec{\tau}}\right|} \delta_{\sigma_0, \vec{\tau}'} \\ &= (1-w)^n \delta_{\vec{\sigma}, \vec{\tau}}, \end{aligned}$$

since  $D_{\ell(1,\vec{\sigma})}^{\vec{\sigma}} = D_{\ell(1)}^{\vec{\sigma}}$  and  $\vec{\sigma} = \vec{\tau} \Leftrightarrow \sigma_0 = \vec{\tau}'$ .  $\square$

# Bibliography

- [1] AFFLECK, I., AND LUDWIG, A. W. W. The Kondo effect, conformal field theory and fusion rules. *Nucl. Phys. B* 352, 3 (1991), 849–862.
- [2] AFFLECK, I., AND LUDWIG, A. W. W. The Fermi edge singularity and boundary condition changing operators. *J. Phys. A* 27, 16 (1994), 5375.
- [3] ATKINSON, D., AND VAN STEENWIJK, F. J. Infinite resistive lattices. *Am. J. Phys.* 67, 6 (1999), 486–492.
- [4] AZIMI-TAFRESHI, N., DASHTI-NASERABADI, H., MOGHIMI-ARAGHI, S., AND RUELLE, P. The Abelian sandpile model on the honeycomb lattice. *J. Stat. Mech.* (2010), P02004.
- [5] BAK, P., CHEN, K., SCHEINKMAN, J. A., AND WOODFORD, M. Self-Organized Criticality and Fluctuations in Economics. *Ric. Econ.* (1993), 3–30.
- [6] BAK, P., TANG, C., AND WIESENFELD, K. Self-organized criticality: An explanation of the  $1/f$  noise. *Phys. Rev. Lett.* 59, 4 (1987), 381–384.
- [7] BAUER, M. A Short Introduction to Critical Interfaces in 2D. In *Conformal Invariance: an Introduction to Loops, Interfaces and Stochastic Loewner Evolution*, M. Henkel and D. Karevski, Eds. Springer, 2012, 51–111.
- [8] BAUER, M., AND BERNARD, D. SLE( $\kappa$ ) growth processes and conformal field theories. *Phys. Lett. B* 543 (2002), 135–138.

- 
- [9] BAUER, M., AND BERNARD, D. Conformal Field Theories of Stochastic Loewner Evolutions. *Commun. Math. Phys.* 239, 3 (2003), 493–521.
- [10] BAUER, M., BERNARD, D., AND KYTÖLÄ, K. Multiple Schramm–Loewner Evolutions and Statistical Mechanics Martin-gales. *J. Stat. Phys.* 120, 5 (2005), 1125–1163.
- [11] BAUER, R. O., AND FRIEDRICH, R. M. Stochastic Loewner evolution in multiply connected domains. *C. R. Math.* 339, 8 (2004), 579–584.
- [12] BELAVIN, A. A., POLYAKOV, A. M., AND ZAMOLODCHIKOV, A. B. Infinite conformal symmetry in two-dimensional quantum field theory. *Nucl. Phys. B* 241, 2 (1984), 333–380.
- [13] BELIAEV, D., AND VIKLUND, F. J. Some Remarks on SLE Bubbles and Schramm’s Two-point Observable. *Commun. Math. Phys.* 320, 2 (2013), 379–394.
- [14] BENEŠ, C., LAWLER, G. F., AND VIKLUND, F. Scaling limit of the loop-erased random walk Green’s function. *Probab. Theory Relat. Fields* 166, 1 (2016), 271–319.
- [15] BIGGS, N. L. Chip-Firing and the Critical Group of a Graph. *J. Algebraic Combin.* 9, 1 (1999), 25–45.
- [16] BJÖRNER, A., LOVÁSZ, L., AND SHOR, P. W. Chip-firing Games on Graphs. *Eur. J. Combin.* 12, 4 (1991), 283–291.
- [17] BOUTTIER, J., BOWICK, M., GUITTER, E., AND JENG, M. Vacancy localization in the square dimer model. *Phys. Rev. E* 76, 4 (2007), 041140.
- [18] BRANKOV, J. G., IVASHKEVICH, E. V., AND PRIEZZHEV, V. B. Boundary effects in a two-dimensional Abelian sandpile. *J. Phys. I France* 3, 8 (1993), 1729–1740.
- [19] BRANKOV, J. G., POGHOSYAN, V. S., PRIEZZHEV, V. B., AND RUELLE, P. Transfer matrix for spanning trees, webs and colored forests. *J. Stat. Mech.* (2014), P09031.

- 
- [20] CALABRESE, P., AND CARDY, J. Entanglement entropy and quantum field theory. *J. Stat. Mech.* (2004), P06002.
- [21] CALABRESE, P., AND CARDY, J. Time Dependence of Correlation Functions Following a Quantum Quench. *Phys. Rev. Lett.* *96*, 13 (2006), 136801.
- [22] CALABRESE, P., AND CARDY, J. Entanglement and correlation functions following a local quench: a conformal field theory approach. *J. Stat. Mech.* (2007), P10004.
- [23] CAMIA, F., AND NEWMAN, C. M. Critical percolation exploration path and SLE<sub>6</sub>: a proof of convergence. *Probab. Theory Relat. Fields* *139*, 3 (2007), 473–519.
- [24] CARACCILO, S., PAOLETTI, G., AND SPORTIELLO, A. Explicit characterization of the identity configuration in an Abelian sandpile model. *J. Phys. A* *41*, 49 (2008), 495003.
- [25] CARACCILO, S., AND SPORTIELLO, A. Exact integration of height probabilities in the Abelian Sandpile model. *J. Stat. Mech.* (2012), P09013.
- [26] CARDY, J. Conformal Field Theory and Statistical Mechanics. In *Exact methods in low-dimensional statistical physics and quantum computing (Les Houches, Session LXXXIX)* (2008).
- [27] CARDY, J. L. Conformal invariance and surface critical behavior. *Nucl. Phys. B* *240*, 4 (1984), 514–532.
- [28] CARDY, J. L. Critical percolation in finite geometries. *J. Phys. A* *25*, 4 (1992), L201.
- [29] CHELKAK, D., DUMINIL-COPIN, H., HONGLER, C., KEMPAINEN, A., AND SMIRNOV, S. Convergence of Ising interfaces to Schramms SLE curves. *C. R. Math.* *352*, 2 (2014), 157–161.
- [30] CHELKAK, D., AND SMIRNOV, S. Discrete complex analysis on isoradial graphs. *Adv. Math.* *228*, 3 (2011), 1590–1630.
- [31] CHELKAK, D., AND SMIRNOV, S. Universality in the 2D Ising model and conformal invariance of fermionic observables. *Invent. Math.* *189*, 3 (2012), 515–580.

- 
- [32] CHEN, W.-K. *Applied Graph Theory: Graphs and Electrical Networks*. North Holland, 1976.
- [33] CIMASONI, D. A generalized Kac–Ward formula. *J. Stat. Mech.* (2010), P07023.
- [34] CIMASONI, D. The Critical Ising Model via Kac-Ward Matrices. *Commun. Math. Phys.* 316, 1 (2012), 99–126.
- [35] CORI, R., AND ROSSIN, D. On the Sandpile Group of Dual Graphs. *Eur. J. Combin.* 21, 4 (2000), 447–459.
- [36] CREUTZ, M. Abelian sandpiles. *Comput. Phys.* 5, 2 (1991), 198–203.
- [37] CSERTI, J. Application of the lattice Green’s function for calculating the resistance of an infinite network of resistors. *Am. J. Phys.* 68, 10 (2000), 896–906.
- [38] DARTOIS, A., FIORENZI, F., AND FRANCI, P. Sandpile group on the graph  $D_n$  of the dihedral group. *Eur. J. Combin.* 24, 7 (2003), 815–824.
- [39] DHAR, D. Self-organized critical state of sandpile automaton models. *Phys. Rev. Lett.* 64, 14 (1990), 1613–1616.
- [40] DHAR, D. Theoretical studies of self-organized criticality. *Physica A* 369, 1 (2006), 29–70.
- [41] DHAR, D., AND MANNA, S. S. Inverse avalanches in the Abelian sandpile model. *Phys. Rev. E* 49, 4 (1994), 2684–2687.
- [42] DHAR, D., RUELLE, P., SEN, S., AND VERMA, D.-N. Algebraic aspects of Abelian sandpile models. *J. Phys. A* 28, 4 (1995), 805.
- [43] DI FRANCESCO, P., MATHIEU, P., AND SÉNÉCHAL, D. *Conformal Field Theory*. Springer, 1997.
- [44] DROSSEL, B., AND SCHWABL, F. Self-organized critical forest-fire model. *Phys. Rev. Lett.* 69, 11 (1992), 1629–1632.
- [45] DUBÉDAT, J. Euler Integrals for Commuting SLEs. *J. Stat. Phys.* 123, 6 (2006), 1183–1218.

- 
- [46] DUMINIL-COPIN, H., AND SMIRNOV, S. Conformal Invariance of Lattice Models. In *Probability and Statistical Physics in Two and More Dimensions*, *Clay Math. Proc.* 15 (2012), 213–276.
- [47] DUMINIL-COPIN, H., AND SMIRNOV, S. The connective constant of the honeycomb lattice equals  $\sqrt{2 + \sqrt{2}}$ . *Ann. Math.* 175, 3 (2012), 1653–1665.
- [48] DUPLANTIER, B. Loop-erased self-avoiding walks in two dimensions: exact critical exponents and winding numbers. *Physica A* 191, 1 (1992), 516–522.
- [49] DÜRRE, M. Conformal covariance of the Abelian sandpile height one field. *Stochastic Process. Appl.* 119, 9 (2009), 2725–2743.
- [50] FLOHR, M. A. I. Bits and pieces in logarithmic field theory. *Int. J. Mod. Phys. A* 18, 25 (2003), 4497–4591.
- [51] FLORY, P. J. *Principles of Polymer Chemistry*. Cornell University Press, 1953.
- [52] FOMIN, S. Loop-Erased Walks and Total Positivity. *Trans. Amer. Math. Soc.* 353, 9 (2001), 3563–3583.
- [53] FORMAN, R. Determinants of Laplacians on graphs. *Topology* 32, 1 (1993), 35–46.
- [54] FORTUIN, C. M., AND KASTELEYN, P. W. On the random-cluster model: I. Introduction and relation to other models. *Physica* 57, 4 (1972), 536–564.
- [55] FRIEDAN, D., MARTINEC, E., AND SHENKER, S. Conformal invariance, supersymmetry and string theory. *Nucl. Phys. B* 271, 1 (1986), 93–165.
- [56] FRIEDRICH, R., AND WERNER, W. Conformal Restriction, Highest-Weight Representations and SLE. *Commun. Math. Phys.* 243, 1 (2003), 105–122.
- [57] GABERDIEL, M. R., AND KAUSCH, H. G. Indecomposable fusion products. *Nucl. Phys. B* 477, 1 (1996), 293–318.

- 
- [58] GABERDIEL, M. R., AND KAUSCH, H. G. A local logarithmic conformal field theory. *Nucl. Phys. B* 538, 3 (1999), 631–658.
- [59] GAINUTDINOV, A., RIDOUT, D., AND RUNKEL, I. (EDS.) Logarithmic conformal field theory. *J. Phys. A* 46, 49 (2013). Special issue.
- [60] GAMSA, A., AND CARDY, J. The scaling limit of two cluster boundaries in critical lattice models. *J. Stat. Mech.* (2005), P12009.
- [61] GINSPARG, P. Applied Conformal Field Theory. In *Fields, Strings and Critical Phenomena, (Les Houches, Session XLIX)* (1989).
- [62] GRIGOREV, S. Y., POGHOSYAN, V. S., AND PRIEZZHEV, V. B. Three-leg correlations in the two-component spanning tree on the upper half-plane. *J. Stat. Mech.* (2009), P09008.
- [63] GURARIE, V. Logarithmic operators in conformal field theory. *Nucl. Phys. B* 410, 3 (1993), 535–549.
- [64] HAGENDORF, C. A generalization of Schramm’s formula for  $SLE_2$ . *J. Stat. Mech.* (2009), P02033.
- [65] HAGENDORF, C. *Évolutions de Schramm-Loewner et théories conformes. Deux exemples de systèmes désordonnés de basse dimension*. PhD thesis, Université Pierre et Marie Curie, 2009.
- [66] HAGENDORF, C., BERNARD, D., AND BAUER, M. The Gaussian Free Field and  $SLE_4$  on Doubly Connected Domains. *J. Stat. Phys.* 140, 1 (2010), 1–26.
- [67] HOLROYD, A. E., MÉSZÁROS, K., PERES, Y., PROPP, J., AND WILSON, D. B. Chip-Firing and Rotor-Routing on Directed Graphs. In *In and Out of Equilibrium 2*, V. Sidoravicius and M. E. Vares, Eds. Birkhäuser, 2008, 331–364.
- [68] HONGLER, C., AND SMIRNOV, S. The energy density in the planar Ising model. *Acta Math.* 211, 2 (2013), 191–225.
- [69] HOU, Y., WOO, C., AND CHEN, P. On the sandpile group of the square cycle  $C_n^2$ . *Linear Algebra Appl.* 418, 2 (2006), 457–467.

- 
- [70] HU, C.-K., AND LIN, C.-Y. Universality in critical exponents for toppling waves of the BTW sandpile model on two-dimensional lattices. *Physica A* 318, 1 (2003), 92–100.
- [71] IKHLEF, Y., AND PONSANG, A. K. Finite-Size Left-Passage Probability in Percolation. *J. Stat. Phys.* 149, 1 (2012), 10–36.
- [72] ITZYKSON, C., SALEUR, H., AND ZUBER, J. B., Eds. *Conformal Invariance and Applications to Statistical Mechanics*. World Scientific, 1988.
- [73] IVASHKEVICH, E. V. Boundary height correlations in a two-dimensional Abelian sandpile. *J. Phys. A* 27, 11 (1994), 3643.
- [74] IVASHKEVICH, E. V., KTITAREV, D. V., AND PRIEZZHEV, V. B. Critical exponents for boundary avalanches in two-dimensional Abelian sandpile. *J. Phys. A* 27, 16 (1994), L585.
- [75] IVASHKEVICH, E. V., KTITAREV, D. V., AND PRIEZZHEV, V. B. Waves of topplings in an Abelian sandpile. *Physica A* 209, 3 (1994), 347–360.
- [76] IZYUROV, K. Critical Ising interfaces in multiply-connected domains. *Probab. Theory Relat. Fields* 167, 1 (2017), 379–415.
- [77] JACOBSON, B., NIEDERMAIER, A., AND REINER, V. Critical groups for complete multipartite graphs and Cartesian products of complete graphs. *J. Graph Theory* 44, 3 (2003), 231–250.
- [78] JENG, M. Boundary conditions and defect lines in the Abelian sandpile model. *Phys. Rev. E* 69, 5 (2004), 051302.
- [79] JENG, M. Conformal field theory correlations in the Abelian sandpile model. *Phys. Rev. E* 71, 1 (2005), 016140.
- [80] JENG, M. Four height variables, boundary correlations, and dissipative defects in the Abelian sandpile model. *Phys. Rev. E* 71, 3 (2005), 036153.
- [81] JENG, M., PIROUX, G., AND RUELLE, P. Height variables in the Abelian sandpile model: scaling fields and correlations. *J. Stat. Mech.* (2006), P10015.

- 
- [82] KAC, M., AND WARD, J. C. A Combinatorial Solution of the Two-Dimensional Ising Model. *Phys. Rev.* 88, 6 (1952), 1332–1337.
- [83] KARRILA, A., KYTÖLÄ, K., AND PELTOLA, E. Boundary correlations in planar LERW and UST. [arXiv:1702.03261](https://arxiv.org/abs/1702.03261) [math-ph].
- [84] KASSEL, A., AND WILSON, D. B. The Looping Rate and Sandpile Density of Planar Graphs. *Am. Math. Mon.* 123, 1 (2016), 19–39.
- [85] KENYON, R. Conformal Invariance of Domino Tiling. *Ann. Probab.* 28, 2 (2000), 759–795.
- [86] KENYON, R. The asymptotic determinant of the discrete Laplacian. *Acta Math.* 185, 2 (2000), 239–286.
- [87] KENYON, R. Dominos and the Gaussian Free Field. *Ann. Probab.* 29, 3 (2001), 1128–1137.
- [88] KENYON, R. Spanning forests and the vector bundle Laplacian. *Ann. Probab.* 39, 5 (2011), 1983–2017.
- [89] KENYON, R. Conformal Invariance of Loops in the Double-Dimer Model. *Commun. Math. Phys.* 326, 2 (2014), 477–497.
- [90] KENYON, R. W., AND WILSON, D. B. Double-Dimer Pairings and Skew Young Diagrams. *Electron. J. Comb.* 18, 1 (2011), #P130.
- [91] KENYON, R. W., AND WILSON, D. B. Spanning trees of graphs on surfaces and the intensity of loop-erased random walk on planar graphs. *J. Amer. Math. Soc.* 28, 4 (2015), 985–1030.
- [92] KIRCHHOFF, G. Ueber die Auflösung der Gleichungen, auf welche man bei Untersuchung der linearen Vertheilung galvanischer Ströme geführt wird. *Ann. Phys.* 148, 12 (1847), 497–508.
- [93] KOZDRON, M. J., AND LAWLER, G. F. The Configurational Measure on Mutually Avoiding SLE Paths. In *Universality and Renormalization: From Stochastic Evolution to Renormalization of Quantum Fields*, I. Binder and D. Kreimer, Eds. Amer. Math. Soc., 2007, 199–224.

- 
- [94] KTITAREV, D. V., AND PRIEZZHEV, V. B. Expansion and contraction of avalanches in the two-dimensional Abelian sandpile. *Phys. Rev. E* 58, 3 (1998), 2883–2888.
- [95] KYTÖLÄ, K. On Conformal Field Theory of  $SLE(\kappa, \rho)$ . *J. Stat. Phys.* 123, 6 (2006), 1169–1181.
- [96] KYTÖLÄ, K., AND RIDOUT, D. On staggered indecomposable Virasoro modules. *J. Math. Phys.* 50, 12 (2009), 123503.
- [97] LANGLANDS, R., POULIOT, P., AND SAINT-AUBIN, Y. Conformal invariance in two-dimensional percolation. *Bull. Amer. Math. Soc.* 30, 1 (1994), 1–61.
- [98] LAWLER, G. F. A self-avoiding random walk. *Duke Math. J.* 47, 3 (1980), 655–693.
- [99] LAWLER, G. F. A Connective Constant for Loop-Erased Self-Avoiding Random Walk. *J. Appl. Probab.* 20, 2 (1983), 264–276.
- [100] LAWLER, G. F. Loop-Erased Random Walk. In *Perplexing Problems in Probability: Festschrift in Honor of Harry Kesten*, M. Bramson and R. Durrett, Eds. Birkhäuser, 1999, 197–217.
- [101] LAWLER, G. F. Partition Functions, Loop Measure, and Versions of SLE. *J. Stat. Phys.* 134, 5 (2009), 813–837.
- [102] LAWLER, G. F. Defining SLE in multiply connected domains with the Brownian loop measure. [arXiv:1108.4364](https://arxiv.org/abs/1108.4364) [math.PR].
- [103] LAWLER, G. F. The probability that planar loop-erased random walk uses a given edge. *Electron. Commun. Probab.* 19 (2014), 1–13.
- [104] LAWLER, G. F. Topics in loop measures and the loop-erased walk. [arXiv:1709.07531](https://arxiv.org/abs/1709.07531) [math.PR].
- [105] LAWLER, G. F., SCHRAMM, O., AND WERNER, W. Conformal Invariance of Planar Loop-Erased Random Walks and Uniform Spanning Trees. *Ann. Probab.* 32, 1 (2004), 939–995.
- [106] LE BORGNE, Y., AND ROSSIN, D. On the identity of the sandpile group. *Discrete Math.* 256, 3 (2002), 775–790.

- 
- [107] LENELLS, J., AND VIKLUND, F. Coulomb gas integrals for commuting SLEs: Schramm's formula and Green's function. [arXiv:1701.03698](https://arxiv.org/abs/1701.03698) [math.PR].
- [108] LEVINE, L., AND PERES, Y. The looping constant of  $Z^d$ . *Random Struct. Algor.* *45*, 1 (2014), 1–13.
- [109] LIN, C.-Y., AND HU, C.-K. Renormalization-group approach to an Abelian sandpile model on planar lattices. *Phys. Rev. E* *66*, 2 (2002), 021307.
- [110] MAHIEU, S., AND RUELLE, P. Scaling fields in the two-dimensional abelian sandpile model. *Phys. Rev. E* *64*, 6 (2001), 066130.
- [111] MAJUMDAR, S. N., AND DHAR, D. Height correlations in the Abelian sandpile model. *J. Phys. A* *24*, 7 (1991), L357.
- [112] MAJUMDAR, S. N., AND DHAR, D. Equivalence between the Abelian sandpile model and the  $q \rightarrow 0$  limit of the Potts model. *Physica A* *185*, 1 (1992), 129–145.
- [113] MALDACENA, J. The Large-N Limit of Superconformal Field Theories and Supergravity. *Int. J. Theor. Phys.* *38*, 4 (1999), 1113–1133.
- [114] MANNA, S. S. Two-state model of self-organized criticality. *J. Phys. A* *24*, 7 (1991), L363.
- [115] MANNA, S. S., DHAR, D., AND MAJUMDAR, S. N. Spanning trees in two dimensions. *Phys. Rev. A* *46*, 8 (1992), R4471–R4474.
- [116] MARCHAL, P. Loop-Erased Random Walks, Spanning Trees and Hamiltonian Cycles. *Electron. Commun. Probab.* *5* (2000), 39–50.
- [117] MOORE, G., AND READ, N. Nonabelions in the fractional quantum Hall effect. *Nucl. Phys. B* *360*, 2 (1991), 362–396.
- [118] MORLEY, P. D., AND GARCIA-PELAYO, R. Scaling Law for Pulsar Glitches. *Europhys. Lett.* *23*, 3 (1993), 185.

- 
- [119] NIENHUIS, B. Exact Critical Point and Critical Exponents of  $O(n)$  Models in Two Dimensions. *Phys. Rev. Lett.* *49*, 15 (1982), 1062–1065.
- [120] NIENHUIS, B. Critical behavior of two-dimensional spin models and charge asymmetry in the Coulomb gas. *J. Stat. Phys.* *34*, 5 (1984), 731–761.
- [121] OLAMI, Z., FEDER, H. J. S., AND CHRISTENSEN, K. Self-organized criticality in a continuous, nonconservative cellular automaton modeling earthquakes. *Phys. Rev. Lett.* *68*, 8 (1992), 1244–1247.
- [122] ORR, W. J. C. Statistical treatment of polymer solutions at infinite dilution. *Trans. Faraday Soc.* *43* (1947), 12–27.
- [123] PANOVA, G., AND WILSON, D. B. Pfaffian Formulas for Spanning Tree Probabilities. *Comb. Probab. Comp.* *26*, 1 (2017), 118–137.
- [124] PAPOYAN, V. V., AND POVOLOTSKY, A. M. Renormalization group study of sandpile on the triangular lattice. *Physica A* *246*, 1 (1996), 241–252.
- [125] PELTOLA, E., AND WU, H. Global and Local Multiple SLEs for  $\kappa \leq 4$  and Connection Probabilities for Level Lines of GFF. [arXiv:1703.00898](https://arxiv.org/abs/1703.00898) [math.PR].
- [126] PEMANTLE, R. Choosing a Spanning Tree for the Integer Lattice Uniformly. *Ann. Probab.* *19*, 4 (1991), 1559–1574.
- [127] PIROUX, G., AND RUELLE, P. Pre-logarithmic and logarithmic fields in a sandpile model. *J. Stat. Mech.* (2004), P10005.
- [128] PIROUX, G., AND RUELLE, P. Boundary height fields in the Abelian sandpile model. *J. Phys. A* *38*, 7 (2005), 1451.
- [129] PIROUX, G., AND RUELLE, P. Logarithmic scaling for height variables in the Abelian sandpile model. *Phys. Lett. B* *607*, 1 (2005), 188–196.
- [130] POGHOSYAN, V. S., GRIGOREV, S. Y., PRIEZZHEV, V. B., AND RUELLE, P. Pair correlations in sandpile model: A check of conformal field theory. *Phys. Lett. B* *659*, 3 (2008), 768–772.

- 
- [131] POGHOSYAN, V. S., GRIGOREV, S. Y., PRIEZZHEV, V. B., AND RUELLE, P. Logarithmic two-point correlators in the Abelian sandpile model. *J. Stat. Mech.* (2010), P07025.
- [132] POGHOSYAN, V. S., AND PRIEZZHEV, V. B. The Problem of Predecessors on Spanning Trees. *Acta Polytech.* 51, 2 (2011), 59–62.
- [133] POGHOSYAN, V. S., PRIEZZHEV, V. B., AND RUELLE, P. Jamming probabilities for a vacancy in the dimer model. *Phys. Rev. E* 77, 4 (2008), 041130.
- [134] POGHOSYAN, V. S., PRIEZZHEV, V. B., AND RUELLE, P. Return probability for the loop-erased random walk and mean height in the Abelian sandpile model: a proof. *J. Stat. Mech.* (2011), P10004.
- [135] POLYAKOV, A. M. Conformal symmetry of critical fluctuations. *JETP Lett.* 12 (1970), 381–383.
- [136] POTTS, R. B., AND WARD, J. C. The Combinatorial Method and the Two-Dimensional Ising Model. *Progr. Theor. Phys.* 13, 1 (1955), 38–46.
- [137] PRIEZZHEV, V. B. Structure of two-dimensional sandpile. I. Height probabilities. *J. Stat. Phys.* 74, 5 (1994), 955–979.
- [138] PRIEZZHEV, V. B., DHAR, D., DHAR, A., AND KRISHNAMURTHY, S. Eulerian Walkers as a Model of Self-Organized Criticality. *Phys. Rev. Lett.* 77, 25 (1996), 5079–5082.
- [139] PRIEZZHEV, V. B., KTITAREV, D. V., AND IVASHKEVICH, E. V. Formation of Avalanches and Critical Exponents in an Abelian Sandpile Model. *Phys. Rev. Lett.* 76, 12 (1996), 2093–2096.
- [140] ROZANSKY, L., AND SALEUR, H. Quantum field theory for the multi-variable Alexander-Conway polynomial. *Nucl. Phys. B* 376, 3 (1992), 461–509.
- [141] RUELLE, P. A  $c=-2$  boundary changing operator for the Abelian sandpile model. *Phys. Lett. B* 539, 1 (2002), 172–177.

- 
- [142] RUELLE, P. Wind on the boundary for the Abelian sandpile model. *J. Stat. Mech.* (2007), P09013.
- [143] RUELLE, P. Logarithmic conformal invariance in the Abelian sandpile model. *J. Phys. A* 46, 49 (2013), 494014.
- [144] SCHRAMM, O. Scaling limits of loop-erased random walks and uniform spanning trees. *Isr. J. Math.* 118, 1 (2000), 221–288.
- [145] SCHRAMM, O. A Percolation Formula. *Electron. Commun. Probab.* 6 (2001), 115–120.
- [146] SCHRAMM, O., AND SHEFFIELD, S. Contour lines of the two-dimensional discrete Gaussian free field. *Acta Math.* 202, 1 (2009), 21.
- [147] SCHRAMM, O., AND SHEFFIELD, S. A contour line of the continuum Gaussian free field. *Probab. Theory Relat. Fields* 157, 1 (2013), 47–80.
- [148] SHIGECHI, K., AND ZINN-JUSTIN, P. Path representation of maximal parabolic Kazhdan–Lusztig polynomials. *J. Pure Appl. Algebr.* 216, 11 (2012), 2533–2548.
- [149] SHROCK, R., AND WU, F. Y. Spanning trees on graphs and lattices in  $d$  dimensions. *J. Phys. A* 33, 21 (2000), 3881.
- [150] SIMMONS, J. J. H., AND CARDY, J. Twist operator correlation functions in  $O(n)$  loop models. *J. Phys. A* 42, 23 (2009), 235001.
- [151] SMIRNOV, S. Critical percolation in the plane: conformal invariance, Cardy’s formula, scaling limits. *Comptes Rendus Acad. Sci. Série I* 333, 3 (2001), 239–244.
- [152] SMIRNOV, S. Discrete Complex Analysis and Probability. In *Proceedings of the International Congress of Mathematicians (Hyderabad, India)* (2010).
- [153] SPITZER, F. *Principles of Random Walk*. Springer, 1976.
- [154] STANLEY, R. P. *Enumerative Combinatorics, Volume 2*. Cambridge University Press, 1999.

- 
- [155] TEMPERLEY, H. N. V. London Math. Soc. Lecture Notes Series #13. In *Combinatorics: Proceedings of the British Combinatorial Conference* (1974), 202–204.
- [156] TOUMPAKARI, E. On the sandpile group of regular trees. *Eur. J. Combin.* 28, 3 (2007), 822–842.
- [157] WILSON, D. B. Generating random spanning trees more quickly than the cover time. In *Proc. 28th Annual ACM Symposium on the Theory of Computing (STOC)* (1996), 296–303.
- [158] WU, F. Y. The Potts model. *Rev. Mod. Phys.* 54, 1 (1982), 235–268.
- [159] WU, H. Hypergeometric SLE and Convergence of Critical Planar Ising Interface. [arXiv:1703.02022](https://arxiv.org/abs/1703.02022) [math.PR].
- [160] ZHAN, D. Stochastic Loewner evolution in doubly connected domains. *Probab. Theory Relat. Fields* 129, 3 (2004), 340–380.